On the Ubiquitination and Protein:Protein Interactions of p53

David George Saliba

Thesis submitted for the Degree of Doctor of Philosophy

The University of Edinburgh

2007

To my family, my Mother Carmen, my Father George and my Brother Edward

and

To my Grandfather Carmelo and Uncle Guido, may they rest in peace.

"IF AT FIRST YOU DON'T SUCCEED, TRY, TRY AGAIN!"

- My father George Saliba

Contents

List of Figures

Acknowledgements

I would like to express my sincere gratitude to my supervisor Prof. Ted Hupp for augmenting my passion for scientific research through his guidance and patience. I am also grateful to Prof. Kathryn Ball for our fruitful discussions on the subject presented in this thesis. I would also like to thank Dr. Pat Langdridge-Smith for inculcating in me an interest of mass-spectrometry. I also have to thank Dr. Jim Creanor and Dr. Logan McKay of SIRCAMS for their help with the mass spectrometers

All members of both the Hupp and Ball laboratories were vital in contributing to this project through constant discussions about the topic. A special thanks goes to Sarah and Nicky for meticulously proof reading my thesis.

I would like to thank my family to whom this work is dedicated, and who have always encouraged me when mishaps (and there were plenty!) arose.

On a lighter note, I am also grateful to the distilleries of Glenlivet, Auchentoshan, Caol ila, Glenrothes, Bruiladdich for being a source of inspiration when writing up this thesis. In fact, if there are any mistakes please blame it on them!

GLOSSARY

17-AAG	17-(Allylamino)-17-demethoxy-geldanamycin
AD	Alzheimer's disease
AMP	Adenosine monophosphate
AMPK	5'AMP-activated protein kinase
ANT	ADP/ATP translocase
AP	apurinic/apyrimidinic
ARF	Cyclin-dependent kinase inhibitor 2A
ARF-BP1	ARF binding protein 1
AT	Ataxia telangiectasia
ATM	Ataxia telangiectasia mutated
ATP	Adenosine 5'-triphosphate
ATR	ATM and RAD3-related kinase
BAG-1	Bcl-2-associated athanogene 1
Bcl-2	B-cell CLL/lymphoma 2
BER	Base excision repair
BRCA1	Breast cancer 1, early onset
BSA	Bovine serum albumin
CARPs	Caspase 8/10-associated RING proteins
CBP	Creb binding protein
CCT	T-complex protein
Cdc25A	Cell division cycle 25 homolog A (S. pombe)
Cdc25C	Cell division cycle 25 homolog C (S. pombe)
CDC37	Cell division cycle 37 homolog (S. cerevisiae)
CDC45	Cell division cycle 45
Cdk2	Cyclin dependent kinase 2
Cdk4	Cyclin dependent kinase 4
CHIP	Carboxyl terminus of Hsp70-interacting protein
CHK1	Checkpoint kinase 1
CHK2	Checkpoint kinase 2
CID	Collision induced decay
CMV	Cyto megalovirus
c-MYC	Cellular myelocytomatosis
COP-1	Constitutively photomorphogenic 1
CPB	Central peptide-binding
CRM	Charge residue model
Cys	Cysteine
Da	Dalton
DAPK-1	Death Associated Protein Kinase-1
DAPK-3	Death Associated Protein Kinase-3

DBD	DNA binding domain
DMEM	Dulbecco's modified eagle's medium
DMSO	Dimethyl sulfoxide
DNA	Deoxyribonucleic acid
DRAK-1	DAPK-related-kinase-1
DRiPs	defective ribosomal products
DsBs	Double stranded breaks
DSS	Disuccinimidyl suberate
E2F1	E2F transcription factor 1
ECL	Enhanced chemiluminescence
EDTA	ethylenediaminetetraacetic acid
eef1a	Eukaryotic elongation factor 1a
EF-Tu	Elongation factor Tu
EGFR1	Epidermal growth factor receptor
EGS	Ethylene glycolbis(sulfosuccinimidylsuccinate
ELISA	Enzyme linked immunosorbent assay
ESI	Electrospray Ionization
ESTs	Expressed sequence tags
F	Phenylalanine
FBS	Foetal bovine serum
FHA	Fork head associated domain
gadd45	growth arrest and DNA damage-inducible protein 45
GOF	Gain of function
GR	Glucocorticoid hormone receptor
GST	Glutathionine S-transferase
HECT	Homologous to E6AP C-terminus-domain
hnRNP-M4	Heterogeneous nuclear ribonucleoprotein M4
HPLC	High performance liquid chromatography
HRP	Horse radish peroxidase
Hsp	Heat shock protein
IDM	Desorption model
IGF-II	Insulin-like growth factor type II
K	Lysine
kDa	kilo Dalton
L	Leucine
LB	Laura Bertani
LDI	Laser/desorption ionization
Leu	Leucine
m/z	mass-charge ratio
MALDI	Matrix-assisted laser desorption/ionization
Mda	Mega Dalton
MDM2	Murine double minute 2

MDR1	Multidrug resistance protein 1
MG132	Carbobenzoxy-L-leucyl-L-leucyl-L-leucinal Z-LLL-CHO
MOPS	3-(N-morpholino)propanesulfonic acid
MPTP	Mitochondrial permeability transition pore
MRE11	meiotic recombination 11
MS	Mass spectrometry
MYT1	Myelin transcription factor 1
NBS-1	Nijmegen breakage syndrome 1
ND/YAG	Neodynium/yttrium aluminum garnet
NEDD8	neural precursor cell expressed, developmentally down-regulated 8
NEDP1	Sentrin specific peptidase family member 8
NES	Nuclear export signal
NF-Y	Nuclear transcription factor Y
NHS	N-Hydroxysuccinimide
NLS	Nuclear localization signal
OGG1	8-oxoguanine DNA glycosylase
P	Proline
PAGE	Polyacrylamide gel electrophoresis
PBS	Phosphate buffer saline
PBST	PBS-Tween
PCNA	Proliferating cell nuclear antigen
Phe	Phenylalanine
PIN1	Peptidylprolyl cis/trans isomerase
PP1B1	Protein phosphatase 1B1
PRD	Poly-proline conformational element domain
QIT	Quadrupole ion trap
R	Arginine
RAF-1	v-raf-1 murine leukemia viral oncogene homolog 1
Ref-1	Redox factor 1
RING	Really interesting new gene
RL	*Renilla* luciferase
RP	Ribosomal Protein
RPMI	Roswell Park Memorial Institute
SDS	Sodium dodecyl sulfate
Ser	Serine
SMC1	Structural maintenance of chromosomes-1
SQ/TQ	Serine glutamine/Threonine glutamine
SUMO	Small ubiquitin-related modifier
TAD	Transactivation domain
TAFII31	TBP-associated factor II31
TAP	Tandem affinity purification

TBP	TATA binding protein
TCP1	T-complex protein
TF	Trigger Factor
TFIID	TATA binding protein of transcription factor IID
Thr	Threonine
TNF	Tumor necrosis factor
TOF	Time of flight
TOPORS	Topoisomerase I- and p53-binding protein
TPRs	Tetratricopeptide repeats
TRAP1	TNF receptor-associated protein 1
TRIS	Trishydroxymethylaminomethane
Trp	Tryptophan
Tyr	Tyrosine
Uba	ubiquitin-activating
Ubc	ubiquitin-conjugating
VEGF	Vascular endothelial growth factor
VS	Vinyl Sulphone
W	Tryptophan
Z-VAD (OMe)-FMK	Z-Val-Ala-Asp(OMe)-CH2F

ABSTRACT

p53 protein is a tumour suppressor that is frequently mutated in human cancers, resulting in a protein with altered biochemical functions. The Interactome of the wild-type and mutant p53 revolves around core interactions with components of the transcriptional machinery and/or the chaperone-assisted degradation machinery. The balance between these two Interactomes regulates the activity of p53. In this study $p53^{F270A}$, $p53^{R175H}$, and wild-type (wt) p53 were used as a panel to dissect how oligomeric protein conformation affects p53 ubiquitination and binding of other proteins to p53. $p53^{F270A}$ is hyperubiquitinated in cells as determined by p53-immunoprecipitation and immunoblotting with an anti-ubiquitin antibody. Using a mass-spectrometric approach, eukaryotic elongation factor 1a (eef1a) was identified as binding specifically to hyperubiquitinated $p53^{F270A}$. In this study, using a one-strep tagged approach, the interactome of p53 was extended by defining stable cellular binding proteins to wild-type and mutant p53. The system faithfully recapitulates the enhanced ubiquitination pattern of the unfolded oncogenic forms of p53. Further, mutually exclusive binding partners were identified for wt and mutant p53: the wild-type protein interacted predominantly with MDM2; whilst the mutant interacted selectively with Heat shock protein 70 (Hsp70) and the TCP-1 beta chaperonin. Upon analyzing the effects of stresses on the p53-interactomes, we identified a Nutlin and 17-(Allylamino)-17-demethoxy-geldanamycin (17-AAG)-induced binding to a novel spliced form of HSP90 lacking the N-terminus (HSP90ΔN). Ionizing radiation did not induce the formation of a p53: HSP90ΔN complex. By contrast, the oncogenic and hyperubiquitinated mutant p53 was constitutively bound to HSP90ΔN. These data expand on the Interactome of p53 and identify eef1a and HSP90ΔN as novel components of signalling pathways that control p53 homeostasis.

1.0 The DNA Damage Checkpoint Cascade

Throughout evolution, organisms have evolved a complex network of checkpoints that act concertedly to maintain genomic stability [1], [2]. Activation of checkpoints by DNA damage ultimately interface with cell cycle regulators and lead to several downstream effects including cell cycle arrest, DNA repair, apoptosis and cellular senescence, thus preventing the proliferation of damaged cells – a hallmark of cancer. The cascade of events in checkpoint pathways requires the cooperation of proteins broadly characterised as sensors, transducers and effectors. (Figure 1)[i] [2]. DNA lesions include single and double stranded breaks, and changes in higher order structures of chromatin [3]. For reasons of brevity the proteins that will be discussed in the following literature review are the checkpoint kinase 2 (CHK2) and p53 transducer, tumour suppressor proteins.

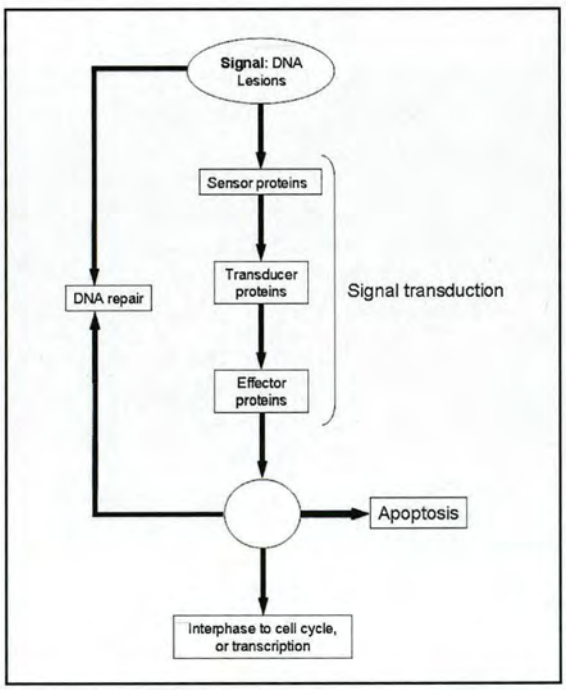

Figure 1.1 Conceptual Organization of the essential components and outcomes of checkpoint responses.[i]

[i] Figure 1.1 adapted from Iliakis, G., et al., *DNA damage checkpoint control in cells exposed to ionizing radiation.* Oncogene, 2003. **22**(37): p. 5834-47.

1.1 CHK2 tumour suppressor protein – structure related to function

CHK2 is a 543 amino acid, nuclear serine/threonine, stable kinase that is expressed throughout the cell cycle [4] [5]. CHK2 has been conserved through eukaryotic evolution [4] as a pivotal protein in checkpoint signal cascades. CHK2 is the human homologue of the yeast checkpoint kinases Cds1 (*Schizosaccharomyces pombe*) and Rad53 (*Saccharomyces cerevisiae*) [5].

The CHK2 protein (Figure 1.2) consists of three distinct functional domains; a serine-glutamine (SQ)/threonine-glutamine (TQ) cluster domain (amino acid residues 19-69); a forkhead associated domain (FHA amino acid residues 112-175) and a Ser/Thr kinase domain (amino acid residues 220-486). The SQ/TQ domain contains five SQ and two TQ motifs, which satisfy the primary substrate motif for ataxia-telangiectasia mutated (ATM) which is a protein that interacts with DNA damage sensor proteins and acts upstream of CHK2.

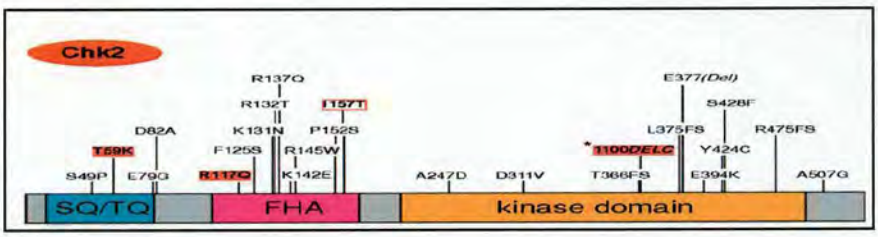

Figure 1.2[ii] Schematic view showing functional domains of human CHK2. SQ/TQ, a regulatory domain containing multiple (ATM/ATR)-recognition sites; FHA a forkhead associated domain required for CHK2 homodimerization and other protein-protein interactions. Positions of tumour associated mutations are indicated (top) Red boxes highlight three mutations associated associated with familial cancer; 1100delC is the most frequent mutation found both in sporadic and familial cancer.

[ii] Figure 1.2 Bartek J, Lukas J. *Chk1 and Chk2 kinases in checkpoint control and cancer.* Cancer Cell. 2003 May; **3**(5):421-9.

1.1.1 CHK2 activation in response to DNA damage

CHK2 is inactive in the absence of genotoxic stress but is activated in the presence of DNA double stranded breaks (DsBs). As depicted in Figure 1.3 activation of CHK2 occurs via the ATM dependent phosphorylation of CHK2 on Thr^{68}. Following phosphorylation at Thr^{68}, two CHK2 molecules dimerize at the FHA domains leading to trans activation of other CHK2 proteins via phosphorlyation at Thr^{383}/Thr^{387}. CHK2 also undergoes autophosphorlyation at Ser^{516} and Thr^{68}. [6]

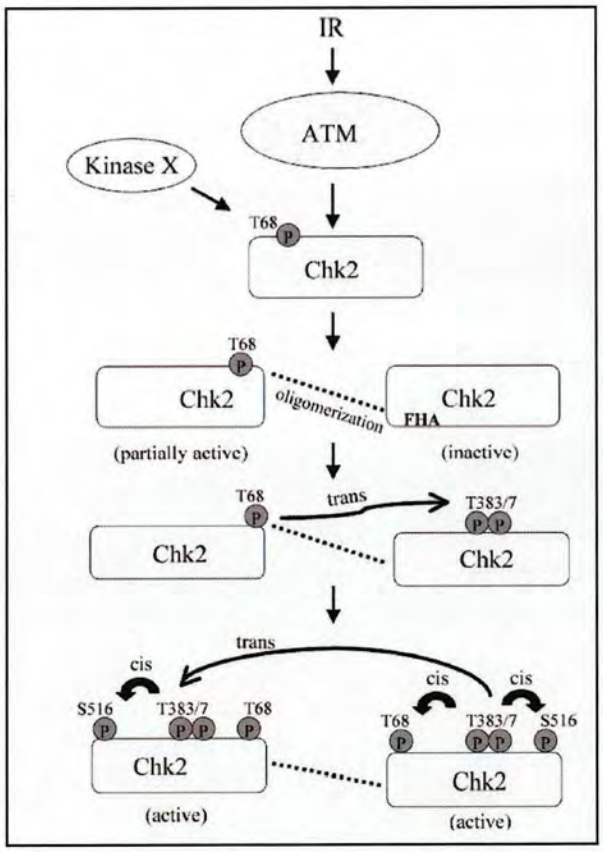

Figure 1.3[iii] Autoactivation of CHK2 is responsible for the rapid relay of the signal down the checkpoint signalling pathway.

[iii] Figure 1.3 Schwarz, J.K., C.M. Lovly, and H. Piwnica-Worms, *Regulation of the Chk2 protein kinase by oligomerization-mediated cis- and trans-phosphorylation.* Mol Cancer Res, 2003. **1**(8): p. 598-609.

1.1.2 CHK2 propagation of signal at various stages of the cell cycle

Activation of CHK2 leads several downstream effects such as DNA replication and cell cycle progression, chromatin restructuring, and apoptosis. The downstream targets of CHK2 include cell cycle phosphatases Cdc25C and Cdc25A [7] [8], breast cancer 1, early onset protein (BRCA1) [9] and the transcription factors E2F1 [10], p53 and p21 waf/cip1 [11] [12]. Live-cell imaging of CHK2 in human cells exposed to DNA damage revealed immediate redistribution of the activated CHK2 throughout the nucleus supporting the role of CHK2 as a checkpoint signal amplifier [5]. Figure 1.4 illustrates the checkpoint signalling pathway in the G1-phase of the cell cycle. In this phase key regulatory steps determine whether a cell will progress into G/S. These regulatory steps fall under the control of two key kinases, cyclin dependent kinase 4 (Cdk4) and cyclin dependent kinase 2 (Cdk2), in association with Cyclin D and cyclin E.

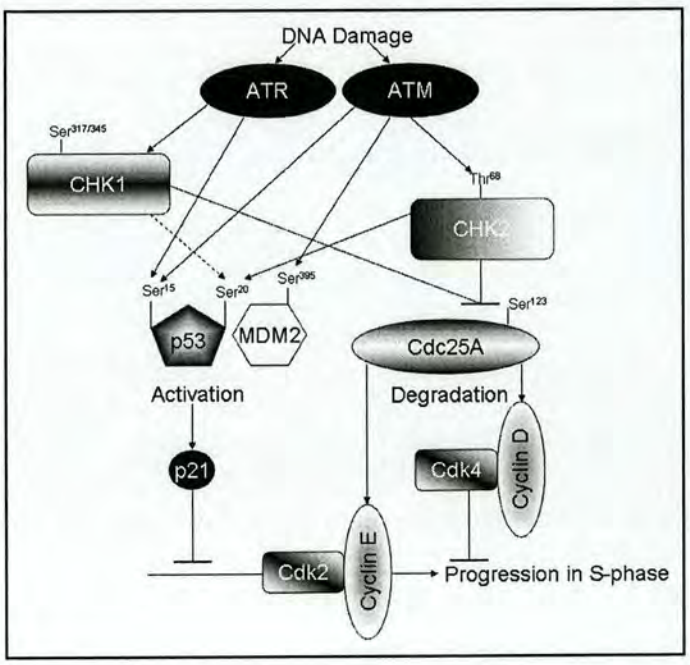

Figure. 1.4[iv] G1-checkpoint signalling cascade

[iv] Figure 1.4: adapted from: Iliakis, G., et al., *DNA damage checkpoint control in cells exposed to ionizing radiation.* Oncogene, 2003. **22**(37): p. 5834-47.

These proteins phosphorylate target proteins, such as CDC45 that ultimately lead to the progression into the S-phase of the cell cycle. Cyclin E-Cdk2 is therefore a regulator of cell cycle progression into the S-phase and is an important target of two distinct checkpoint cascade processes. The first, prompt pathway is the ubiquitin/proteasome mediated degradation of CDC25A which maintains Cyclin E-CDK2 locked in the inactive state. This is occurs through phosphorylation of CDC25A at Ser^{123} by CHK2 and checkpoint kinase 1 (CHK1). Once CDC25A is inactivated, Cyclin E-CDK2 cannot be activated since the former protein cannot remove inhibitory phosphates positioned at Thr^{14} and Tyr^{15}. [2] The second, delayed pathway, involves the stabilisation and activation of the transcription factor p53. This leads to the transcription of a large number of genes. $P21^{waf/cip1}$ is one of the genes to be transcribed, and this protein inhibits Cyclin E-CDK2. In nonirradiated cells, p53 is kept at low levels via the interaction with murine double minute 2 (MDM2) which through a negative feedback loop targets p53 for ubiquitination and proteasome mediated degradation. The MDM2 oncoprotein is a RING (really interesting new gene)-finger-type ubiquitin ligase that ubiquitinates both itself and p53, through its binding to the N-terminus of p53 leading to the ubiquitination of the latter (*c.f.* Sections 1.5). [1] Following DNA damage, phosphorylation of p53 at Ser^{15} by ATM and ATM and RAD3-related kinase (ATR), and Ser^{20} by a broad range of calcium calmodulin kinase superfamily members, including CHK2, CHK1, Death Associated protein kinase-1 (DAPK-1), death associated protein kinase-3 (DAPK-3), DAPK-related-kinase-1 (DRAK-1), and 5'AMP-activated protein kinase (AMPK), leads to the disruption of the p53-MDM2 interaction [13].

Although most of the cells in an adult organism are in the G1 phase, damage to DNA in the S-phase leads to the severe genomic abnormalities if not properly dealt with [2].

Indeed, radio-resistant DNA synthesis is a phenotypic feature of cells derived from patients with ataxia-telangiectasia (AT), AT-like disorder and Nijmegen breakage syndrome [1]. Two main pathways operate as checkpoint cascades in the S-phase. The first, the ATM-CHK2-CDC25A path, and operates in the same fashion as described in the G1-checkpoint. The other pathway involves the MRE11-RAD50-NBS-1 complex. ATM phosphorylates NBS1 on Ser^{343} resulting in the activation of the intra-S checkpoint. The protein structural maintenance of chromosomes-1 (SMC1) is also phosphorylated by ATM in an NBS-dependent manner and this leads to the activation of the intra-S checkpoint.

The key target protein in the G2/M checkpoint cascade is the Cdc2 kinase. Together with its partner cyclin B this protein promotes the progression of the cell into mitosis. Analogous to the regulation of the Cyclin E-CDK2 in the G1 phase the inhibitory phosphates are present on Tyr^{15} and Thr^{14}. These phosphates are added by Weel (Tyr^{15}) and MYT1 (Thr^{14}) [14 15 16]. In a manner similar to the checkpoint in the G1 phase, ATM phosphorylates CHK2 at Thr^{68}, which in turn blocks CDC25C by phosphorylation at $Ser2^{16}$. CDC25C is responsible for the removal of the inhibitory phosphates on CDC2-cyclin B. Once CDC25C is phosphorylated it interacts with the 14-3-3 protein resulting in sequestration to the cytoplasm, loss of activity in the nucleus and halt in the cell cycle.

1.2 p53 structure and function

The p53 tumour suppressor gene encodes a 393-amino acid, DNA binding, nuclear phosphoprotein which functions as a transcription factor that is activated in response to genotoxic and non-genotoxic cellular stress. Examples of cellular stresses that lead to p53 activation include agents that create single or double-strand breaks in DNA (γ - or UV radiations, free radical damage, inhibitors of topoisomerases), mutagens that form bulky DNA adducts (aflatoxins, benzo(*a*)pyrene, alkylating agents) or agents that block elongation by RNA polymerases. In addition, damage to the mitotic spindle, ribonucleotide depletion, hypoxia, heat shock and exposure to nitric oxide can also induce p53. Induction follows a different time-course, depending upon the nature and intensity of the stress [17], [18], [19], [20].

p53 is a modular protein (Figure 1.5) with five functional domains, namely an N-terminal transactivation domain (TAD), a poly-proline conformational element domain (PRD), a core sequence-specific DNA-binding domain, a tetramerisation domain and a basic, regulatory C-terminal domain [21].

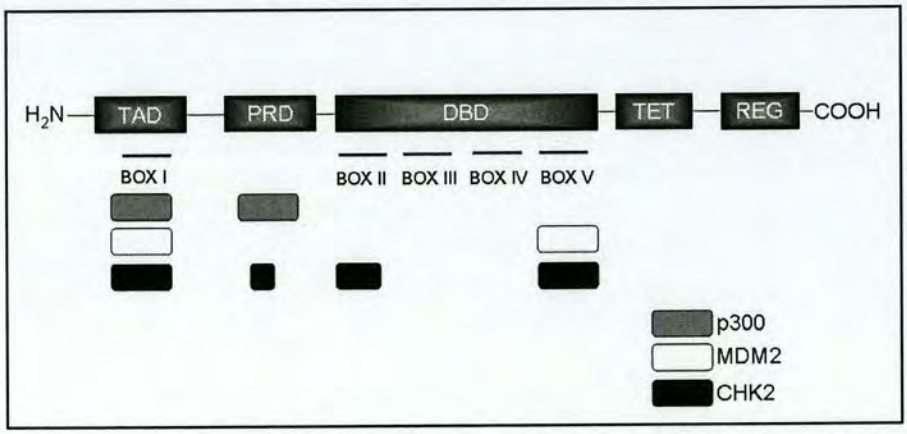

Figure 1.5 Schematic view showing functional domains of p53 and binding sites of regulatory proteins p300, MDM2 and CHK2

1.2.1 p53 N-terminus

The TAD is a classical acidic activation domain, which is known to be potent at activating transcription and allows the recruitment of the basal transcription machinery including the TATA binding protein (TBP) and the TBP-associated factor II31 (TAFII31) components of TFIID [22]. The N-terminal conserved BOX-I domain (amino acid residues 13-23) of p53 found within the TAD encompasses approximately 15 amino acids and has evolved as a multiprotein binding domain, resulting in an interaction with a set of acetyltransferases, ubiquitin ligases and protein kinases [13]. The BOX-I domain contains the *LXXLL*-motif (where *X* is any amino acid), transactivation domain and provides a binding site for other regulatory proteins, including the transcriptional co-activators, p300 and its homolog CREB binding protein (CBP) [23], [24], as well as components of the DNA repair machinery, including subunit p62 of the dual function transcription/repair factor TFIIH [25], [26]. The BOX-I domain also contains the *FXXWXXXL* consensus binding site that is required for MDM2-mediated inhibition of p53 and will be further discussed in Section 1.5.

The PRD of p53 (amino acid residues 63-97) contains five evolutionary conserved PxxP motifs (where x is any amino acid) [27]. Phosphorylation within the BOX-I at ser^{15} and ser^{20} and the adjacent Thr^{18} enables binding of the prolyl isomerase PIN1 to induce cis-trans prolyl isomerizations within the PRD. This leads to stabilization of p300 docking and promotes DNA-dependent acetylation of p53 [28]. It is important to note that phosphorylation at Thr^{18} has the most striking effect on blocking MDM2 binding [29], while phosphorylation at Ser^{20} has no effect on MDM2 binding [30].

1.2.2 p53 core DNA-binding-domain

The core DNA-binding-domain (DBD) of p53 (amino acid residues 102-292) is responsible for the binding of p53 to specific gene promoters. The arrangement of the promoter sequence suggests that p53 binds DNA as a tetramer [31]. X-ray crystallography of the p53 DBD in complex with consensus DNA solved at 2.2 Å demonstrated that the DBD consists of three molecules contained in an asymmetric unit that acts as a scaffold for three-loop based elements. One of the three core domains is bound to a DNA consensus site, the second to a non-consensus region of DNA, and the third molecule makes no significant contact with DNA, thus representing a DNA-free state of the coredomain. The main structural feature of the core domain is an immunoglobulin-like central β-sandwich of two antiparallel β-sheets, which provides the basic scaffold for the DNA-binding surface (Figure 1.6). This surface is formed by two large loops (L2 comprising residues 164–194, which is interrupted by a short helix, and L3 comprising residues 237–250) that are stabilized by a zinc ion, and a loop–sheet–helix motif (loop L1, β-strands S2 and S20, the end of the extended β-strand S10, and the C-terminal helix H2) [32], [33]. Loops L1, L2 and L3 correspond to the most highly evolutionary conserved domains, being encoded by the sequences BOX II-V, thereby highlighting their importance in p53 function.

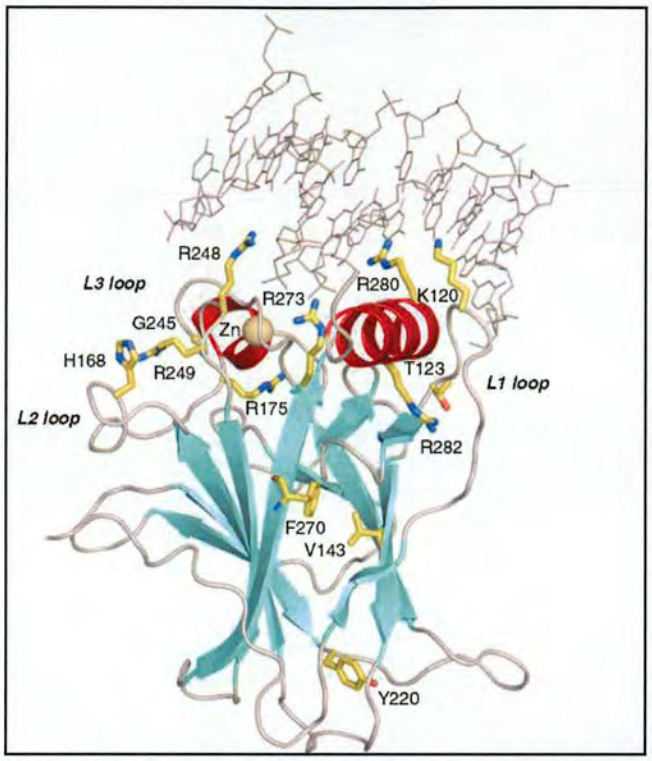

Figure 1.6[v] Ribbon diagram of the structure of DNA-bound p53 core domain

1.2.3 p53 C-terminus

The C-terminus of p53 (amino acid residues 300-393) consists of a tetramerisation domain (amino acid residues 323-356) and a basic regulatory domain (amino acid residues 360-393) which are connected by a flexible linker (amino acid residues 300-318) [34]. The crystal structure of the tetramerisation domain resolved at 1.7 Å revealed a highly symmetrical structure composed of a dimer with each monomer composed of a turn, a β-strand, a second turn and an α-helix. The monomers interact with each other across an antiparallel β-sheet and an antiparallel helix-helix interface to form the dimer. Two of these dimers associate across a second and distinct parallel helix-helix interface to form the tetramer [34].

[v] Figure 1.6 Joerger AC, Fersht AR. *Structure-function-rescue: the diverse nature of common p53 cancer mutants.* Oncogene. 2007 Apr **2;26**(15):2226-42.

The basic regulatory domain controls the active/inactive state of p53 by allosteric regulation of the DNA binding domain. The C-terminal region interacts with the core domain to induce a conformational shift that prevents DNA binding [35], [36], and this can be regulated by post-translation modification of the C-terminus, such as phosphorylation, or binding to regulators, such as 14-3-3 proteins [37]. The C-terminus exclusively binds non-specifically to ssDNA, RNA and DNA mismatches [38], [39] as well as to reannealing ssDNA and RNA complementary strands [40], [41].

The C-terminus of p53 also hase three nuclear localization signals (NLS), which have been mapped to amino acid residues 316-325, 369-375 and 379-384 and have been termed NLS1, NLS2 and NLS3 respectively [42]. Interestingly, a nuclear export signal (NES) (amino acid residues 340-351) cooperates with the p53 N-terminal NES for p53 nuclear export [43].

1.3 p53 mutations

"The history of p53 is a chaotic voyage from the world of oncogenes to the world of tumour suppressor genes, while retaining a certain degree of individuality (Lane and Benchimol, 1990). Apart from artefactual problems related to involuntary cloning of mutant p53, this ambiguity is also due to our propensity to over categorize in order to satisfy our Cartesian and oversimplistic view of science."

- T Soussi p53 alterations in human cancer: more questions than answers Oncogene (2007) 26, 2145–2156

It is important to stress that wild-type p53 cannot be pigeon holed into a single category of tumour suppressor gene and concomitantly, mutant p53 should be considered in context with its interacting proteins namely the 'mutant p53 megacomplex'. The properties of the 'mutant p53 megacomplex' are defined by the

heterogenous loss of activity, dominant-negative activity (antimorphic) and gain of function (GOF) (neomorphic) [44]. Almost 80% of p53 gene mutations are missense mutations resulting in the synthesis of a stable protein lacking specific DNA-binding activity and accumulating in the nucleus of tumour cells [44]. The observation of high incidence of missense mutations in the p53 gene strongly supports the view of the oncogenic activity of mutant p53 in malignant transformation since selection of missense mutation hotspots could have two consequences. Firstly, a dominant negative effect by heteroligomerization with wild-type p53 expressed in the second allele [45], and secondly, a specific GOF of mutant p53 [46]. In the latter scenario, some mutants are capable of transactivating target genes such as MDR1, EGFR, c-MYC, PCNA, IGF-II or VEGF which are not transactivated by the wild-type p53 protein and the resultant GOF properties are associated with growth-promoting phenotypes as well as resistance to anti-cancer drugs [47]. Interestingly, in a recent work by Di-Agostino and co-workers has shown that mutant p53 physically interacts with the transcription factor NF-Y, whose DNA-binding consensus sequences are present in the regulatory regions of many key genes involved in the regulation of the cell cycle such as cyclin A, cyclin B1, Cdk1 and Cdc25C [48].

Somatic p53 mutations have been described in all types of cancers with a variable prevalence depending on the type of cancer [20]. p53 is mutated in 75% of invasive cancers of the mouth, oesophagus and bronchi, particularly in smokers who are exposed to mutagens, and the mutation is often detectable in early, pre-neoplastic lesions. In colon and other lower-digestive tract cancers p53 mutations are less common in at early stages (polyps or adenomas) but become highly prevalent at the adenoma-carcinoma transition. In breast cancers, mutations are detected in about 25% of the

cases, but it has been suggested that inactivation of p53 may occur by other mechanisms in a proportion of the cases. Cancers in which p53 mutations are infrequent include cancers of the cervix, testicular cancers, neuroblastoma and malignant melanomas, in which the overall p53 mutation prevalence is less than 5% [20]. In the latter types of cancers, the p53 pathway may be functionally inactivated by viral or cellular oncogenes. For example, in cervical cancers, the viral antigen E6 of the oncogenic types of Human Papilloma Virus binds to the wild-type p53 protein and induces its rapid degradation, thus effectively bypassing the need of an inactivating mutation to remove p53 protein function [49].

80% of the missense mutations of p53 are located within the DNA-binding domain (DBD). The N-terminus and C-terminus of p53 are rarely targeted by mutations (less than 2% of all mutations) [20]. The spectrum of p53 mutation can be explained by the observation that the DBD, which is encoded by 600 nucleotides, is very fragile and each residue in this region has been found to have been the target of at least one mutation in cancer [44]. However, 30% of the mutations fall at five hot spot codons (175, 245, 248 273 and 282). Four of these residues correspond to arginine residues (175, 245, 248, 273, and 282) and are involved in protein-DNA interactions, either by direct contact with DNA (residues 248 and 273) or by stabilization of the DNA-binding surface (residues 175 and 282) [32].

1.4 The Ubiquitin/Proteasome pathway

In the 1980's, pioneering work by Hershko and co-workers found that energy, in the form of ATP, is needed to modify proteolytic substrates with ubiquitin, a highly conserved 76 amino acid polypeptide that is joined to a substrate lysine side chain through an isopeptide bond to ubiquitin's C terminus [50], [51]. Ubiquitination occurs through sequential steps catalyzed by activating (E1), conjugating (E2), and ligase (E3) enzymes (Figure 1.7) [52]. E1 activates ubiquitin by using ATP to synthesize ubiquitin C-terminal adenylate, which then serves as an enzyme bound substrate for the formation of an E1-ubiquitin thiol ester [53]. The latter ubiquitin is passed to an E2 cysteine residue and from there, in an E3-dependent manner, to the substrate [52].

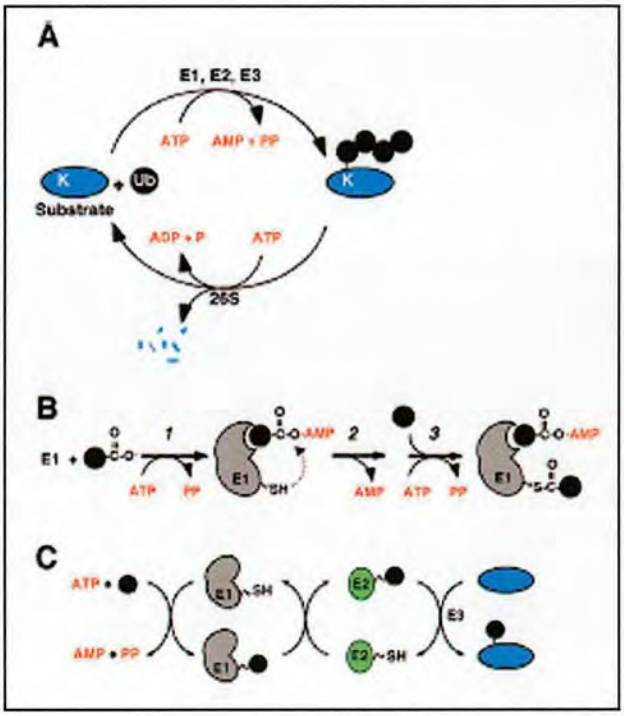

Figure 1.7[vi] Components and mechanisms in the ubiquitin proteasome pathway (**A**) Overview of pathway showing how ATP is used in its conjugative (top) and degradative (bottom) phases. (**B**) E1 calysed reaction. Step 1, ubiquitin adenylate formation; Step 2 second round of adenylate formation to yield fully loaded enzyme. (**C**) Ubiquitin conjugation cascade involving E1, E2 and E3 enzymes.

[vi] Figure 1.7 Pickart CM. *Back to the future with ubiquitin.* Nat Struct Mol Biol. 2007 Oct;**14**(10):885-887.

E3 ligases fall into two groups: those that utilize a covalent mechanism, namely Homologous to E6AP C-Terminus-domain (HECT-domain-E3s) and those that do not, including but not exclusively RING-domain-E3s. The mammalian RING-domain family is very large and it is likely that a substantial fraction of its members are E3s. Some consist of just one subunit [54], whereas others are multiprotein complexes in which each subunit is a member of a distinct protein family, with the RING subunit acting to recruit the E2 [55]. RING domain E3s act as bridging factors that bring the E2 enzyme with its activated ubiquitin into the vicinity of the substrate. It is however unclear how RING E3s bring about the exact structural placement of reactants, given the tens of angstroms that are inferred to separate the bound E2 and substrate molecules based on data derived from X-ray crystallography [56], [57].

Following polyubiquitination of the proteolytic substrate, the 26S proteasome, a 2.5 MDa complex, uses energy derived from ATP hydrolysis to unfold the substrate polypeptide chain and translocate it into an interior chamber [58] . Once inside this chamber, the substrate is hydrolysed by a nucleophilic mechanism to produce small peptides. Ubiquitin is recycled by release from the substrate prior to degradation by deubiquitinating enzymes [51]. The 26S proteasome (Figure 1.8) is made up of the 20S core particle (CP) and the 19S regulatory particle (RP). The core particle contains the proteases that can be degrade proteins to small peptides. It consists of 28 subunits – 14 α and 14 β proteins which form 4 stacked rings of 7 subunits each 2 α rings and 2 β rings. The rings sandwich the β rings to form a cylindrical structure. In this way a central channel is formed with three chambers: two antechambers on either side of a central chamber. This central chamber is lined with at least three active sites whose combined specificities can hydrolyse almost all peptide bonds. Access to these active

sites is controlled by the α subunits which form the antechambers and can exhibit closed or open conformations. The protein to be degraded passes through this pore and the proteases degrade it to 6-9 amino-acid peptide products which are released and recycled [i].

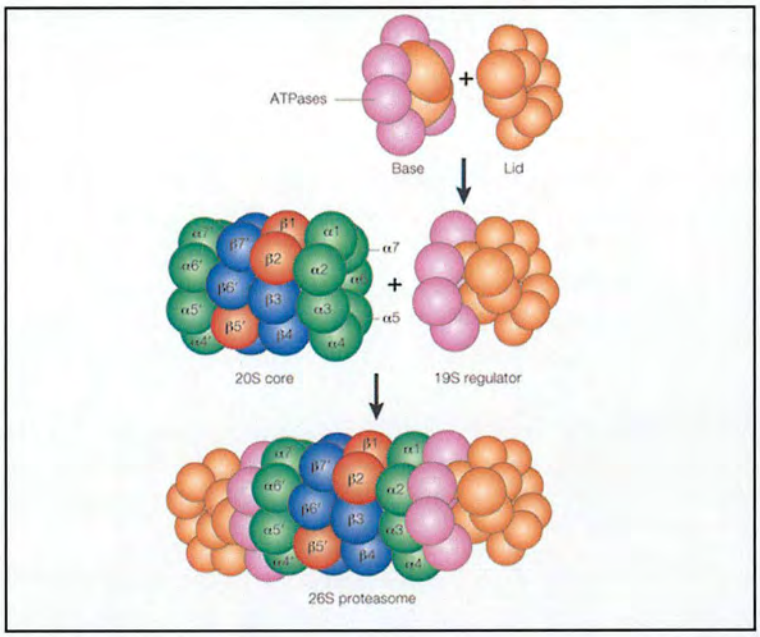

Figure 1.8 Schematic view of 26S proteasome

1.4.1 Proteasome inhibitors

Ever since the discovery of the proteasome as a key player in protein turnover, several studies have been undertaken involving the use of small molecular inhibitors. These fall under the catagories of Peptide Aldehydes, Lactacystin, Peptide Epoxyketones, Cyclic Peptides, Peptide Boronates, Peptide Vinyl Sulfones (VS). For reasons of brevity, only the inhibitors used in this study shall be discussed, namely,

MG132 (Z-Leu-Leu-Leu-Al) and $AdaAhx_3Leu_3VS$ that belong to the Peptide Aldehydes and Peptide VS categories respectively. MG132 is one of the standard tools used to modulate proteasome activity. The inhibitor's aldehyde moiety presumably forms a hemiacetal linkage with a catalytic threonine residue. Although this linkage is covalent, it can be hydrolysed under physiological making MG132 reversible, competitive inhibitors. A major drawback of MG132 is its propensity to cross-react with other proteolytic activities, primarily cysteine proteases [59]. $AdaAhx_3Leu_3VS$ is an irreversible proteasome inibitor that covalently modifies the catalytic subunits through Michael reaction of the threonine hydroxyl with the VS moiety, resulting in the formation of a physiologically stable β-sulfonyl ether linkage [60]. The nature of the peptide portion attached to the electrophylic trap, directs most of the activity of $AdaAhx_3Leu_3VS$ towards the proteasome rather than cysteine proteasome inhibitors, underscoring the importance of peptide-based recognition elements in attaining protease specificity.

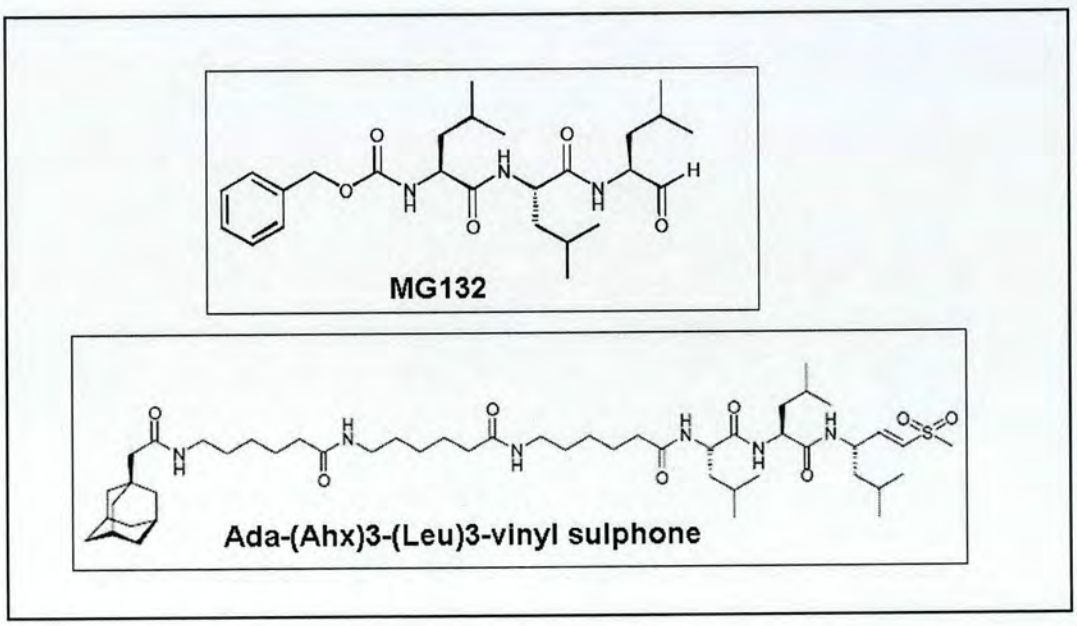

Figure 1.9 Structures of 26S proteasome inhibitors MG132 and $AdaAhx_3Leu_3VS$

1.5 The p53:MDM2 interaction

Following the discovery of the MDM2 gene, compelling evidence has emerged that MDM2 has a physiological role in controlling p53. MDM2-null mouse embryos die after early implantation but are fully rescued if they are co-deficient for p53. [61].

Principally, MDM2 is an E3 ligase and promotes degradation through a ubiquitin-dependent pathway on nuclear and cytoplasmic 26 proteasomes. [62] The ability of MDM2 to inactivate p53 relies on a direct interaction between the two proteins. The N-terminal portion of MDM2 contains the p53-binding domain. MDM2 also contains a central acidic region capable of interaction with ribosomal protein L5 [63] as well as the ARF tumour suppressor protein. MDM2 contains a C-terminal ring finger domain and a zinc finger located downstream of the acidic region. There are also structural requirements for the p53 protein for MDM2-dependent p53 degradation. Deletion analysis has established that the last 30 amino acid residues of p53 are important for MDM2-dependent degradation. [64] Lysines within the C-terminal part of p53 might therefore be targets for modification by ubiquitination. Mutation of 6 lysine residues within the C-terminus of p53 to arginine (at amino acid residues 370, 372, 373, 381, 382 and 386) termed 6 KR, was found to confer increased resistance of the mutant p53 protein to MDM2-mediated degradation. Nonetheless significant residual MDM2-dependent ubiquitination of the 6KR mutant was observable both *in vitro* and *in vivo*. [65] Another structural requirement for optimal p53 ubiquitination relates to p53 oligomerization. Amino acids 333-353 in the tetramerisation domain are crucial for Mdm2 binding and Mdm2-dependent degradation. [66] The hydrophobic side of the amphipatic p53 α-helix, which is formed by amino acid residues 19-26 (with Phe^{19}, Trp^{23} and Leu^{26} making contact), fits deeply into the hydrophobic cleft of MDM2. The

MDM2 cleft is formed by the amino acid residues 26-108 and consists of two structurally similar portions that fold up into a deep groove lined by 14 hydrophobic and aromatic residues. (Figure 7)

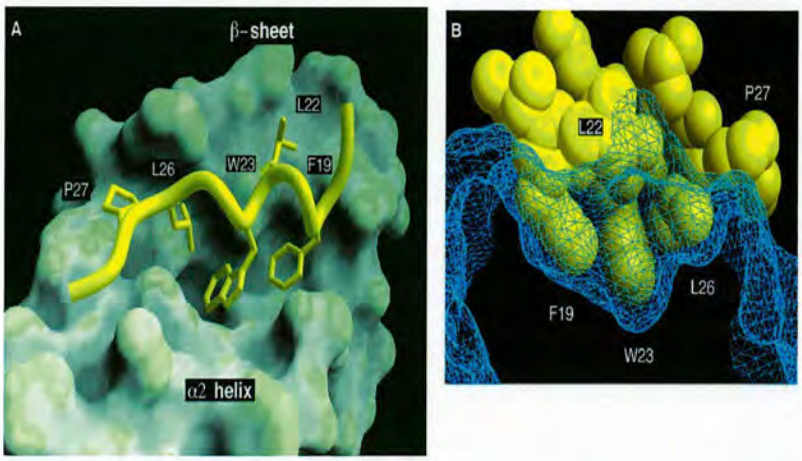

Figure 1.10[vii]. MDM2 cleft containing the p53 peptide sequence represented in yellow.

Apart from the p53 N-terminal binding site for MDM2, the latter also binds a secondary conformationally flexible loop within the S10 β-sheet in the central DNA-binding *BOX-V* domain of p53. The *BOX-V* region has therefore been defined as a key ubiquitination signal for MDM2, which is driven by a dual-site docking mechanism by MDM2 on the p53 tetramer [67]. The interaction between the N-termini of p53 and MDM2 seems to promote a conformational change in MDM2. This stabilizes the interaction between the MDM2 acid-domain and the ubiquitination signal located in the above mentioned secondary site within the DNA binding domain of the p53 tetramer resulting in enhanced ubiquitination [68]. These studies thereby highlight the importance of p53 conformational status in MDM2-dependent ubiquitination. Interestingly, the *BOX-V* domain of p53 forms a docking site for the calmodulin kinase superfamily

[vii] Figure 1.10 Kussie, P.H., et al., *Structure of the MDM2 oncoprotein bound to the p53 tumor suppressor transactivation domain.* Science, 1996. **274**(5289): p. 948-53.

which include CHK2, CHK1, DAPK-1, DAPK-3, DRAK-1, and AMPK. It therefore appears that the *BOX-V* interface is a conformationally flexible multiprotein binding domain with a potential for cross-talk through competition for the same *BOX-V* interface: CHK1/DAPK-1 and MDM2 resulting in p53 activation and degradation respectively [13].

1.5.1 The MDM2-ARF and MDM2-L5-L11-L23 ribosomal complex interaction

The p14ARF (ARF) protein is the alternate product of the INK4A tumour suppressor locus. ARF binds to the ring finger domain of MDM2, which houses the E3 ligase activity thereby acting as a direct inhibitor of the E3 activity of MDM2 [69]. Studies suggest that ARF binds to MDM2 and sequesters it into the nucleolus, away from p53 that remains in the nucleoplasm [70 71].

A recent study [72] suggests that overexpressed ribosomal proteins L5, L11 and L23 can inhibit MDM2 function and activate p53. In response to ribosomal biogenesis stress by actinomycin D, the same authors suggest that these ribosomal proteins can also form a quaternary complex with MDM2, probably working in concert to negate the MDM2 feedback regulation of p53. The finding that the quadruple complex is markedly reduced in the presence of p53 suggests that these ribosomal proteins may compete with p53 for binding to MDM2 (Figure 8). Since all three ribosomal proteins can inhibit MDM2-mediated ubiquitination, it is likely that they execute inhibitory effects by sterically hindering the transfer of the ubiquitin moiety from E2 to p53 – in other words blocking the E3 ligase activity of MDM2.

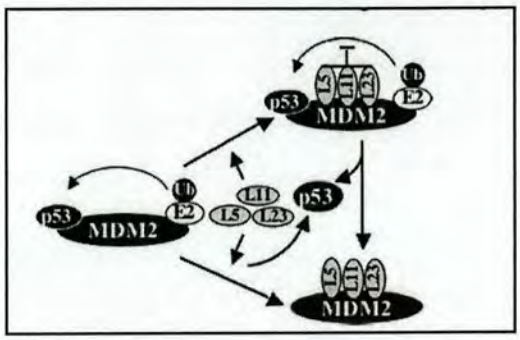

Figure 1.11[viii].Inhibition of E3 ligase activity of MDM2 by quadruplex formation of ribosomal proteins L5, L11 and L23 with MDM2

1.5.2 SUMO protein modification of p53

SUMO (*s*mall *u*biquitin-related *mo*difier) family proteins are structurally and mechanistically related to ubiquitin in that they are posttranslationally attached to other proteins. Like ubiquitin, SUMO is covalently linked to its substrates via amide (isopeptide) bonds formed between its C-terminal glycine residue and the ε-amino group of internal lysine residues. The enzymes involved in the reversible conjugation of SUMO are analagous to those mediating the ubiquitin conjugation. [73] In contrast to most ubiquitination functions, sumolation appears to affect the ability of the modified protein to interact with other cellular components.

Modification of proteins by SUMO-1 requires the activity of the SUMO-activating enzyme E1 and the SUMO-conjugating enzyme hUbc9. M.Gotissa and co-workers [74] have shown that p53 transcriptional activity is enhanced by SUMO-1 or hUbc9 overexpression, indicating that both factors are rate limiting in the conjugation process.

[viii] Figure 1.11 Dai, M.S. and H. Lu, *Inhibition of MDM2-mediated p53 ubiquitination and degradation by ribosomal protein L5.* J Biol Chem, 2004. **279**(43): p. 44475-82.

Indeed co-expression of SUMO-1 and hUbc9 increases the amount of sumolated p53. A potential outcome of the sumolation of p53 might be the direct alteration of the growth-suppressive properties of p53. This outcome might arise via several mechanisms including allosteric regulation, interference with the ubiquitin/proteasome-mediated degradation, and changes in subcellular distribution.

1.5.3 NEDD8 conjugation of p53 via MDM2

Among the ubiquitin-like family, NEDD8 is most homologous to ubiquitin. NEDD8 like SUMO and ubiquitin, is transferred to substrates by E1 and E2 enzymes. Unlike the ubiquitin E1 enzyme, which is a single polypeptide, the NEDD8 E1 enzyme is a heterodimer composed of the amyloid precursor protein binding protein (APP-BP1) and Uba3 protein. The E2 conjugating enzyme for NEDD8 is the Ubc-12 E2-like protein [75 76]. Recently Xirodimas and co-workers [77] demonstrated that the MDM2 RING finger E3-ubiquitin ligase is NEDDylated and promotes conjugation of NEDD8 to p53. The critical Cys^{462} in the ring finger domain of the protein, which is required for the E3 ubiquitin ligase activity of MDM2, is also required for MDM2-dependent NEDDylation. The same authors indicate that three lysine residues at the C-terminus of p53 are required for MDM2-mediated NEDDylation, namely lys^{370}, lys^{372} and lys^{373}. Mutation of these three lysines resulted in an increased transcriptional activity compared to wild–type p53 in H1299 cells, suggesting that NEDDylation of p53 inhibits its function.

MDM2 can therefore be envisaged as a gatekeeper protein with independent regulation of ubiquitin and NEDD8 mediated conjugation of p53.

1.6 Molecular Chaperones

The finding that up to 30% of newly synthesised proteins never reach their native state (termed defective ribosomal products, DRiPs [78]) highlights the importance of the relationship between the three-dimentional structure of proteins and biological activity. Maintaining the three-dimensional, native structure is a delicate process that is under constant threat of unfolding as a consequence of chemical equilibrium and cellular stress [79]. Misfolded proteins have a tendency to form aggregates thus posing a major threat to cell function and viability due to non-specific protein:protein interactions. Organisms have therefore evolved systems that actively maintain and control protein structure, and involve both molecular chaperones and energy-dependent degradation [80]. Molecular chaperones are defined by their ability to bind non-native proteins. These specialized proteins have evolved to participate in the folding of newly translated and damaged polypeptides, in the transport of proteins across cellular membranes and in the assembly of protein complexes [81], [82], [83] . These folding events are regulated by interactions between chaperones and ancillary proteins, the co-chaperones, which in general assist in cycling unfolded substrate proteins on and off the active chaperone complex [84], [85]. Signalling proteins and apoptosis regulators are among the most important substrates of molecular chaperones [86], [87]. Another important feature of chaperones that has been recently discovered revolves around their active participation in protein degradation [88], [89], an activity that, once again, depends on the ability of chaperones to selectively associate with non-native proteins. The ability of molecular chaperones to direct the substrate to a folding pathway or to the degradation machinery (e.g. by the ubiquitin-proteasome system) has been termed 'The Protein Triage Hypothesis'[90]. In agreement with their essential functions, chaperones are ubiquitously

expressed in high abundance and are found in all cellular compartments of the eukaryotic cells (except for peroxisomes). Moreover, cells induce chaperone concentration as a response to diverse stresses, when proteins when proteins require protection and stabilization [ii]. It is, therefore, not surprise that many chaperones are heat shock proteins (Hsps). There are four families of cytoplasmic chaperones, namely, the Hsp70s, the Hsp90s, the small heat shock proteins and the chaperonins.

1.6.1 The Hsp70 family

Members of this family are highly conserved throughout the prokaryotic and eukaryotic phylogeny and are typically in the range of 70 kDa in size. The Hsp70 proteins bind to misfolded proteins during translation or after stress-mediated protein damage [91]. The Hsp70s contain three functional domains, namely an amino-terminal ATPase domain, a central peptide-binding cleft and a carboxyl terminus that seems to form a lid over the peptide-binding cleft [92], (Figure 1.12). Hsp70s recognize short segments of the protein substrate, which are composed of clusters of hydrophobic amino acids flanked by basic residues which are frequently found in exposed sequences of non-native proteins [93]. Hsp70 proteins apparently prevent protein aggregation and promote proper folding by shielding hydrophobic segments of the protein substrate which are recognized by the central peptide-binding (CPB) domain of Hsp70 proteins. An X-ray crystallographic approach of the CPB of a bacterial Hsp70 revealed a structure composed of two β-sheets that together with connecting loops form a cleft to accommodate extended peptides of about seven amino acids in length [94]. The adjacent C-terminal domain of Hsp70 folds back over the β-sandwich, suggesting that the domain may function as a lid in permitting entry and release of protein substrates [94].

ATP binding and hydrolysis by the amino-terminal ATPase domain of Hsp70 induce conformational changes of the carboxyl-terminus, which lead to lid opening and closure which ultimately, allows stable holding of the protein substrate [92]. Co-chaperones of the Hsp40 family stimulate ATP hydrolysis, thereby promoting substrate binding whereas the carboxyl terminus of Hsp70-interacting protein (CHIP) attenuates ATP hydrolysis thereby inhibiting substrate binding [95]. Also, nucleotide exchange on Hsp70 is under the control of co-chaperones Hip, which slows down nucleotide exchange [96] and Bcl-2-associated athanogene 1 (BAG-1), which assists substrate unloading from Hsp70 [97], [98].

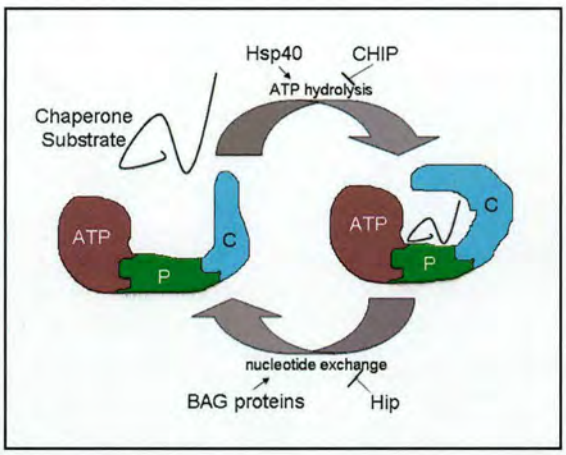

Figure 1.12 Schematic view of the Hsp70 chaperone cycle. ATP = ATPase domain, P = Peptide binding domain, C = carboxy-terminal domain

1.6.2 The Hsp90 family

The members of this family are typically in the 90 kDa range and exhibit several features in common with Hsp70 chaperones in that both possess ATPase activity and are regulated by cycling of ATP binding and hydrolysis, and both are further regulated by ancillary co-chaperones. In contrast to Hsp70, however, Hsp90 is not generally involved in the folding of nascent polypeptide chains, but plays a key role in the regulation of signal transduction networks. Hsp90 binds to substrates at a late stage in

the folding pathway, and aids the activation of the latter prior to ligand binding or associations with other factors. In fact, Hsp90 accepts non-native, but partially folded conformations from Hsp70 for further processing [79]. A chaperone-binding motif found in several Hsp70 and Hsp90 cofactors is characterized by a tandem arrangement of three degenerate 34 amino acid repeats (tetratricopeptide repeats, TPRs) [85]. The transfer of the substrate from Hsp70 to Hsp90 requires the Hsp70/Hsp90 organizing protein (Hop), which possesses multiple, non-overlapping TPR domains for Hsp70 and Hsp90 thereby acting as a coupling factor between the two chaperones during the regulation of signal transduction pathways [85], [99], [100]. In each domain, three tandem TPRs align with an adjacent α-helix to form a groove that accommodates conserved peptide motifs present at the C-terminus of Hsp70 and Hsp90 [101]. Similar to Hsp70, CHIP binds Hsp90 preventing the cooperation of the chaperone with other cofactors required for productive chaperone function [102]. Other interactors that regulate Hsp90 function include p23 and different cyclophillins [iii]. Since Hsp90 substrate proteins are involved in regulating cell proliferation and cell death, significant research is currently been undertaken to inhibit the Hsp90 chaperone function therapeutically.

1.6.3 Chaperonins

The chaperonins are defined by a barrel-shaped, double-ring structure [84], [92]. Members of this family include bacterial GroEL, mitochondrial and chloroplast Hsp60, and the Tri-CCT complex localized in the eukaryotic cytoplasm. A central cavity is formed in the ring-structure, where non-native proteins are contained via hydrophobic interactions. Conformational changes of the chaperonin subunits, induced through ATP hydrolysis, change the inner lining of the cavity from a hydrophobic to a hydrophilic

nature[103], [104], [105] , resulting in the release of the unfolded protein into the central cavity were folding proceeds in protected environment [106].

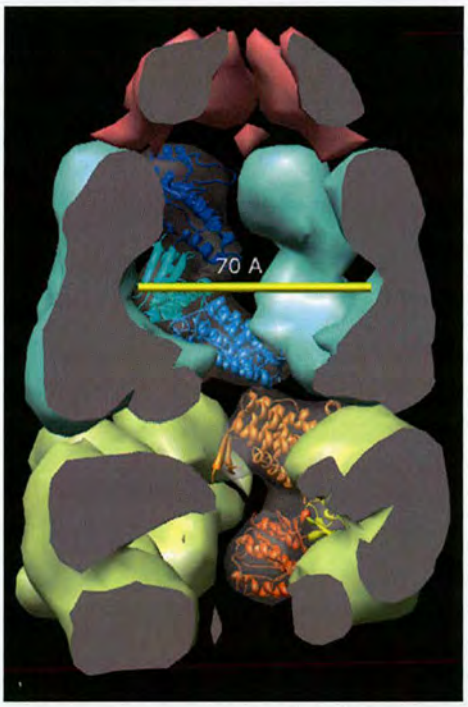

Figure 1.13[ix] Sliced chaperonin complex from Escherichia coli. Misfolded proteins are refolded inside the cavity formed by this 21 protein complex. The blue and yellow rings (GroEL) each consist of 7 copies of the same protein, while the red cap (GroES) is composed of 7 copies of a different protein. The two rings of GroEL exhibit different conformations

1.6.4 CHIP - a key factor in protein triage

Ballinger and co-workers initially identified CHIP by screening human TPR-containing proteins. The N-terminus of CHIP contains three TPRs which, together with an adjacent, highly charged α-helix, form an adaptor for Hsp70 or Hsp90 chaperones [95]. Furthermore, the C terminus of CHIP contains a U-box that confers E3 ligase activity. Therefore, the modular structure of CHIP may thus enable the cofactor to link molecular chaperones directly to the degradation machinery. In support of this concept, CHIP was

[ix] Figure 1.13 http://www.rbvi.ucsf.edu/chimera/ImageGallery/entries/1aon/1aon.html

recently shown to promote the degradation of chaperone substrates by the ubiquitin/proteasome system. Among these substrates are glucocorticoid hormone receptor (GR) [102], cystic fibrosis transmembrane conductance regulator (CFTR) [107] and p53 [108], [109].

Since CHIP associates with molecular chaperones, the latter can therefore be seen as an integral part of the ubiquitin ligase complex. Through its ability to recognize non-native proteins and specific client proteins, the chaperone apparently selects substrates for CHIP-mediated ubiquitination and degradation [79].

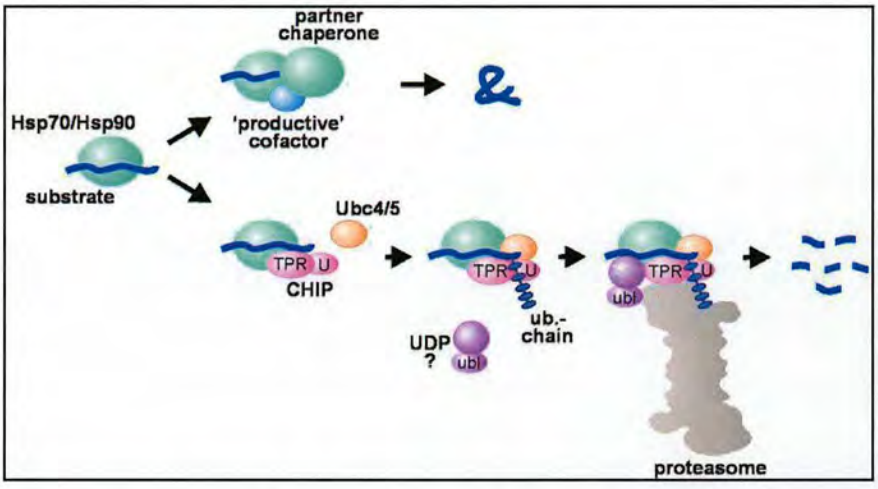

Figure 1.14[x] Schematic view of protein triage. Molecular chaperones Hsp70/Hsp90 interact with either ancillary co-chaperones for the folding of the substrate or CHIP for degradation of mislfolded proteins via the 26S proteasome

[x] Höhfeld J, Cyr DM, Patterson C. *From the cradle to the grave: molecular chaperones that may choose between folding and degradation.* EMBO Rep. 2001 Oct;**2**(10):885-90.

1.7 Mass Spectrometry

Mass spectrometry (MS) is an analytical technique used to measure the mass of individual molecules and atoms expressed as their mass-charge (m/z) ratio. All mass spectrometers consist of three basic parts: an ion source, a mass analyzer, and a detector system. The first essential step in MS analysis, which occurs in the ion source, is the conversion of the neutral analyte molecules into gas-phase ionic species, for downstream manipulation and detection. Furthermore, the excess energy during the ionization event leads to fragmentation of small molecules which provides additional structural information. The mass analyzer separates these molecular ions and their charged fragments according to their m/z ratio. Finally, the ion current due to these mass-separated ions is detected by a suitable detector and displayed in the form of a mass spectrum. To prevent collisions and interactions between different ion species, each of these steps is carried out under high vacuum. The following sections provide a brief outline of the soft ionization sources and mass analyzers used in this study.

1.7.1 Ionization methods

1.7.1.1 Matrix-assisted laser desorption/ionization (MALDI)

In MALDI, the sample is mixed with a suitable matrix, and bombarded with a high energy particle beam to produce, just above the point of impact, a high concentration of the gas-phase neutral and ionic species. By depositing a large amount of energy into the analyte molecule on a timescale that is fast compared with the vibrational time period, vaporization generally occurs before thermal decomposition

begins. In early mass spectrometry lasers were applied directly to the sample. The infrared laser (e.g. ND/YAG (neodynium/yttrium aluminum garnet; 1.06 μm), pulsed CO_2 laser (10.6 μm) and UV lasers (frequency-quadrupled Nd/YAG laser that emits light at 266 nm) were used. In this direct mode of laser application, termed laser/desorption ionization (LDI), the extent of energy transfer often leads to excessive thermal decomposition of the sample. Furthermore, not all compounds absorb radiation at the laser wavelength. Consequentially, the LDI mode is applicable to a limited number of compounds, usually those with a molecular mass < 1000 Da. Karas and Hikkenkamp, and Tanaka and co-workers, reported the development of MALDI in 1988 [110], , which revolutionized the study of large biomolecules by mass spectrometry. In principle, the sample is mixed with surplus matrix material that absorbs at the wavelength of the laser radiation which occurs in short pulses 10-20 ns duration and approximately 10^6 W/cm^2 irradiance power [iv]. Since the matrix absorbs at the wavelength of the laser irradiation, a large amount of energy is absorbed efficiently by the matrix, and subsequently transferred to the sample in a controlled manner, hence resulting in the co-desorption of sample and matrix. In addition to absorbing the laser energy via electronic or vibrational excitation, a useful matrix should provide a number of different functions. Firstly, it should disperse the analyte molecules by dilution within the preparation, thus minimizing analyte aggregation. Secondly, disintegration of the condensed phase has to take place with concomitant analyte ionization (via gas-phase proton-transfer reactions) and without excessive destructive heating of the embedded analyte molecules [111]. Three different models have been proposed to explain desorption of the matrix-sample from the crystal surface: (1) quasithermal evaporation as a result of increased molecular motion, (2) expulsion of upper lattice layers, and (3)

an increase in the hydrodynamic pressure due to rapidly expanding molecules in the crystal lattice [v]. The widely accepted view for analyte molecule ionization following desorption is that following their desorption as neutrals, the sample molecules are ionized by acid-base proton transfer reactions with the protonated matrix ions in a dense phase just above the surface of the matrix [111]. The MALDI mass spectra of proteins and peptides typically contain signals due to singly protonated target molecules and their oligomeric ions (e.g $[M+H]^+$, $[2M+H]^+$). In addition, Na^+ and K^+ adducts are also a common feature of MALDI spectra of peptides or proteins.

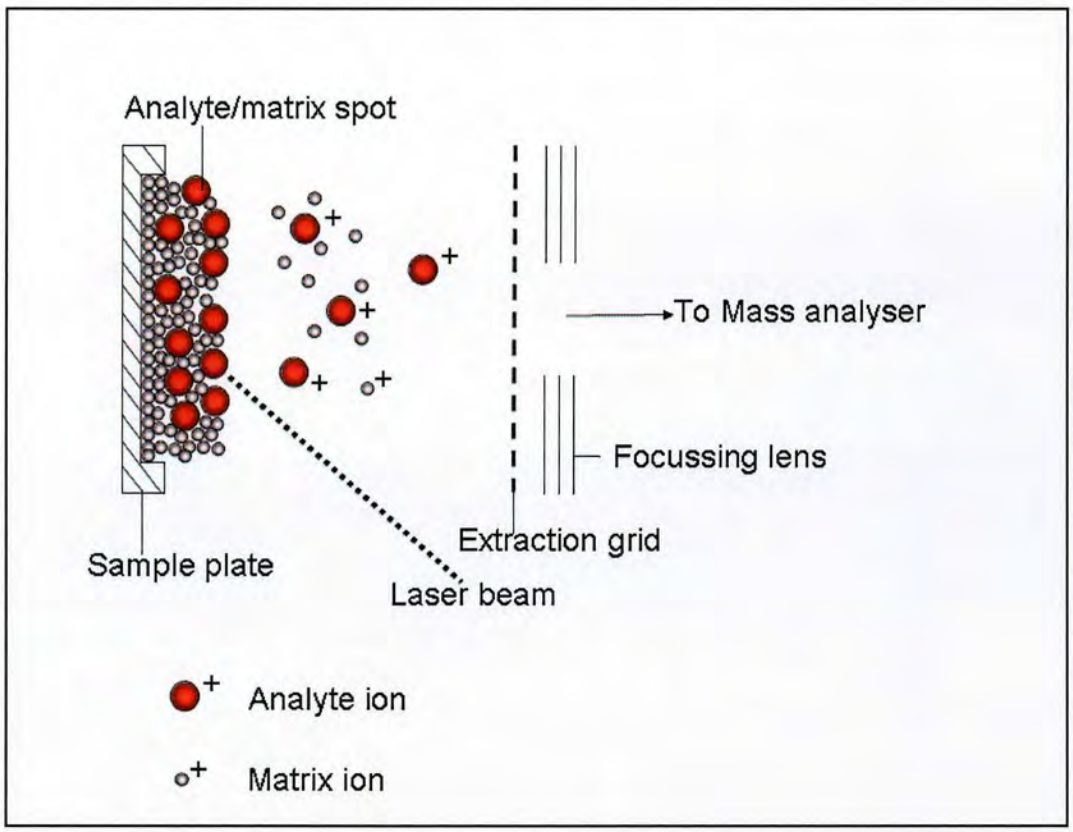

Figure 1.15 Schematic diagram of MALDI

1.7.1.2 Electrospray Ionization

Electrospray Ionization (ESI) is a type of atmospheric pressure ionization (API) which is a means of analysing non-volatile samples without first converting them to the gaseous phase [vi]. As seen in the schematic diagram of a typical ESI source, the capillary tube continuously delivers organic solvent (mobile phase from HPLC) containing the dissolved sample. A potential difference of 3-4 kV between the tip of the capillary and the walls of the surrounding atmospheric pressure region produces an electrostatic field sufficiently strong to disperse the emerging solution in a fine mist of charged droplets. The ions are transported from the atmospheric pressure region to the high-vacuum region of the mass-analyser via a low-pressure transport region. Prior to entering the mass analyzer, all sample ions are stripped off the solvent molecules. Hence, ESI incorporates three processes, namely, droplet formation, droplet shrinkage, and gaseous ion formation. The electrostatic force exerted on the eluate from the capillary causes it to emerge from the tip in the shape of a "Taylor cone" [112]. A thin liquid extends from this cone which breaks up in a fine mist. There are two views concerning the formation of gas-phase ions from the charged droplets, namely, the charge residue model (CRM) and the desorption model (IDM). In CRM, as the droplets shrink in size due to solvent evaporation, the charge density on their surface increases until it reaches the Rayleigh instability limit. Once this point is reached, repulsive Coulombic forces exceed the droplet surface tension and cause droplets to break into smaller and highly charged droplets. This process is repeated until the droplet contains only one solute molecule and as the remaining solvent evaporates, the analyte is dispersed into ambient gas retaining some of the charge on the droplets [113]. In IDM the sequence of events related to solvent evaporation and droplet shrinkage is repeated, but

instead of proceeding to droplets so small to contain one solute molecule, at an intermediate droplet size the electric field due to the surface charge density is sufficiently high to overcome the droplet cohesive forces leading to direct ion desorption [vii].

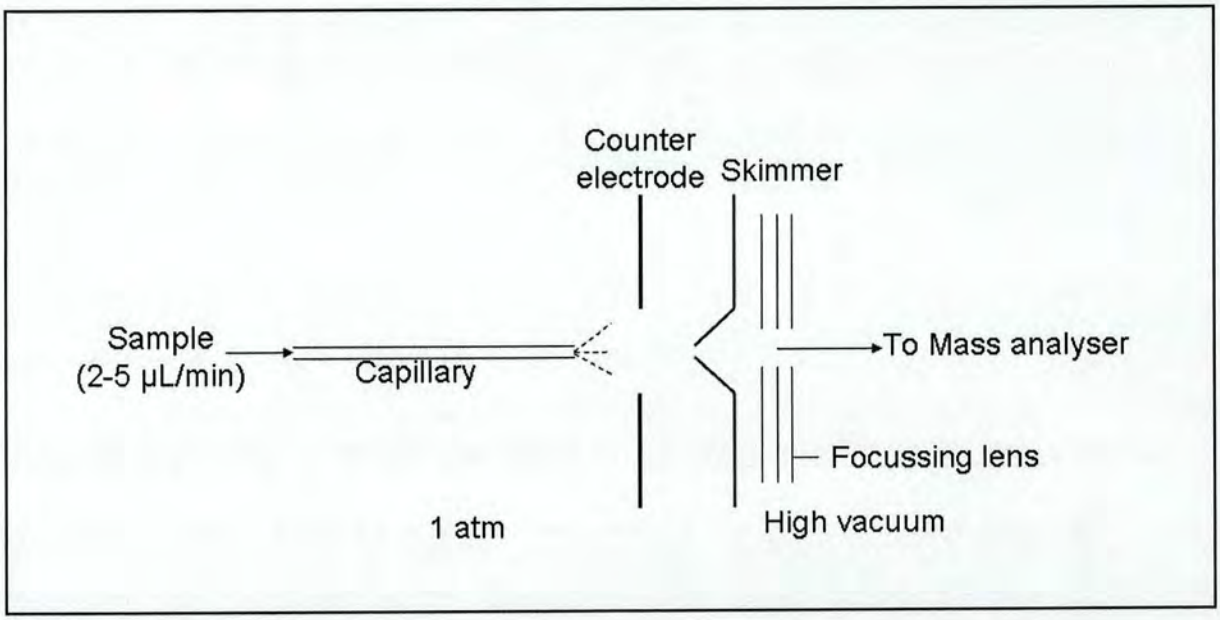

Figure 1.16 Schematic representation of an electrospray ion source

1.7.2 Mass analyzers

1.7.2.1 Time of flight mass spectrometer

The time of flight (TOF) mass spectrometer is one of the simplest mass-analyzing devices and describes the method used to measure the time it takes for a particle, object of stream to reach a detector while traveling over a known distance. In TOFMS ions are separated on the basis of their velocity differences [114]. The charged ions generated at the ion source are dispersed in time by allowing it to drift in a field-free region of a long flight tube (Figure). As seen in the equation below, after

acceleration to a constant kinetic energy (equal to zV, where z is the charge on the ion and V the accelerating potential), ions travel at velocities, v, that are an inverse function of the square root of their m/z values:

$$v = \left(\frac{2zV}{m}\right)^{1/2} \quad \text{..... Equation 1.1}$$

Lighter ions travel faster and reach the detector placed at the end of the flight tube earlier than do the heavier ones. Therefore, mass analysis of ions that enter the flight tube can be accomplished by determining their time of arrival given by:

$$t = \frac{L}{v} = L\left(\frac{m}{2zV}\right)^{1/2} \quad \text{.....Equation 1.2}$$

In order to convert the time spectrum into a mass spectrum, the instrument is mass calibrated by measuring the flight times of two different known mass ions [viii].

Recent success to TOFMS can be attributed to its coupling to the MALDI ion source. In the past, however, poor mass resolution was one of the major limitations of TOFMS. The determining factor that restricted resolution in early TOFMS instruments was the kinetic lack of homogeneity within the ion beam resulting in higher-initial-energy ions arriving at the detector sooner than do the same-mass lower initial energy ions. Resolution can be improved in MALDI-TOF by allowing the initial burst of ions and neutrals produced by the laser pulse to equilibrate and dissipate before the ions are accelerated into the flight tube. This is referred to as "time-lag focusing" for ionization of a gas and "delayed extraction" for desorption ionization [115]. The kinetic energy distribution in the direction of ion flight can be corrected by using a reflectron. This

device is an electrostatic mirror that consists of a series of electrical lenses, each with progressively increasing repelling potential, and reflects the ion beam back to the detector. The more energetic ions travel deeper into the reflectron, and take a slightly longer path to the detector. Less energetic ions of the same charge and mass travel a shorter distance into the reflectron and take a shorter path to the detector. The detector is placed at the focal point where ions of different energies but same mass focused by the reflectron strike the detector at the same time [116].

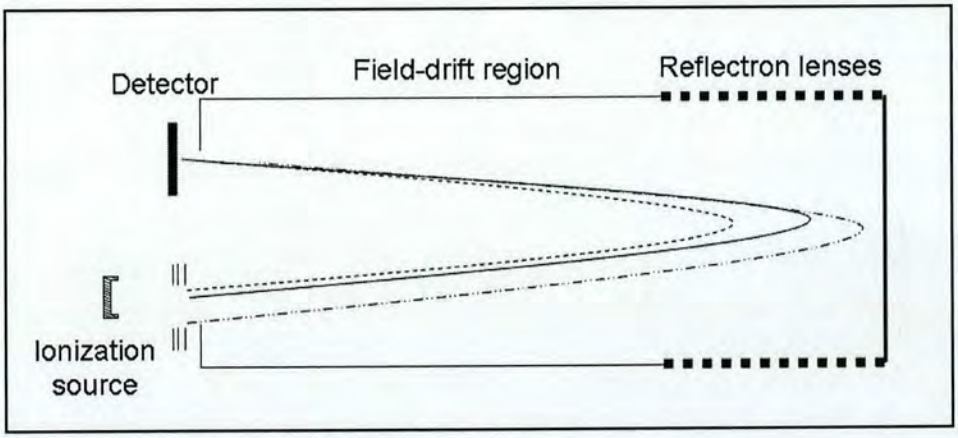

Figure 1.17 Schematic representation of a reflectron time-of-flight mass spectrometer

1.7.2.2 Quadrupole ion trap mass spectrometer

Quadrupole ion trap (QIT) mass spectrometers are made up of three hyperbolic electrodes, consisting of a ring central electrode and two end-cap electrodes each with a hyperbolic cross-section, which form the core of the instrument. One of the end-cap electrodes has a small opening through which a gated electron beam can enter the trap for *in-situ* ionization of the analyte, while the other end-cap electrode has several perforations through which ions escape for external detection. QITMSs are dynamic mass analyzers that use an oscillating electric potential applied to the ring electrode,

called the "fundamental rf", to focus ions to the centre of the trap. This is accomplished by creating a parabolic potential, shaped like a saddle [117], inside the trapping volume. Ultimately a population of trapped ions is therefore observed to occupy only the space near the centre of the trap due to the focusing effect of the electric fields. The trapped ions precess in the trapping field in the trapping field with a frequency that is dependent on their m/z ratio. By increasing the magnitude of the rf voltage and the frequency of the rf signal, ions of higher m/z become sequentially unstable in the axial direction and ultimately exit the trap through perforations in the end-cap electrodes and are detected by a detector.

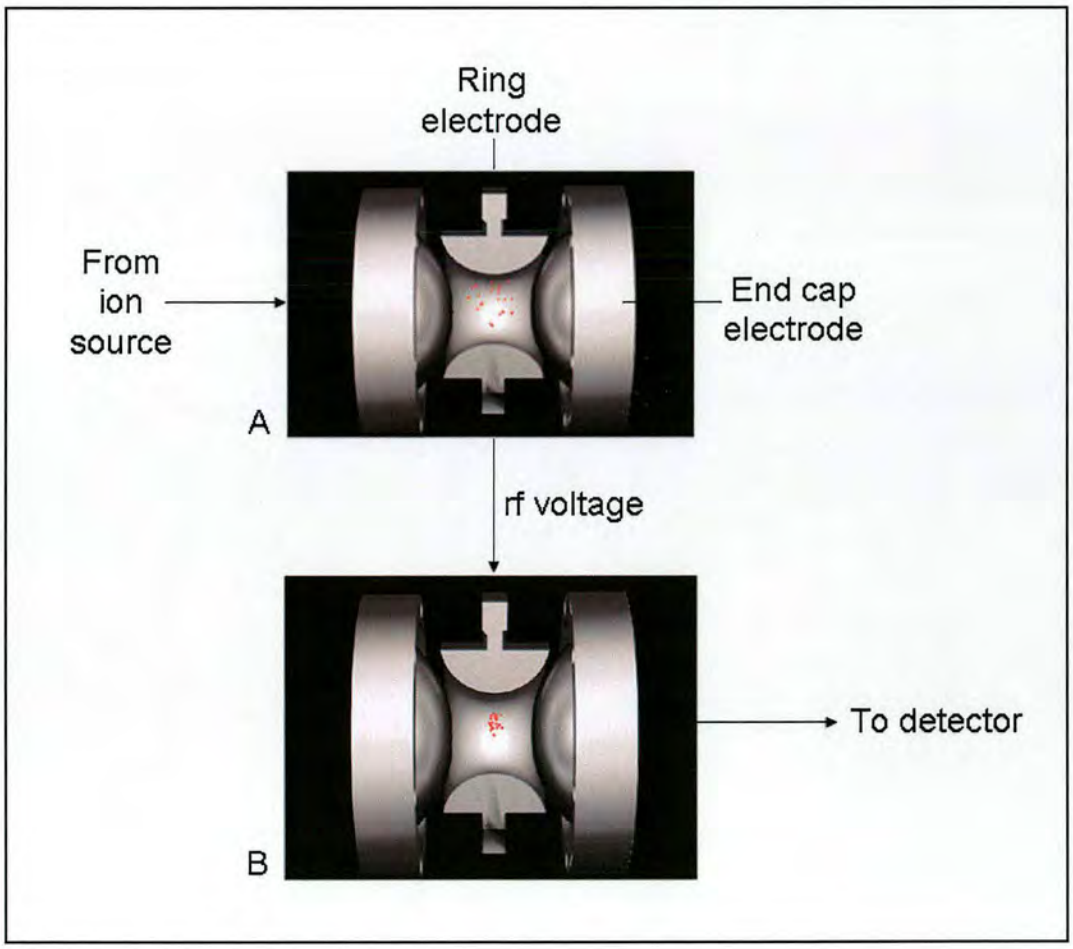

Figure 1.18 Quadrupole mass analyzer. Ionized species from the ion source (**A**) are trapped in a small space at the centre of the core (**B**) following application of an rf voltage.

1.7.3 Tandem mass spectrometry

The IUPAC Compendium of Chemical Terminology defines a tandem mass spectrometer as:

"An arrangement in which ions are subjected to two or more sequential stages of analysis (which may be separated spatially or temporally) according to the quotient mass/charge. A hybrid mass spectometer is an instrument which combines analysers of different types, e.g. magnetic plus electric sector combined with quadrupole. The study of ions involving two stages of mass analysis has been termed mass spectrometry/mass spectrometry."

- IUPAC Compendium of Chemical Terminology 1991, *63*, 1546

Tandem mass spectrometry involves mass-selection, fragmentation, and mass analysis and involves two stages of mass analysis. The first stage (MS^1) performs the mass selection of a specified ion from a mixture of ions that are produced in the ion source. This mass-selected ion undergoes fragmentation in the intermediate region, usually via collisions with neutral gas atoms [118]. The mass selected ion is termed the "precursor ion", and the ionic fragments are called "product ions". The second stage (MS^2) of MS/MS is used to mass analyze the product ions that are formed in the intermediate step.

For reasons of brevity the tandem mass spectrometer used in this study shall be discussed, namely the Tandem Ion-Trap mass spectrometer (QITMS). The QITMS acts as a tandem-in-time mass spectrometer. Hence, all the steps of MS/MS are performed within the same space, but with a temporal sequence. Following ion trapping in the MS^1 stage, all ions except the precursor are ejected out of the trap with the resonance ejection procedure [119]. The precursor ion is then subjected to an excitation pulse to facilitate collisions with helium bath gas, a process termed collision induced decay (CID). The

MS^2 step involves analysis of the fragmented ions as described in Section 1.7.6. CID is a two-step process, which involves collision activation and unimolecular dissociation. In the former, the fast moving precursor ions collide with atoms of an inert gas, and are excited to higher states [120]. During this excitation process, a part of the initial translational energy of the incident ions is converted into the excitation energy to cause its fragmentation.

1.7.4 Protein identification by gel electrophoresis-mass spectrometry and database search

With the development of MALDI and ESI, mass spectrometry has become a widely used technique in the analysis of gel separated proteins [121]. Following gel separation the protein band of interest is excised, reduced, carboxymethylated and digested within the gel by a proteolytic enzyme. A variety of amino acid-specific enzymes are available that will yield reproducible peptide maps of a protein. Trypsin was used in this study because of its excellent properties as a protease. Trypsin produces peptides ideal for mass spectrometry analysis and since trypsin cleaves an amide on the C-terminal side of lysine or arginine residue, the tryptic peptides that result contain a basic amino acid at the C-terminus. This is particularly useful for the ESI process and for subsequent sequencing by tandem MS.

Various databases exist for protein, DNA and expressed sequence tags (ESTs). In the single MS mode the peptide-mass fingerprints, which are generated following a digestion step with trypsin, are matched with theoretical peptide fragment mass values of each protein in the database. The theoretical mass values are created for the protease that was used specifically in the digestion step by applying the protease-specific

fragmentation rules to all of the protein sequences in the database. In MALDIMS, from a list of experimentally derived $[M+H]^+$ values of peptides, the output of the search gives a ranked list of most likely candidates. The database that produces the best score is assumed to be the sequence of the protein. In the MS/MS mode identification of the protein occurs following correlation of the fragmentation patterns with the amino acid sequences in the protein databases [122]. Following digestion of the protein, the individual peptides are fragmented in MS/MS mode (e.g. CID as used in this study). The observed pattern of the fragment ions of individual peptides are then compared with patterns of fragment ions that are calculated from the database sequences .

1.7.5 CID fragmentation of peptides

A notation has been developed for indicating peptide fragments that arise from an MS/MS spectrum [123]. Peptide fragment ions are indicated by a, b, or c if the charge is retained on the N-terminus and by x, y or z if the charge is retained on the C-terminus. The subscript indicates the number of amino acid residues in the fragment. Although peptide backbone cleavage is the most useful for sequencing and peptide identification other fragment ions may be observed under certain conditions including side chain loss ions d, v, w and immonium ions.

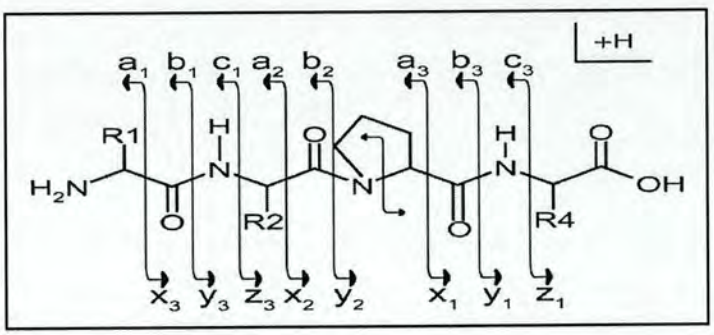

Figure 1.19 Nomenclature used for the fragmentation pattern of a peptide in MS^2 mode

1.8 Objectives of this study

The DNA damage checkpoint network, as discussed in the above literature review, depends on promotional and inhibitory, synergistic and antagonistic molecular interactions that are investigated by an enormous experimental effort in numerous laboratories worldwide. To place this checkpoint network in context of tumorigenesis, it is useful to use Waddington's (1957) "epigenetic landscape" (Figure 1.20). Waddington was a prolific biologist who was interested in reconciling Lamarck's ideas on the inheritance of acquired characters with modern biology. The epigenetic landscape is a clever metaphor for the hierarchical nature of embryogenesis. The pegs at the bottom of the figure represent genes, and the guy ropes pulling on the landscape surface represent the products of genes. The different tensions produced by each peg on the ropes and the surface of the landscape represent (and are directly proportional to) the phenotypes that develop during the life of an organism. So the "deeper" a groove is on the surface, the less variation there is on a given phenotype (i.e. the stronger the phenotype). It is clear to see in this fashion how every single developmental feature depends on the production of a myriad of genes. Intra- and extra-cellular pathways may therefore be envisaged to be largely redundant, analogous to the overlapping neural networks of the brain rather than to traffic grids of intersecting streets and interacting vehicles. Understanding the dynamic, non-linear interactions of individual components in these pathways is intrinsic to understanding the maintenance of genomic stability or conversely, when things go haywire, the progression into tumorigenesis. This requires the integration of genomic, proteomic, and bioinformatics approaches. Proteomics is a sphere of research that comprises the identities, quantities, structures, and biochemical and cellular functions of all proteins in an organism, organ, or organelle, and how these properties vary in space,

time, or physiological state. Interactomics, is a recent, further elaboration on proteomics, and comprises the complex, dynamic and non-linear interactions between individual proteins, which ultimately influences the biochemistry of the cell.

The following treatise is, primarily, an investigation on the degradation interactome of wild-type and mutant p53, which revolves around interactions with the chaperone-assisted, ubiquitin-proteasome degradation machinery. The main objective of this study was therefore to investigate key differences in wild-type and mutant p53 interactomes by revealing novel key interactors through the use of standard biochemical techniques and mass spectrometry.

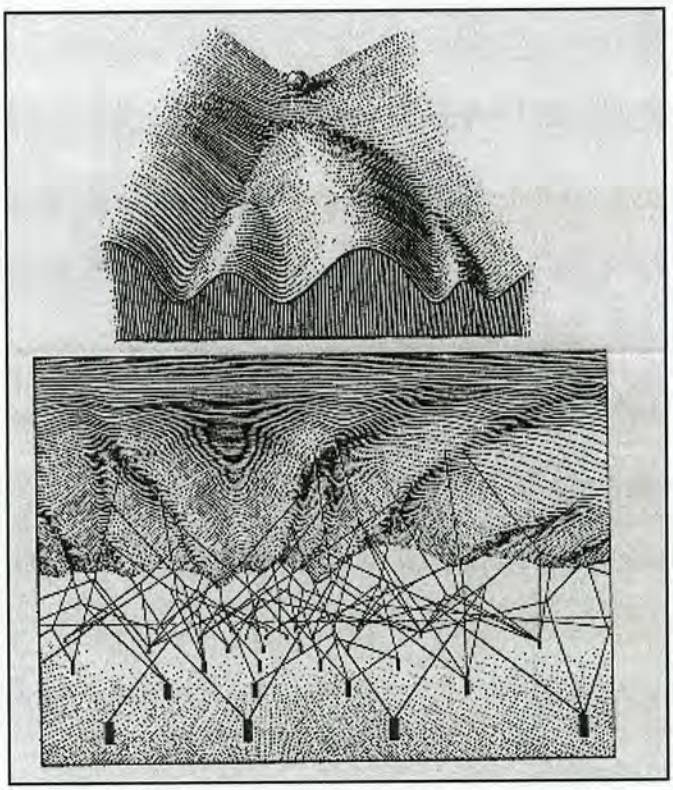

Figure 1.20 Waddington's "Epigenetic Landscape" (Waddington, 1957): A. "The path followed by the ball, as it rolls down towards the spectator, corresponds to the developmental history of a particular [organ]. There is first an alternative, towards the right or the left. Along the former path, a second alternative is offered; along the path to the left, the main channel continues leftwards, but there is an alternative path which, however, can only be reached over a threshold." B. Interacting network of signal transduction pathways. "The pegs in the ground represent genes; the strings leading from them the [pathways initiated by gene expression]. The modeling of the epigenetic landscape, which slopes down from above one's head towards the distance, is controlled by the pull of these numerous guy-ropes [pathways] which are ultimately anchored to the genes."

2.0 Materials and Methods

2.1 Reagents and Materials

All reagents were supplied by Sigma unless otherwise stated. p3XFLAG-*myc*-CMV™-26 plasmid was supplied by Sigma. One-STrEP-tag vector pEXPR-IBA 105 was supplied by IBA Biotagnology.

DNA Mini and Maxi Prep, PCR purification kits were supplied by Qiagen. Restriction enzymes were supplied by New England Biolabs. Oligonucleotides were synthesised by Sigma-Genosys. QuikChange Site-Directed mutagenesis kit was supplied by Stratagene. Foetal bovine serum (FBS), Dulbecco's modified eagle's medium (DMEM), RPMI-1640 and trypsin-EDTA solution were supplied by (Gibco-BRL). Lipofectamine 2000 was supplied by Invitrogen. Handee Mini-Spin Columns were supplied by Pierce. Protein G Sepharose 4 Fast Flow and enhanced chemiluminescence (ECL) hyperfilm were supplied by Amersham.

2.2 Molecular biology methods

2.2.1 Growing Bacterial Cultures

Luria-Bertani (LB) broth

1% (w/v) Tryptone
0.5 % (w/v) Yeast extract
1% (w/v) NaCl
Sterilized by autoclaving at 121°C for 20 minutes

2.2.2 Agar bacterial culture dishes and broths

8 g of LB Agar mix (Fisher Bioreagents) were diluted in 200 mL of dH_2O and sterilized by autoclaving at 121 °C for 20 minutes. The LB agar mix consists of:

1 % (w/v) Tryptone

0.5 % (w/v) Yeast extract

1 % (w/v) NaCl

1.5% (w/v) Agar, granulated

LB agar was liquefied by heating in a microwave oven and allowed to cool until handwarm. Ampicillin was added to a final concentration of 100 μg/mL and the agar poured into 90 mm Petri dishes (sterilin) and left to cool. The culture plates were stored at 4 °C for no more than a month. Before use the plates were dried at 37 °C for 1 h.

5-10 mL LB broth containing 100 μg/mL ampicillin selective antibiotic (Sigma) was inoculated with a colony of bacteria from a stock plate and incubated for 8 h at 37 °C (225 rpm). This starter culture was then transferred to 250 mL of LB broth and incubated under the same conditions overnight in 2 L culture flasks.

2.2.3 Glycerol stocks

Glycerol stocks of bacterial cells were prepared by adding 0.15 mL of sterile glycerol to 0.85 mL of liquid bacterial culture in a cryotube (Nunc) and snap frozen. The cells were stored at -70 °C.

2.2.4 Preparation of heat shock competent cells

Transforming Buffer 1	**Transforming Buffer 2**
30 mM CH_3COOK	10 mM MOPS
100 mM RbCl	75 mM $CaCl_2$
10 mM $CaCl_2$	10 mM $RbCl_2$
50 mM $MnCl_2$	15 % (v/v) Glycerol
15 %(v/v) Glycerol	Adjusted to pH 6.8 with NaOH
pH adjusted to 5.8 with dilute acetic acid	

2-3 mL of LB broth were inoculated with DH5α competent cells from a glycerol stock and grown overnight with shaking (225 rpm) at 37 °C. 250 µL of the overnight stock was added to 50 mL LB broth in a 250 mL culture flask and incubated at 37°C with shaking (225rpm) until the OD_{600nm} was approximately 0.4 (log phase). The cells were pelleted by centrifugation (4000 rpm, 15 min, 4 °C) and resuspended gently in 16 mL of ice cold Transforming buffer 1. The cells were incubated for 10 minutes on ice. The cells were pelleted by centrifugation (4000 rpm, 15 min, 4 °C) and resuspended gently in 2 mL of ice cold Transforming buffer 2. The cells were incubated once again for 10 minutes on ice and 200 µL aliquots were added to pre-chilled microcentrifuge tubes. The aliquots were snap frozen and stored at -70 °C.

2.2.5 KCM transformation

An aliquot of DH5-α competent cells was thawed on ice and 100 µL of the thawed cells was incubated on ice for 20 minutes with 200 ng of DNA and 100 µL of KCM (100 mM KCl, 30 mM $CaCl_2$ and 50 mM $MgCl_2$). The cells were then incubated at room temperature for 10 minutes. 400 µL of LB was added to the competent cell/DNA mixture and incubated for 1 hour at 37°C to allow growth of transformed

bacteria. Cells were then plated onto LB agar plates with ampicillin and incubated at 37°C overnight for colony formation.

2.2.6 Heat shock transformation

An aliquot of DH5-α competent cells was thawed on ice and 100 μL of the thawed cells was incubated on ice for 20 minutes with 200 ng of DNA. The cells were subjected to heat shock by incubating at 42°C for 45 seconds and quickly returned to ice for 2-5 minutes. 500 μL of LB was added to the competent cell/DNA mixture and incubated for 1 hour at 37°C with agitation to allow growth of transformed bacteria. The cells were then spun at 2000 x g. The pellet was resuspended in 250 μL of LB. 50 and 100 μL of the cell suspension was plated onto LB agar plates with the appropriate selection antibiotic for the plasmid transformed. Plates were incubated overnight at 37°C for colony formation.

2.2.7 DNA amplification and purification

Single colonies were selected and allowed to grow in 5 mL LB with the selection antibiotic at 37°C for 8 hours. The culture was used directly in a mini-prep DNA purification (Qiagen) and carried out according to manufacturer's instructions. For maxi-prep, the culture was used as pre-culture and added to 200 mL of LB with ampicillin and allowed to grow overnight at 37°C before carrying out the protocol according to the manufacturer's protocol (Qiagen).

2.2.8 Quantitation of DNA by UV spectrophotometry

1-5 µL of DNA was diluted to 100 µL in water. The absorbance of the samples was measured by a UV Powerwave XS 96 well plate reader (Bio-tek) reader at 260 nm. The amount of DNA was determined by the following formula:

$$DNA\ concentration\ (\mu g / \mu L) = \frac{Absorbance\ at\ 260\ nm \times Dilution\ factor \times 50}{1000}$$

2.2.9 Agarose gel electrophoresis

DNA loading buffer

40% v/v glycerol

50 mM EDTA

0.1 % w/v bromophenol blue

DNA samples were mixed with DNA loading buffer and loaded onto 0.8% agarose ethidium bromide gels. As a size reference, a 1 Kb DNA ladder (Invitrogen) was loaded next to the DNA samples. Electrophoresis was performed at 80 V for 1 hour before analysing under a UV transilluminator.

2.3 DNA Plasmids

2.3.1 Primer Design

Primers were designed to achieve a melting temperature (T_m) of 55-70°C using the following formula[xi]:

$$T_M = \{81.5 + 0.41(\%\ GC\ content)\} - 16.6 - (672/N)$$

were N is the number total of bases in the primer

HPLC purified oligonucleotide primers were purchased from Sigma/Genosys and were reconstituted in nuclease-free dH_2O.

Table 2.1 Primers designed for cloning into the respective vectors.

Gene	Vector	Primer	Primer melting temperature (°C)
CHK2	p3XFLAG-myc-CMV™-26	**Upstream**: HIND III 5' – *GAT* GAC A|AG CTT GGA TCT GGA ATG TCT CGG GAG TCG GAT GTT – 3'	70
CHK2	p3XFLAG-myc-CMV™-26	**Downstream**: Xba I 5' – CTC CGC T|CT AGA TCC CAC AGC AGC ACA CAC AGC –3'	70
CHK2	pEXPR-IBA 105	**Upstream**: ECO-RI 5'-G ATA ATC GCA G|AA TTC G TCT CGG GAG TCG GAT GTT G – 3'	67

[xi] Sambrook, J., Fritsch, E.F., and Maniatis, T., in Molecular Cloning: A Laboratory Manual. Cold Spring Harbor Laboratory Press, NY, Vol. 1, 2, 3 (1989).

CHK2	pEXPR-IBA 105	**Downstream**: HIND III 5'- G AGC AGT GAC A|AG CTT TCA CAA CAC AGC AGC ACA C – 3'	67
P53	pEXPR-IBA 105	**Upstream**: ECO-RI 5'-G ATA TAT GTA G |AA TTC G GAG GAG CCG CAG TCA GAT CC -3'	67
P53	pEXPR-IBA 105	**Downstream**: HIND III 5'- G ATA AGT GAC A|AG CTT TCA GTC TGA GTC AGG CCC TTC - 3'	67
Rps3	pEXPR-IBA 105	**Upstream**: ECO-RI 5'-G AGT GAC GCA G |AA TTC G GCA GTG CAA ATA TCC AAG AAG	67
Rps3	pEXPR-IBA 105	**Downstream**: HIND III 5'- G AGC AGT GAC A|AG CTT TTA TGC TGT GGG GAC TGG 3'	67

2.3.2 Polymerase Chain Reaction (PCR)

Reaction mixtures were set up as in thin-wall PCR tubes as following:

dH_2O	40.6 µL
10x cloned Pfu reaction buffer (Stratagene)	5.0 µL
dNTPs (25 mM each dNTP)	0.4 µL
DNA template (100 ng/µL)	1.0 µL
Upstream primer (100 ng/µL)	1.0 µL
Downstream primer (100 ng/µL)	1.0 µL
PfuTurbo® DNA polymerase (Stratagene) (2.5 U/µl)	1.0 µL

Table 2.2 PCR cycling conditions.

Segment	Number of Cycles	Temperature	Duration
1	1	95°C	2 mins
2	30	95°C Primer T_m - 5°C 72°C	30 sec 30 sec 1.5 mins
3	1	72°C	10 mins
4	1	4°C	forever

2.3.3 Restriction endonuclease digestion

Double restriction endonuclease digestions were set up by adding 1 µL of each enzyme (NEB) to c.a 1 µg of DNA in a final volume of 50 µL of 1 x NEB buffer. The reaction mixture was incubated for 1 hour at 37 °C. The digests were subsequently run on a 0.8 % agarose ethidium bromide gels. The products were excised with a scalpel and purified with a QIAquick gel extraction kit (Qiagen).

2.3.4 Ligation

Three ligation reactions were set up using molar ratios of 1:1, 1:3, or 3:1 of vector:insert DNA in a final volume of 10 µL of T4 DNA ligase buffer and 1 Weiss units of T4 DNA ligase (Promega). The reactions were incubated overnight at 4 °C. 3 µL of reaction mixture was used to transform DH5α by heat shock (see Section 2.2.6)

2.3.4.1 CHK2 in p3XFLAG-myc-CMV™-26

p3XFLAG-*myc*-CMV™-26-CHK2 was subcloned from a pENTR21 (Invitrogen) vector encoding the full-length human CHK2 in a HIND III and Xba I digested p3XFLAG-*myc*-CMV™-26 vector (Sigma).

2.3.4.2 CHK2 in pEXPR-IBA 105

pEXPR-IBA 105-CHK2 (wild-type and mutants) were subcloned from the p3XFLAG-*myc*-CMV™-26-CHK2 vector in an Eco RI and Hind III digested pEXPR-IBA 105 vector (IBA Biotagnology).

2.3.4.3 p53 in pEXPR-IBA 105

pEXPR-IBA 105-p53 (wild-type and mutants) were subcloned from the pCDNA 3.1 vector encoding full-length human p53 in an Eco RI and Hind III digested pEXPR-IBA 105 vector (IBA Biotagnology).

2.3.4.4 rps3 in pEXPR-IBA 105

pEXPR-IBA 105-rps3 was subcloned from the pCMV6- XL5 vector encoding full-length human rps3 (Origene) in a Eco RI and Hind III digested pEXPR-IBA 105 vector (IBA Biotagnology).

2.3.5 Site directed mutagenesis

QuickChange™ Site-Directed Mutagenesis Kit (Stratagene) was used to create CHK2 mutants. Primers were designed to achieve a melting temperature (T_m) of 55-70°C.

HPLC purified oligonucleotides were purchased from Sigma/Genosys and were reconstituted in nuclease-free dH_2O.

UPSTREAM PRIMER FOR $CHK2^{R145W}$

5' –GC AAG AAA CAC TTT **TGG** ATT TTC AGG GAA GTG GG – 3'

DOWNSTREAM PRIMER FOR R145W

5' – CC CAC TTC CCT GAA AAT **CCA** AAA GTG TTT CTT GC– 3'

%GC - 44

N - 34

T_M - 63°C

UPSTREAM PRIMER FOR $CHK2^{I157T}$

5' – GGT CCT AAA AAC TCT TAC **ACA** GCA TAC ATA GAA GAT CAC – 3'

DOWNSTREAM PRIMER FOR I157T

5' –GTG ATC TTC TAT GTA TGC **TGT** GTA AGA GTT TTT AGG ACC – 3'

%GC - 38

N - 39

T_M - 63°C

UPSTREAM PRIMER FOR $CHK2_{INSA1368}$

5'-CTGGGCAGAAGTCTC**A**AGAGAAAGCTCTGGACC-3'

DOWNSTREAM PRIMER FOR INSA1368

5'-GGTCCAGAGCTTTCTCT**T**GAGACTTCTGCCCAG-3'

%GC - 57

N - 33

T_M - 68°C

UPSTREAM PRIMER FOR $CHK2_{delC1100}$

5' – GTC TTA TAA AGA TTA TGA TTT TGG GCA CTC C – 3'

DOWNSTREAM PRIMER FOR C1100del

5' – G GAG TGC CCA AAA TCA TAA TCT TTA TAA GAC – 5'

%GC - 35

N - 31

T_M - 58°C

2.3.6 DNA sequencing

Automated sequencing was carried out by the DNA analysis facility within the Wellcome trust clinical research facility at the Western General Hospital.

2.4 Protein Purification Procedures

2.4.1 Purification of antibodies (IgG) by protein G from ascites

200 µL of a 50% slurry of protein G sepharose beads (Pierce) were pipetted into a Handee Mini-Spin column (Pierce). The beads were washed five times with 500 µL of Phosphate Buffered Saline (PBS 140 mM NaCl, 2.6 mM KCl, 10 mM Na_2HPO_4, 1.7 mM KH_2PO_4).

The ascites were thawed at 4°C overnight to prevent the aggregation of proteins. The ascites were subsequently centrifuged at 13,000 rpm at 4°C to sediment aggregates of degraded proteins and lipids.

500 µL of ascites containing approximately 5-10 mg/mL of IgG were added to the washed beads and the resulting slurry rotated on a rotating wheel for 1 hour at room temperature. The beads were washed with 500 µL of PBS and a fraction of the wash used to test for the presence of protein by Bradford Assay. The wash procedure was repeated until no protein was detectable in the wash. The beads were drained from the final wash of PBS and 100 µL of elution buffer (0.1M glycine pH 2.8) was added to the beads. The eluate was collected in 1.7 mL eppendorfs containing 8 µL of neutralisation buffer (TRIS-HCl 1.5M pH 8.8). A fraction of the eluate was used to determine the concentration of purified antibody. The elution procedure was repeated until no protein was detected in the eluate. The eluates containing the antibody were pooled and concentrated with ultrafree 0.5 centrifugal columns with a molecular weight cut off membrane of 10 kDa. The final concentration of the purified antibody was determined by Bradford assay.

2.4.2 Preparation of Protein G Immunomatrix (cross-linked IgG)

200 µL of a 50% slurry of protein G sepharose beads were pipetted into a Handee Mini-Spin column. The flow-through was discarded and the beads washed five times with 500 µL of Phosphate Buffered Saline (PBS 140 mM NaCl, 2.6 mM KCl, 10 mM Na_2HPO_4, 1.7 mM KH_2PO_4) and resuspendend in 100 µL of PBS.

The required amount of protein G purified antibody (typically 50-100 µg) was added to the beads and the resultant slurry rotated on a rotator wheel for 1 hr at room temperature. The columns were centrifuged and the flow through kept to determine the amount of antibody bound to the beads by Bradford assay (typically > 80%). The beads were resuspended in 400 µL of PBS and 12.5 µL of a 25 µg/µL disuccinimidyl suberate

(DSS) in dimethyl sulfoxide (DMSO) stock solution added. The contents of the column were rotated for 1 hour at room temperature. The tube was centrifuged and the flow-through discarded. The column was washed 5 times with 500 μL of TBS (TRIS-HCl 1.0M pH 6.8) to remove excess and quench the DSS.

2.4.3 Preparation of NHS-crosslinked IgG to sepharose beads

200 μL of a 50% slurry of NHS-activated sepharose beads (Amersham) were pipetted in a 1.0 mL column. The isopropanol was allowed to flow out of the column at a rate of 1 drop/sec. 200 μL of ice cold HCl was added to the beads and allowed to flow out of the column at a rate of 1 drop/sec. 200 μL of PBS was added to the column and allowed to flow out at a rate of 1 drop/sec. The beads were resuspended in PBS. The antibody was diluted in 0.2 M NaHCO3, 0.5 M NaCl, pH 8.3 so that the final volume was 50 μL. An aliquot of the antibody solution was taken prior to adding to the beads. The antibody was added to the beads and the resulting suspension was mixed thoroughly on a rotator for 1 hr at room temperature. The beads were drained by gravity flow and an aliquot of the eluate was taken. A Bradford assay was performed on the aliquots taken prior to and after binding to the beads to determine the coupling efficiency.

The beads were washed and excess NHS moieties deactivated by the following sequence of buffer additions:

Buffer A: 0.5 M ethanolamine, 0.5 M NaCl, pH 8.3

Buffer B: 0.1 M acetate, 0.5 M NaCl, pH 4

a. Injected 3 × 200 µL of Buffer A.

b. Injected 3 × 200 µL of Buffer B.

c. Injected 3 × 200 µL of Buffer A.

d. Left the column for 15–30 min in room temperature.

e. Injected 3 × 200 µL of Buffer B.

f. Injected 3 × 200 µL of Buffer A.

g. Injected 3 × 200 µL of Buffer B.

h. Finally, injected 2 ml of PBS to adjust the beads to a neutral pH.

2.4.4 Immunoprecipitation of ubiquitinated p53

Cells were lysed in Triton X-100 lysis buffer containing Complete ® protease inhibitor mix. Lysates were centrifuged with 13000 rpm for 10 minutes at 4°C and filtered through 0.2 µM button filters to remove cellular debris and lipids. Lysates were precleared with Sepharose CL-4b (Sigma) overnight at 4°C. The precleared lysates were added to 1 mL columns containing 20 µL of DO-1 NHS-conjugated sepharose beads. The columns were placed on a rotator at 4°C overnight. The beads were washed three times with 500 µL PBS-T for 5 minutes. The beads were eluted with 3 x 100 µL of 0.1 M glycine pH 3.5 into eppendorfs containing 10 µL of 1.5M TRIS-HCl pH 8.8.The eluates were combined and concentrated with ultrafree 0.5 mL spin columns MWCO 10 kDa. The eluates were run on a on 4-12% NuPAGE® Novex precast gel (Invitrogen) and immunoblotted with an antibody that recognized ubiquitinated proteins (Biomol).

2.4.5 Immunoprecipitation of p53 ^{R175H} from sf9 cells.

A 15 cm plate of p53^{R175H} baculovirus infected sf9 cells was lysed in 4 mL of X-100 lysis buffer containing Complete ® protease inhibitor mix. Lysates were centrifuged with 13000 rpm for 10 minutes at 4°C and filtered through 0.2 μM button filters to remove cellular debris and lipids. Lysates were precleared with Sepharose CL-4b (Sigma) overnight at 4°C. The precleared lysates were added to 5 mL columns containing 100 μL of DO-1 NHS-conjugated sepharose beads. The columns were placed on a rotator at 4°C overnight. The beads were washed three times with 5 mL PBS-T for 5 minutes. The beads were eluted with 3 x 100 μL of 0.1 M glycine pH 3.5 into eppendorfs containing 10 μL of 1.5M TRIS-HCl pH 8.8. The eluates were run on a on 4-12% NuPAGE® Novex precast gel (Invitrogen) and stained with colloidal blue stain (Invitrogen) to visualize eluted proteins.

2.4.6 Purification of One-Strep-tag fusion proteins

The storage buffer of 0.2 mL Strep-Tactin columns was removed prior to equilibration with 0.4 mL of washing buffer (100 mM Tris/HCl, 150 mM NaCl, 1 mM EDTA, pH8.0). The soluble cell extracts were added to the column and allowed to flow through by gravity. The flow through was re-added to the column. This step was repeated 5 times. The column was washed 5 times with wash buffer. The column was eluted with 6 x 100 μL of elution buffer (100 mM Tris/HCl, 150 mM NaCl, 1mM EDTA, 2 mM biotin, pH 8.0).

2.5. Tissue Culture

2.5.1 Cell maintenance

H1299 human lung carcinoma cells were incubated in RPMI 1640 (Roswell Park Memorial Institute), and A549 human alveolar epithelial cell line and MCF7 human breast adenocarcinoma were incubated in DMEM (Dulbecco's Minimal Essential Medium). Both media were supplemented with foetal bovine serum (FBS) at 10% (v/v). Cells were cultured in a humidified incubator (Hera) at 37°C with an atmosphere of 10% CO_2. Cultures were seeded in 6 cm and 10 cm dishes and subcultured 2-3 times per week in 10 cm diameter culture dishes in sterile conditions and split to a maximal dilution of 1/10. The media was discarded and the cells were washed with sterilized PBS. 1-3 mL of 1x Trypsin-EDTA solution was added per dish and then incubated at 37°C for 2-3 minutes. The trypsinised cells were taken up into media (9mL/10cm diameter culture dishes) and then split into new culture dishes with fresh media (10mL/10cm diameter culture dishes)

Cells were kept in liquid nitrogen for long-term storage as follows. A 10 cm diameter culture dish with confluent cells was trypsinised and the cells collected by centrifugation (1000 rpm, 5 min at room temperature). The cell pellet was gently resuspended in 3 mL of freezing medium (90 % (v/v) Foetal Bovine serum, 10 % (v/v) DMSO) and transferred to cryotubes (Nunc) at 1mL per tube. The cells were placed in Nalgene™ Cryo freezing containers and transferred to liquid nitrogen to freeze the cells at 1°C/min.

To recover the cells the cryotubes were thawed quickly in a 37°C water bath and transferred to a 10 mL falcon tube containing 10 mL of culture medium. The cells were collected by centrifugation (1000 rpm, 5 min at room temperature) and the cell pellet

gently resuspended in 10 mL of fresh culture medium. The resuspended cells were plated out in a 10 cm diameter culture dish.

2.5.2 Cell Treatments

Table 2.3 Cell treatments that were directly added to the cell culture medium.

Treatment	**Description**	**Diluen t**	**Concentration s used**
17-AAG (17-(Allylamino)-17-demethoxy-geldanamycin	HSP90 inhibitor (Calbiochem)	DMSO	10 μM
MG132 (Carbobenzoxy-L-leucyl-L-leucyl-L-leucinal Z-LLL-CHO)	26S proteasome complex inhibitor (Calbiochem)	DMSO	10 μM
ADA(AHX)$_3$(LEU)$_3$vinyl sulphone	20S proteasome inhibitor (Biomol)	DMSO	10 μM
(Z-Val-Ala-Asp(OMe)-CH_2F) Z-VAD (OMe)-FMK	pan-caspase inhibitor (Caliobchem)	DMSO	5-25 μM
Nutlin-3	Inhibitor of p53/MDM2 interaction (Alexis biochemicals)	DMSO	8 μM
Cycloheximide	Inhibitor of protein synthesis (Supleco)	DMSO	10 μM
EGS (Ethylene glycolbis(sulfosuccinimidylsuccinate))	In-vivo Cross-linking reagent (Pierce)	DMSO	2-8 mM

2.5.3 Transient transfection

Cells were plated in dishes and seeded for 24 hours. All transfections were performed using the liposome-mediated method using Lipofectamine™ 2000 (Invitrogen) based on the manufacturer's recommendations. The quantity of DNA was normalized in each transfection by adding the appropriate amount of empty vector. The amount of plasmid DNA is detailed in figure legends. For a 10 cm diameter culture dish the plasmid DNA was diluted in 1.25 mL of Optimem (Gibco-BRL). 12 μL of Lipofectamine™ 2000 was added to 1.25 mL of Optimem (Gibco-BRL) and incubated for 5 min at RT. The diluted Lipofectamine™ 2000 was added to the diluted DNA in equal amounts, mixed and incubated at RT for 20 min to allow DNA/ Lipofectamine™ 2000 complexed to form. 2.5 mL of the mixture was added to each culture dish. Cells were harvested in ice-cold PBS 24 hours post transfection unless cell treatment followed.

2.5.4 Stable transfection

2.5.4.1 Determinination of G418 working concentration for H1299 cells

Untransfected H1299 cells were plated in ten 10 cm plates in RPMI 1640. Once the cells reached 40-50 % confluency the medium was removed and the cells washed with 1xPBS prior to adding RPMI 1640 medium containing G418 selection antibiotic at a concentration of 100 - 1000 μg/mL. The cells were allowed to grow and the medium replenished every 3 days. The concentration at which untransfected H1299 cells were killed in 2 weeks was used as the G418 working concentration (500 μg/mL for H1299 cells).

2.5.4.2 Transfection and pooling of clones

H1299 cells at 90% confluency were transfected with Lipofectamine™ 2000 as indicated in Section 2.5.3. 24 hours post transfection the cells were split (1:10) in RPMI 1640 containing 500 μg/mL G418. The medium was replenished every 3 days until stably tranfected clones were visible (approx 2 weeks). The clones were pooled by trypsinisation and grown in RPMI 1640 supplemented with 300 μg/mL G418.

2.6 SDS-polyacrylamide gel electrophoresis (PAGE)

2.6.1 Cell Lysis and SDS sample buffers

Triton X-100 Lysis buffer

50 mM Tris-HCl pH 7.4

1 mM EDTA pH 7.4

150 mM NaCl

1% (w/v) Triton X-100

10 % (w/v) Glycerol

One-strep Lysis Buffer

50 mM Tris-HCl pH 7.4

7.5 % glycerol

150 mM NaCl

1 mM EDTA

SDS sample buffer (SB)

5% (w/v) SDS

25% (v/v) Glycerol

125 mM Tris-HCl pH 6.8

0.02 % (w/v) Bromophenol Blue

DTT (1M) added to buffer (1DTT : 4 SB prior to use)

2.6.2 Cell harvesting and lysis

Cells were washed in ice cold PBS, and harvested by scraping with 1 mL of PBS into a pre-chilled microcentrifuge tube. Cells were collected by centrifugation at 1200 rpm for 5 min at 4 °C. The supernatant was removed and cells snap frozen and stored at -70 °C until required for lysis. To 10 mL of Lysis Buffer 1 Complete-Mini protease inhibitor cocktail tablet (Roche) was added. For cell lysis, the cell pellet was resuspended in 500 - 1000 µL of lysis buffer. The cells were disrupted further with a 2.5 mL syringe equipped with a 0.6 mm x 25 mm syringe needle (Microlance^{TM} BD). Samples were incubated on ice for 20 min. The cell lysate was centrifuged at 13000 rpm for 5 min at 4 °C to pellet insoluble cellular debris.

2.6.3 Bradford assay

Bradford assay dye reagent (Biorad) was diluted one in five in water to give a 1x working solution. Bovine serum albumin (BSA) standards ranging from 0.1 – 2 mg/mL were prepared in water. 1 µL of each standard was pipetted in 500 µL of 1x Bradford reagent and the absorbance of the resultant solution determined at 595 nm with a Powerwave XS 96 well plate reader (Bio-tek). A standard curve was generated from the BSA standard from which sample readouts were converted to concentrations.

2.6.4 SDS-PAGE

SDS-Running Buffer

Tris-Glycine

192 mM Glycine

25 mM Tris-HCl

0.1 % (w/v) SDS

Equal volumes of SDS sample buffer were mixed with the protein samples and incubated at 96°C for 3 minutes before loading onto 6,8,12% polyacrylamide gel or 4-12% NuPAGE Bis-Tris gel (Invitrogen). The samples on 6,8 and 12% polyacrylamide gels were resolved by electrophoresis in SDS-tris-glycine running buffer on mini-protean 3 apparatus (BioRad) at 150 V for approximately 1 hour. The samples on a 4-12% NuPAGE Bis-Tris gel were resolved by electrophoresis in SDS-MOPS running buffer (Invitrogen) on a Novex XCell SureLock (Invitrogen) gel apparatus at 200V for approximately 1 hour.

2.6.5 Detection of separated protein

2.6.5.1 Colloidal Blue Staining

For colloidal blue staining of proteins the Colloidal Blue staining kit (Invitrogen) was used and the manufacturer's instructions for Nupage® Novex Bis-tris gels were followed.

2.6.5.2 Silver staining

Fixing Solution	**Developing solution**
50% (v/v) methanol	0.04% formaldehyde solution (37% v/v)
5% (v/v) glacial acetic	2% Na_2CO_3

The resolved proteins were incubated in fix solution for 20 minutes and washed in 50% methanol for 10 minutes. Gels were subsequently washed in water overnight. Gels were subsequently incubated in cold sensitization solution (0.02% $Na_2S_2O_3$) for 1 minute. Gels were subsequently washed twice in water for 1 minute. Gels were then incubated in cold 0.1% $AgNO_3$ for 20 minutes and washed twice with water for 1 minute. The gels incubated in developing solution. Staining was terminated washing the gel in 5% glacial acetic acid.

2.6.5.3 Immunoblotting

Transfer buffer	**ECL Solution 1**
192 mM Glycine	100 mM Tris pH 8.5
25 mM Tris	2.5 mM Luminol
20% (v/v) Methanol	0.4 mM p-coumaric acid

ECL Solution 2	**10 x Phosphate Buffered Saline (PBS)**
100 mM Tris pH8.5	1.37 M NaCl
0.02 % (v/v) H_2O_2	0.1 M Na_2HPO_4
	0.027 M KCl

0.018 M KH_2PO_4

adjusted to pH 7.4 with HCl

PBS-tween (PBST)

1x PBS + 0.1% (v/v) Tween 20

Blocking Buffer

PBST + 5 %(w/v) low fat dry Milk (Marvel)

Resolved proteins were transferred onto Hybond-C nitrocellulose membrane (Amersham) in Transfer Buffer at 300 mA for 1 hour or 25 mA overnight. For 300 mA blotting, an ice pack was placed in the transfer tank to maintain a low temperature. Following transfer, to prevent non-specific binding of the antibody, the membrane was blocked in Blocking Buffer for 1 hour. The membrane was subsequently incubated with primary antibody, as indicated in Table 2.4, in Blocking Buffer for 1 hour at room temperature or overnight at 4°C. The blot was then washed 3 times for 10 minutes in PBST before incubating for 1 hour in horse radish peroxidase (HRP) coupled secondary antibody in Blocking Buffer to detect specific antibody binding (Dako). Finally, the blot was washed 3 times with PBST for 10 minutes prior to incubating with ECL solutions 1 and 2 (mixed 1:1) for 1 min. Specific bands were detected by being exposed to Hyperfilm™ ECL (Amersham).

Primary antibody	Species	Dilution	Company
Anti-p53 (DO-1)	Mouse	1:4000	Moravian Biotechnology
Anti-ubiquitin (P4D1)	Mouse	1:1000	Santa Cruz (Cat # sc8017)
Anti-eef1a (CBP-KK1)	Mouse	1:1000	Upstate (Cat # 05-235)
Anti-MDM2 (2A10)	Mouse	1:1000	Moravian Biotechnology
Anti-CHIP (Stub1)	Rabbit	1:1000	Abcam (Cat # ab2917)
Anti-Hsp/Hsc70	Mouse	1:4000	Stressgen (Cat # SPA-822)
Anti- Hsp70	Mouse	1:2000	Stressgen (Cat # SPA-810
Anti-Hsp40	Rabbit	1:250	Immunokontact (code 221-25-Hsp40
Anti-$p50^{cdc37}$	Mouse	1:500	BD Transduction Laboratories (Cat # 610576)
Anti-p21	Mouse	1:500	Calbiochem (Cat # OP64)
Anti-β-actin (AC-15)	Mouse	1:5000	Sigma (Cat # A5441)
Anti-vimentin (v9)	Mouse	1:250	Sigma (Cat # V6630)
Anti-TCP1beta (F39P7F11)	Mouse	1:250	Abcam (Cat # 50605)
Anti-CHK2 (A-12)	Mouse	1:500	Santa Cruz (Cat # sc5278)
Anti-Flag (M2)	Mouse	1:5000	Sigma (Cat # F3165)
Anti-c-myc (9E10)	Mouse	1:500	Sigma (Cat # M5546)
Anti-c-myc (4A6)	Mouse	1:500	Upstate (Cat # 05-724)
Anti-ADP, ATP Translocator (5F51BB5AG7)	Mouse	1:500	Calbiochem (Cat # AP1034)

Table 2.4 Primary antibodies and respective dilutions used in immunoblotting

2.7 Mass Spectrometry

2.7.1 In-Gel digestion of protein samples

Reducing Solution

10 mM DTT

0.2 % EDTA

100 mM NH_4HCO_3

Alkylating Solution

50 mM iodoacetamide

100 mM NH_4HCO_3

Extraction Solution

50 µL of 5% Formic acid

50 % Acetonitrile

Destaining solution

0.1 M NH_4HCO_3

50 % Acetonitrile

Trypsin Solution

0.04 µg/µL trypsin (Promega) in 0.1 M NH_4HCO_3/10% acetonitrile

The stained protein bands were excised from the gel with a clean scalpel, cut in ca. 1x1 mm cubes and placed in a microcentrifuge tube. The colloidal blue stained gels were incubated with 250 µL of destaining solution at 37 °C until all visible blue colour was removed. Samples were dried in a Gyrovap for about 15 minutes. Gels slices were then incubated for 30 minutes at 56 °C with 10-15 µL reducing solution and cooled to room temperature. The reducing solution was removed and gel slices incubated with 10-50 µL alkylating solution at room temperature and in the dark for 30 minutes.

The alkylating solution was removed and gel slices washed and dehydrated twice by first incubating with 200 μL of 100 mM NH_4HCO_3 for 10 minutes and then with 200 μL of neat acetonitrile for 10 minutes. The gel slices were dried in a Gyrovap for approximately 15 minutes. The gel slices were incubated for 15 minutes at 37°C with 5 μL trypsin and then covered with 10-15 μL of 50 mM NH_4HCO_3 followed by an incubation at 37°C for 12-16 hours. 50 μL of 20 mM NH_4HCO_3 were added to the gel slices and incubated at room temperature for 20 minutes. The free liquid was transferred to a new eppendorf tube. The gel slice was placed in Extraction solution twice for 20 minutes. The extraction solution and free liquid were pooled and dried in a Gyrovap. The peptides were dissolved in 10 μL of 2 % formic acid prior to analysis by MALDI-TOF or ESI-MS-MS.

2.7.2 Online Nano LC-MS/MS

Online separation by reverse phase nanoLC of in-gel trypsin digests was performed on an UltiMate 3000 (Dionex) equipped with a C18 PepMap100 trap (C18, 300μm i.d. X 5mm; 5μm, 100Å, Dionex) and C18 PepMap100 analytical column (C18, 75μm i.d X 15cm; 3μm, 100Å, Dionex). Each analysis was performed using approximately 1pmol of protein. The trap column was loaded and washed with 98% H_2O, 2% acetonitrile at a flow rate of 30uL/min. Analysis was performed at a flow rate of 0.3μl/min. A 60minute increasing gradient of 4 to 90% of solvent B (80% water + 20% acetonitrile + 0.05% formic acid) at 0.3μl/min was applied for the first 40min for the elution of peptides from the reverse phase column. This was followed by a 4%

solvent B wash for 10mins to recondition the column. UV absorbance was collected at 214nm and 280nm at 0.5s steps.

The eluent was electrosprayed directly into the mass spectrometer using a 360μm o.d, 20μm i.d, 10μm i.d tip, distally coated picotip (New Objective, MA) mounted on an online nanospray source (Agilent).

The HCT ion trap was operated in positive ion mode and MS-MS was achieved by collision-induced fragmentation (CID). Ions with a mass range of 200-2000m/z were accumulated in the ion trap for a maximum time of 200ms.The Auto MS/MS function was used for alternating precursor ion scanning and the MS/MS of the 2 most abundant precursor ions. After a spectrum was collected on an ion, it was added to an exclusion list for 45s. Data obtained was processed in Data Analysis, Biotools software packages and searched using an in-house MASCOT server (Matrix science).

2.7.3 MALDI-ToF MS

Matrix

3 mg/mL α-cyano-4-hydroxycinnamic acid

75 % (v/v) ethanol

25 % (v/v) acetone

1 μL of matrix was mixed by pipetting with 1 μL of sample peptide digest (refer to Section 2.7.1 for details of sample preparation). 0.5 - 1 μL of this mixture was spotted onto a MALDI target. Data were collected in positive reflectron mode on a MALDI De-STR (ABI) using a 337nm nitrogen laser. Each spectrum was an average of

200 spectra (200 laser shots per spot). The spectra were batch processed in Data Explorer with default settings of advanced background correction, noise removal, noise filtered and 5points Gaussian smoothing.

2.8 Fluorometric assays

2.8.1 Sandwich-type enzyme-linked immunosorbent assay (ELISA)

This technique was used mainly to study the conformations of wild type and mutant forms of p53. 96-PVC-wells were coated with monoclonal antibodies (DO-1, DO-12, PAb1620 for p53) at 50 – 100 ng/well in $NaHCO_3$ pH 8.0 overnight and washed 3 times with 18 μL of PBST (0.02% v/v) to remove non-binding antibodies. To prevent non-specific binding, non reactive sites were blocked with 200 μL of 3% BSA-PBST and incubated for 1 hour. Cell lysates from baculovirus infected insect cells or transfected H1299 cells at the appropriate dilution was added to the antibody-coated ELISA wells and incubated for 1 hour. Unbound proteins were washed away with 200 μL of PBST (0.02 %v/v) for 3 times. p53 captured by anti-p53 monoclonal antibodies were incubated with anti-p53 polyclonal antibody CM-1 in 3% BSA in PBS-T (1 in 2000) for 2 hours at 4°C. After binding of the secondary antibodies, the wells were washed with 200 μL PBST (0.02% v/v) for 6 times. The amount of CM-1 captured in the wells was visualised by the ECL method. 50 μL of ECL solution was added to each well to develop chemiluminescence and the luminescence was immediately detected and quantitated in a Fluoroskan Ascent FL (Labsystems) luminometer.

2.8.2 Dual-luciferase reporter assay

H1299 cells were plated in 6-well plates a day prior to transfection. The cells were co-transfected with p53-wild type plasmid (50 ng), p53-responsive p21 reporter plasmid, *Renilla* luciferase (pRL-CMV) for 24 hrs using Lipofectamine 2000. To assess the effect ribosomal protein s3 on the transcriptional activity of p53, the plasmid encoding the rps3 gene was titrated at the levels indicated in the experiments. The total amount of DNA was kept constant with empty pcDNA 3.1 and empty onestrep tag (pEXPR105). The cells were lysed in lysis buffer provided by the manufacturer (Promega).

The activities of *Firefly* luciferase expressed by the p53-responsive p21-reporter plasmid were measured using the Dual-Luciferase reporter assay system (Promega) and a Fluoroskan Ascent FL (Labsystems) and corrected according to the *Renilla* luciferase activities derived from pRL-CMV for assessment of the transfection efficiency. The relative luciferase activity was calculated using the formula: (*Firefly* luciferase activity)/(*Renilla* luciferase activity).

2.9 In-vitro translation

2.9.1 TNT® coupled reticulocyte transcription/translation reactions

The plasmids used for the in vitro transcription/translation contained the T7 RNA polymerase promoter.

The reagents (Promega) were removed from storage at -70°C. TNT® rabbit reticulocyte lysate was thawed by hand warming and immediately placed on ice. The following reaction components were pipetted in a 1.5 mL microcentrifuge tube.

- TNT® Rabbit Reticulocyte Lysate 25 µL
- TNT® Reaction Buffer 2 µL
- TNT® RNA Polymerase 1 µL
- Amino Acid Mixture, Minus Leucine, 1mM 0.5 µL
- Amino Acid Mixture, Minus Methionine, 1mM 0.5 µL
- RNasin® Ribonuclease Inhibitor (40 U/µL) 1 µL
- DNA templates (0.5 µg/µL) 2 µL/template
- Water 16 µL

The reaction components were gently mixed by pipetting and the resultant mixture incubated at 30°C for 90 minutes. The in-vitro translated proteins were resolved on 4-12% Novex gels.

2.10 Fluorescent Microscopy

2.10.1 Cell transfections

Transfections were performed with the Lipofectamine reagent (InVitrogen). H1299 cells were seeded at a density of 0.13×10^6 cell/ml and plated in sterile four-chambered slides (NUNC) until 80-90% confluency was reached. Twenty-four hours post-plating the medium from the cells was removed and fresh media was added. Cells

were transfected with 0.5μg/ml of the pCDNA 3.1 + construct encoding wild-type p53, $p53^{F270A}$ or a control empty vector

2.10.2 Immunofluorescence for detection of transfected p53 DAPI staining

Twenty-four hours post-transfection H1299 cells were washed in 1xPBS, fixed and permeabilized in 1:1 (v/v) Methanol:Acetone for 6 min at -20°C. Following washes with 1xPBS, nonspecific sites were blocked for 1h with 3% (w/v) BSA/PBS in room temperature. After 3 washes in 1xPBS, the chambers from each slide were removed and cells were incubated overnight with the anti-p53 (DO-1) primary antibody (1:6000) diluted in 1% (v/v) BSA/PBS at 4°C. Twenty-four hours post-incubation, the slides were washed in 0.1% (v/v) PBS-Tween and incubated with the secondary anti-rabbit antibody conjugated with Alexa-568 for 30min at RT. After incubation cells were washed thrice in 1xPBS containing 0.1% (v/v).Tween. Nuclei were counterstained using DAPI. Coverslips were mounted with Fluorescent Mounting Media (DakoCytomation). The control for non-specific binding of the secondary antibody was the 1% (w/v) BSA/PBS, where no primary antibody was added. Microscopy analysis was performed on Zeiss microscope (Zeiss Axionplan Imaging Systems, kindly provided by the Medical Research Council, Human Genetics Unit). Transfected and non-transfected cells were localized using excitation in blue light (488nm) and images were sequentially acquired using DAPI and TexasRed filter blocks. Captured images were analysed using the Limelight microscope (Zeiss) and the Photometric CoolSnap HQ camera was used to capture them.

3.0 Destabilising mutation F270A in p53 core domain enhances its ubiquitination *in vivo* and associates with eef1a

3.1 Introduction

p53 transcriptional activity is influenced by two pathways, namely protein degradation (negative regulation) and transcriptional co-activation (positive regulation). p53 degradation occurs by the ubiquitin/proteasome pathway and is mediated by four distinct proteins with E3 ubiquitin ligase activity that catalyse the final step in linking the ubiquitin moiety to the ε-amino group of lysine residues. The p53 E3 ligases discovered so far are MDM2 (murine double minute clone 2 oncoprotein), PirH2 [124], COP-1 (constitutively photomorphogenic 1) [125], TOPORS [topoisomerase I- and p53-binding protein] [126], ARF-BP1/Mule [127], Synoviolin [128], CARPs [Caspase 8/10-associated RING proteins] [129] and CHIP [C-terminus of Hsc70 (heat-shock cognate 70)-interacting protein [108]. p53 is positively co-activated by p300, which is essential for p53 protein stabilisation in response to DNA damage. MDM2 and p300 share a binding site on the N-terminal domain of p53 characterised by an LXXLL motif. Binding of p300 or p53 at this site leads to the monoubiquitination of p53 on lysine residues in the C-terminus of p53 or acetylation catalysed by p300. Mutation of the phenylalanine residue at position 19 that flanks the LXXLL motif in the N-terminus of p53 can inhibit MDM2-dependent ubiquitination. Interestingly, monomeric p53 is not ubiquitinated by MDM2 despite having an intact N-terminal domain, thereby highlighting the importance of p53 oligomeric status as a prerequisite for MDM2-dependent ubiquitination.

Apart from the p53 N-terminal binding site for MDM2, the latter also binds a secondary conformationally flexible loop within the S10 β-sheet in the central DNA-

binding domain of p53 [67]. The interaction between the N-termini of p53 and MDM2 seems to promote a conformational change in MDM2 that stabilizes the interaction between the MDM2 acid-domain and the ubiquitination signal located in the above mentioned secondary site within the DNA binding domain of the p53 tetramer resulting in enhanced ubiquitination [68]. These studies thereby highlight the importance of p53 conformational status in MDM2-dependent ubiquitination.

Polypeptides emerging from ribosomes necessitate the folding into three-dimensional structures prior to performing their routine functions within the cell. Failure of proper folding leads to an enhanced probability of protein aggregation and non-specific interactions with cellular components leading to deleterious effects in the cell. An example of the damaging effects of protein aggregation can be observed in Alzheimer's disease (AD) which has been identified as a protein misfolding disease due to the accumulation of abnormally folded amyloid beta protein and tau protein in the brains of AD patients [130].

Heat shock proteins are chaperones that assist the proper folding of nascent and mis-folded proteins by lowering the activation energy of the process. On the other hand, the ubiquitin-proteasome system is an error-checking system that targets improperly and/or unnecessarily synthesized proteins for destruction. The partitioning of proteins to either one of these pathways has been referred to as the "protein triage" and depends on the unfolding state at the ribosome. In fact, a significant fraction of newly synthesized proteins is degraded cotranslationally. These nascent damaged proteins can be ubiquitinated while bound to the ribosome, demonstrating that there exists a close coupling between the pathways of protein synthesis and protein degradation [131].

The aim of the following chapter was to focus on the role of p53 substrate conformation in MDM2-dependent ubiquitination of p53. A link was identified between substrate misfolding and susceptibility to ubiquitination. An immunoaffinity approach coupled with mass-spectrometry was used to elucidate potential key factors that discriminate between folded and misfolded p53. Using this technique a pool ribosomal proteins and ribosome associated proteins were identified as binding to p53. Moreover, eukaryotic elongation factor 1a (eef1a) was found to bind exclusively to the misfolded p53 mutant.

3.2 Extent of mutant p53 unfolding and oligomeric status in cells

To determine the relative ratios of folded or unfolded p53 in cells grown at 37°C, lysates from H1299 p53-null cells transfected with wild-type or mutant p53 alleles were incubated in ELISA wells coated with monoclonal antibodies PAb1620 or DO-12 that are specific for wild-type and unfolded p53, respectively [132]. Total p53 levels captured by the conformation-specific antibodies were then detected using a polyclonal antibody to p53 (Figure 3.1 (**A**) and (**B**)). Transfection of wild-type p53 into cells led to the synthesis of a pool of p53 that was predominantly in the PAb1620 positive conformation with a minor pool of wild-type p53 in the unfolded conformation. The ratio of folded to unfolded wild-type p53 was approximately 9:1. In contrast, the transfection of $p53^{F270A}$ into cells produced a pool of mutant p53 that was predominantly in the DO-12 conformation. The ratio of folded to un-folded wild-type p53 was approximately 1:9. These data indicate that $p53^{F270A}$ is significantly unfolded in cells at physiological temperatures when compared to wild-type p53.

p53 functions as a transcription factor in a homotetrameric form. *In-vivo* cross-linking with EGS was used to determine whether the oligomeric status of mutant $p53^{F270A}$ differed from wild-type p53. As seen in Figure 3.1 (**C**) the oligomeric status of wild-type p53 was very similar to that of mutant $p53^{F270A}$ as similar higher-molecular-weight species were resolved on the 4-12% gradient gel (Figure 3.1 (**C**) *Lanes 5-7 vs. 1-3*).

Figure 3.1

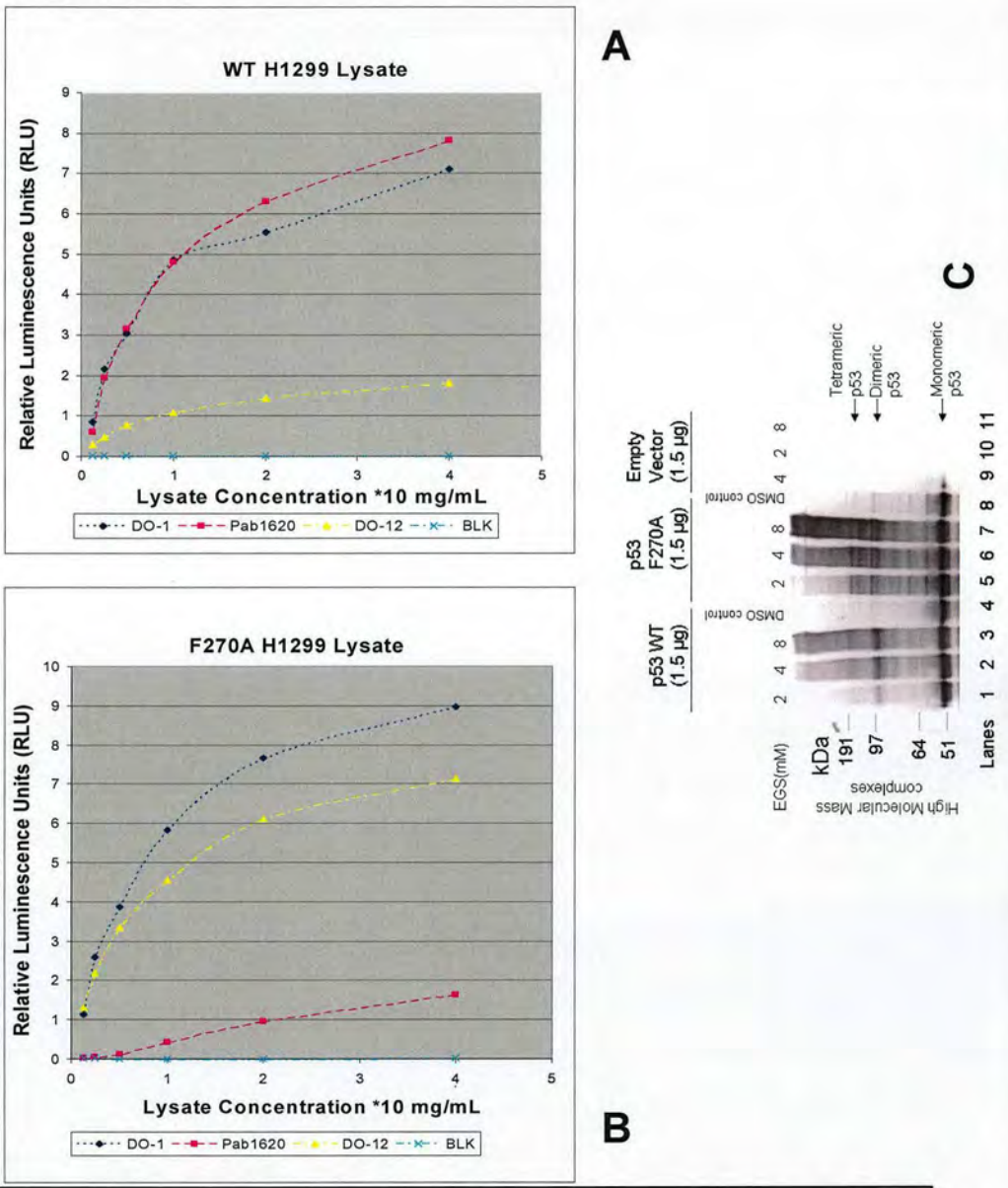

Figure 3.1 Extent of mutant p53^{F270A} unfolding and oligomeric status in cells

Antibody capture ELISA revealed that most of the p53^{F270A} mutant shows an unfolded conformation. Expression vector encoding wild-type p53 (**A**), or p53^{F270A} (**B**) (1.5 µg of DNA) was transfected into cells, and the conformation of p53 protein was examined by antibody capture ELISA. p53 proteins in the lysates were captured by monoclonal antibodies PAb1620 or DO-12 coated on to ELISA wells, followed by polyclonal antibody CM1 incubation and ECL® detection. The data are represented as luminescence in RLU (relative luminescence units) as a function of the monoclonal antibody used to capture p53. (**C**) In-vivo cross-linking of p53. The indicated p53 genes were transfected into cells and treated with EGS for 1 hr prior to cell harvesting, lysis and immunoblotting on a 4-12% gel with anti-p53 antibody (DO-1).

3.3 $p53^{F270A}$ displays enhanced ubiquitination *in-vivo* that is MDM2 dependent

Transfection of the $p53^{F270A}$ allele in H1299 cells resulted in enhanced ubiquitination when compared to wild-type p53 as determined by the higher molecular-mass ladder of p53 positive bands (arrows, *Figure 3.2 Lane 1 vs. 2*). Co-transfection of MDM2 into cells resulted in the enhanced ubiquitination of wild-type p53 to a level similar of the ubiquitination of $p53^{F270A}$ (arrows, *Figure 3.2 Lane 8 vs. 1*). A modest increase in intensity of the higher molecular-mass ladder resulted following the addition of proteasome inhibitor MG132 to cells transfected with $p53^{F270A}$ (Figure 3.2 *Lane 4 vs. 1*). Furthermore, co-transfection of MDM2 (arrows, *Figure 3.2 Lane 7*) and addition of proteasome inhibitor MG132 resulted in distinct novel bands appearing in the high molecular-mass ladder in cells transfected with $p53^{F270A}$ (arrows, *Figure 3.2 Lane 11 vs. 4*).

To ascertain whether the high-molecular-mass ladder was the ubiquitinated form of p53, genes encoding for wild-type p53 and $p53^{F270A}$ were transfected in H1299 cells followed by precipitation with monoclonal antibody DO-1 and immunoblotting with anti-ubiquitin antibody. Presumably, due to the heterogeneous nature of ubiquitin conjugation polyubiquitinated forms of p53 could only be detected as a large molecular size smear. This experiment demonstrated the enhanced ubiquitination of $p53^{F270A}$ when compared to wild-type p53 in the presence of MG132 (Figure *3.3 Lane 3 vs. 4*). The transfection of MDM2 also led to increased ubiquitin-adduct formation on wildtype p53 in the presence of MG132 (Figure 3.3 *Lane 8 vs. lane 4*) to a level similar to $p53^{F270A}$ under the same conditions (Figure 3.3 *Lane 7*).

Figure 3.2

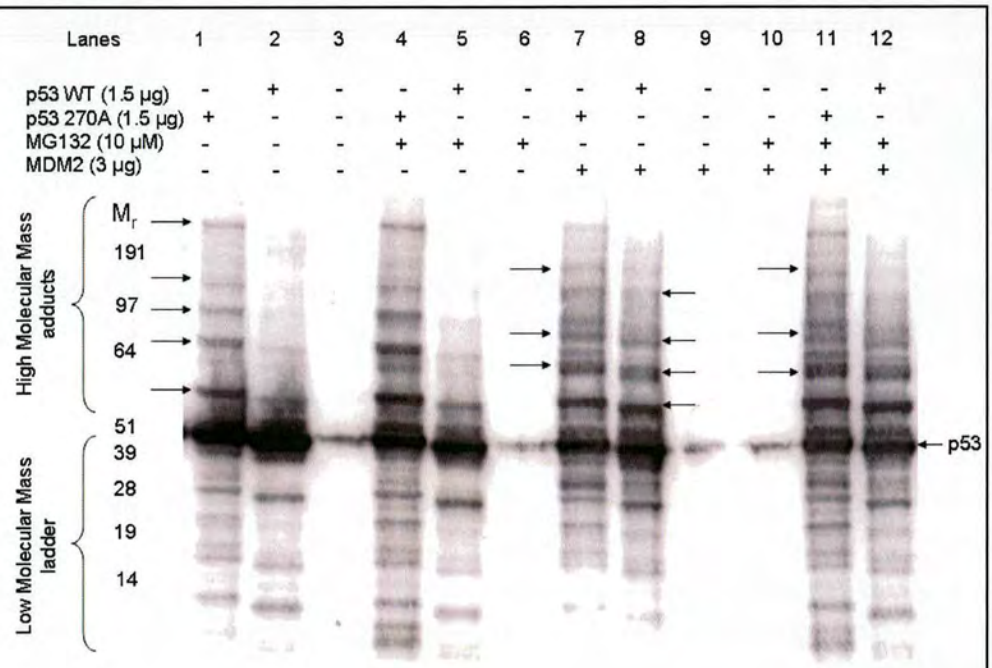

Figure 3.2 Monomeric p53 encoded by the $p53^{F270A}$ allele yields higher and lower molecular peptides when compared to wild-type p53.

Expression vectors (pCMV 3.1) encoding wild-type p53 or $p53^{F270A}$ (1.5 µg) were co-tranfected with MDM2 in H1299 cells in the presence of proteasomal inhibitor MG132 or DMSO control. The expressed proteins were examined for changes in their steady-state levels of p53 with the amount of ubiquitination products determined by immunoblotting with anti-p53 antibody (DO-1). The arrows highlight high-molecular mass p53-positive bands.

Figure 3.3

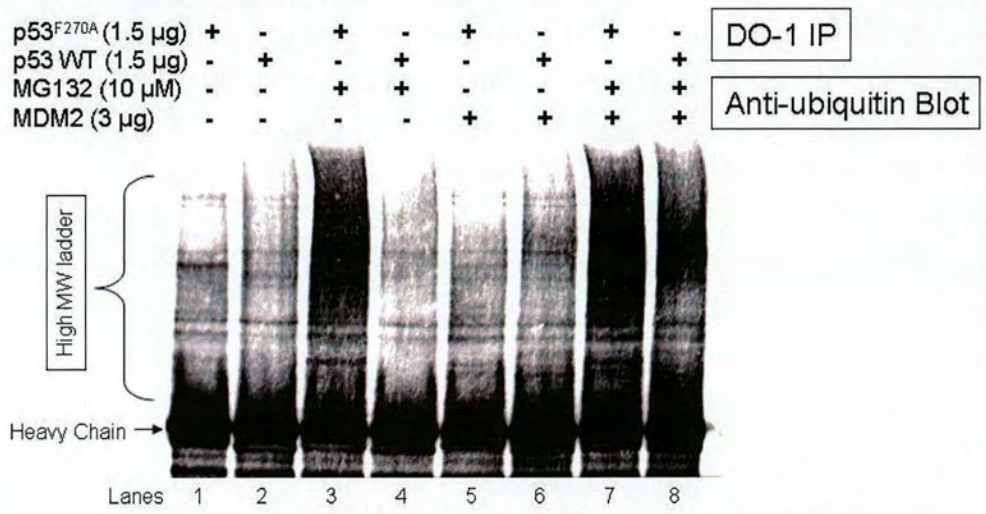

Figure 3.3 Immunoprecipitation of $p53^{F270A}$ in a hyperubiquitinated state

H1299 cells were transfected with either wildtype or mutant pcDNA-p53 (1.5 µg)or pCMV-MDM2 (3 µg), as indicated. DO-1 was used to pull down ubiquitinated conjugates of p53. Immunoblots of the eluates with anti-ubiquitin showed that mutant $p53^{F270A}$ exhibits enhanced ubiquitination *in-vivo* in the presence of MG132 (*Lane 3 vs. 4*). The transfection of MDM2 impacts on the ubiquitin-adduct formation on wild-type p53 (*Lane 8 vs. 4*)..

3.4 $p53^{F270A}$ displays enhanced proteasomal processing but not NEDD8 conjugation when compared to wild-type p53

These data indicate that a large proportion of proportion of the high-molecular-mass forms of p53-positive bands are ubiquitinated, but they do not address whether the lower-molecular-mass pattern of p53-positive bands arise from cleaved fragments of p53 or whether the high-molecular-mass bands might also stem from other adducts such as NEDD8 conjugation. The latter scenario was evaluated by co-transfection of NEDP1 (a specific cysteine protease which specifically cleaves NEDD8 molecules from substrates [133]; a kind gift of D. Xirodimas) into cells together with either wild-type p53 (and MDM2) or $p53^{F270A}$. A proportion of wild-type p53 adducts was reduced upon deconjugation by NEDP1 (Figure 3.4 (**A**) *Lanes 2-5 vs. 1*), a result which is in agreement with Xirodimas and co-workers. Conversely, mutant p53 adducts remained unchanged when co-transfected with NEDP1 (Figure 3.4 (**A**) *Lanes 7-10 vs. 6*) thereby leading to the conclusion that the lower- and higher-molecular-mass adducts of $p53^{F270A}$ do not stem from NEDD8 conjugation.

In an attempt to elucidate whether the lower-molecular-mass pattern of bands arise from intermediates in polyubiquitin coupled proteolysis, cells were transfected with mutant p53 and incubated with increasing amounts of the proteasome inhibitor Ada-$(Ahx)_3$-$(Leu)_3$-vinyl sulphone. This resulted in an accumulation of higher-molecular-mass adducts and also resulted in changes of some lower-molecular-mass bands (Figure 3.4 (**B**) arrows *Lanes 7-9 vs. 6 and 10*). The predominance of the lower-molecular-mass banding on mutant p53 might be due to its enhanced susceptibility for proteolysis owing to its unfolded nature.

Figure 3.4

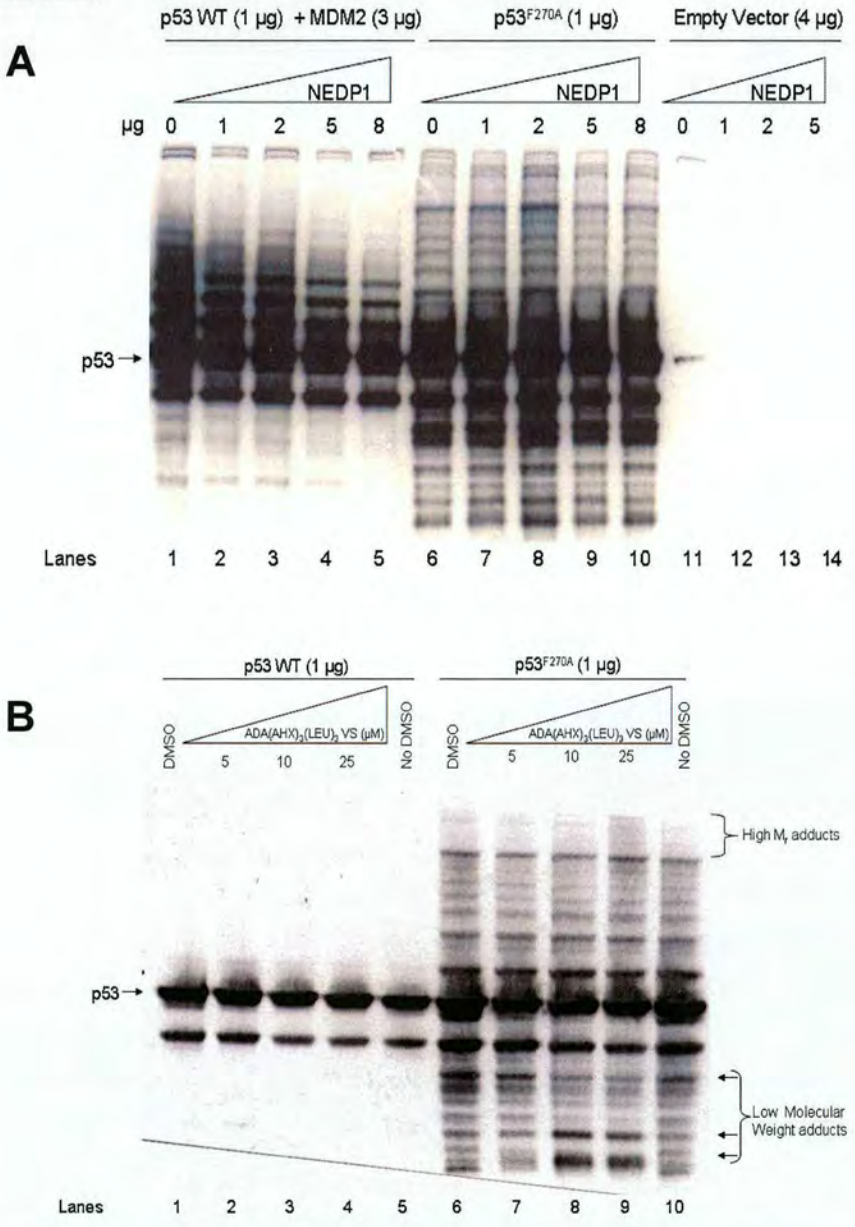

Fig 3.4 Mutant p53 ubiquitin adducts are not cleaved by NEDP1 protease but are cleaved by the proteasome.
(**A**) The indicated p53 allele (wild-type p53+MDM2, lanes 1–5; or $p53^{F270A}$, lanes 6–10) was transfected into cells alone or with increasing amounts of NEDP1 (1–8 μg, as indicated). After 24 h, cells were harvested and immunoblotted with an anti-p53 antibody. (**B**) Accumulation of lower- and higher-molecular-mass adducts on mutant p53 using a broad-range proteasome inhibitor. The mutant-p53-specific ubiquitination system was assembled *in vivo* as described above using transfected genes, followed by addition of increasing amounts of Ada-(Ahx)3-(Leu)3-vinyl sulphone. Lysates were immunoblotted to quantify changes in mutant p53 adducts, and higher-molecular-mass accumulation and production of lower-molecular-mass adducts are highlighted with arrows

3.5 Mutant $p53^{F270A}$ and $p53^{R175H}$ display caspase cleavage-dependent polypeptides

To investigate the possibility that the lower-molecular mass p53-derived peptides could arise from caspase cleavage, H1299 cells were transfected with empty vector, wild-type p53, $p53^{R175H}$ (a structural mutant, found in the zinc binding regions of the DNA binding domain [33]) or $p53^{F270A}$, with or without MDM2, incubated with either caspase inhibitor (Z-VAD (OMe)-FMK (20μM)) or DMSO control and harvested at incremental time-points. Generation of some of lower-molecular-mass bands on mutant $p53^{F270A}$ (Figure 3.5 (**A**) *Lanes 6-8 vs. 5* and (**B**) *Lanes 14-16 vs. 13*) and $p53^{R175H}$ (Figure 3.5 (**C**) *Lanes 2-4 vs. 1 and lanes 6-8 vs. 5*) is caspase dependent since it was blocked by Z-VAD (OMe)-FMK. Nonetheless, some of the p53 fragments were not blocked by Z-VAD (OMe)-FMK suggesting caspase-independent formation of these products.

Figure 3.5

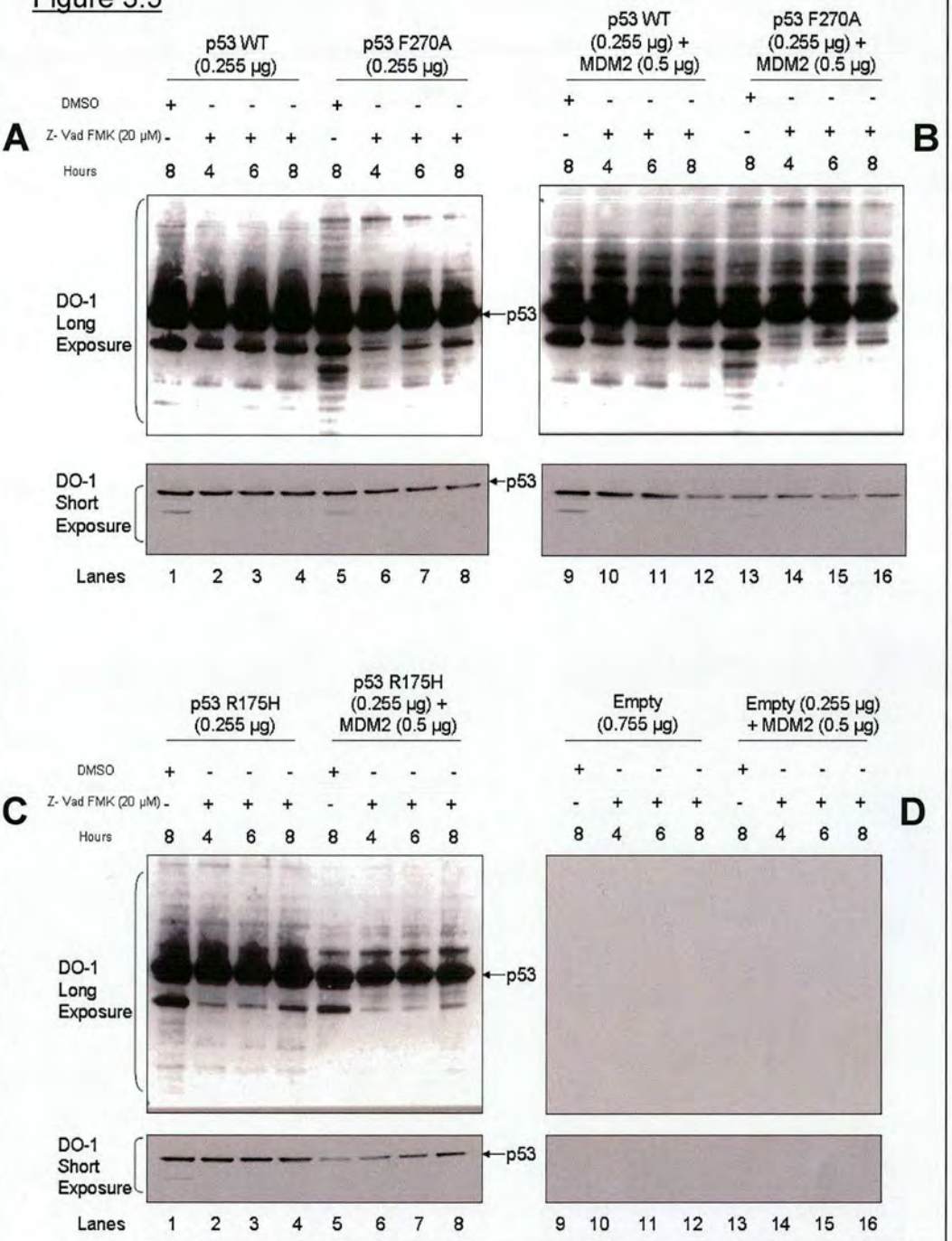

Figure 3.5 Mutant p53 is susceptible to caspase-dependent cleavage.
H1299 cells were transfected with (**A**) wild-type p53 (lanes 1-4) or $p53^{F270A}$ (lanes 5-8), (**B**) wild-type p53 (lanes 9-12) or $p53^{F270A}$ (lanes 13-16) and MDM2, (**C**) $p53^{R175H}$ (lanes 1-4) or $p53^{R175H}$ and MDM2 (lanes 5-8), or (**D**) empty vector (lanes 9-12) or empty vector and MDM2 (lanes 13-16). 24 hrs post transfection the cells were treated with 20 µM Z-VAD (OMe)-FMK (**A**, **B**, **C** and **D** lanes 2-4, 6-8,10-12, 14-16) or DMSO (**A**, **B**, **C** and **D** lanes 1, 5, 9, 13). Lysates were immunoblotted to quantify changes in p53 adducts.

3.6 Mutant p53 is more susceptible to ubiquitination *in vitro* on lysine residues outside the C-terminus

The previous studies, demonstrating a connection between p53 conformation and ubiquitination is somewhat limiting since the assays are based *in vivo*, thereby, the link between unfolded p53 conformation and its ubiquitination might be indirect. For example, the mutant unfolded p53 might be mis-localised in a cellular compartment different from wild-type p53, leading to an enhanced ubiquitination that is indeed unrelated directly to the degree of folding. In this respect, an *in vitro* protein-synthesis system was used that resolves p53 into folded or unfolded conformational variants.

MDM2 protein was synthesized by co-translation *in vitro* with wild-type p53, $p53^{F270A}$, $p53^{F19A}$ (mutation of the critical Phe residue of the p53 α-helix, that binds to the hydrophobic cleft of MDM2, to an Ala residue, thereby resulting in the disruption of the MDM2:p53 N-terminal domain interaction [134]) and $p53^{F270A/F19A}$ (double mutant). $p53^{F270A}$ displayed high molecular-mass adducts in the absence of MDM2 co-translation in contrast to wild type p53 (Figure 3.6 (**A**) *Lane 3 vs 1*). Both wild-type p53 and $p53^{F270A}$ demonstrated enhanced high-molecular-mass adducts after co-translation with MDM2 (Figure 3.6 (**A**) *Lanes 4 and 2*). Additionally, although $p53^{F19A}$ was not ubiquitinated by MDM2 co-translation (Figure 3.6 (**A**) *Lane 8*) a high molecular-mass adduct appeared upon re-introduction of the F270A allele into the F19A genetic background, which was further augmented by co-translated MDM2 *in vitro*. (Figure 3.6(**A**) *Lanes 9 and 10*).

An attempt to confirm the identity of the high-molecular-mass adducts resulting from *in-vitro* translated mutant-p53 as ubiqutin by immunoprecipitation with a p53 antibody (DO-1) and subsequent immunoblotting with anti-ubiquitin antibody proved

elusive, probably due to the inefficiency of the anti-ubiquitin antibody to cross-react with the rabbit ubiquitin immunogen.

In this respect a different approach was adopted, namely, the use of small peptides that inhibit the E3 ligase activity of MDM2 (summarized in Table 3.1).

Table 3.1 Small peptide inhibitors of MDM2 E3 ligase activity

Peptide Name	**Peptide-Sequence**	**Effect on MDM2-p53 interaction**
Retinoblastoma Peptide 1 (Rb1)	SGSGDQIMMCSMYGICKVKNIDLK	Inhibits p53 degradation by binding the acidic domain of MDM2 $IC_{0.5}$ in the range of 0.2–0.3 μM
BOX V domain of p53 (s9-s10 linker in the core DNA binding domain of p53)	SGSGRNSFEVRVCACPGRD	Domain that forms part of a binding surface for MDM2 that is involved in signalling p53 ubiquitination. The peptide inhibits p53 degradation by MDM2 with an $IC_{0.5}$ in the range of 20–30 μM
BOX V_{C276A} domain of p53 (BOX V_{276})	SGSGRNSFEVRVCAAPGRD	Increase inhibition of p53 degradation by MDM2 when compared to BOX V

Constructs encoding wild-type p53, $p53^{F270A}$ and $p53^{F270A/6KR}$ were *in-vitro* translated. The latter construct consists of the introduction of the F270A mutation in a 6KR background, a mutant form of p53 that can enter the nucleus similarly to wild-type p53 and which has all six ubiquitin conjugation target, C-terminal lysine residues (at positions 370, 372, 373, 381, 382 and 386) replaced by arginine [65]. The *in-vitro*

translations of the above mentioned constructs were performed with Rb I (5mM), Box V (5mM) and Box V_{276} (5mM) in the presence or absence of proteasome inhibitor Ada-$(Ahx)_3$-$(Leu)_3$-vinyl sulphone. $p53^{F270A/6KR}$ displayed high-molecular-mass adducts similar to that obtained with $p53^{F270A}$. The addition of proteasome inhibitor did not have an effect on the high-molecular-mass banding of mutant p53. Addition of retinoblastoma peptide I resulted in an attenuation of the high-molecular-mass adducts of *in-vitro* translated $p53^{F270A}$ (Figure 3.6 (**C**) *Lanes 12 and 17 vs Lane 16 and 21*) and also, but to a lesser extent, of *in-vitro* translated $p53^{F270A/6KR}$ (Figure 3.6 (**E**) *Lane 12 vs 16*). No significant reduction was observed with Box V or Box $_{V276}$. These results indicate that the majority of mutant p53 ubiquitination *in-vitro* occurs on lysine residues that are not in the C-terminus since $p53^{F270A/6KR}$ displayed similar adducts to $p53^{F270A}$.

To further confirm that mutant and wild-type p53 are not present in different cell compartments an immunohistochemical approach was adopted. H1299 cells transfected with wild-type p53 or $p53^{F270A}$ were permeabilized 24 hours post transfection and incubated with anti-p53 antibody (DO-1), anti-PDI endoplasmic reticulum marker antibody followed by DAPI staining. Mutant $p53^{F270A}$ was also incubated with caspase inhibitor (Z-VAD (OMe)-FMK (20μM)) for 6 hours prior to permeabilization. No significant difference was observed in cellular location of $p53^{F270A}$ (Figure 3.7 as indicated) or wild-type p53 (Figure 3.7 as indicated) with the protein found to be overexpressed heterogeneously throughout the cell. Interestingly, however, addition of caspase inhibitor to $p53^{F270A}$ (Figure 3.7 as indicated) expressing cells resulted in an enhanced signal of p53 observed at the periphery of the cell outside the nucleus and outside the endoplasmic reticulum.

Figure 3.6

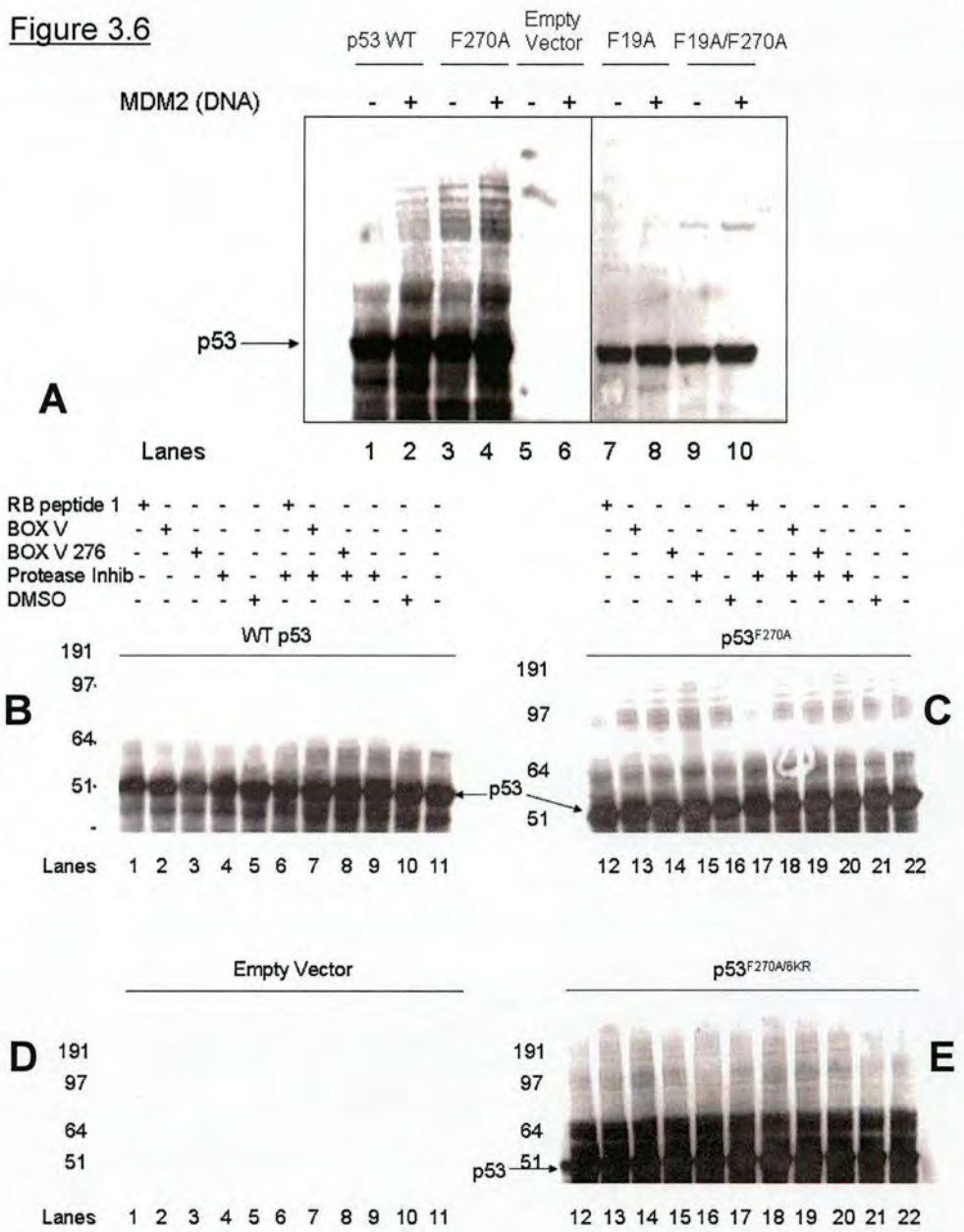

Figure 3.6 Mutant p53 is susceptible to ubiquitination *in vitro*.
(**A**) Co-translation of MDM2 with mutant p53 in reticulocyte lysates stimulates ubiquitination *in vitro*. Reticulocyte lysates containing co-translated MDM2 (+) or vector control (−) and p53 protein isoform (as indicated) were incubated at 30°C. After 90 min the reactions were quenched and the material was processed for immunoblotting to reveal p53 protein (arrow) and high-molecular-mass modifications of the indicated p53 protein isoforms. (**B**), (**C**), (**D**) and (**E**) *In vitro* translation of p53 and peptide inhibition of ubiquitination. Reticulocyte lysates containing p53 WT (**B**), $p53^{F270A}$ (**C**), empty vector (**D**), or $p53^{F270A/6KR}$ (**E**) were incubated with retinoblastoma peptide I (5mM), Box V (5mM) and Box V276 (5mM) in the presence or absence of proteasome inhibitor Ada-(Ahx)3-(Leu)3-vinyl sulphone (as indicated). RB peptide I attenuated the high-molecular mass adducts of $p53^{F270A}$ and $p53^{F270A/6KR}$.

Figure 3.7

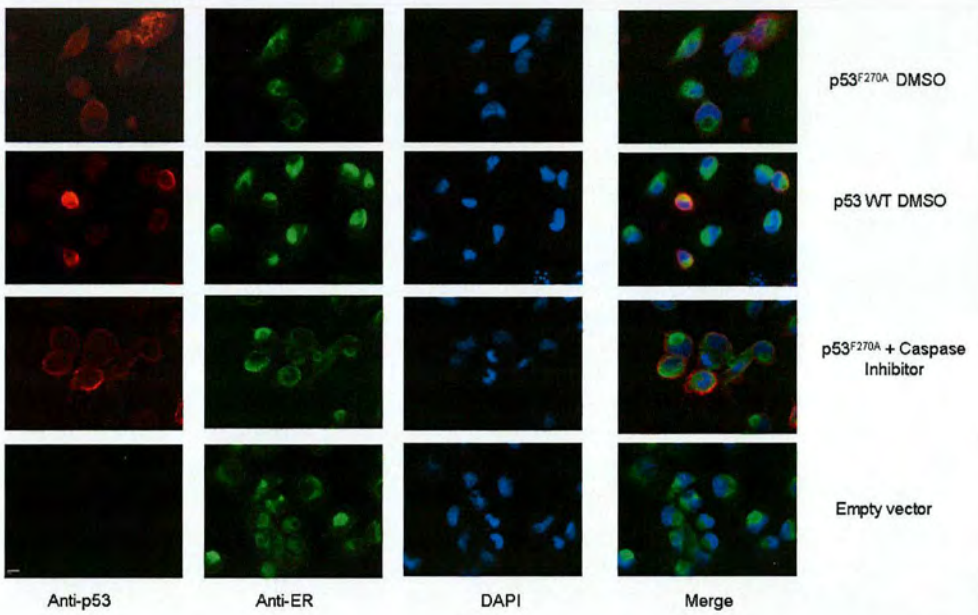

Figure 3.7 Cellular localization of wild-type and mutant p53.
H1299 cells were transfected with wild-type or $p53^{F270A}$ as indicated. 24 hrs post transfection, cells were fixed, permeabilized, and probed with DO-1 antibody. The nucleus was stained with with 4_,6-diamidino-2-phenylindole (*DAPI*) and anti-PDI endoplasmic reticulum. No significant difference was observed in cellular location of $p53^{F270A}$ or wild-type p53 with the protein found to be overexpressed heterogeneously throughout the cell with predominant nuclear staining. Addition of caspase inhibitor results in $p53^{F270A}$ localising to the cell periphery.

3.7 Immunoprecipitation coupled mass-spectrometry identifies a ribosomal pool of proteins associated with p53

An immunoaffinity coupled to mass-spectrometry approach was employed to identify novel factors that discretely discriminate between mutant and wild-type p53. $p53^{R175H}$ expressing baculovirus was used to infect insect *Spodoptera frugiperida* cells followed by precipitation with DO-1 antibody cross-linked to sepharose beads. Immunoblotting with anti-p53 antibody (DO-1) of the protein eluates confirmed the successful immunoprecipitation of p53 along with the high and low-molecular-mass adducts associated with the mutant form (Figure 3.8 B). Protein eluates were resolved on a 4-12 % gradient gel and stained with colloidal-blue stain. Uninfected insect cells were used as a control to eliminate false positives. Protein bands stained in the $p53^{R175H}$ infected cell eluates but absent in the uninfected control eluates were cut out with a scalpel for identification with nano-spray-LC-MS/MS.

The use of sepharose beads that directly cross-link the antibody via an NHS-ester moiety significantly reduced the background from control un-infected immunoprecipitation (Figure 3.8 (**A**) and data not shown). Nonetheless, despite the antibody being cross-linked to the sepharose beads, a small amount of antibody bled into the eluates from uninfected cells.

Table 3.2 summarizes the significant protein hits obtained from the colloidal blue stained gel slices. It is important to point out that the top hits for most of the proteins identified were not from the protein database of the species used in this study, namely *Spodoptera frugiperida*, possibly because the genome of this species has not been completely sequenced. In this respect, the high scoring matches from other closely related species are of interest because they are likely to be homologous to the unknown

protein in *Spodoptera frugiperida*. Interestingly, all the gel slices resulted in the p53 protein having the highest significance according to the Mowse ion score. This data corroborates the immunoblotting data showing that indeed all the DO-1 positive high and low-molecular mass bands are p53 peptides. Furthermore, all the other proteins identified, with the exception of ADP/ATP translocase and proteasome subunit alpha type 5, were ribosomal or ribosome-associated proteins. It is however, puzzling that no co-eluting chaperones were identified in this study. A possible explanation for this observation is that maximal expression of exogenous p53 by the baculovirus impedes the expression of host molecular chaperones. In fact a study by Yun and co-workers showed that there is indeed a rate-limited expression of endoplasmic reticulum molecular chaperones that is strongly associated with the maximal expression of exogenous proteins obtained from baculovirus expression vector systems [135].

Ribosomal proteins L5 and L23 have been previously shown to bind MDM2 and activate p53 by inhibiting MDM2-mediated p53 degradation [136]. It is tempting to suggest that a feedback loop exists were interaction of ribosomal proteins with MDM2 and p53 modulates the ribosome filter [137] thereby altering cellular growth and proliferation.

3.8 Identification of eukaryotic elongation factor 1a as a factor that discriminates between wild-type and hyperubiquitinated p53

Eukaryotic elongation factor 1a (eef1a) can bind nascent polypeptide chains following their release from the ribosome [138]. Furthermore, eef1a having a central role

in translation elongation, has been demonstrated to bind damaged nascent proteins that are ubiquitinated and facilitate their delivery to the proteasome [131].

Gel Band B from the colloidal blue stained gel depicted in Figure 3.8 (**A**) resulted in the identification of eef1a. The MS/MS spectrum of tryptic peptide with sequence IGGIGTVPVGR from eef1a is shown in Figure 3.9 (**B**). Alignment of *Spodoptera frugiperda* eef1a with human eef1a1 by clustalW protein alignment program showed that the protein was highly conserved between the two species (Figure 3.9 (**A**)). Thereby, to confirm the identity of eef1a in the eluates from DO-1 immunoprecipitation of sf9 cells infected with $p53^{R175H}$, immunoblotting with anti-human eef1a was carried out (Figure 3.8 (**D**). This experiment, indeed confirmed an eef1a positive band being present in the eluate from $p53^{R175H}$ cells but not in the eluate of un-infected cells. The lower molecular mass of the eef1a positive cells from the insect eluate when compared to the marker of human cell-lysate might be due to the shorter length of the insect protein compared to the human protein, 413 amino acids vs. 462 amino acids respectively (Figure 3.8 (**D**) as indicated).

In order to verify the interaction between eef1a and mutant p53, H1299 cells were transfected with $p53^{F270A}$, $p53^{6KR}$ and $p53^{F19A}$ and clones stably expressing the constructs were selected with geneticin (Invitrogen). Although multiple clones for the above mentioned mutants were created, generation of wild-type p53 clones in this cell background proved elusive, a result which is in agreement with findings of Dumont and co-workers who were "consistently unable to generate stably transfected clones for the Arg72 [polymorphic form of p53] variant" [139]. An immunoblot with anti-p53 antibody (DO-1) of cell lysates from H1299 cells that stably express mutant forms of p53 demonstrated that $p53^{F270A}$ protein displayed similar low and high-molecular-mass

adducts to lipofectamine 2000-mediated transfection of the same construct (Figure 3.9 (**C**) as indicated). These high and low-molecular mass adducts were absent in $p53^{6KR}$ and $p53^{F19A}$ clones (Figure 3.9 (**C**) as indicated). H1299 cell lysates stably expressing $p53^{F270A}$, $p53^{F19A}$ or $p53^{6KR}$ were immunoprecipitated with anti-eef1a antibody crosslinked to sepharose beads and eluates were immunoblotted with anti-p53 (DO-1) antibody. This experiment demonstrated that eef1a specifically interacts with the unfolded and hyperubiquitinated form of p53, namely $p53^{F270A}$ (Figure 3.9 (**B**), *Lanes 5 and 6*), while no interaction could be observed with non-ubiquitinated and wild-type-similar $p53^{6KR}$ and $p53^{F19A}$ (Figure 3.9 (**B**) *Lanes 7 and 8/ 3 and 4*). eef1a should therefore be investigated more thoroughly as a potential player in the degradation pathway of mutant p53, especially in view of the recent finding that eef1a also interacts with MDM2 [140].

In corroboration with the previous finding that mutant p53 is degraded by the proteasome, it is interesting to note that the proteasome subunit alpha type 5 was identified in the mass-spectrometry approach. The proteasome subunit alpha type 5 from *Plasmodium yoelii yoelii* has a high sequence homology with human proteasome subunit zeta (data not shown). This result is not surprising since the enzymes involved in ubiquitin metabolism are highly conserved among eukaryotes, particularly since mutation of the yeast homolog DOA5 (also known as PUP2) results in the accumulation of multi-ubiquitinated proteins [141].

Figure 3.8

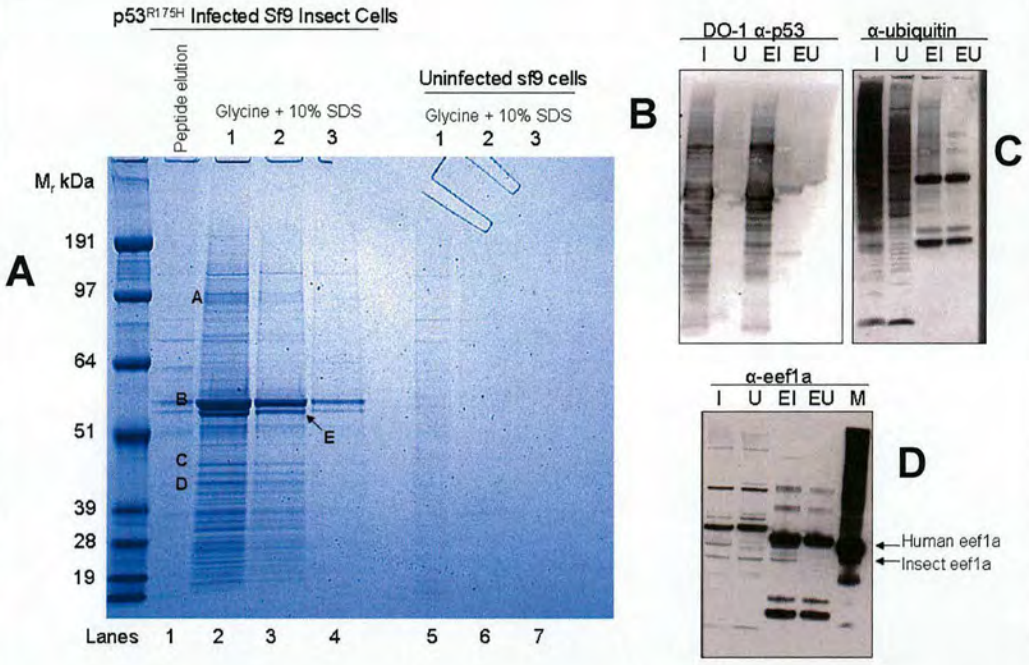

Figure 3.8 Co-immunoprecipitation of Sf9 infected with p53^{R175H}.
(**A**) Colloidal blue stain of eluates from DO-1 immunoprecipitated p53^{R175H} infected Sf9 cells. Sf9 cells were infected with p53^{R175H} baculovirus. Cells were harvested and lysed in Triton X-100 lysis buffer followed by DO-1 precipitation and 3 sequential glycine (0.1 M, pH 2.5) +10% SDS elutions. Gel Bands labelled A-E were excised with a scalpel, trypsinized and subjected to nano-spray-LC-MS/MS. Proteins identified are listed in table 2.1. (**B**), (**C**), (**D**) Immunoblots of p53^{R175H} eluates with DO-1 (**B**), anti-ubiquitin (**C**) and anti-human eef1a (**D**) (I = input p53^{R175H} infected sf9 cells; U = input uninfected sf9 cells; EI = eluate p53^{R175H} infected sf9 cells; EU= eluate uninfected sf9 cells; M = Marker for human eEF1a). Arrows indicate gel-migration size for human and insect eef1a.

Gel Slice	Protein description	Species	Nominal M_r	NCBI non redundant accession number	Number of matched peptides	Ion score (MASCOT)
A	cellular tumor antigen p53	*Homo sapiens*	44196	gi|120407068	12	437
B	cellular tumor antigen p53	*Homo sapiens*	44196	gi|120407068	13	568
	translation elongation factor eEF-1 alpha chain	*Apis mellifera*	50747	gi|58585198	4	113
	Ribosomal protein L3	*Spodoptera frugiperda*	47416	gi|18253047	8	249
	Ribosomal protein L4	*Bombyx mori*	48195	gi|112982800	5	192
	Ribosomal protein 23	*Lonomia obliqua*	31257	gi|56462224	5	182
C	cellular tumor antigen p53	*Homo sapiens*	44196	gi|120407068	10	411
	Ribosomal protein L23A	*Bombyx mori*	35943	gi|112984266	6	253
	Ribosomal protein L13	*Spodoptera frugiperda*	25005	gi|15213760	3	85
	Ribosomal protein S16	*Spodoptera frugiperda*	17113	gi|16566734	2	84
D	cellular tumor antigen p53	*Homo sapiens*	44196	gi|120407068	9	510
	Ribosomal protein L5	*Bombyx mori*	34443	gi|112983276	5	354
	Ribosomal protein L7	*Bombyx mori*	30502	gi|112983462	7	278
	ADP/ATP translocase	*Bombyx mori*	33041	gi|28261391	5	230
	Ribosomal protein S4	*Spodoptera frugiperda*	29706	gi|16566725	3	171
E	cellular tumor antigen p53	*Homo sapiens*	44196	gi|120407068	15	1107
	Ribosomal protein L3	*Spodoptera frugiperda*	47416	gi|18253047	7	399
	Proteasome subunit alpha type 5	*Plasmodium yoelii yoelii*	28629	gi|23489205	1	50

Table 3.2 Proteins Identified from agarose gel bands by nano-LC-MS/MS

Figure 3.9

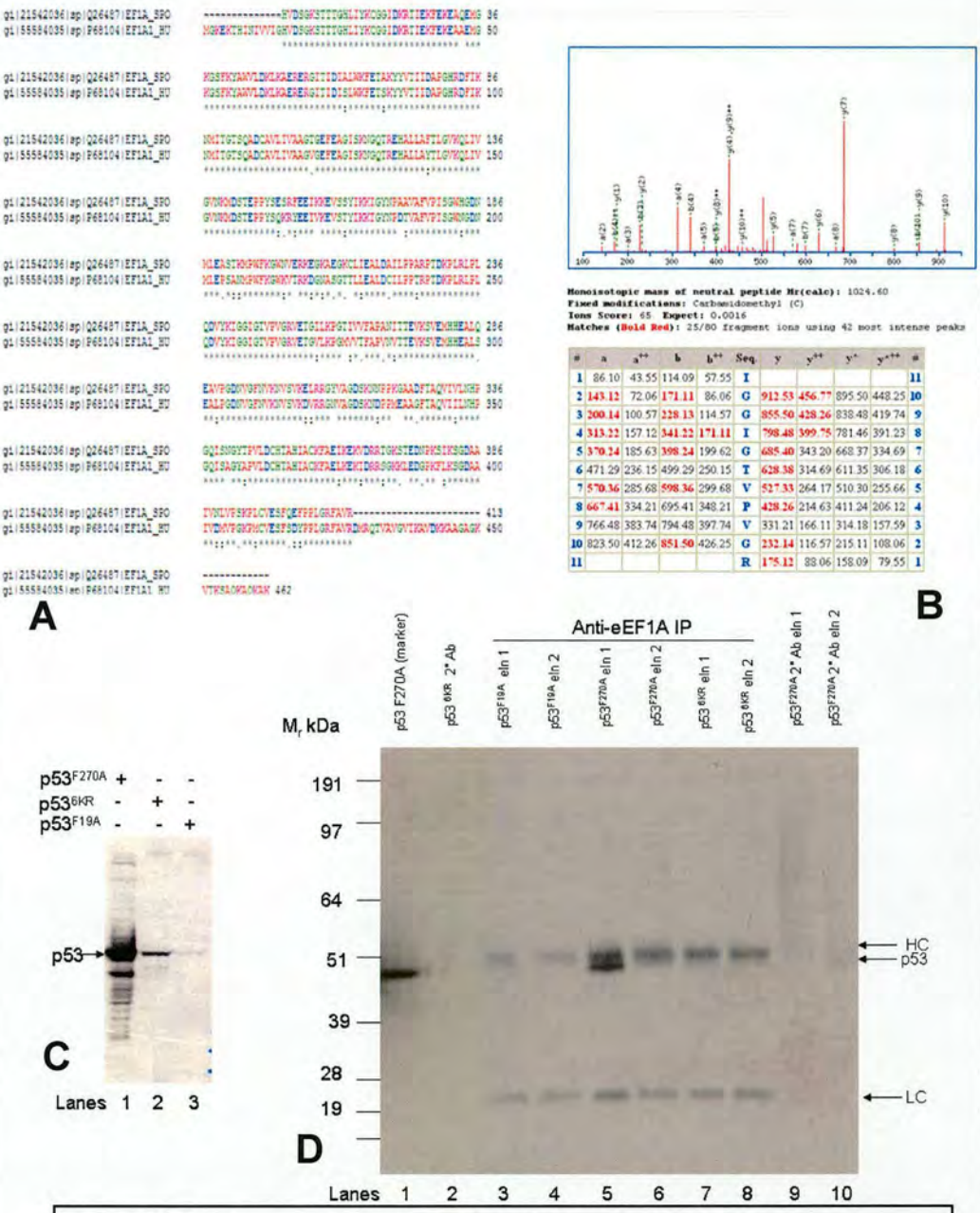

Figure 3.9 Co-immunoprecipitation of p53^{F270A} with eef1a
(**A**) ClustalW alignment of S*podoptera frugiperida* eef1a with human eef1a shows high sequence conservation between the two proteins. (**B**) MS/MS spectrum of trpytic peptide from insect eef1a. (**C**) DO-1 immunoblot of H1299 stably expressing p53^{F270A}, p536KR and p53^{F19A} (as indicated) under geneticin selection. (**D**) eef1a immunoprecipitation followed by 2 sequential glycine elutions (0.1 M, pH 2.5) of H1299 cells stably expressing p53^{F19A} (*lanes 3 and 4*), p53^{F270A} (*lanes 5 and 6*) and p53^{6KR} (*lanes 7 and 8*). Control immunoprecipitation with rabbit anti-mouse antibody crosslinked to sepharose beads are also shown for p53^{6KR} (*lane 2*) and p53^{F270A} (*lanes 9 and 10*). HC = DO-1 Heavy chain; LC = DO-1 Light chain.

3.9 Discussion

Tumour suppressor protein p53 functions as conformationally flexible transcription factor that is allosterically regulated by post-translational modifications (phosphorylation, acetylation, sumoylation, neddylation and ubiquitination) and protein-protein interactions. MDM2 has been well characterized as a binding partner to p53 with an idiosyncratic negative regulatory role on p53 stability by catalysing ubiquitination that results in the 26 S proteasome-dependent degradation of p53. Concomitantly, MDM2 itself, is also conformationally flexible and its binding to its substrates is regulated by additional cofactors such as zinc and RNA [142].

MDM2 forms a tight interaction with the p53 N-terminal domain and catalyses its monoubiquitination. In fact, mutation of a critical phenylalanine residue in the N-terminus of p53 blocks ubiquitination. Although most studies of the p53:MDM2 interaction are focussed on the N-terminal docking of MDM2 previous work from our lab has demonstrated the location of a second binding site for MDM2 in the DNA-binding domain of p53 [67, 68], using phage display of RNA-bound MDM2. This secondary site was confirmed by NMR spectroscopy of MDM2 peptides from the acidic domain and part of the zinc finger domain [143]. Furthermore, by deconstructing the MDM2 mediated ubiquitination of p53 *in vitro*, it has been shown that interaction of MDM2 with the N-terminus of p53 induces a conformational change in MDM2 that stabilizes the interaction of the acid-domain of MDM2 with a ubiquitination signal in the DNA binding domain of p53 [68].

The intrinsic instability of p53 and such a complex dual interaction with MDM2 might be important when considered from an evolutionary perspective. This allows for tight regulation of the tumour suppressor protein but also allows for a certain degree of

flexibility which is central in importance to a nodal protein at the core of numerous cellular networks.

The mutants analysed in this study, namely $p53^{F270A}$ and $p53^{R175H}$ can be classified as structural mutants since these residues play a role in maintaining the structural integrity of the DNA binding surface and are found in the β- sandwich and zinc binding regions of the DNA binding domain respectively [33]. Joerger and co-workers have determined that mutation of the phenylalanine residue at position 270 to a leucine created an internal cavity with a capacity of 51 $Å^3$ in the hydrophobic core of the β-sandwich without collapse of the surrounding structure [144]. In this study antibodies were used to characterize the degree of folding of mutant p53 vs wild-type. The PAb1620 antibody is specific for the 'wild-type' or folded conformation but does not bind to denatured, unfolded p53 [132]. DO-12 binds to denatured, destabilized mutants at amino residues 256-270 which is cryptic in wild-type p53 and becomes accessible upon denaturation. Denaturation is not necessarily accompanied by complete unfolding of a protein, but rather results in the appearance of new conformations. It is important to stress that this conformational assay has no predictive value for the conformation of a mutant in the folded state. In fact, whilst $p53^{R175H}$ and $p53^{F270L}$ significantly destabilize the core domain by 3 kcal/mol and 4.1 kcal/mol as shown by urea denaturation, the former mutation could not bind *gadd45* DNA (a transcriptional target of p53) at the permissive temperature of 20 °C (a temperature at which all mutants adopt an intrinsically folded structure) whereas the latter could bind *gadd45* DNA at a level similar to wild-type [33]. The finding that mutant p53 was unfolded with respect to the wild-type as defined by 'conformational' antibodies is due to the marginal thermodynamic stability of p53 at body temperature.

In this study the use of *in-vivo* cross-linking demonstrated that mutant and wild-type p53 have similar oligomeric status which is an important prerequisite when comparing ubiquitination levels of p53, since, remarkably, p53 in a monomeric, rather than tetrameric conformation is not ubiquitinated by MDM2 [145].

This study showed that transfected mutant p53 is ubiquitinated to a higher degree by endogenous MDM2 than wild-type p53. Comparable ubiquitination levels of wild-type p53 are obtainable only upon ectopic transfection of MDM2 suggesting that mutant p53 has a higher sensitivity to small amounts of MDM2. These results together with the observation of high level of expression of MDM2 in primary breast cancers with mutant p53 suggest that MDM2 might have a role in mutant p53 conformation [146]. Furthermore, the finding that MDM2 stabilizes the p53:DNA interaction in a chaperone-like way [147] suggests that MDM2 might function differently depending on whether the p53 substrate is native or non-native. In this light, the finding that MDM2 catalyses the neddylation of wild-type p53 [77] but not mutant p53 further points to the idea that the difference in p53 processing by MDM2 may be related to the native or non-native nature of p53.

The finding that mutant p53 transfection also leads to proteasome and caspase cleavage- dependent low-molecular mass adducts in contrast to wild-type p53 also points to a cellular detection system that discretely discriminates between mutant and wild-type p53.

One surprising finding in this study was the data acquired using $p53^{6KR}$ as a substrate for ubiquitination in the *in-vitro* translation system showing that introduction of the F270A mutation in a 6KR background leads to ubiquitination levels comparable to $p53^{F270A}$. This suggests that ubiquitination of mutant p53 occurs on lysine residues

that are not the widely reported C-terminal lysines. The data demonstrating that the level of mutant $p53^{F270A/6KR}$ ubiquitination is not different *in vitro* from that of the $p53^{F270A}$ mutant further points to ubiquitination sites that are not in the C-terminus, since $p53^{6KR}$ has all C-terminal lysine residues mutated to arginine residues. In fact a key report on the ubiquitination of p53 using a method involving *in vitro* proteolytic cleavage at specific sites after ubiquitination found that the lysines in the NH_2-terminal and DNA-binding domains of p53 are important for ubiquitination [148]. In this respect, it was found that the COOH-terminal lysine residues are not essential for p53 regulation but may contribute to a fine-tuning mechanism *in vivo* [149]. This study thereby suggests that mutant p53 ubiquitination is operating along a control pathway different from that followed by wild-type p53 and that transfected HIS-tagged ubiquitin and MDM2 cannot necessarily be employed to dissect out mutant p53 ubiquitination mechanisms. Moreover, although specific residues are normally ubiquitinated (lysines in the C-terminus and the DNA binding domain) in wild-type p53, native structure-disrupting mutations may allow other cryptic sites to be ubiquitinated.

Although *Drosophila* p53 and human p53 share much sequence and biochemical homology, one major difference between *Drosophila* p53 and human p53 is that *Drosophila* p53 lacks the consensus box I sequence found in all vertebrate p53 proteins which is located in the p53-MDM2 interaction region. Moreover, genome-wide searches in *Drosophila* have failed to identify an MDM2 homolog. Therefore, MDM2-mediated p53 degradation could be a later evolutionary event. In this study human $p53^{R175H}$ mutant was used to infect sf9 cells. Intriguingly, this experiment resulted in p53 high and low-molecular-mass peptides as seen in human H1299 cells transfected with mutant p53. In experiments to identify a eukaryotic cell component that associates

with human mutant p53 in insect cells, it was found that many proteins that co-eluted were associated with the ribosome. Previously, Marcheal *et al.* identified a ribonucleoprotein complex composed of 5S RNA, L5 ribosomal protein, MDM2 and p53 covalently linked to 5.8S rRNA [63]. Furthermore, it has been previously shown that L5 ribosomal protein, 5S rRNA, and 5.8S rRNA form a ternary complex in solution [150]. The occurrence of these complexes suggests that p53 may be involved in one or more of the following mechanisms: (i) regulation of the transcription of rRNA genes; (ii) processing of rRNA precursors; (iii) transport of ribosomes from the nucleus to the cytoplasm; and (iv) translational control. In fact, a cytoplasmic fraction of p53 as the mature protein rather than the nascent form was demonstrated to bind to a small fraction of ribosomes in which 5.8S rRNA is covalently linked to the protein [151]. Ribosomal protein L13 as identified in this study to bind p53 also binds 5.8S rRNA [152]. Moreover, probably the best characterised p53 activation involves expression of the ARF gene product [153]. When induced, $p14_{ARF}$ disrupts the interaction between p53 and MDM2 and sequesters the latter to the nucleolus [71 153]. Sherr and Webber postulated that since the nucleolus transcribes ribosomal RNA and processes pre-ribosomes for nuclear export, the p53-MDM2 complex exits the nucleus via the nucleolus, and that ARF binding to MDM2 interferes with this transport which is described as p53-MDM2 complexes 'riding the ribosome'. Rubbi and Milner described nuclear-bound p53 being readily detectable in the nucleoli of cells grown under non-stressed conditions [154]. Furthermore, Klibanov and co-workers have demonstrated accumulation of nucleolar p53 after proteasome inhibition [155]. In light of this bibliographic background supporting the nucleolar export model of p53, it is interesting to point out that ribosomal protein L7

identified in this study is in fact not a ribosomal protein but a nucleolar protein that plays a critical role in processing of precursors to the large ribosomal subunit RNAs [156]. Another possible reason for the observation of p53 bound to a ribosomal pool is that ribosomes tether molecular chaperones as the first line of defence against protein misfolding. In this light, it is interesting to point out that the ribosomal protein L23a identified as one of the p53 interacting partners in this study has some degree of homology with the *Escherichia coli* ribosomal protein L23. In *Escherichia coli* ribosomal protein L23 acts as a docking site on the ribosome for trigger factor (TF) which acts as a chaperone of nascent polypeptide chains [157]. Moreover the exposed glutamine residue at position 18 that is involved in the interaction with TF is conserved in the insect homolog [157]. The role of corresponds to the role played by Hsc70 and Mpp11 TF in mammalian cells as proteins recruited to the ribosomes to chaperone nascent polypeptide chains. DnaK is a chaperone found in the cytosol of *Escherichia coli* that assists folding of newly synthesized proteins to their native states [158]. DnaK requires ATP and its co-chaperones DnaJ and GrpE to refold a large variety of misfolded proteins through repeated cycles of substrate binding and release [92]. In a study using peptide libraries, *Escherichia coli* TF was shown to bind elongation factor Tu (EF-Tu) at sites buried within the hydrophobic interior [159]. Moreover, TF and DnaK have been shown to bind similar hydrophobic and basic residues on EF-Tu [160]. Intriguingly, EF-Tu has been demonstrated to possess chaperone-like properties with nascent polypeptide chains [161, 162]. The authors of this study argue that since two EF-Tu molecules might be involved per translation cycle, there might be some interaction between one EF-Tu molecule and the nascent peptidyl chain probably via the C-terminal 2 amino acids in the nascent chain at the ribosomal P site, which influences

efficiency of EF-Tu-dependent read-through of stop codons. Furthermore, a separate study has shown that mitochondrial EF-Tu (EF-Tumt) binds to nascent polypeptides under stress conditions, prevents thermal aggregation of proteins while promoting their refolding and also recruits damaged unfolded proteins to the mitochondrial proteasome complex post-translationally [162].

Another consequence of the binding of mutant $p53^{R175H}$ to ribosomal proteins, even though speculative, is that such binding promotes the oncogenic function of mutant p53. This stems from a study in zebra fish (*Danio rerio*) showing that many ribosomal genes act as tumour suppressors. Despite the fact that ribosomal proteins have been implicated in a wide range of biological functions independent of their role in the ribosome, the authors of the study suggest that it is a shared ribosome-associated function that allows them to be tumour suppressors [163]. Therefore by sequestering ribosomal proteins, mutant p53 might lead to reduced protein synthesis leading to a reduction of a positive regulator of apoptosis or differentiation, either of which could favour growth. Alternatively, a reduction in the number of ribosomes might alter the identity of the messages recruited to ribosomes—similar to the way that modulation of the translational capacity of mammalian cells by oncogenes such as *Ras* or *Akt* is known to alter the identity of mRNAs recruited to polysomes—changing the translation rate of growth-promoting genes [164].

In eukaryotes, the homolog of EF-Tu termed eukaryotic elongation factor 1a (eef1a) has been demonstrated to bind damaged proteins that are ligated to polyubiquitin chains and mediate the transfer to the proteasome [131]. Hence, eef1a has been shown to play an important role in protein degradation. This study demonstrated that eef1a binds selectively to hyperubiquitinated, unfolded mutant $p53^{F270A}$ but not the

folded, mutant $p53^{6KR}$ which is not ubiquitinated by endogenous levels of MDM2. Hence, this study identifies a key player in a cellular detection system that exists to discriminate between folded and unfolded proteins and interacts exclusively with mutant unfolded but not wild-type folded p53.

Intriguingly, a recent proteomic study on binding partners of MDM2 revealed an interaction with eef1a. Moreover, the binding of MDM2 to eef1a did not alter the translation function of eef1a [140]. Collectively, these results and results from the present study, suggest that eef1a might cooperate with MDM2 for the ubiquitination-mediated degradation of mutant unfolded p53. A striking study by Chen and Madura reports elevated levels of eef1a in primary human breast cancer tissues indicating a failure in the fidelity of protein synthesis resulting in the accumulation of damaged proteins in neoplastic cells [165]. Hence, further studies are warranted to biochemically characterise the interaction between MDM2, p53 and eef1a, its influence on neoplastic growth and the consequential development of novel cancer therapeutics.

4.0 Mutant and wild-type p53 chaperomes

4.1 Introduction

In the post-genomic era elucidation of protein function remains an important challenge in biological sciences. In this respect, protein-protein interactions are a key element in deciphering the intricate cellular networks, recently referred to as the 'interactome'. Mapping the interactome may better define the organization of individual molecular machines and their dynamic nature in the cells. While genetic methods like yeast two hybrid screens allow large scale systematic analysis, they also yield a substantial amount of false results. In addition, interactions requiring more than two partners or cofactors e.g. the authentic cellular environment for human proteins are not found in yeast. To overcome these limitations, pull-down assays in mammalian cells have been used. However, they require a tedious optimization of binding and washing conditions because of the high purification background they produce.

An improvement to this method was the tandem affinity purification (TAP) which requires two successive purification steps, but this method has the disadvantage of missing some transient interactions.In order to prevent loss of transient but nonetheless important proteins that interact with p53 in the mutant and/or wild-type conformation the One-STrEP purification system was employed.

MDM2 oncoprotein plays a central role in the regulation of p53 tumour suppressor protein. MDM2 binds to p53, blocks its activity as a tumour suppressor and promotes its degradation in many tumour cells. The p53 E3 ligases discovered so far are MDM2 (murine double minute clone 2 oncoprotein), PirH2 [124], COP-1 (constitutively photomorphogenic 1) [125], TOPORS [topoisomerase I- and p53-binding protein] [126], ARF-BP1/Mule [127], Synoviolin [128], CARPs [Caspase 8/10-associated RING proteins

[129]and CHIP [C-terminus of Hsc70 (heat-shock cognate 70)-interacting protein [108].In H1299 cells, overexpression of CHIP appeared to reduce the levels of co-expressed mutant $p53^{R175H}$ and to a lesser extent wild-type p53 while ablation of CHIP by siRNA resulted in an increase in endogenous p53 levels in U2OS cells. Moreover, *in vitro* CHIP appears to co-operate with UbcH5b and Hsc70 to mediate ubiquitination of mutant $p53^{R175H}$ [108]. Recent data by K. Vousden's laboratory, which are in contrast with findings reported in this study (*c.f.* Chapter 3) suggest that the MDM2 function as a ubiquitin ligase is less important in the degradation of mutant p53, which is heavily ubiquitinated in an MDM2 independent manner. The same group suggest that CHIP is the main ubiquitin ligase of mutant p53 and not MDM2 [166]. Further proteomic studies are therefore warranted to identify all ubiquitin ligases responsible for mutant p53 ubiquitination.

Molecular chaperones are a class of proteins that interact with diverse protein substrates to assist in their folding; with a critical role during cell stress to prevent the appearance of folding intermediates that lead to misfolded or otherwise damaged molecules. Consequently, heat shock proteins assist in the recovery from stress either by repairing damaged proteins (protein refolding) or by degrading them, thus restoring protein homeostasis and promoting cell survival [167]. The interaction between Hsp70 or Hsc70 and mutant p53 has been widely reported. In mammary tumour cell lines, both Hsc70 and Hsp90 were found associated with mutated $p53^{V143A}$ in the cytoplasm [168]. Mutant $p53^{Y205C}$ appears to form a complex with Hsp40 [169]. An elegant study by Whitesell *et al.* demonstrates a shift in a Hsc70, Hsp90, p23 and cyclophylin 40 chaperone complex which formed with temperature sensitive mutant murine $p53^{A135V}$ at 37° C (p53 adopting a mutant conformation at this temperature) but was absent at 30° C

(p53 adopting a wild-type conformation at this temperature) [170]. The same authors have speculated that wild-type p53 may undergo highly transient interactions with molecular chaperones. In fact, King and co-workers have demonstrated, with the use of highly purified proteins, that both mutant ($p53^{R175H}$) and wild-type p53 form an in initial complex with Hsc70 and Hsp40 under non-stress conditions. The authors argue that following this initial step, wild-type and mutant p53 diverge in molecular chaperone associations. In the case of wild-type p53, Hsp90 is tethered to p53 resulting in dissociation of the p53-Hsc70-Hsp40 heterocomplex and ultimately Hsp90-mediated p53 nuclear import. Bag-1 dissociates the Hsp90-p53 complex, so p53 can be targeted for proteolysis. In the case of mutant p53, Hsp90 and Hop do not dissociate the p53-Hsc70-Hsp40 heterocomplex thereby facilitating the stabilization and cytoplasmic sequestration of mutant p53 by masking the p53 domains required for proteolysis and nuclear import [171].

Protein–protein interactions usually involve large and flat surfaces and such interactions are difficult to disrupt by low molecular weight compounds [172]. In the case of the p53–MDM2 interaction, however, it has been demonstrated that a limited number of amino acid residues are crucial for the binding of these two proteins [134]. In fact, just three p53 amino acids –Phe19, Trp23 and Leu26 – have been found essential for the binding between the two proteins and they are inserted into a deep hydrophobic pocket on the surface of the MDM2 molecule. The first potent and selective small-molecule MDM2 antagonists, the nutlins could displace p53 from MDM2 *in vitro* with nanomolarpotency (IC_{50} = 90 nM for nutlin-3a, the active enantiomer of nutlin-3). Nutlins bind to the p53 pocket from MDM2 in a way that mimics the molecular interactions of the crucial amino acid residues from p53 [173].

The aim of this chapter was to investigate the specific interactions between the above-mentioned molecular chaperones and MDM2 with mutant ($p53^{R175H}$ and $p53^{F270A}$) and wild-type p53 ('p53 chaperome') *in vivo*. The effect of drug inhibition of Hsp90 by 17-AAG, MDM2 by nutlin-3 and X-ray induced DNA damage on the p53 chaperome was also investigated. Finally a mass spectrometric approach was adopted to identify potential new chaperones of p53.

4.2 One-strep purification of $p53^{F270A}$, $p53^{R175H}$ and wild-type p53

The one-strep purification strategy (Figure 4.1) was adopted to identify key molecular chaperones that bind to p53 mutant and wild-type *in vivo* ('the p53 chaperome'). The immunoaffinity approach using anti-p53 specific antibody DO-1 was used successfully in this work (*c.f.* chapter 3) to purify *bona fide* protein complexes. However, since DO-1 binds to the N-terminus (Box I) domain of p53 it is possible that any chaperones binding to this site might be competitively detached. Also, even though chemical crosslinking of the antibody via the Fc portion to the surface of the sepharose beads by an NHS-ester moiety decreased the degree of bleeding of the antibody in the eluate, it was not possible to eliminate this contamination completely. Taking these factors into consideration, the $p53^{F270A}$, $p53^{R175H}$ and wild-type p53 alleles were subcloned into the one-strep vector pEXPR-IBA105 containing an N-terminal one-strep tag from the pCDNA-3.1(+) vector using Eco RI and Hind III restriction sites. Lipofectamine mediated transfection of the above mentioned constructs into H1299 cells led to the expression of p53 protein, together with associated high and low-molecular mass adducts, (Figure 4.2 *Lane 1*) in the case of mutant p53 in a similar fashion to the pc-DNA3.1(+) vector encoding these alleles (*cf.* Figure 3.2 *Lane 1*).

To isolate protein complexes containing one-strep tagged p53, lysates from mutant or wild-type one-strep-p53-expressing H1299 cells and from control cells (empty vector transfected H1299) were subjected to affinity chromatography on strep-tactin macroprep columns (polymethacrylate resin). Following a wash step, bait mutant or wild-type p53 was eluted with six sequential biotin (2mM) elutions. As shown in Figure 4.2 approximately 80% of the bait p53 bound to the strep-tactin resin (Figure 4.2 *Lanes 1 vs. 2*) and was successively eluted in biotin elutions 2-6 (Figure 4.2 *Lanes 4*-8) with a peak in elution 3 (Figure 4.2 *Lane 5*). Moreover, in the case of mutant $p53^{F270A}$ and $p53^{R175H}$ the high and low-molecular-mass adducts also successfully eluted (Figure 4.2 *Lanes 4-8, as indicated*).

4.3 Effect of 17AAG on co-precipitation of MDM2 with wild-type and ubiquitinated mutant one-strep tagged p53

In order to rule out the possibility that the one-strep tag interferes with the physical binding of MDM2 to p53, H1299 cells were transiently transfected with one-strep N-terminal tagged $p53^{F270A}$, $p53^{R175H}$, wild-type p53 or control empty vector followed by strep-tactin precipitation and immunoblotting of biotin eluates with anti-MDM2 (2A10) antibody. As expected, and as shown in Figure 4.3(**A**) expression of wild-type p53 induces MDM2 protein when compared to mutant $p53^{F270A}$ or $p53^{R175H}$ (Figure 4.3(**A**) *Lane 1 and 5 as indicated*). Moreover, higher levels of MDM2 were obtained in biotin eluates from wild-type p53 when compared to mutant $p53^{F270A}$ or $p53^{R175H}$ (Figure 4.3(**A**) 90 arrow *Lane 2-4 and 6-8, as indicated comparing lower 3 panels to each other*). Interestingly, apart from the 90 kDa SDS-migrating form of MDM2 this system also precipitated a 2A10-positive MDM2 band migrating at 60 kDa

with both wild-type and mutant p53. Intriguingly, mutant and wild-type p53 display differing binding affinities to the two forms of MDM2 with a higher 90 kDa : 60 kDa ratio for wild-type p53 when compared to mutant $p53^{F270A}$ or $p53^{R175H}$ (Figure 4.3(**A**) 90 and 60 arrows *Lane 2-4 and 6-8, as indicated*). The 60 kDa form of MDM2 has been demonstrated to be a product of a p53-dependent caspase cleavage which lacks E3 ligase activity [174]. By binding to mutant p53 the cleaved form of MDM2 might exert a dominant negative effect to stabilize mutant p53.

17-AAG acts as a nucleotide mimetic that binds in the deep ADP/ATP pocket of the amino-terminus of Hsp90 ultimately blocking the assembly of an Hsp90-p23 complex implicated in Hsp90-dependent protein folding [175]. In order to investigate the effect of 17-AAG on the binding of MDM2 to mutant and wild-type p53 cells were incubated with 10 μM 17-AAG for 2hrs prior to cell-harvesting, strep-tactin precipitation and immunoblotting with anti-MDM2 antibody (2A10). As shown in Figure 4.3(**A**) addition of 17-AAG did not result in an appreciable difference in the binding of either the 90 kDa or 60 kDa forms of MDM2 to wild-type or mutant p53 (Figure 4.3(**A**) arrows *Lane 2-4 vs. 6-8, as indicated*).

As discussed in Chapter 3 mutant $p53^{F270A}$ is hyperubiquitinated in cells when compared to wild-type. In this respect, the one-strep purification system was evaluated to determine whether ubiquitinated p53 could be successfully pulled-down from cell lysates. H1299 cells were transiently transfected with one-strep N-terminal tagged $p53^{F270A}$, $p53^{R175H}$, wild-type p53 or control empty vector followed by strep-tactin precipitation and immunoblotting of biotin eluates with anti-ubiquitin antibody. Using the one-strep purification system the hyperubiquitinated forms of mutant $p53^{F270A}$ and $p53^{R175H}$ were efficiently pulled-down (Figure 4.3 (**B**) *arrows Lanes 9-12 vs. Lane 7-8*).

Morover, addition of 17-AAG (10 μM for 2 hrs) to the cells prior to harvesting resulted in a modest increase in p53-ubiquitination levels (Figure 4.3 (**B**) *Lanes 7 vs. 8; Lanes 9 vs. 10; Lanes 11 vs. 12*).

Figure 4.1

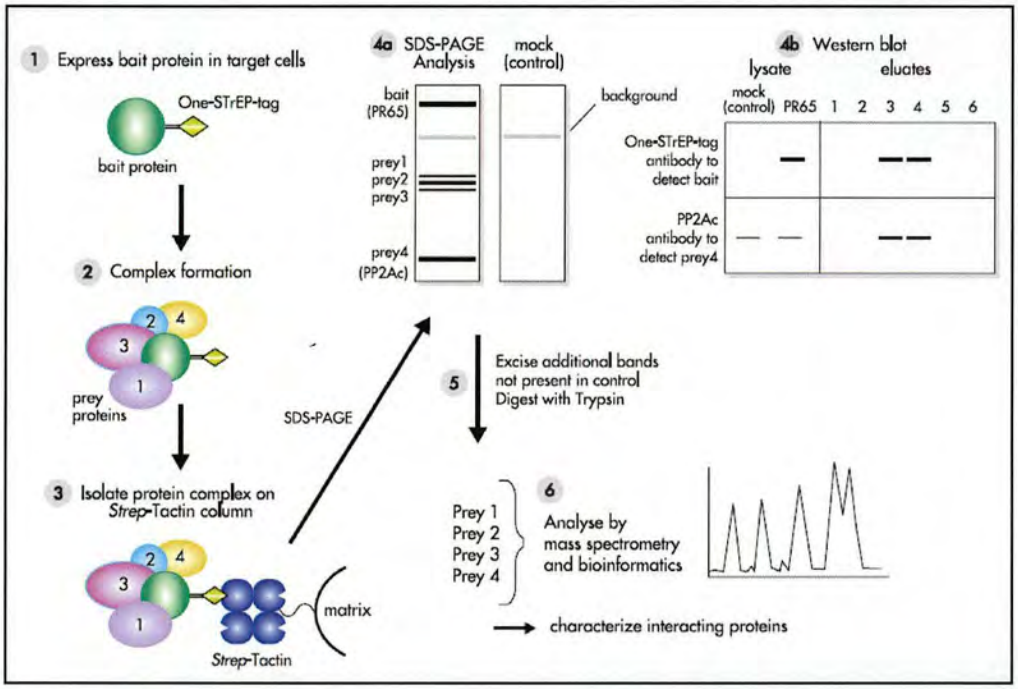

Figure 4.1 Schematic representation of One-Strep purification procedure.

Cells are transfected with the plasmid coding for the bait protein fused to the One-STrEPtag. After an appropriate expression period, cells are lysed and the bait together with bound proteins are isolated using a *Strep*-Tactin column. Following a biotin elution the proteins are resolved on an SDS-gel (4a) and specifically bound proteins e.g. proteins not appearing in the mock control can be identified. This is done by either excising the protein bands form the gel and subsequent mass spectrometric analysis or, if interaction partners are known or expected, by Western blot using specific antibodies (4b).

Figure 4.2

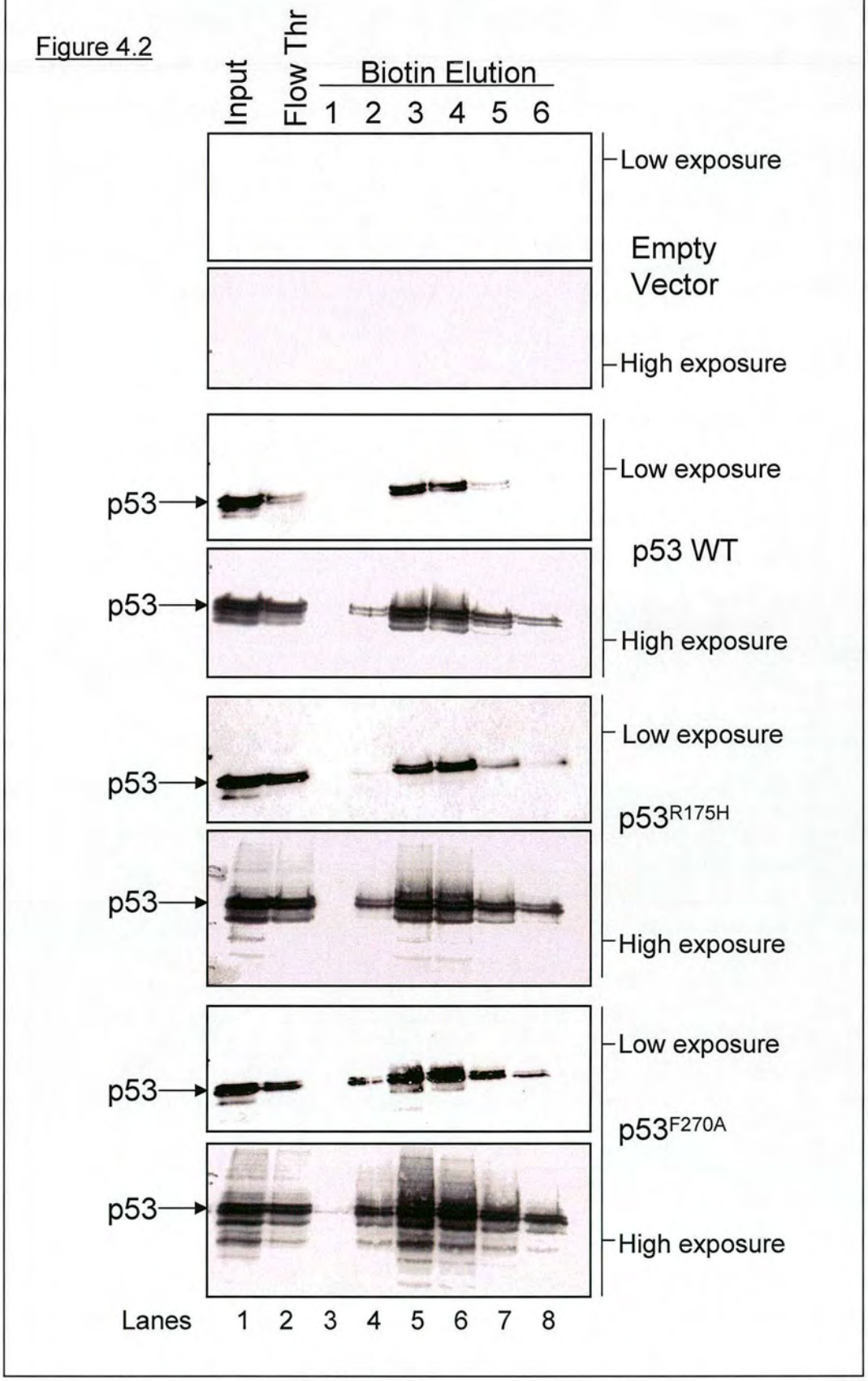
Input
Flow Thr
Biotin Elution
1 2 3 4 5 6
Low exposure
Empty Vector
High exposure
p53
Low exposure
p53 WT
p53
High exposure
p53
Low exposure
p53R175H
p53
High exposure
p53
Low exposure
p53F270A
p53
High exposure
Lanes 1 2 3 4 5 6 7 8

Figure 4.2 One-Strep purification of wild-type p53, $p53^{F270A}$ and $p53^{R175H}$.

Expression vectors (pEXPR-IBA 105) encoding N-terminus tagged One-strep wild-type p53, $p53^{R175H}$ and $p53^{F270A}$ (1.5 μg) or control empty vector were transfected in H1299 cells. The expressed proteins (Input, *Lane 1*) were purified on macroprep Strep-tactin columns; the flow-through (*Lane 2)* from the column and biotin eluates (*Lane 3-8*) were resolved on a 10% SDS-PAGE gel prior to immunoblotting for p53 (DO-1). Expression of N-terminus tagged One-strep mutant $p53^{F270A}$ or $p53^{R175H}$ yielded high and low molecular mass adducts in a similar fashion to the pc-DNA3.1(+) vector encoding these alleles. Approximately 80% of the bait p53 bound to the strep-tactin resin and was successively eluted in biotin elutions 2-6 (*Lanes 4-8*) with a peak in elution 3 (*Lane 5*). The high and low molecular-p53-positive bands also successfully co-eluted (*High exposure immunoblot*).

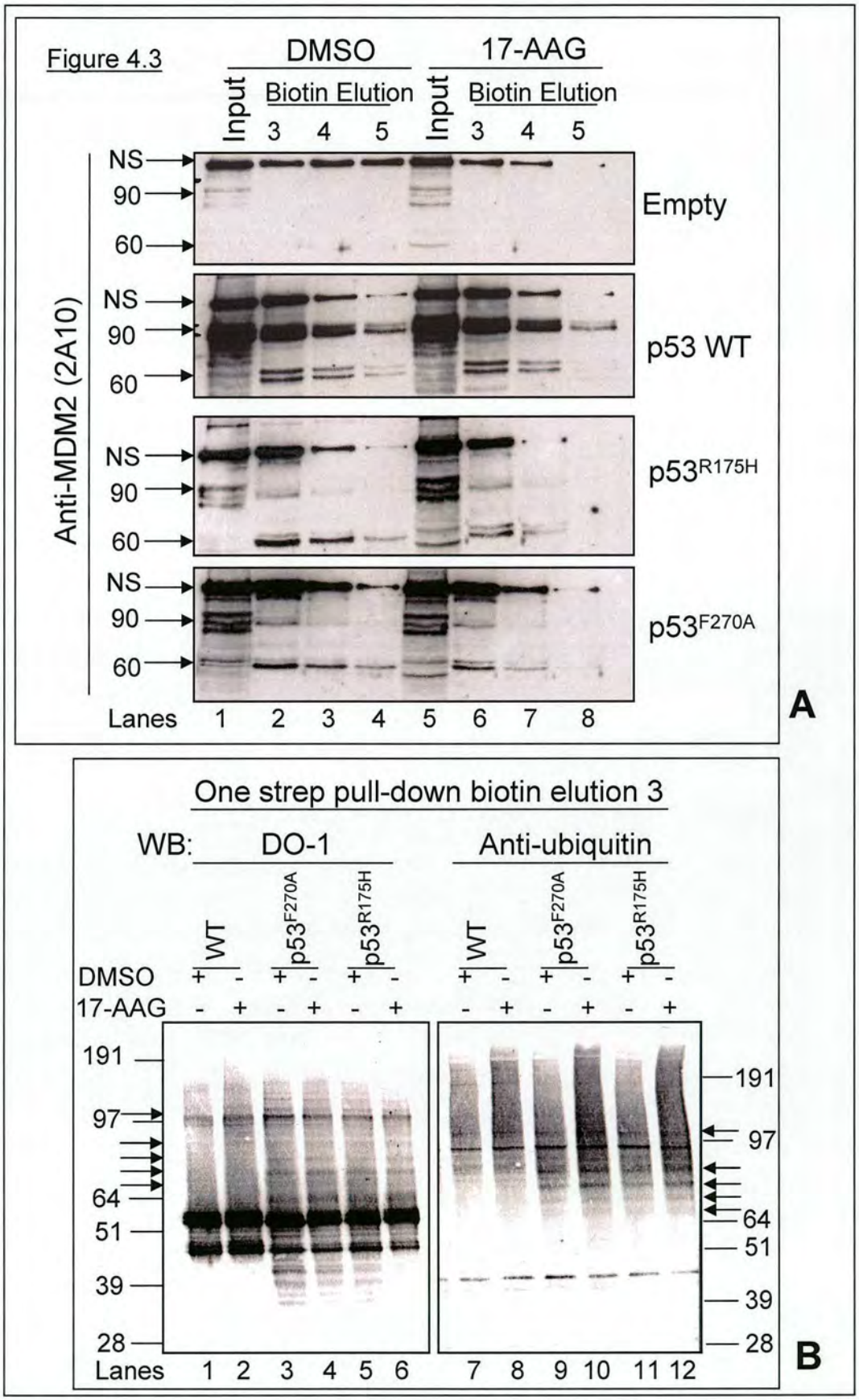
Figure 4.3
DMSO
17-AAG
Input
Biotin Elution
3 4 5
Anti-MDM2 (2A10)
NS
90
60
Empty
p53 WT
p53R175H
p53F270A
Lanes 1 2 3 4 5 6 7 8
A
One strep pull-down biotin elution 3
WB: DO-1
Anti-ubiquitin
WT
p53F270A
p53R175H
DMSO
17-AAG
191
97
64
51
39
28
Lanes 1 2 3 4 5 6 7 8 9 10 11 12
B

Figure 4.3 No effect of 17-AAG on wild-type and mutant p53 ubiquitination levels and co-precipitation of MDM2 with p53 following One-strep purification.

(**A**) H1299 cells transfected with N-terminus one-strep tagged wild-type p53, mutant ($p53^{F270A}$ or $p53^{R175H}$) or control empty vector (1.5 μg) in the presence of Hsp90 inhibitor 17-AAG (10 μM for 2 hours) or DMSO-control. The expressed proteins were purified on Strep-tactin macroprep columns. Proteins from cell lysate (Input, *Lane 1 and 5*) and biotin eluates (*Lanes 2-4 and 6-8*) were resolved on 10% SDS-PAGE and immunoblotted for endogenous MDM2 (2A10). Wild-type p53 induced endogenous MDM2 when compared to empty vector, $p53^{F270A}$ or $p53^{R175H}$ (*Lane 1 as indicated*). Mutant and wild-type p53 display differing binding affinities to the two forms of MDM2 with a higher 90 kDa : 60 kDa ratio for wild-type p53 when compared to mutant $p53^{F270A}$ or $p53^{R175H}$ (90 and 60 arrows *Lanes 2-4 as indicated*). Hsp90 inhibition by 17-AAG (10 μM for 2 hours) revealed no effect on the binding of MDM2 to wild-type or mutant p53. (*Lanes 2-4 vs. 6-8*).

(**B**) H1299 cells transfected with N-terminus one-strep tagged wild-type p53, mutant ($p53^{F270A}$ or $p53^{R175H}$) or control empty vector (1.5 μg) in the presence of Hsp90 inhibitor 17-AAG (10 μM for 2 hours) or DMSO-control. The expressed proteins were purified on Strep-tactin macroprep columns. Proteins from biotin eluates were resolved on 4-12 % gel (MOPS running buffer) and immunoblotted for transfected p53 (*Lanes 1-6*) (DO-1) and endogenous ubiquitin (*Lanes 7-12*) (on separate gels). The hyperubiquitinated forms of $p53^{F270A}$ (*arrows Lanes 9 and 10*) and $p53^{R175H}$ (*arrows Lanes 11 and 12*) were efficiently pulled-down. A modest increase in p53 ubiquitination was observed following the addition of 17-AAG (*Lanes 7 vs. 8; Lanes 9 vs. 10; Lanes 11 vs. 12*)

4.4 Effect of 17AAG co-precipitation of CHIP, HSP70 and HSP40 with wild-type and mutant one-strep-tagged p53

To investigate the interaction of mutant or wild-type p53 with CHIP, Hsp70 and HSP40, H1299 cells were transiently transfected with one-strep N-terminal tagged $p53^{F270A}$, $p53^{R175H}$, wild-type p53 or control empty vector followed by strep-tactin precipitation and immunoblotting of p53-normalised (data not shown) biotin eluates with anti-CHIP, anti-Hsp70 and anti-Hsp40 respectively. CHIP interacted with wild-type and mutant p53 to similar extent (Figure 4.4 *arrows Lanes 2-4, as indicated*) showing that this E3 ligase does not differentiate between p53 conformations [176]. This is in accordance with recent findings by Tripathi and co-workers, who show that CHIP interacts with the N-terminus of p53 which is intrinsically unstructured in both mutant and wild-type p53 [177]. Interestingly, both mutant and wild-type p53 bind to a 51 kDa CHIP-positive band that may correspond to the di-ubiquitinated form of CHIP (Abcam anti-CHIP Cat No. PC711 datasheet) (Figure 4.4 *arrows Lanes 2-4, as indicated*).

On the other hand, mutant $p53^{F270A}$ or $p53^{R175H}$ forms a more stable complex with the Hsc/Hsp70 than wild-type p53 (Figure 4.5(**A**) *Lanes 2-5 and 7-10, as indicated*). Using an Hsp70 antibody to immunoblot the biotin eluates, further demonstrated the conformation-specific interaction of the Hsp70 molecular chaperone with p53 (Figure 4.5 (**B**) *Lanes 2-4 and 6-8*). Transient transfection of H1299 thus reiterates the findings obtained in p53-expressing cell lines and tumour specimens that conformational mutants but not wild-type p53 form stable complexes with molecular chaperones [170, 178, 179] (37–39)

Protein complexes between mutant and wild-type p53 and molecular chaperone Hsp40 were readily detectable following one-strep purification. However, as for Hsp70,

Hsp40 bound with higher affinity to the unfolded conformations of p53 (Figure 4.5 (**C**) *Lanes 2-5 and 7-10, as indicated*)

The effect of Hsp90 inhibition by 17AAG on the binding affinity of CHIP, Hsp 40 and Hsp70 to mutant and wild-type p53 was evaluated by incubating the cells with the inhibitor (10 μM for 2 hrs) prior to harvesting and precipitation with strep-tactin columns. Addition of 17AAG did not statistically change on the binding of CHIP (both full-length and di-ubiquitinated) or inducible Hsp70 to mutant or wild-type p53 (Figure 4.5 (**B**) *Lanes 2-4 and 6-8*). On the other hand, however, a modest decrease in binding to constitutive Hsc70 and Hsp40 were observed upon addition of the 17-AAG (Figure 4.5 (**A**) and (**C**) *Lanes 2-5 vs .7-10, as indicated*). Further analyses are warranted to confirm or refute this observation, preferably by direct knockdown experiments on Hsp90.

Figure 4.4

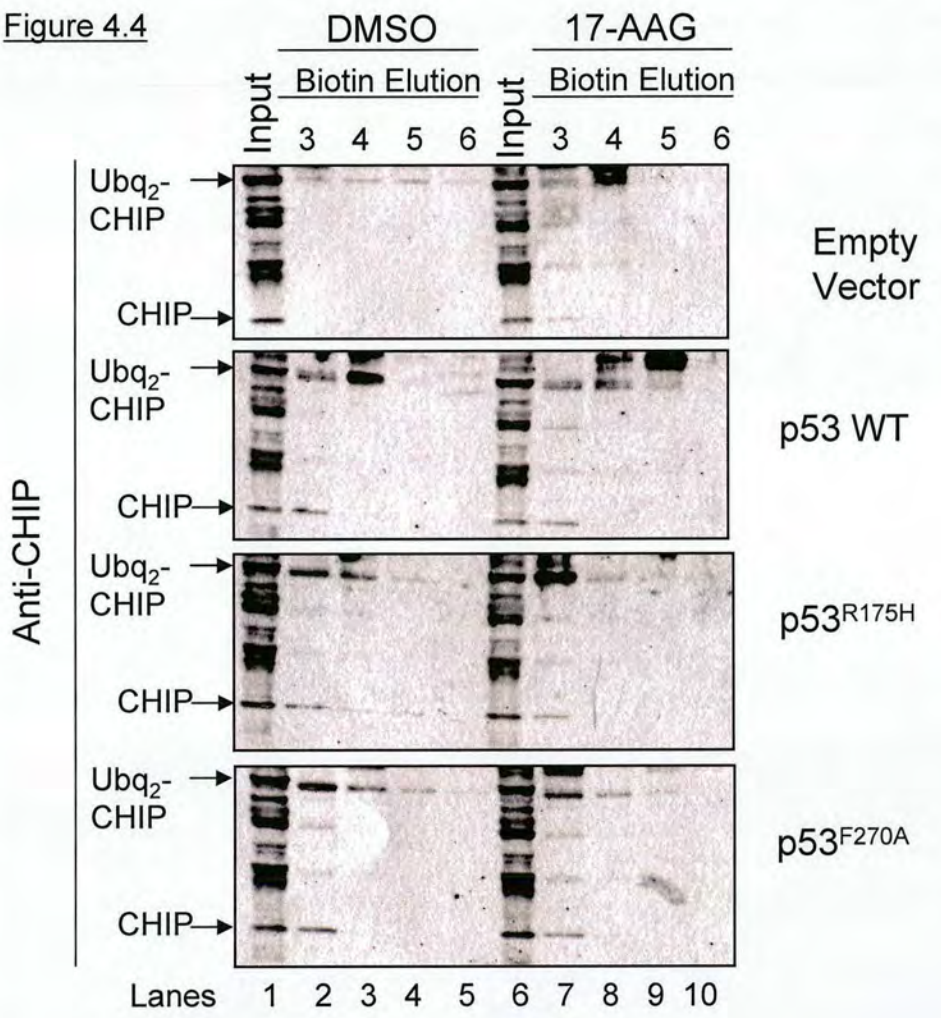

Figure 4.4 Effect of 17-AAG on on co-precipitation of CHIP with wild-type and mutant p53 following One-strep purification.

H1299 cells transfected with N-terminus one-strep tagged wild-type p53, mutant ($p53^{F270A}$ or $p53^{R175H}$) or control empty vector (1.5 μg) in the presence of Hsp90 inhibitor 17-AAG (10 μM for 2 hours) or DMSO-control. The expressed proteins (Input, *Lane 1 and 6*) were purified on macroprep Strep-tactin columns and biotin eluates (*Lane 2-8 and 7-10*) were resolved on a 4-12% precast gel (MOPS running buffer) prior to immunoblotting for CHIP (Calbiochem). Both wild-type and mutant p53 bound to CHIP and di-ubiquitinated CHIP (*arrows Lanes 2-4 as indicated*) to a similar extent. The effect of Hsp90 inhibition by 17-AAG (10 μM for 2 hours) revealed no effect on the binding of CHIP or di-ubiquitinated CHIP to wild-type or mutant p53 (*Lanes 2-5 vs. 7-10*).

Figure 4.5

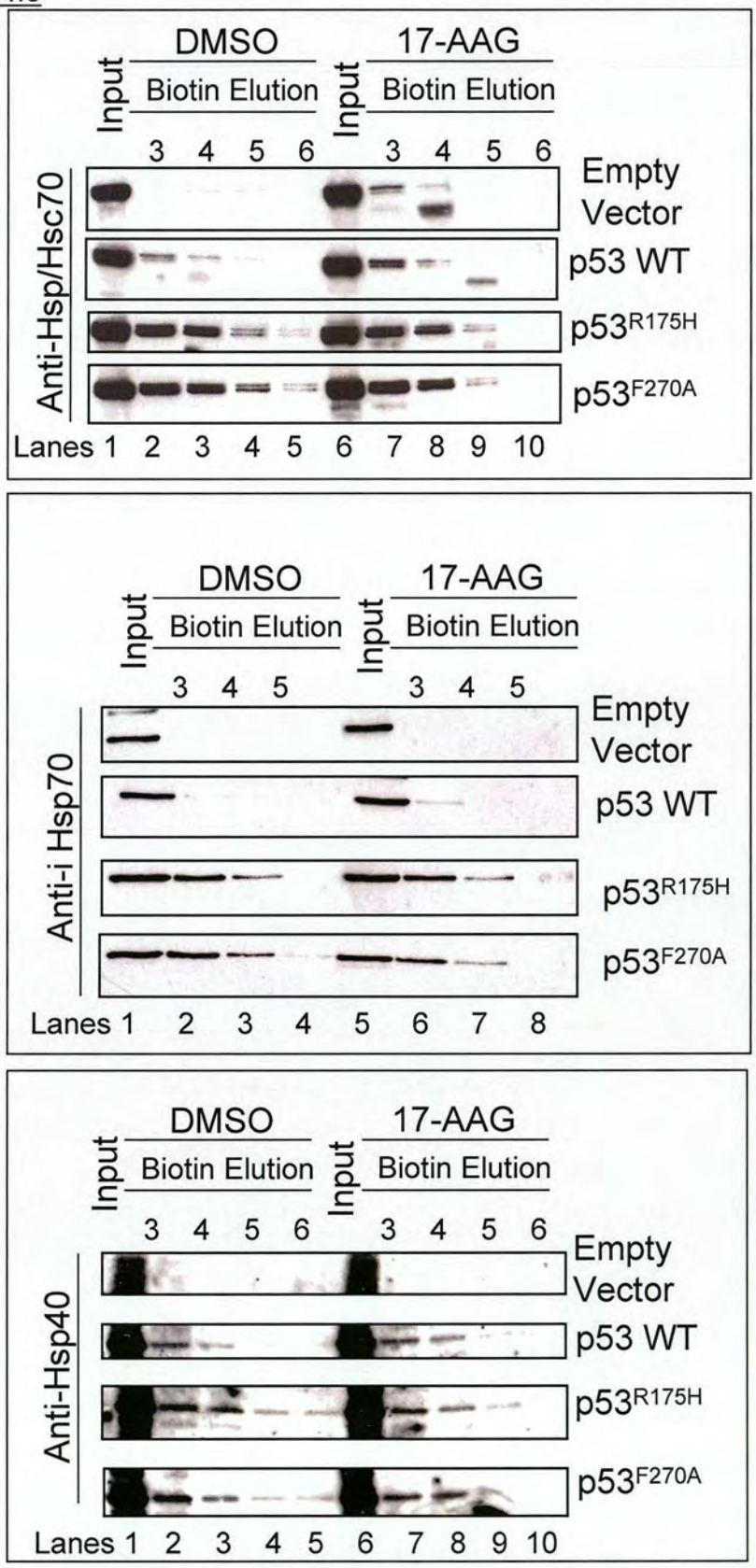
DMSO
17-AAG
Input
Biotin Elution
3 4 5 6
Anti-Hsp/Hsc70
Empty Vector
p53 WT
p53R175H
p53F270A
Lanes 1 2 3 4 5 6 7 8 9 10
A
Anti-i Hsp70
3 4 5
Lanes 1 2 3 4 5 6 7 8
B
Anti-Hsp40
Lanes 1 2 3 4 5 6 7 8 9 10
C

Figure 4.5 Co-precipitation of Hsp/Hsc70 and HSP40 with wild-type and mutant p53 following One-strep purification and effect of 17-AAG.

H1299 cells transfected with N-terminus one-strep tagged wild-type p53 mutant ($p53^{F270A}$ or $p53^{R175H}$) or control empty vector (1.5 μg) in the presence of Hsp90 inhibitor 17-AAG (10 μM for 2 hours) or DMSO-control. The expressed proteins were purified on Strep-tactin macroprep columns. Proteins from cell lysate (Input, *Lane 1 and 5 or 6*) and biotin eluates (*Lanes 2-4 or 5 and 7-10 or 6-8*) were resolved on 10% SDS-PAGE and immunoblotted for endogenous Hsp/Hsc70 (Stressgen) (**A**); Hsp70 (Stressgen) (**B**); and Hsp40 (Stressgen) (**C**). Mutant $p53^{F270A}$ and $p53^{R175H}$ bound to Hsc70 (**A** *Lanes 2-5 and 7-10 as indicated*) and Hsp40 (**C** *Lanes 2-5 and 7-10 as indicated*) with a higher affinity when compared to wild-type p53. Inducible Hsp70 (**B** *Lanes 2-4 and 6-8*) bound mostly to mutant p53 and not wild-type p53. A modest decrease in binding affinity to Hsc70 and Hsp40 was observed following the addition of 17-AAG (**A** and **C** *Lanes 2-5 vs.7-10 as indicated*)

4.5 Identification of novel interaction between Hsp 90ΔN isoform and conformational mutants of p53

To investigate the transient interaction of Hsp90 with p53 in the folded or unfolded conformation the p53 null human lung cancer cell line H1299 was used. In an initial experiment, the interaction of wild-type p53 and the conformational mutants $p53^{F270A}$ and $p53^{R175H}$ with Hsp90 was investigated following transient transfection of the p53-deficient cell line with the corresponding one-strep plasmid. Immunoblotting of biotin eluates with anti-Hsp90 antibody specific to an epitope mapped to amino acids 604-697 of human Hsp90, surprisingly revealed no distinguishable interaction between wild-type or mutant p53 and Hsp90 when compared to mock, empty vector control pull-down (Figure 4.6 (**A**) *Hsp90 arrow Lanes 2-4 and 6-8 as indicated*). The presence of Hsp90 in the empty vector biotin eluates probably arises from the interaction between Hsp90 and the streptactin-column matrix. This result is not surprising since the interaction between Hsp90 and wild-type or mutant p53 is a transient one and possibly disrupted by cell lysis (*cf*.Section 4.1), hence, future work should address this problem by *in-vivo* protein cross-linking prior to precipitation with strep-tactin beads.

Intriguingly, however, the antibody used for assaying Hsp90 also recognized a faster migrating band at approximately 75 kDa in the wild-type and mutant p53 cell lysates (Figure 4.6 (**A**) bottom 3 panels compared to top panel, ΔN arrow *Lane 1* and *5*). There are two major cytoplasmic forms of Hsp90, Hsp90α and Hsp 90β which are the inducible/major form and constitutive/minor form respectively [180]. A recent report added another isoform to the Hsp90 family, namely Hsp90ΔN, which is associated with cellular transformation [181]. Other Hsp90 analogues include Grp93 in the endoplasmic reticulum and Hsp75/TRAP1 in the mitochondrial matrix [180]. The TRAP1 and Hsp 90ΔN proteins both have a molecular mass of 75 kDa, however the former lacks the

carboxy-terminus of Hsp90α/ β, whereas the latter lacks the amino-terminus [182]. Since the antibody used in this assay binds to the carbox-terminal amino acid residues 604-697, it is possible to infer that the Hsp90-positive 75 kDa migrating band is Hsp90ΔN and not TRAP1.

Interestingly, Hsp90ΔN appeared to bind preferentially to conformational mutants $p53^{F270A}$ and $p53^{R175H}$ rather that wild-type p53 (Figure 4.6 (**A**) *ΔN arrow Lanes 2-4 and 6-8, as indicated*). The effect of Hsp 90 inhibition by 17AAG on the binding affinity of Hsp 90ΔN to mutant and wild-type p53 was evaluated by incubating the cells with the inhibitor prior to harvesting and precipitation with strep-tactin columns. Addition of 17AAG resulted in a very slight interaction between wild-type p53 and Hsp90ΔN (*cf.* Section 4.7 for better example of this interaction). A possible reason for the previous observation is that Hsp90α/β may form oligomers with Hsp90ΔN, which are disrupted following the addition of 17AAG. Addition of 17AAG did not have an effect on the binding of Hsp90ΔN to mutant $p53^{F270A}$ or $p53^{R175H}$ (Figure 4.6 (**A**) *ΔN arrow Lanes 2-4 vs. 7-8*). This surprising result arises from the fact that Hsp 90ΔN lacks the 17-AAG-specific binding site which is located in the amino-terminus of Hsp 90α/β.

In order to further confirm the binding of Hsp 90ΔN to mutant p53, biotin eluates from strep-tactin pull-downs of one-strep mutant, wild-type p53 and empty vector control transfected H1299 cells were immunoblotted with an antibody specific to Hsp 90ΔN (a kind gift of Nicholas Grammatikakis). As shown, in Figure 4.6 (**B**) Hsp 90ΔN specifically interacted with conformationally mutant rather than wild-type p53 (Figure 4.6 (**B**) *ΔN arrow Lane 6 vs. 7-8*). Furthermore, the Hsp 90ΔN-specific antibody

also recognized a faster migrating band at approximately 51 kDa in the mutant $p53^{F270A}$ and $p53^{R175H}$ pulldowns (Figure 4.6 (**B**) *arrow and question marks Lanes 5-8*). Hsp90-associated pp50 has been identified immunologically and by peptide mapping to be the 50-kDa gene product of the mammalian Cdc37 homologue $p50^{cdc37}$ [183]. It has been further proposed that $p50^{cdc37}$ may serve to target Hsp90 to a subset of protein kinases and thereby help them achieve an active conformation [184, 185]. However, the distantly related yeast Cdc37p by itself has been shown to have chaperone activity *in vitro* [186]. Moreover, Grammatikakis and co-workers have shown that $p50^{cdc37}$ and Hsp90 each interact directly with Raf-1 but that $p50^{cdc37}$ is the main determinant of the assembly of heterotrimeric complex. Disruption of the Raf-1-$p50^{cdc37}$-Hsp90 ternary complex with the Hsp90 inhibitor geldanamycin or with a dominant negative $p50^{cdc37}$ inhibits Raf-1 activity [187].

In this respect, to investigate the possible interaction of $p50^{cdc37}$ with mutant or wild-type p53 biotin eluates from strep-tactin pull-downs of one-strep mutant, wild-type p53 and empty vector control transfected H1299 cells were immunoblotted with an antibody specific to $p50^{cdc37}$. $p50^{cdc37}$ appears to interact with mutant $p53^{F270A}$, $p53^{R175H}$ and wild-type p53 (Figure 4.6 (**C**) doublet arrows *Lanes 1-4*). Moreover, $p50^{cdc37}$ appears to migrate as a doublet with non phosphorylated $p50^{cdc37}$ and phosphorylated $p50^{cdc37}$ (Figure 4.6 (**C**) bottom and top band of the doublet respectively, (Nicholas Grammatikakis personal communication) appearing to bind differentially to wt p53 and mutant p53 (Figure 4.6 (**C**) doublet arrows *Lanes 1-4*). Wild-type p53 might be bound to the phosphorylated form while mutant p53 might be bound to the unphosphorylated form. (Figure 4.6 (**C**) doublet arrows *Lanes 2 vs. 3-4*). In order to confirm or refute the differential binding of p53 to phosphorylated or unphosphorylated $p50^{cdc37}$ a

phosphoenrichment procedure ought to be adopted followed by classical phosphomapping and phosphosite mutagenesis.

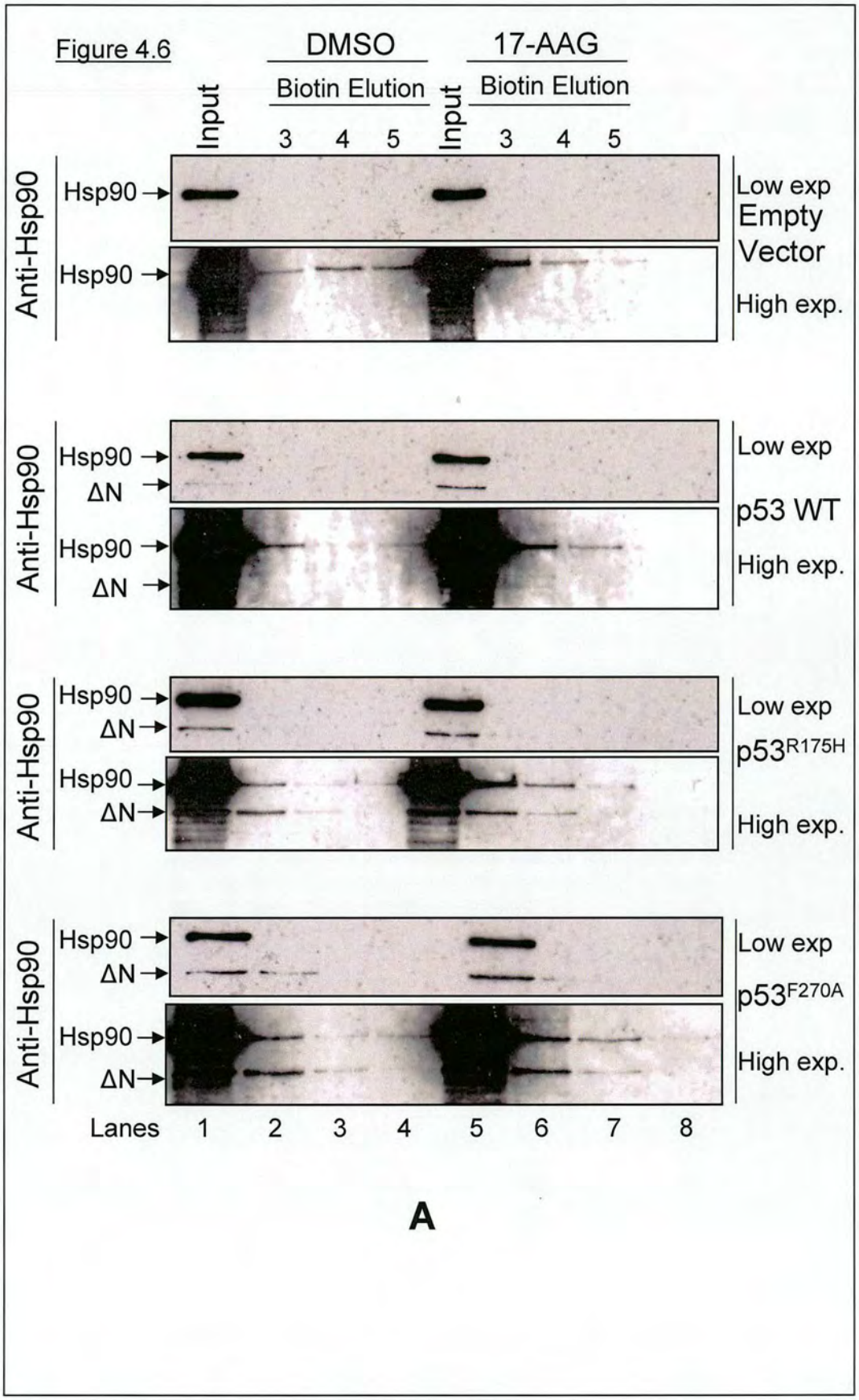
Figure 4.6
DMSO
17-AAG
Biotin Elution
Biotin Elution
Input
3 4 5
Input
3 4 5
Anti-Hsp90
Hsp90
Hsp90
Low exp
Empty Vector
High exp.
Anti-Hsp90
Hsp90
ΔN
Hsp90
ΔN
Low exp
p53 WT
High exp.
Anti-Hsp90
Hsp90
ΔN
Hsp90
ΔN
Low exp
p53R175H
High exp.
Anti-Hsp90
Hsp90
ΔN
Hsp90
ΔN
Low exp
p53F270A
High exp.
Lanes 1 2 3 4 5 6 7 8
A

Figure 4.6 (cont.)

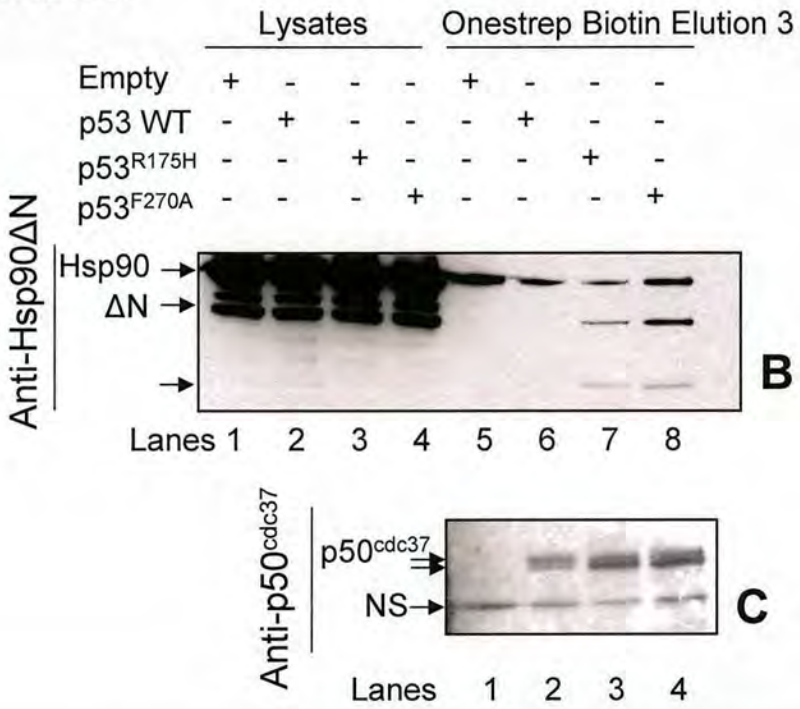

Figure 4.6 Identification of $p50^{cdc37}$ and Hsp90 isoform lacking the N-terminus that binds mutant p53.

(**A**) H1299 cells transfected with N-terminus one-strep tagged wild-type p53, mutant ($p53^{F270A}$ or $p53^{R175H}$) or control empty vector (1.5 µg) in the presence of Hsp90 inhibitor 17-AAG (10 µM for 2 hours) or DMSO-control. The expressed proteins were purified on Strep-tactin macroprep columns. Proteins from cell lysate (Input, *Lane 1 and 5*) and biotin eluates (*Lanes 2-4 and 6-8*) were resolved on 10% SDS-PAGE and immunoblotted for endogenous Hsp90 (Stressgen). There was no distinguishable interaction between wild-type or mutant p53 and Hsp 90 when compared to mock, empty vector control pull-down (*Hsp90 arrow Lanes 2-4 and 6-8 as indicated*). Hsp90ΔN bound exclusively to mutant p53 and not to wild-type p53 (*ΔN arrow Lanes 2-4 and 6-8 as indicated; see text for details*). Addition of 17AAG did not have an effect on the binding of Hsp 90ΔN to mutant $p53^{F270A}$ or $p53^{R175H}$ (Figure 4.6 (**A**) *ΔN arrow Lanes 2-4 vs. 6-8*) .

(**B**) and (**C**) H1299 cells transfected with N-terminus one-strep tagged wild-type p53, mutant ($p53^{F270A}$ or $p53^{R175H}$) or control empty vector (1.5 µg). The expressed proteins were purified on Strep-tactin macroprep columns. (**B**) Proteins from cell lysates (*Lanes 1-4*) and biotin eluates (*Lanes 5-8*) were resolved on 4-12 % precast gel (MOPS running buffer) and immunoblotted for endogenous Hsp90ΔN (kind gift from N. Grammatikakis). Hsp90ΔN bound exclusively to mutant p53 and not to wild-type p53 (*ΔN arrow Lanes 7+8 vs. 6 as indicated*). (**C**) Proteins from biotin eluates (*Lanes 1-4*) were resolved on 4-12 % precast gel (MOPS running buffer) and immunoblotted for endogenous $p50^{cdc37}$. Wild-type p53 might be bound to phosphorylated $p50^{cdc37}$ whereas mutant $p53^{F270A}$ or $p53^{R175H}$ might be bound preferentially to the unphosphorylated form (*arrows $p50^{cdc37}$ doublet Lanes 2-4 as indicated; see text for details*).

4.6 Effect of the addition of Nutlin-3, 17-AAG and X-ray irradiation on transfected onestrep p53

The effect of inhibition of MDM2 and Hsp 90 molecular chaperone activities on wild-type p53 was evaluated in H1299 cells transfected with one-strep wild-type p53. 24 hours post transfection the cells were incubated with either 8 μM Nutlin-3 and/or 10 μM 17 AAG; or DMSO control for 6 hours prior to harvesting (a longer treatment was adopted in this and following experiment when compared to previous experiments in this chapter in order to augment any subtle differences of Hsp90 inhibition) One plate of cells was also harvested 4 hours post irradiation with 5 Gy X-ray (this is the time point were p53 Ser^{15} phosphorylation [which increases p53-transactivation via increased p300 binding but has no effect on MDM2 binding] is maximal, Lisa Pang personal communication). Cells were lysed in onestrep lysis buffer and resolved on a 4-12 % gradient gel prior to immunoblotting with anti-p53 antibody (DO-1). Addition of single inhibitors nutlin-3, 17-AAG and a combination of nutlin-3 and 17AAG resulted in an increase in intensity of a DO-1 positive band at 90 kDa when compared to DMSO control (Figure 4.7 (**A**) *Lanes 2-4 vs. 1*). Moreover, this 90 kDa DO-1 positive band decreased following X-ray irradiation (Figure 4.7 (**A**) *Lane 5 vs. 1*). Since this band usually appeared predominantly with the hyperubiquitinated mutant $p53^{F270A}$ rather than wild-type p53, a conformational ELISA using DO-1 and Pab1620 was carried out to investigate the folding status of ectopically transfected one-strep tagged wild-type p53. Lysates were serially diluted in onestrep lysis buffer and the degree of wild-type conformation-specific antibody Pab 1620 reactivity was normalized against the total levels of p53 derived from levels of DO-1 binding reactivity. X-ray irradiation appeared to increase the wild-type conformation as indicated by the higher affinity of normalized

Pab 1620 affinity to X-ray treated cell lysates when compared to DMSO control cell lysates (Figure 4.7 (**B**). No appreciable difference in normalized Pab 1620 affinity was observed following the addition of single inhibitors nutlin-3, 17-AAG and a combination of nutlin-3 and 17AAG (Figure 4.7 (**B**).

The effect of nutlin-3 on the conformation ectopically transfected wild-type p53 in H1299 may not be representative of what would happen in cells expressing endogenous levels of p53, since subtle changes in p53 conformation might be cancelled out due to overexpression of the ectopically transfected p53. In this respect, the effect of addition of incremental concentrations of Nutlin-3 on endogenous levels of p53 and MDM2 was evaluated in A375 cells as well as the folding status of endogenous p53 in the same lysates defined by a conformational ELISA using DO-1 and Pab 1620. As shown in Figure 4.8 (**A**) the level of p53 increased steadily with incremental addition of nutlin-3 up to a concentration of 8 μM (Figure 4.8 (**A**) *Lanes 2-5 vs. 1*) after which it p53 levels remained constant from 8-20 μM (Figure 4.8 (**A**) *Lanes 6 and 7*). Interestingly, a significant steady increase was observed for p21 and MDM2 up to a concentration of 8 μM nutlin-3 Figure 4.8 (**A**) *Lanes 2-5 vs. 1*) after which it levelled off at 16 and 20 μM (Figure 4.8 (**A**) *Lanes 6 and 7*), thereby closely mirroring the levels of p53. The degree of p53 folding was determined by normalizing the reactivity of wild-type specific antibody Pab 1620 against the total levels of p53 derived from levels of DO-1 binding reactivity. Intriguingly, a steady increase in wild-type conformation was observed up to a concentration of 8 μM after which it levelled off at 16 and 20 μM (Figure 4.8 (**B**), once again mirroring the increase in levels of p53, p21 and MDM2.

Figure 4.7

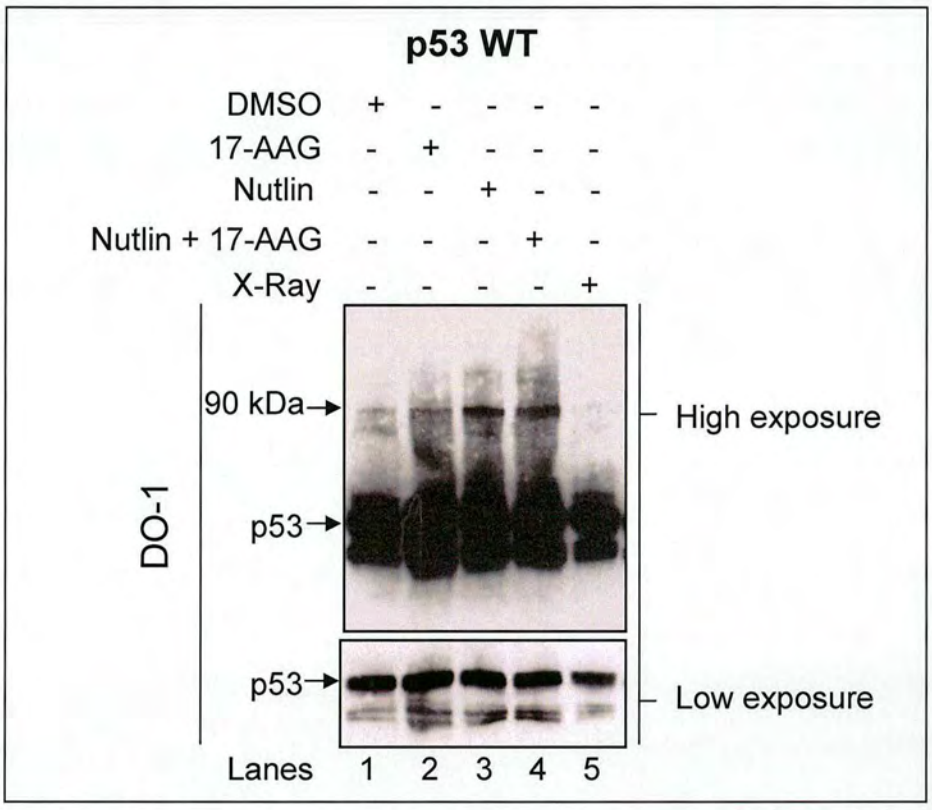
p53 WT
DMSO + - - - -
17-AAG - + - - -
Nutlin - - + - -
Nutlin + 17-AAG - - - + -
X-Ray - - - - +
90 kDa
p53
p53
DO-1
High exposure
Low exposure
Lanes 1 2 3 4 5
A

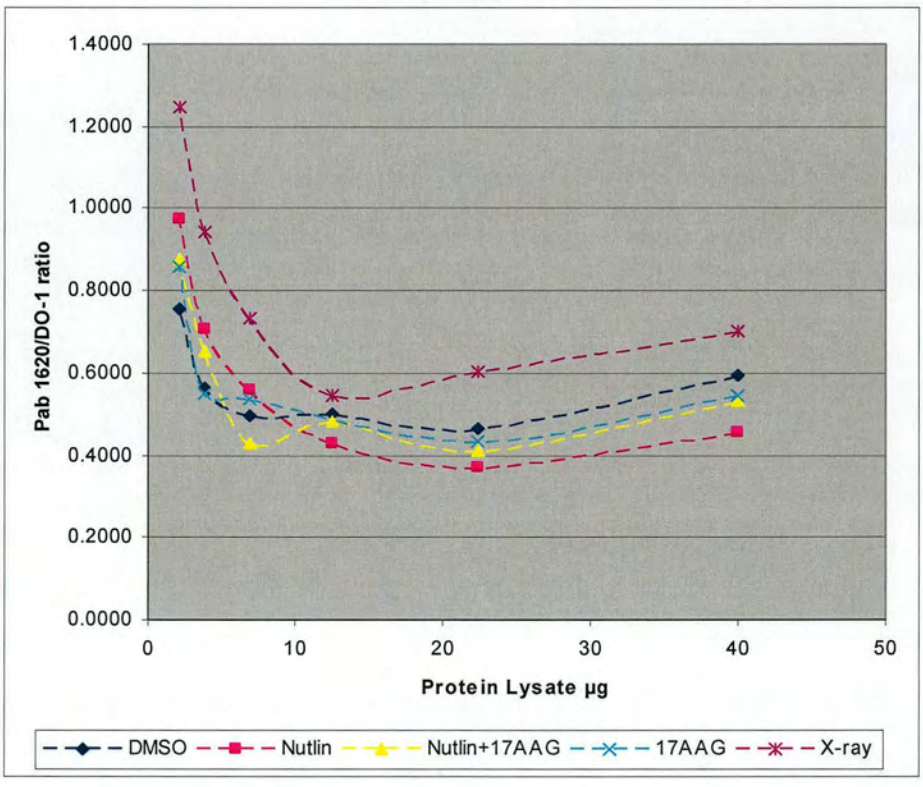
1.4000
1.2000
1.0000
0.8000
0.6000
0.4000
0.2000
0.0000
Pab 1620/DO-1 ratio
0
10
20
30
40
50
Protein Lysate µg
DMSO
Nutlin
Nutlin+17AAG
17AAG
X-ray
B

Figure 4.7 Effect of the addition of Nutlin-3, 17-AAG and X-ray irradiation on transfected onestrep p53

(**A**) H1299 cells transfected with N-terminus one-strep tagged wild-type p53 (1.5 µg). 24 hours post transfection the cells were incubated with either 8 µM Nutlin-3; 10 µM 17 AAG; 8 µM Nutlin-3 and 10 µM 17 AAG; or DMSO control for 6 hours prior to harvesting. One plate of cells was also harvested 4 hours post irradiation with 5 Gy X-ray. Cell lysates were resolved on a 4-12 % gradient gel prior to immunoblotting with anti-p53 antibody (DO-1) (*Lanes 1-5*). Addition of single inhibitors 17-AAG (*Lane 2*), nutlin-3 (*Lane 3*) and a combination of nutlin-3 and 17AAG (*Lane 4*) resulted in an increase in intensity of a DO-1 positive band at 90 kDa when compared to DMSO control (*Lane 1*). X-ray irradiation resulted in a decrease of the 90 kDa band (*Lane 5*).
(**B**) An ELISA conformation assay of cell lysates (*from 4.7 **A***) of H1299 cells transfected with N-terminus one-strep tagged wild-type p53 (1.5 µg). The signal from wild-type conformation specific antibody Pab 1620 was normalized against the total levels of p53 derived from levels of DO-1 binding reactivity. X-ray treatment led to an increase in wild-type p53 conformation when compared to DMSO control. No appreciable difference in wild-type conformation in cells treated with single inhibitors 17-AAG, nutlin-3 and a combination of nutlin-3 and 17AAG was observed.

Figure 4.8

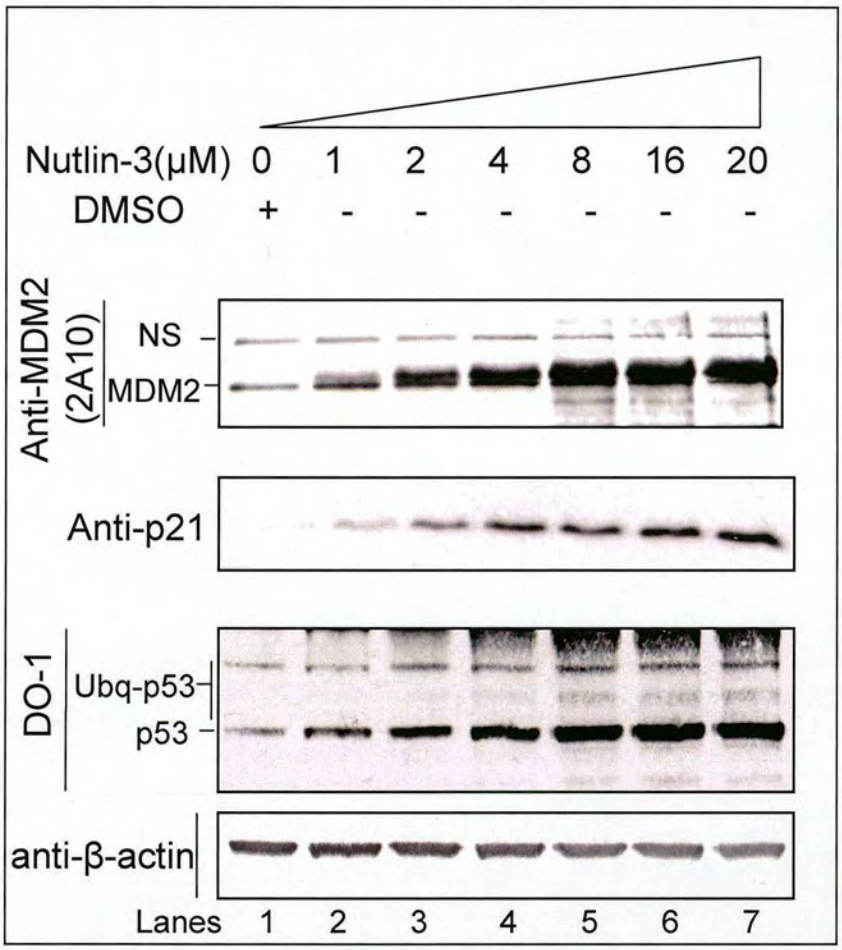
Nutlin-3(μM) 0 1 2 4 8 16 20
DMSO + - - - - - -
Anti-MDM2 (2A10)
NS
MDM2
Anti-p21
DO-1
Ubq-p53
p53
anti-β-actin
Lanes 1 2 3 4 5 6 7

A

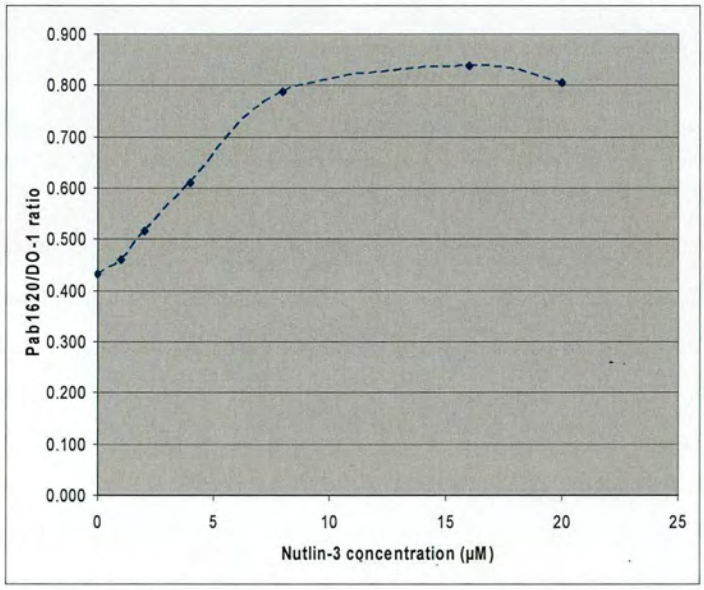
Pab1620/DO-1 ratio
0.900
0.800
0.700
0.600
0.500
0.400
0.300
0.200
0.100
0.000
0
5
10
15
20
25
Nutlin-3 concentration (μM)

B

Figure 4.8 Effect of the addition of Nutlin-3 on endogenous levels of p53 and MDM2 in A375 cells

(**A**) Nutlin titration of A375 cells. Cells were treated with DMSO control (*Lane 1*) or incremental amounts (1 to 20 μM) of Nutlin-3 (*Lanes 2-7*). Cells were harvested follwing a 6 hr incubation. Proteins from Triton X-100 cell lysates were resolved on a 10% SDS-PAGE gel prior to immunoblotting with anti-MDM2 (2A10), anti-p21, anti-p53 (DO-1) or β-actin (loading control). MDM2, p21, p53 and ubiquitinated p53 increased following nutlin-3 up to a concentration of 8 μM (Figure 4.8 (**A**) *Lanes 2-5 vs. 1*) after which they levelled off at 16 and 20 μM (Figure 4.8 (**A**) *Lanes 6 and 7*) .

.

(**B**) An ELISA conformation assay of cell lysates (*from 4.8 **A***) of A375 cells treated with DMSO control or incremental amounts (1-20 μM) of Nutlin-3. The response of wild-type conformation specific antibody Pab 1620 reactivity was normalized against the total levels of p53 derived from levels of DO-1 binding reactivity. A steady increase in wild-type conformation was observed up to a concentration of 8 μM nutlin-3 after which it levelled off at 16 and 20 μM.

4.7 Effect of the addition of Nutlin-3, 17-AAG and X-ray irradiation on binding of MDM2 and Hsp 90ΔN with transfected onestrep p53

The effect of inhibition of MDM2 and Hsp 90 molecular chaperone activities by nutlin-3 and/or 17-AAG on the binding of MDM2 and Hsp 90ΔN to mutant $p53^{F270A}$, $p53^{R175H}$ and wild-type p53 was evaluated in H1299 cells transiently transfected with the corresponding N-terminal one-strep tagged constructs. 24 hours post transfection the cells were incubated with either 8 μM Nutlin-3 and/or 10 μM 17 AAG; or DMSO control for 6 hours prior to harvesting. One plate of cells was also harvested 4 hours post irradiation with 5 Gy X-ray. Following a pull-down with strep-tactin columns the biotin eluates were normalized for p53 levels and immunoblotted with anti-MDM2 or anti-Hsp 90ΔN antibodies.

As indicated previously (*cf.* Figure 4.6 (**A**), Hsp 90ΔN co-precipitates with mutant $p53^{F270A}$ (Figure 4.9 *Lane 12*) and $p53^{R175H}$ (Figure 4.9 *Lane 6*) but not wild-type p53 (Figure 4.9 *Lane 1*) in DMSO control treated H1299 cells. Interestingly, however, wild-type p53 appears to bind to Hsp 90ΔN upon addition of nutlin-3, 17-AAG or a combination of nutlin-3 and 17-AAG (Figure 4.9 *Lanes 2-4 vs. Lane 1*). The same effect is also observed with mutant $p53^{F270A}$ and to a lesser extent with $p53^{R175H}$ (Figure 4.9 *Lane 13-15 vs.12* and *Lanes 7,8,10,11 vs. 6*). X-ray irradiation of mutant $p53^{F270A}$ (Figure 4.9 *Lane 16*), $p53^{R175H}$ (Figure 4.9 *Lane 10*) resulted in a decrease in binding of Hsp 90ΔN. In the case of wild-type p53 these modulations of Hsp 90ΔN binding correlate with the change observed in the levels of the high-molecular mass of p53 (Figure 4.7 (**A**). It is therefore possible that addition of these inhibitors and induction of DNA damage by X-rays modifies the p53 chaperome in cells.

This modification of the p53 chaperome is indeed further reinforced with the effect of the above mentioned inhibitors or X-ray induced damage on the binding of MDM2 to wild-type p53. As shown in Figure 4.10 nutlin-3 abolishes the interaction of p53 with MDM2 compared to DMSO control (Figure 4.10 *Lane 3 vs. 1*). As expected X-ray induced damage results in a decrease of MDM2 binding to p53 when compared to DMSO control (Figure 4.10 *Lane 5 vs. 1*). On the other hand, addition of 17-AAG results in an increase in binding of p53 to MDM2 when compared to DMSO control (Figure 4.10 *Lane 2 vs. 1*) and the interaction is once again reduced upon concomitant addition of nutlin-3 (Figure 4.10 *Lane 4 vs 2*). These data suggest that the p53:MDM2 interaction is dynamic and can be altered following addition of inhibitors to MDM2 or Hsp90. Further studies are therefore warranted to investigate the modification of this and other interactions by use of highly purified proteins and in-vitro assays. As shown previously in Figure 4.3A, only very low levels of the 90 kDa MDM2 bound to mutant p53 (Figure 4.10 Lanes 6-8 and 10-16). This was unchanged following the addition of inhibitors or X-rays.

Figure 4.9

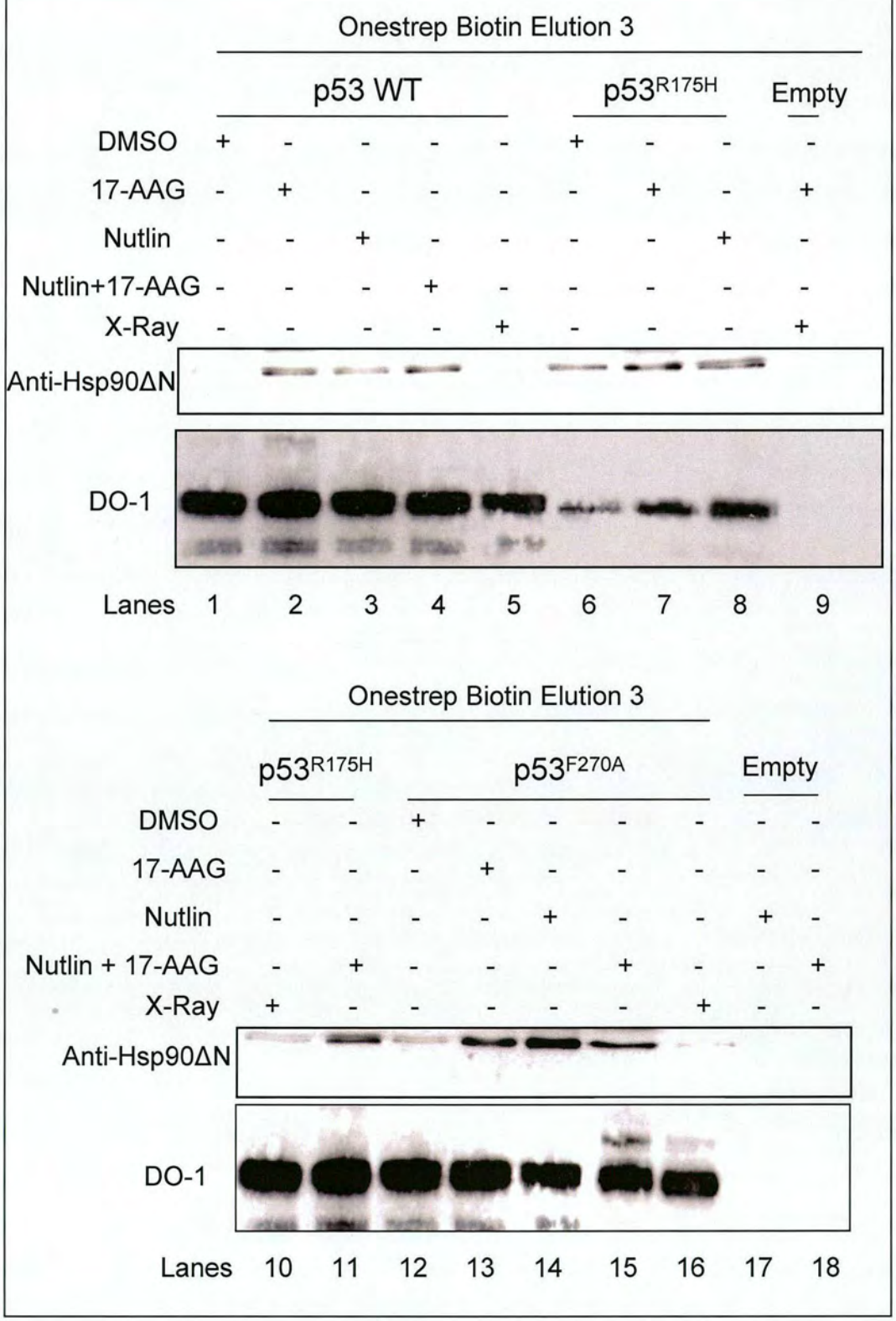
Onestrep Biotin Elution 3
p53 WT
p53R175H
Empty
DMSO
17-AAG
Nutlin
Nutlin+17-AAG
X-Ray
Anti-Hsp90ΔN
DO-1
Lanes 1 2 3 4 5 6 7 8 9
Onestrep Biotin Elution 3
p53R175H
p53F270A
Empty
DMSO
17-AAG
Nutlin
Nutlin + 17-AAG
X-Ray
Anti-Hsp90ΔN
DO-1
Lanes 10 11 12 13 14 15 16 17 18

Figure 4.9 Effect of the addition of Nutlin-3, 17-AAG and X-ray irradiation on binding Hsp 90ΔN with transfected onestrep p53

H1299 cells transfected with N-terminus one-strep tagged wild-type p53, mutant ($p53^{F270A}$ or $p53^{R175H}$) or control empty vector (1.5 μg) 24 hours post transfection the cells were incubated with either 8 μM Nutlin-3; 10 μM 17 AAG; 8 μM Nutlin-3 and 10 μM 17 AAG; or DMSO control for 6 hours prior to harvesting. One plate of cells was also harvested 4 hours post irradiation with 5 Gy X-ray. The expressed proteins were purified on Strep-tactin macroprep columns. Proteins from biotin elution 3 (*Lanes 1-18*) were resolved on 10% SDS-PAGE and immunoblotted for endogenous Hsp90ΔN. Hsp 90ΔN co-precipitates with mutant $p53^{F270A}$ (*Lane 12*) and $p53^{R175H}$ (*Lane 6*) but not wild-type p53 (*Lane 1*) in DMSO control treated H1299 cells. Wild-type p53 appears to bind to Hsp 90ΔN upon addition of nutlin-3, 17-AAG or a combination of nutlin-3 and 17-AAG (*Lanes 2-4 vs. Lane 1*). X-ray irradiation of mutant $p53^{F270A}$ (*Lane 16*), $p53^{R175H}$ (*Lane 10*) resulted in a decrease in binding of Hsp 90ΔN.

Figure 4.10

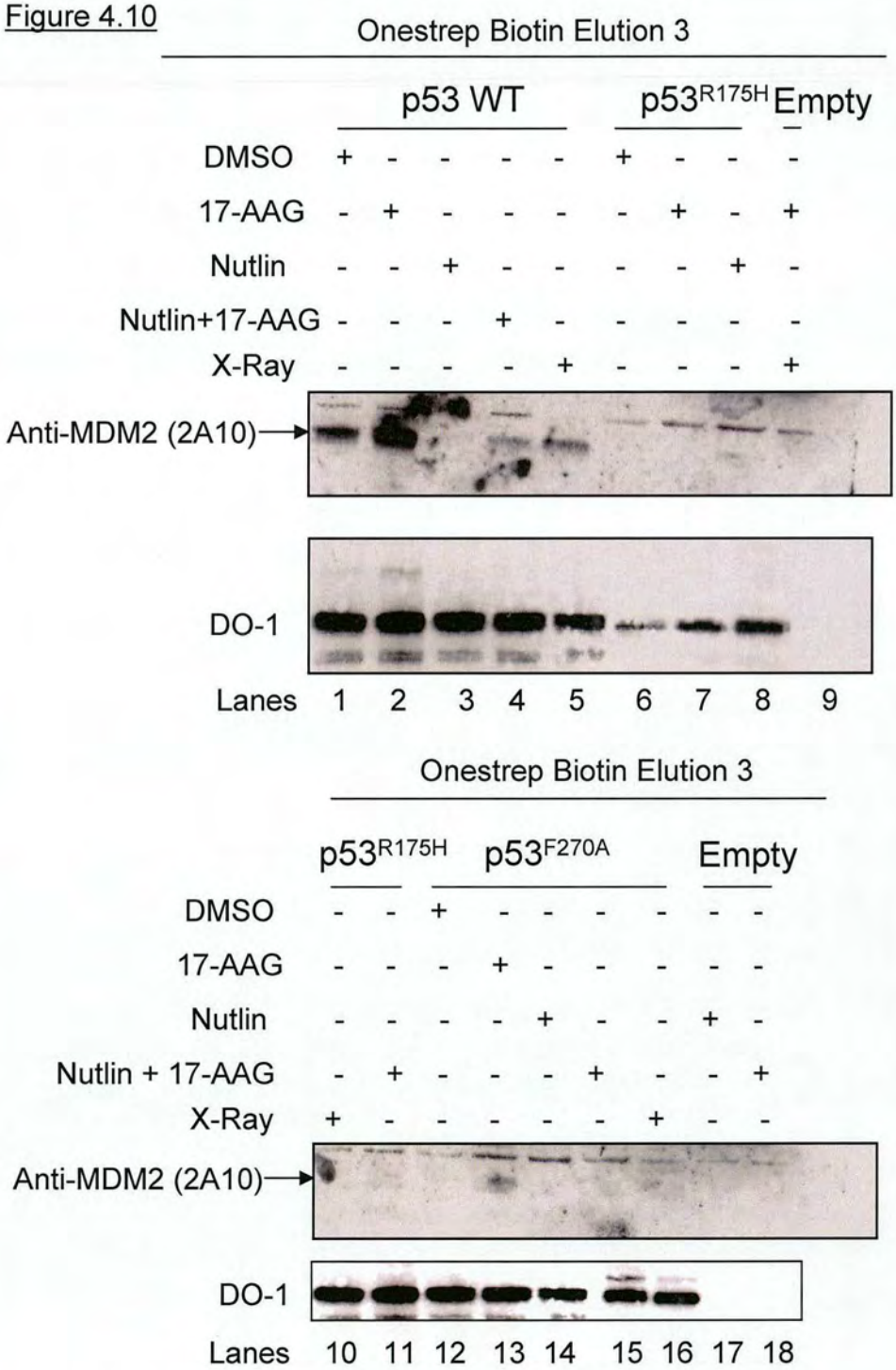
Onestrep Biotin Elution 3
p53 WT
p53R175H
Empty
DMSO + - - - - + - - -
17-AAG - + - - - - + - +
Nutlin - - + - - - - + -
Nutlin+17-AAG - - - + - - - - -
X-Ray - - - - + - - - +
Anti-MDM2 (2A10)
DO-1
Lanes 1 2 3 4 5 6 7 8 9
Onestrep Biotin Elution 3
p53R175H
p53F270A
Empty
DMSO - - + - - - - - -
17-AAG - - - + - - - - -
Nutlin - - - - + - - + -
Nutlin + 17-AAG - + - - - + - - +
X-Ray + - - - - - + - -
Anti-MDM2 (2A10)
DO-1
Lanes 10 11 12 13 14 15 16 17 18

Figure 4.10 Effect of the addition of Nutlin-3, 17-AAG and X-ray irradiation on binding of MDM2 with transfected onestrep p53

(**A**) H1299 cells transfected with N-terminus one-strep tagged wild-type p53, mutant ($p53^{F270A}$ or $p53^{R175H}$) or control empty vector (1.5 μg) 24 hours post transfection the cells were incubated with either 8 μM Nutlin-3; 10 μM 17 AAG; 8 μM Nutlin-3 and 10 μM 17 AAG; or DMSO control for 6 hours prior to harvesting. One plate of cells was also harvested 4 hours post irradiation with 5 Gy X-ray. The expressed proteins were purified on Strep-tactin macroprep columns. Proteins from biotin eluates (*Lanes 1-18*) were resolved on a 4-12 % precast gel (MOPS running buffer) and immunoblotted for endogenous MDM2 (2A10). The p53-MDM2 interaction was abolished following nutlin-3 addition (arrow *Lane 3*) and reduced following X-ray irradiation (arrow *Lane 5*) when compared to DMSO control (arrow *Lane 1*). The p53-MDM2 interaction was augmented following 17-AAG (arrow *Lane 2*) when compared to DMSO control (arrow *Lane 1*). An increase in MDM2 interaction was observed following the concomitant addition of nutlin-3 and 17-AAG (arrow *Lane 4*) when compared to nutlin-3 treatment alone (arrow *Lane 3*).

4.8 Identification of intermediate filament vimentin as a binding partner to p53 and TCP1 beta and hnRNP-M4 that specifically bind to mutant p53 by mass spectrometry

In an attempt to identify novel chaperones that bind mutant and/or wild-type p53, the onestrep purification system was used prior to analysis by nano-LC-MS/MS. Briefly, p53 null H1299 cells were transiently transfected with N-terminus tagged onestrep $p53^{F270A}$, $p53^{R175H}$, wild-type p53 or empty control vector. 24 hours post transfection the cells were harvested and lysed in one-strep lysis buffer prior to affinity purification on strep-tactin columns. The biotin eluates were resolved on 4-12% gradient gels, colloidal blue stained and gel bands (that were present in positive pulldowns but absent in mock control) excised for tryptic digestion and analysis by nano-LC-MS/MS. As a control, gel slices that migrated at a similar molecular weight in the mock empty vector were also subjected to analysis by nano-LC-MS/MS to eliminate any false positive that might have arisen due to lack of colloidal blue staining of the empty control eluate (Figure 4.11 *arrows*).

The results are summarized in Table 4.1.

The colloidal blue stained gels are illustrated in Figure 4.11. As expected, Hsp 70 was positively identified with mutant but not wild-type p53 in the gel bands migrating at 70 kDa (labelled A in Figure 4.11).

Analysis of the gel bands from mutant and wild-type p53 that migrated at approximately 50 kDa (labelled as B in Figure 4.11) showed the presence of p53 and vimentin. Additionally, in the case of mutant $p53^{F270A}$ but not $p53^{R175H}$ or p53 wild-type TCP1 beta and heterogeneous nuclear ribonucleoprotein M4 (hnRNP-M4) were also positively identified. Intriguingly, Gattoni and co-workers have demonstrated that following a 10 minute heat shock at 45°C, hnRNP-M4, which is associated with pre-

mRNA splicing, transiently leaves the hnRNP population and strongly binds to the nuclear matrix [188]. Further investigations should be undertaken to investigate whether the hnRNP-p53 interaction is specific to mutant and not to wild-type p53. Should hnRNP-M4 bind to wild-type p53, this might highlight a novel way of p53-mediated cell-cycle-control/arrest.

To investigate the possibility that binding of vimentin to p53 is altered following the addition of either 8 μM Nutlin-3 and/or 10 μM 17 AAG or DMSO control following a 6 hour incubation, H1299 cells were transfected with N-terminally tagged onestrep mutant wild-type p53. One plate of cells was also harvested 4 hours post irradiation with 5 Gy X-ray. Following a onestrep purification, the protein complexes were resolved on a 4-12% gradient gel and immunoblotted for vimentin (V9 *Sigma*) and anti-p53 (DO-1). The association of vimentin with wild-type p53 was not reproducibly affected by any of the inhibitors or X-ray showing (Figure 4.12 *Lane 2-5 vs. 1*) that the modification on wild-type p53 protein and chaperome by these inhibitors and X-rays (*cf.* Section 4.7) does not result from a shift of the p53-vimentin association.

The above mentioned inhibitors and X-ray irradiation were also used to investigate the effect on TCP1 beta binding to p53 by immunoblotting the one-strep purified eluates with anti-TCP1 beta antibody (*Abcam*). The specific association of TCP1 beta with $p53^{F270A}$ (Figure 4.12 *Lanes 12-16*) and not wild-type (Figure 4.12 *Lanes 1-5*), $p53^{R175H}$ (Figure 4.12 *Lanes 6-10*) or empty vector control (Figure 4.12 Lanes *9, 17 and 18*) was thereby confirmed by this technique. Moreover, the association between TCP1 beta and $p53^{F270A}$ was not statistically affected by the addition of inhibitors or X-ray induced damage highlighting the stability of this interaction (Figure 4.12 *Lanes 13-16 vs. 12*).

Interestingly, $p53^{R175H}$ appeared to bind to TCP1 beta only following concomitant addition of 17-AAG and Nutlin-3 (Figure 4.12 *Lane 11*).

Figure 4.11

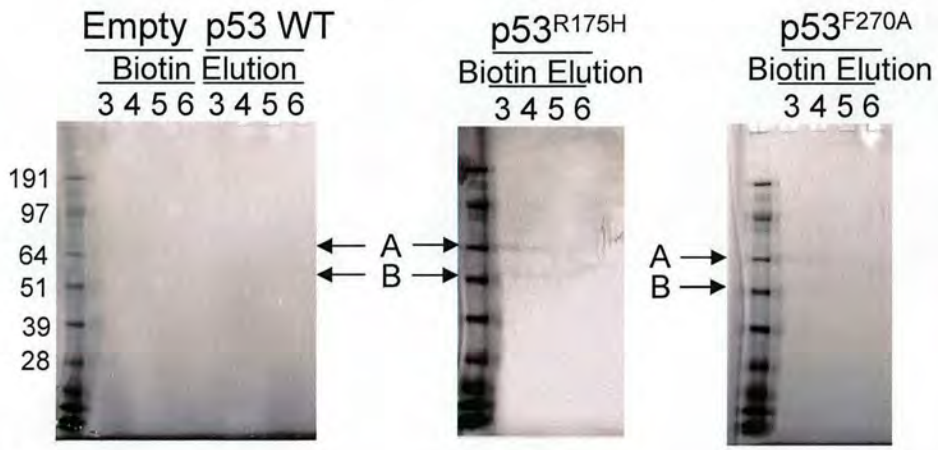

Table 4.1

Gel Slice	Protein description	Species	Nominal M_r	NCBI nonredundant accession number	Number of matched peptides	Ion score (MASCOT)
(A) $p53^{F270A}$	heat shock 70kDa protein 8 isoform 1	*Homo sapiens*	71082	gi|5729877	9	332
	P53	*Homo sapiens*	44226	gi|23491729	13	602
	vimentin	*Homo sapiens*	53710	gi|37852	5	126
	chaperonin containing TCP1, subunit 2 (beta), isoform CRA_c	*Homo sapiens*	53027	gi|119617636	2	65
(B) $p53^{F270A}$	heterogeneous nuclear ribonucleoprotein M 4	*Homo sapiens*	44641	gi|33874022	5*	43
(A) $p53^{R175H}$	heat shock 70kDa protein 8 isoform 1	*Homo sapiens*	71082	gi|5729877	5	221
	P53	*Homo sapiens*	44226	gi|23491729	14	571
(B) $p53^{R175H}$	vimentin	*Homo sapiens*	53710	gi|37852	5	95
(A) p53 WT	keratin 1	*Homo sapiens*	66198	gi|11935049	13	525
	P53	*Homo sapiens*	44226	gi|23491729	12	515
(B) p53 WT	vimentin	*Homo sapiens*	53710	gi|37852	3	76
(A) Empty	keratin 1	*Homo sapiens*	66198	gi|11935049	11	651
(B) Empty	keratin 1	*Homo sapiens*	66199	gi|11935049	15	708

Figure 4.11 Identification of intermediate filament vimentin as a binding partner to p53 and TCP1 beta and hnRNP-M4 that specifically bind to mutant p53 by mass spectrometry

H1299 cells transfected with N-terminus one-strep tagged wild-type p53, mutant ($p53^{F270A}$ or $p53^{R175H}$) or control empty vector (1.5 µg). The expressed proteins were purified on macroprep Strep-tactin columns and biotin eluates were resolved on a 4-12% precast gel (MOPS running buffer) prior to colloidal blue staining. Bands A and B from biotin eluates of each construct were excised, digested with trypsin and the resultant peptides separated and identified on an nano-LC-MS-MS.

Table 4.1 Mass spectrometric identification of gel slices A and B from Fig 4.11

Figure 4.12

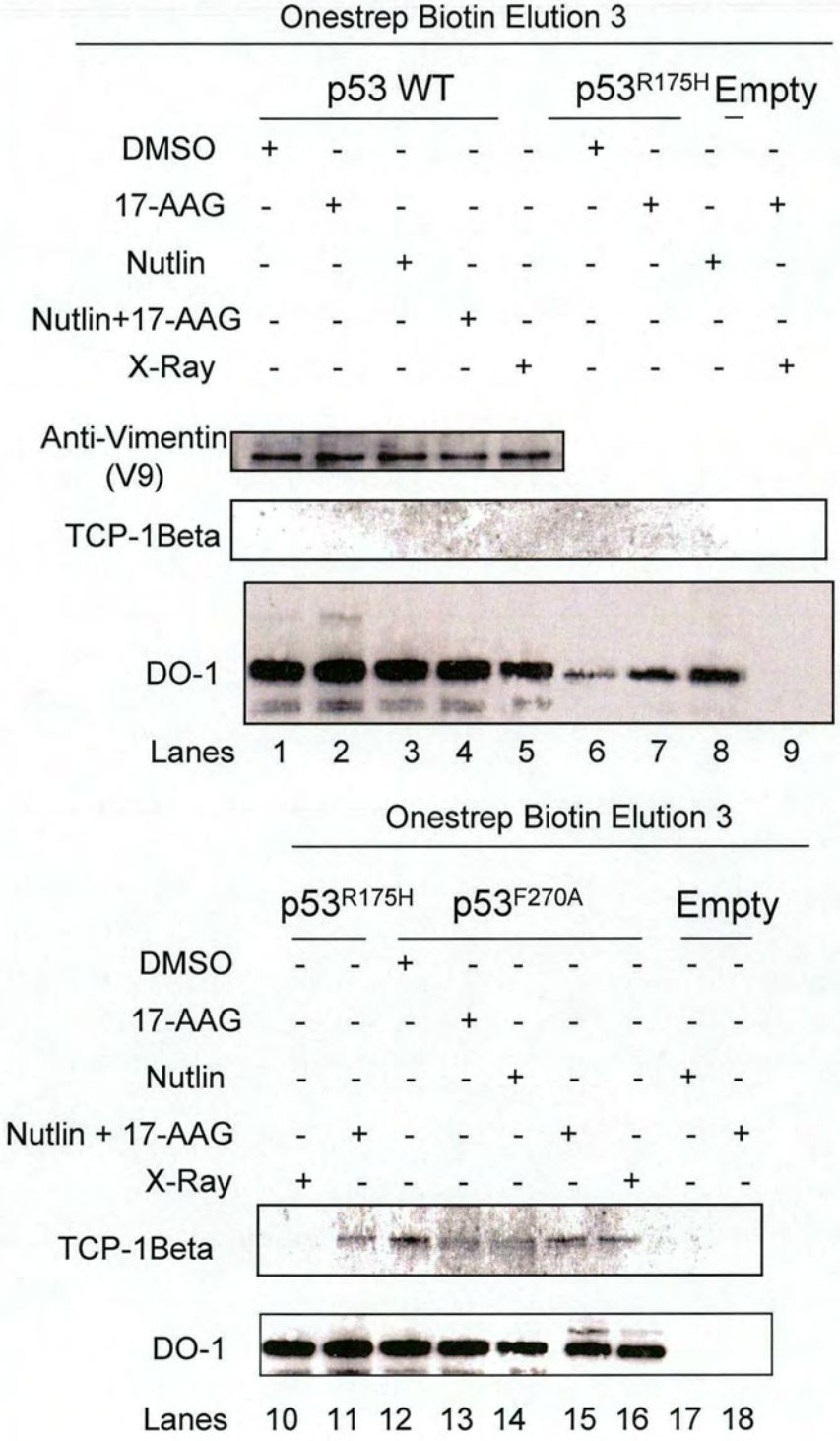
Onestrep Biotin Elution 3
p53 WT
p53R175H
Empty
DMSO + - - - - + - - -
17-AAG - + - - - - + - +
Nutlin - - + - - - - + -
Nutlin+17-AAG - - - + - - - - -
X-Ray - - - - + - - - +
Anti-Vimentin (V9)
TCP-1Beta
DO-1
Lanes 1 2 3 4 5 6 7 8 9
Onestrep Biotin Elution 3
p53R175H
p53F270A
Empty
DMSO - - + - - - - - -
17-AAG - - - + - - - - -
Nutlin - - - - + - - + -
Nutlin + 17-AAG - + - - - + - - +
X-Ray + - - - - - + - -
TCP-1Beta
DO-1
Lanes 10 11 12 13 14 15 16 17 18

Figure 4.12 Effect of the addition of Nutlin-3, 17-AAG and X-ray irradiation on binding of vimentin and TCP-1 beta with transfected onestrep p53

H1299 cells transfected with N-terminus one-strep tagged wild-type p53, mutant ($p53^{F270A}$ or $p53^{R175H}$) or control empty vector (1.5 μg) 24 hours post transfection the cells were incubated with either 8 μM Nutlin-3; 10 μM 17 AAG; 8 μM Nutlin-3 and 10 μM 17 AAG; or DMSO control for 6 hours prior to harvesting. One plate of cells was also harvested 4 hours post irradiation with 5 Gy X-ray. The expressed proteins were purified on Strep-tactin macroprep columns. Proteins from biotin eluates (*Lanes 1-18*) were resolved on 10% SDS-PAGE and immunoblotted for endogenous TCP-1 beta and vimentin. The association of vimentin with wild-type p53 was not affected by any of the inhibitors or X-ray (*Lanes 1-5 as indicated*) TCP-1 beta interacted with $p53^{F270A}$ (*Lanes 12-16*) but not wild-type (*Lanes 1-5*) or $p53^{R175H}$ (*Lanes 6-10*). $p53^{R175H}$ interacted with TCP-1 beta following concomitant addition of nutlin and 17-AAG

4.9 Discussion

Molecular chaperones associate with non-native proteins and participate in the folding of newly translated and damaged polypeptides. Recently, molecular chaperones have also been linked with protein degradation, when the chaperone associated protein is directed to the degradation machinery rather than onto the folding pathway. Chaperone associated ubiquitin ligases, such as the CHIP, are the key component for labelling chaperone substrates for degradation. CHIP binds Hsp70 and Hsp90 via an N-terminal tetratricopeptide repeat (TPR) domain together with a highly charged region. CHIP also possesses a U-box that enables the co-chaperone to interact with ubiquitin-conjugating enzymes, such as human Ubc4/5 family members. In conjunction with Ubc, CHIP mediates the ubiquitination of chaperone substrates presented by Hsp70 and Hsp90. Therefore the chaperone/CHIP/Ubc complex may actually be viewed as a multi-subunit ubiquitin ligase complex, in which the chaperone acts as the main substrate recognition factor [88].

This study has shown that both mutant and wild-type p53 interact with CHIP, a result which is in accordance with previous studies carried out in the Hohfeld and Vousden laboratories [108, 109]. However, this study also highlights an interaction between di-ubiquitinated CHIP with mutant and wild-type p53 [189].

This study has also shown that mutant p53 interacts with a higher affinity with Hsc70 and almost exclusively with induced Hsp70 when compared to wild-type p53. The binding of Hsc70 to wild-type p53 is in accordance with results obtained by King and co-workers [171]. Moreover, Hsp40 binds with a higher affinity to mutant p53 when compared to wild-type, once again in agreement with findings by King and co-workers [171]thereby adding *in-cellulo* evidence to the model that mutant p53 forms a stable mega-

complex with molecular chaperones which ultimately leads to the increased stability and degradation-resistance of mutant p53 within cells.

There is substantial bibliographical information that has highlighted the 90-kDa heat shock protein Hsp90 as a potential target of anticancer therapy [190]. Two main reasons warrant this. Firstly, the majority of Hsp90 substrates are signalling intermediates of clinical importance, which require Hsp90 for proper conformation and activity, and secondly, Hsp90 can be inhibited by anisamycins and radicicol, which bind the nucleotide-binding pocket and inhibit the ATPase activity of the molecule. Although the interaction between Hsp90 and mutant or wild-type p53 has proved elusive, possibly due to the very transient interaction between these two proteins as suggested by King *et al.* [171] an interaction was positively identified between mutant and wild-type p53 and $p50^{cdc37}$, the specific co-factor of Hsp90 [183]. Furthermore, wild-type p53 might be bound to the phosphorylated form while mutant p53 might be bound to the unphosphorylated form. In this context it is relevant to add that Nicholas Grammatikakis showed that while p53 can be found in various kinase complexes, overexpression of $p50^{cdc37}$ titres p53 away from such complexes. Therefore phosphorylation events (on p53 and/or cdc37) might also regulate the formation of p53 complexes (Nicholas Grammatikakis personal communication unpublished data). This study has also identified the specific interaction between Hsp90ΔN, an isoform of Hsp90 lacking the N-terminus and mutant p53. Although wild-type p53 does not appear to interact with Hsp90ΔN under normal conditions, addition of specific inhibitors of MDM2 (nutlin-3), Hsp90 (17-AAG) or a combination of the two results in the formation of a complex between Hsp90ΔN and wild-type p53. Interestingly, induction of DNA damage by ionizing radiation results in a decreased association of Hsp90ΔN mutant p53. The above observations occurred in

conjunction with an increase in intensity of a DO-1 positive band at 90 kDa when compared to DMSO control in wild-type p53 transfected cells. Moreover, this 90 kDa DO-1 positive band decreased following X-ray irradiation of wild-type p53 transfected cells. In the case of nutlin treated cells, an increase in wild-type conformation was observed with endogenous p53 in A375 cells. An increase in endogenous p53 protein levels was also observed in A375 cells together with a concomitant increase of p53 transcriptional targets MDM2 and p21. Together, these results suggest an alteration of the wild-type p53 protein levels and conformation upon nutlin-3 addition which results in an alteration of the interaction between mutant/wild-type p53 and Hsp90ΔN. In other words, reduction of the Hsp90/MDM2:p53 interaction/s, results in an increase of mutant/wild-type p53 interaction with Hsp90ΔN. The above results taken together indicate that Hsp90ΔN might bind to and regulate p53 in its own right. Hsp90ΔN has been shown to interact with and activate Raf in an association that does not require $p50^{cdc37}$ and with a higher affinity than HSP90 [181]. Higher levels of Hsp90ΔN expression resulted in neoplastic transformation, including interruption of gap juntional, intercellular communication and anchorage-independent proliferation [181].

Taken together, results from this study and from Grammatikakis and co-workers suggest a molecular chaperone role for Hsp90ΔN. Backing this notion, *in vitro* work from the Buchner laboratory and *in vivo* work in the Hartl laboratory [191, 192] demonstrated that the C-terminal domain of Hsp90 possesses a chaperone activity of its own which is independent from the activity residing at the N-terminus. In addition the Hsp90 C-terminal binding and release to protein substrates *in vitro* was unaffected by Hsp90 cofactors [191]. Since the C-terminal chaperone activity is apparently conserved in Hsp90ΔN, it is logical to speculate that Hsp90ΔN also possesses the capacity to bind to

and chaperone its substrate(s) in a direct manner. This study, thereby calls for direct analysis of the Hsp90/ Hsp90ΔN interaction with p53 possibly via a crystallographical approach. Furthermore, the interaction between Hsp90ΔN and mutant p53 should be further scrutinized to investigate whether it is responsible, at least in part, for the accumulation of mutant p53 to high levels in tumour cells. If this were the case, it would be important to design specific inhibitors for both the N-terminus and C-terminus of Hsp90. The recent finding of a C-terminal nucleotide binding site [193] and the characterisation of its differential nucleotide binding specificity [194] might help accomplish this task.

This study shows preliminary evidence for the interaction between chaperonin containing TCP1, subunit 2 (beta) (CCT) and the conformationally misfolded mutant $p53^{F270A}$. Chaperonins are the major molecular chaperones in *Escherichia coli*. In *Escherichia coli*, after approximately 50 residues on the nascent polypeptide chain interact with DnaJ (an Hsp40) and DnaK (an Hsp70), the growing polypeptide is passed on to the lumen of a double-ring complex formed by 14 subunits of GroEL (an Hsp60) – a chaperonin [190]. The GroEL ring can be capped by a seven-subunit ring of GroES (an Hsp10), transiently enclosing the nascent polypeptide within the GroEL cavity [190]. Many models depict a folding reaction occurring within the central lumen in the chaperonins, thereby protecting the target protein from interaction with other proteins, following which, release of the native structure occurs [195-199]. This model has been challenged by evidence that target proteins can jump between different chaperonin molecules during a folding reaction ("cycling") [200, 201]. Thus the function of chaperonins might be to unfold and release proteins that have been misfolded. Whereas GroEL is a general nascent chain factor in prokaryotes, the closest Hsp60 homologs in eukaryotes

are in mitochondria and chloroplasts (essentially prokaryotic organelles). In the cytoplasmic compartment there is a family of proteins, termed T-complex polypeptides (TCPs) that are loosely homologous with GroEL and form toroidal structures similar to that of GroEL [202]. TCP ring complexes are less abundant in cytoplasm than would appear to be necessary for general protein folding, so they may have a limited range of substrates. Significantly, tubulin and actin subunits are specific substrates that require the chaperoning of TCP ring complexes [203]. Further work using a crystallographic approach is necessary to elucidate whether CCT binds misfolded p53 in the nucleotide-free conformation, and whether following ATP binding, a closed structure of CCT, is created as observed when CCT interact to chaperone actin and tubulin [204].

This study has also highlighted a potential interaction with heterogeneous nuclear ribonucleoprotein M4 (hnRNP-M4). Although the effects on either mutant or wild-type p53 have not been investigated further studies are warranted since hnRNPs are known to have multiple functions related to other transcription factors. hnRNPs are nuclear RNA-binding proteins that form complexes with RNA polymerase II transcripts. They function in many cellular activities ranging from transcription and premRNA processing in the nucleus to cytoplasmic mRNA translation and turnover [205]. hnRNP K is involved in transcriptional activation and repression, RNA splicing and stability, translation activation and silencing, signal transduction, and chromatin remodelling [206]. hnRNP U participates in regulation of transcription of several genes. It binds to a 65 kDa Yes-associated protein, regulating its co-activation of Bax transcription [207], and it regulates Kruppel-like factor 2 transcription [207]. It regulates initiation of transcription in general by associating with both actin and Pol II [208]. HnRNP F binds to TATAbinding protein, associates with RNA polymerase II, and

interacts with the nuclear cap-binding complex. It binds to the insulin-responsive element of the rat angiotensinogen gene, regulating transcription of that gene [209]. A proteomic approach to determine protein interactions of transcription factor tonicity-responsive enhancer/osmotic response element-binding protein (TonEBP/OREBP) also identified a physical interaction with hnRNP M [210].

Interestingly, a separate proteomic approach by Moumen and co-workers identified hnRNP K as being rapidly induced by DNA damage (*via* ATM and ATR) ultimately cooperating with p53 to elicit the activation of p53 target genes and thereby trigger cell-cycle-checkpoint events. Moroever the same researchers show that hnRNP K is targeted for HDM2/MDM2-dependent proteasomal turnover in undamaged cells and that this degradation promptly ceases upon the creation of DNA damage [211].

5.0 Ubiquitination status of CHK2 naturally occurring mutations

5.1 Introduction

The Checkpoint Kinase 2 (CHK2) regulatory amino-terminus comprises an SQ/TQ cluster domain (amino acid residues 19–69), that is the target for upstream phosphatidylinositol-3 kinase (PI-3K)-like kinase (PIKK) activities, and a phosphopeptide-binding Forkhead- associated (FHA) module (amino acid residues 113–175). The carboxy-terminal catalytic domain (amino acid residues 220–486) is related to the Ca^{2+}/calmodulin- dependent protein kinase (CaMK) family. The CHK2 FHA domain consists of an 11-stranded-β sandwich that binds to phospho-threonine containing peptides [212]. CHK2 is inactive in the absence of genotoxic stress but is activated in the presence of DNA double stranded breaks (DsBs). Activation of CHK2 occurs via the ATM dependent phosphorylation of CHK2 on T68. Following phosphorylation at T68 CHK2 dimerize at the FHA domains leading to transactivation of other Chk2 proteins via phosphorlyation at T383/T387. Chk2 also undergoes autophosphorlyation at S516 and T68 [6]. Two oncogenic mutations reside within the FHA domain, namely R145W and I157T. These mutations have been shown to reside on one face of the FHA β sandwich domain, remote from the site of peptide binding. The R145 residue is located on the β5 and forms the core of a network of hydrogen bonding, nonpolar, and van der Waals interactions involving constellation amino acids on the neighbouring β strands [212]. Other CHK2 inactivating, cancer-associated mutations involve the common frameshift delC1100 and delT1422 mutations which encode premature stop codons within the catalytic domain, and the resulting truncated mutant proteins are both inactive and unstable [213]. A novel breast cancer-derived CHK2 frameshift mutant insA1368 encodes a premature stop codon within the kinase domain,

resulting in expression of a stable protein that is mislocalized to the cytoplasm. Interestingly, the breast cancer expressing the insA1368 mutant was found to be resistant to the chemotherapeutic agent doxorubicin, a characteristic normally associated with mutated p53 in these tumours. Thus, cytoplasmic localization of CHK2 may be a novel marker for breast cancers that are drug resistant [214].

Protein phosphatases comprise several families of enzymes that catalyse the dephosphorylation of intracellular phosphoproteins, thereby reversing the actions of protein kinases. This critical property of the reversibility of intracellular protein phosphorylation allows for great sensitivity of control and integration of cellular regulation. Protein phosphatases, however, must not be considered simply as passive 'off-switches', since they are intricately regulated, particularly in response to extracellular stimuli [ix]. Protein phosphatase 2C (PP2C) exists as two isoforms, with catalytic subunits of 42 and 44 kDa. It is completely dependent on magnesium ions for activity. The amino acid sequence of PP2C is unrelated to its other family members PP1, PP2A or PP2B. The best candidates for PP2C mediated dephosporylation are: inhibitor of kappa light polypeptide gene enhancer in B-cells, kinase beta (IKKbeta), mitogen-activated protein kinase kinase kinase 7 (MAP3K7), cyclin-dependent kinase 2 (CDK2), AMP-activated protein kinase and p53 [215-218].

CHK2 is critical for DNA-damage induced apoptosis, since the CHK2 null cells from knockout mice showed remarkable resistance to ionizing radiation [219]. Consequently, it is important to understand how CHK2 is degraded in cells. Therefore, the aim of the following chapter was to elucidate the ubiquitination status of wild-type and mutant CHK2 in a cellular system *in vivo*. An immunoaffinity approach coupled

with mass-spectrometry was used to identify PP2C as a potential novel binding partner of CHK2.

5.2 Wild-type and mutant CHK2 are degraded by the proteasome

To investigate whether mutant or wild-type CHK2 protein expression was affected by proteasome mediated degradation, A549 cells were transfected with p3XFLAG-*myc*-CMV™-26 vector encoding wild-type CHK2, $CHK2^{R145W}$, $CHK2^{I157T}$, $CHK2_{insA1368}$ or $CHK2_{delC1100}$ (8μg). 24 hours post transfection the cells were treated with proteasome inhibitor MG132 (20 μM) or DMSO control for 6 hours. The steady-state levels of CHK2 proteins were evaluated by resolving the cells lysates on a 4-12% gradient gel (MOPS running buffer) followed by immunoblotting with anti-CHK2 antibody (A12). Wild-type CHK2 and $CHK2^{I157T}$ are expressed at high levels under DMSO control conditions (Figure 5.1 bottom panel, arrows *Lane 7 and 9*). Addition of proteasome inhibitor resulted in a modest increase in expression of wild-type CHK2 protein and $CHK2_{delC1100}$ (Figure 5.1 bottom panel, arrows *Lane 2 vs. 7* and *Lane 6 vs. 11*) with a concomitant increase in high-molecular-mass adducts (Figure 5.1 top panel, bracket *Lane 2 vs. 7 and Lane 4 vs. 9*). A more pronounced effect was observed with mutant $CHK2^{R145W}$ protein (Figure 5.1 bottom panel, arrow *Lane 3 vs. 8*) with a concomitant increase in high-molecular-mass adducts (Figure 5.1 top panel, bracket *Lane 3 vs. 8*). No significant change was observed with $CHK2^{I157T}$ or $CHK2_{insA1368}$ protein (Figure 5.1 bottom panel, arrows *Lane 4 vs. 9* and botton panel, bracket *Lane 5 vs. 10*, respectively), however, an increase in high-molecular-mass adducts could be clearly observed (Figure 5.1 top panel, bracket *Lane 4 vs. 9* and top panel, bracket *Lane 5 vs 10*, respectively).

Figure 5.1

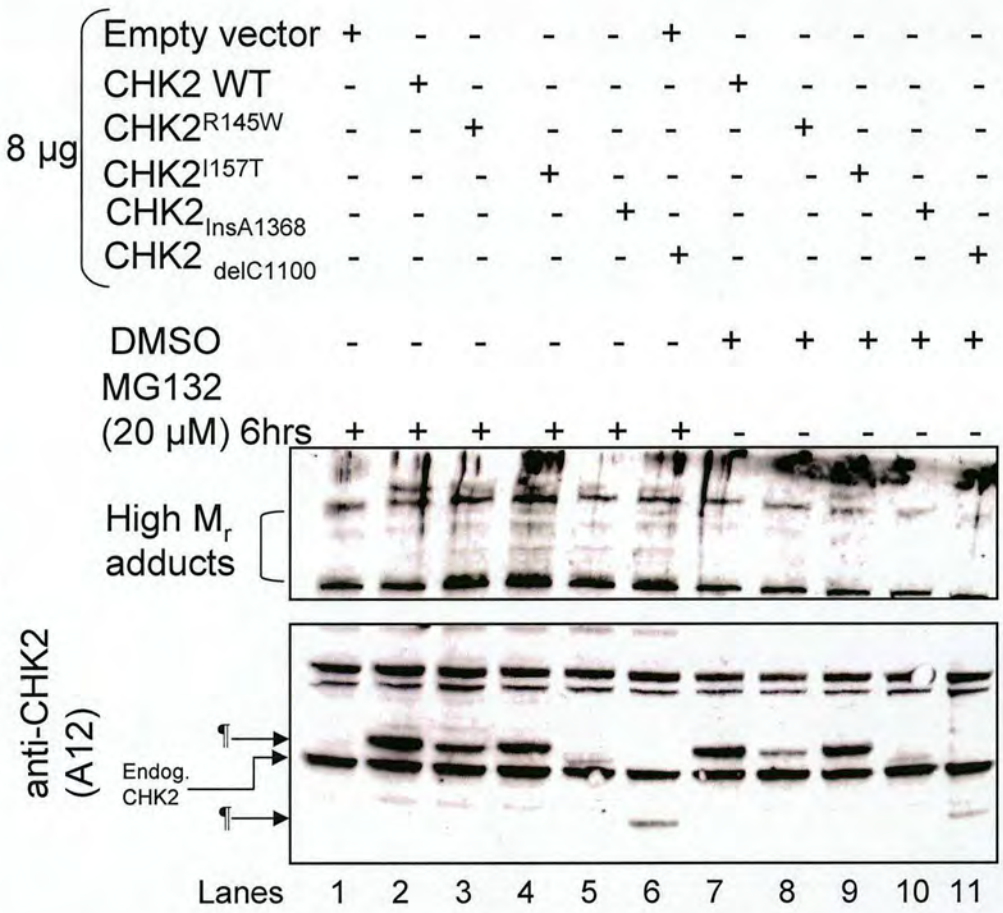

Figure 5.1 Effect of proteasome inhibition on transfected CHK2 wild-type and mutant

Expression vector (p3XFLAG-*myc*-CMV™-26) encoding wild-type CHK2, $CHK2^{R145W}$, $CHK2^{I157T}$, $CHK2_{insA1368}$ or $CHK2_{delC1100}$ (8µg) were transfected in A549 cells and 24 hours post-transfection incubated in the presence of MG132 (20µM) or DMSO control. 6 hours post-treatment the expressed proteins were examined for changes in steady-state levels of CHK2 (bottom panel, ¶ arrows *Lanes 2-11*). Addition of MG132 resulted in an increase of protein levels for wild-type CHK2 (bottom panel, ¶ arrows *Lane 2 vs. 7*), $CHK2^{R145W}$ (bottom panel, ¶ arrows *Lane 3 vs. 8*) and $CHK2_{delC1100}$ (bottom panel, ¶ arrows *Lane 6 vs. 11*). MG132 also resulted in an increase in high molecular mass adducts for wild-type CHK2 and mutant $CHK2^{R145W}$, $CHK2^{I157T}$, $CHK2_{insA1368}$ and $CHK2_{delC1100}$ when compared to DMSO control (top panel, bracket, *Lanes 2-6 vs Lanes 7-11*) as determined by immunoblotting with anti-CHK2 antibody (A12).

5.3 $CHK2^{R145W}$ exhibits a shortened half-life and enhanced ubiquitination when compared to wild-type CHK2 and $CHK2^{I157T}$

The half-lives of wild-type CHK2, $CHK2^{R145W}$ and $CHK2^{I157T}$ were examined to determine whether the low protein level of $CHK2^{R145W}$ stemmed from a high degradation rate when compared to wild-type CHK2 and $CHK2^{I157T}$. A549 cells were transfected with p3XFLAG-*myc*-CMV™-26 vector encoding wild-type CHK2, $CHK2^{R145W}$ or $CHK2^{I157T}$. 24 hours post transfection the cells were treated with cycloheximide (10 μM) at 0.5, 1, 2, 4, 6, 8 and 10 hrs. An untreated, but transfected, control was included. The proteins from cell lysates were examined for turn-over rate by immunoblotting with anti-Flag (M2) antibody. Transfection of wild-type CHK2 and $CHK2^{I157T}$ alleles resulted in the expression of stable proteins with a half-life ($t_{1/2}$) greater than 10 hrs (Figure 5.2 top and middle panels *Lanes 1-16*). In contrast $CHK2^{R145W}$ exhibited a high turn-over rate ($t_{1/2}$ approx. 2 hrs Figure 5.2 bottom panel *Lanes 25-32*).

To elucidate whether the high turn-over rate of $CHK2^{R145W}$ resulted from enhanced ubiquitination levels, A549 cells were transfected with p3XFLAG-*myc*-CMV™-26 wild-type CHK2, $CHK2^{R145W}$, $CHK2^{I157T}$, $CHK2_{delC1100}$ or $CHK2_{insA1368}$ and immunoprecipitated with anti-Flag antibody followed by competitive elution with 3xFlag peptide. Although, CHK2 could be efficiently pulled-down with this procedure (*cf.* Figure 5.7), a high background in the high-molecular-mass range interfered with the interpretation of ubiquitination levels. Due to this hindrance, wild-type CHK2, $CHK2^{R145W}$, $CHK2^{I157T}$, $CHK2_{delC1100}$ and $CHK2_{insA1368}$ alleles were subcloned into one-strep vector pEXPR-IBA105 containing an N-terminal one-strep tag from the

p3XFLAG-myc-CMV™-26 vector using Eco RI and Hind III restriction sites. To isolate one-strep tagged CHK2, lysates from MG132 treated, mutant or wild-type one-strep-CHK2-expressing A549 cells and from control cells (empty vector transfected A549 cells) were subjected to affinity chromatography on strep-tactin macroprep columns (polymethacrylate resin). Following a wash step, bait mutant or wild-type CHK2 was eluted with six sequential biotin elutions (2mM). As shown in Figure 5.3 all proteins were efficiently eluted in elution fractions 1-3 (Figure 5.3 *Lanes 2-4*). The same biotin eluates (following normalization of CHK2 protein level by densitometry) were resolved on a 10% SDS-PAGE gel and immunoblotted with anti-ubiquitin antibody. Due to the heterogeneous nature of ubiquitin conjugation polyubiquitinated forms of CHK2 could only be detected as a large molecular size smear. This experiment demonstrated the enhanced ubiquitination of $CHK2^{R145W}$ when compared to wild-type CHK2 and other mutants in the presence of MG132 (Figure 5.4 *Lanes 2-5* as indicated). This observation might arise due to the inherent nature of the amino acid residue substitution; although arginine and tryptophan are sterically similar, a charge difference might disrupt the hydrophobic interactions with constellation amino acid residues in the β-sandwich that maintain the structure of the FHA, potentially making it more susceptible to proteolysis by the ubiquitin/proteasome pathway.

Figure 5.2

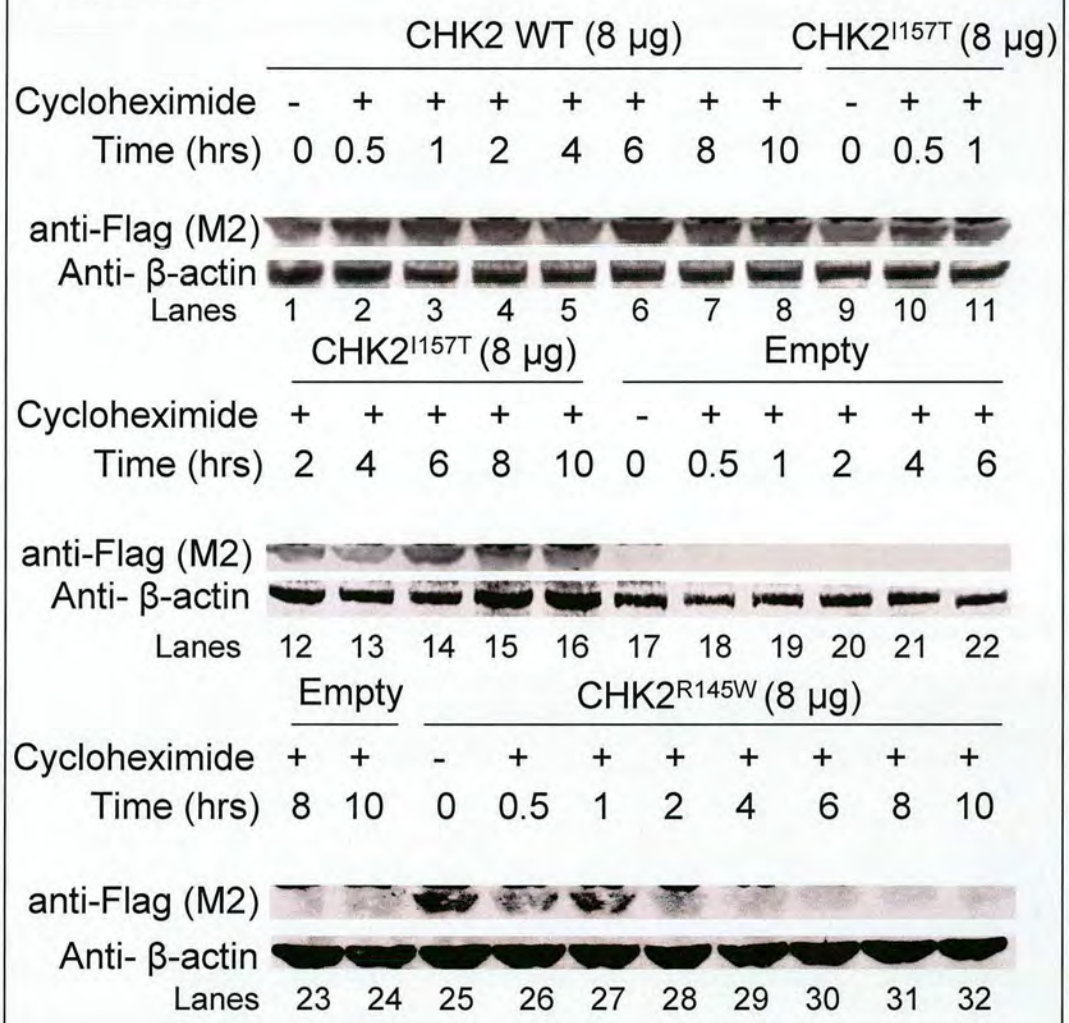

Figure 5.2 The half-life of mutant CHK2^{R175H} is reduced when compared to wild-type CHK2 or mutant CHK2^{I157T}

Expression vector (p3XFLAG-*myc*-CMV™-26) encoding wild-type CHK2, CHK2^{R145W}, CHK2^{I157T}, (8µg, as indicated) were transfected in A549 cells. 24 hours post transfection, cycloheximide was added to the cells and harvested at time points 0 hrs (no cycloheximide addition), 0.5, 1, 2, 4, 6, 8 and 10 hrs. The examined proteins were examined for steady-state levels of CHK2 by immunoblotting with anti-Flag antibody (M2). Transfection of wild-type CHK2 and mutant CHK2^{I157T} led to the expression of a stable protein with a half-life > 10 hrs. CHK2^{R145W} mutant displayed a much reduced half-life (approx 2 hrs) when compared to wild-type CHK2 and mutant CHK2^{I157T}.

Figure 5.3

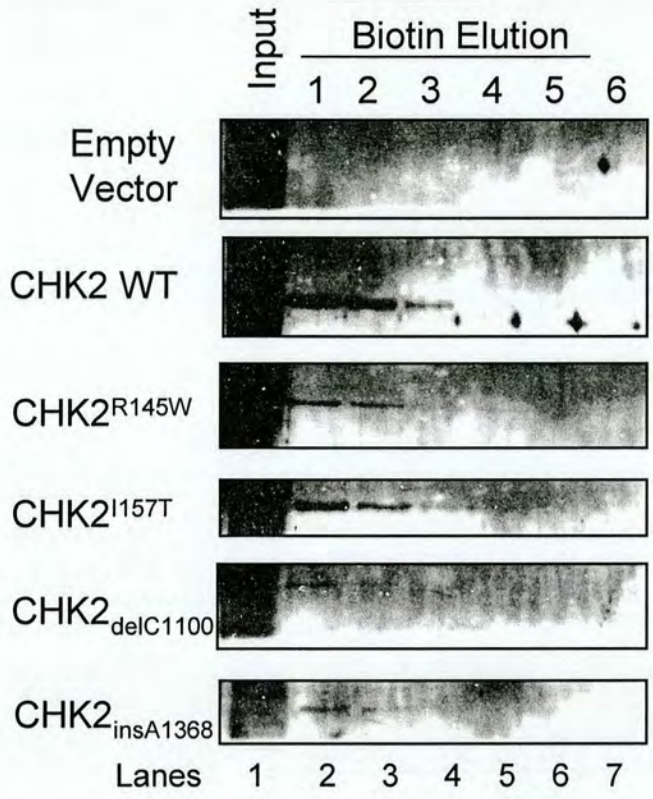

Figure 5.3 One-Strep purification of wild-type CHK2, $CHK2^{R145W}$, $CHK2^{I157T}$, $CHK2_{delC1100}$ and $CHK2_{insA1368}$

Expression vectors (pEXPR-IBA 105) encoding N-terminus tagged One-strep wild-type CHK2, $CHK2^{R145W}$, $CHK2^{I157T}$, $CHK2_{delC1100}$ and $CHK2_{insA1368}$ (8 μg) or control empty vector were transfected in A549 cells and 24 hours post-transfection incubated in the presence of MG132 (20μM). The expressed proteins (Input, *Lane 1*) were purified using macroprep Strep-tactin resin (microcentrifuge tube format) and biotin eluates (*Lane 2-7*) were resolved on a 10% SDS-PAGE gel prior to immunoblotting with anti-strep tag antibody. The CHK2 proteins were successively eluted in biotin elutions 1-3 (*Lanes 2-4*) with a peak in elution 1 (*Lane 2*).

Figure 5.4

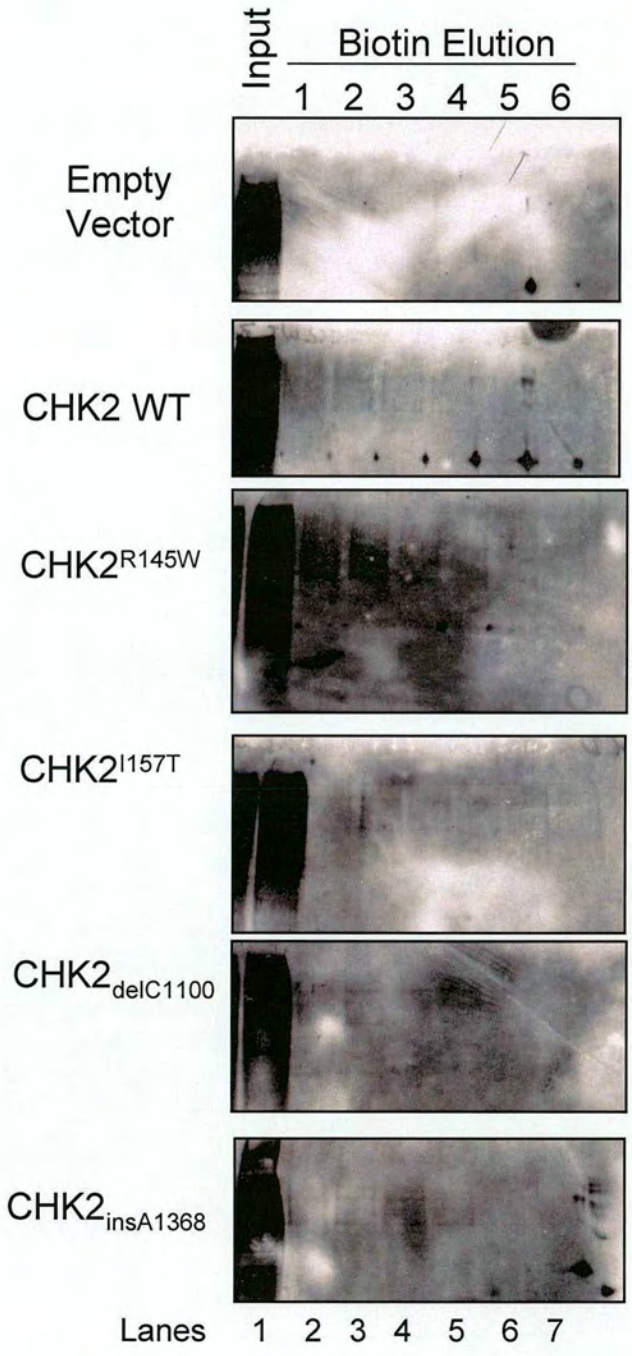
Input
Biotin Elution
1 2 3 4 5 6
Empty Vector
CHK2 WT
CHK2R145W
CHK2I157T
CHK2delC1100
CHK2insA1368
Lanes 1 2 3 4 5 6 7

Figure 5.4 Ubiquitination levels of wild-type CHK2, $CHK2^{R145W}$, $CHK2^{I157T}$, $CHK2_{delC1100}$ and $CHK2_{insA1368}$

Expression vectors (pEXPR-IBA 105) encoding N-terminus tagged One-strep wild-type CHK2, $CHK2^{R145W}$, $CHK2^{I157T}$, $CHK2_{delC1100}$ and $CHK2_{insA1368}$ (8 μg) or control empty vector were transfected in A549 cells and 24 hours post-transfection incubated in the presence of MG132 (20μM). The expressed proteins (Input, *Lane 1*) were purified using macroprep Strep-tactin resin (microcentrifuge tube format) and biotin eluates (*Lane 2-7*) were resolved on a 10% SDS-PAGE gel prior to immunoblotting with anti-ubiquitin antibody. $CHK2^{R145W}$ exhibits enhanced ubiquitination when compared to wild-type CHK2, $CHK2_{insA1368}$, $CHK2^{I157T}$ or $CHK2_{delC1100}$.

5.4 Identification of protein phosphatase 1B as a binding partner to CHK2 by mass spectrometry

Repeated attempts to identify CHK2 binding partners following one-strep purification procedure proved elusive. Therefore, MCF7 cells were transfected with p3XFLAG-*myc*-CMV™-26 wild-type, mutant CHK2 or empty vector. As seen in Figure 5.5 ectopic transfection of these constructs results in similar levels as when the same proteins are expressed following the transfection of the same alleles cloned in the one-strep vector. Due to frameshift mutations in $CHK2_{delC1100}$ and $CHK2_{insA1368}$ result in premature stop codons the c-myc epitope on the C-terminus of these constructs was truncated from these proteins (Figure 5.5 bottom 2 panels, *Lanes 4 and 5 vs. Lanes 1-3*). In addition, incremental amounts of in-vivo cross-linking agent EGS (1-8 mM) to ectopically transfected MCF7 cells with wild-type 3xflag-c-myc-CHK2 resulted in effective cross-linking of CHK2 as a dimer (Figure 5.6 *Lanes 1-5 vs. 7*). In light of these results MCF7 cells were transfected with p3XFLAG-*myc*-CMV™-26 wild-type CHK2 or empty vector and immunoprecipitated with anti-Flag antibody followed by competitive elution with 3xFlag peptide. The 3xFlag-eluates were then immunoprecipitated with anti-c-myc antibody crosslinked to sepharose beads followed by a competitive elution with c-myc peptide. As shown in Figure 5.7 incubation of cell-lysate containing wild-type 3xflag-c-myc-CHK2 for 15 minutes resulted in maximal binding of CHK2 to the Flag-sepharose beads (Figure 5.7 (**A**), top panel, lack of band, *Lane 2 vs. 1*). As shown in Figure 5.7, 3xFlag peptide eluates required an overnight incubation for a maximal binding of protein to the c-myc-sepharose beads (Figure 5.7 (**A**) bottom panel, *Lane 5 vs. 1*). Overnight incubation with c-myc peptide was required for maximal elution of CHK2 (Figure 5.7 (**A**) bottom panel, *Lane 9 vs. 6*). Following

the above mentioned optimization procedure, c-myc peptide eluates from CHK2 wild-type and empty vector control were resolved on a 12 % SDS-PAGE gel, silver stained and gel bands (that were present in positive pulldowns but absent in mock control) excised for tryptic digestion and analysis by MALDI-TOF-MS. As a control, gel slices that migrated at a similar molecular weight in the mock empty vector were also subjected to analysis by MALDI-TOF-MS to eliminate any false positive that might have arisen due to lack of silver staining of the empty control eluate (Figure 5.7 (**B**) arrows *(i)* and *(ii)*). Analysis of gel band (i) resulted in the positive identification of CHK2 protein (Figure 5.7 (**C**). Analysis of gel band (ii) resulted in the positive identification of protein phosphatase 1B1 also known as PP2C beta (Figure 5.7 (**D**).

Figure 5.5

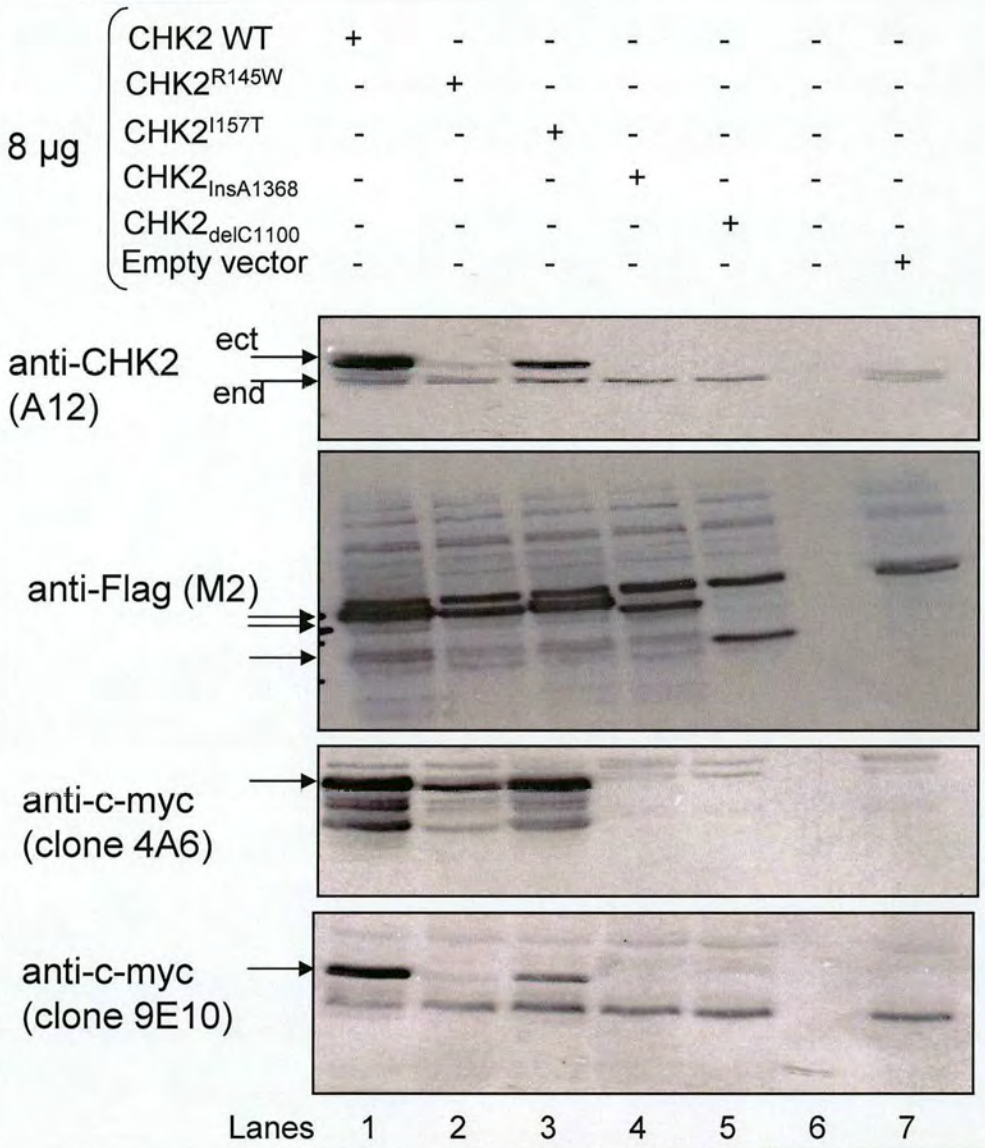

Figure 5.5 Ectopic transfection of Flag-c-myc dual-tagged wild-type CHK2, $CHK2^{R145W}$, $CHK2^{I157T}$, $CHK2_{delC1100}$ and $CHK2_{insA1368}$

Expression vector (p3XFLAG-*myc*-CMV™-26) encoding wild-type CHK2, $CHK2^{R145W}$, $CHK2^{I157T}$, $CHK2_{insA1368}$ or $CHK2_{delC1100}$ (8µg) were transfected in MCF7 cells. The expressed proteins were examined by immunoblotting with anti-CHK2 antibody (A12), anti-Flag (M2) and anti-c-myc (clone 4A6 or 9E10). Frameshift mutations in $CHK2_{delC1100}$ and $CHK2_{insA1368}$ result in premature stop codons so the c-myc epitope on the C-terminus of these constructs was truncated from these proteins (Figure 5.5 bottom 2 panels, *Lanes 4 and 5 vs. Lanes 1-3*)

Figure 5.6

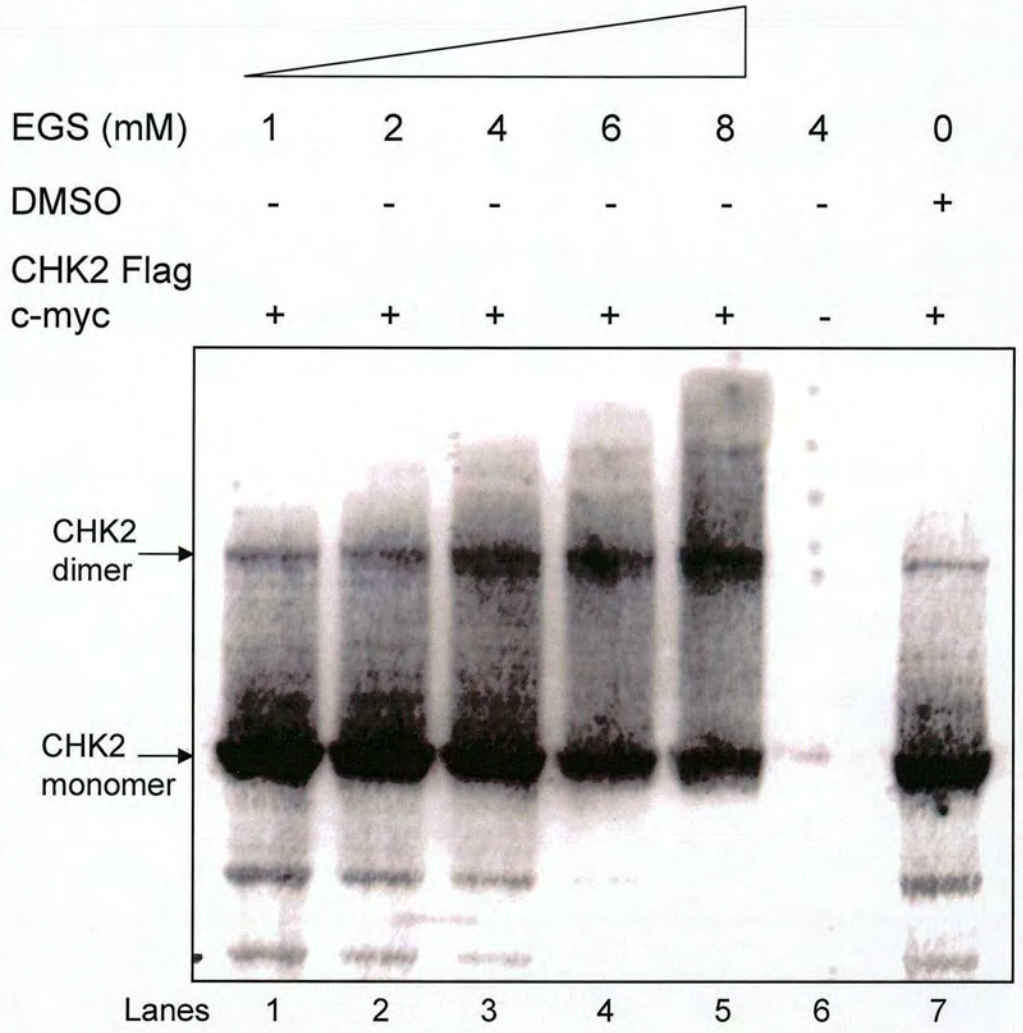

Figure 5.6 Cross-linking of wild-type CHK2

Expression vector (p3XFLAG-*myc*-CMV™-26) encoding wild-type CHK2 (8µg) was transfected in MCF7 cells. 24 hours post-transfection, the cells were incubated with incremental amounts of EGS cross-linker (*Lanes 1-5*) or DMSO control (*Lane 7*). The expressed proteins were examined by immunoblotting with anti-CHK2 antibody (A12) whereas the expressed CHK2 monomer protein decreases with addition of EGS, the CHK2 dimer increases (arrows, as indicated, *Lanes 1-5 vs. Lane 7*).

Figure 5.7

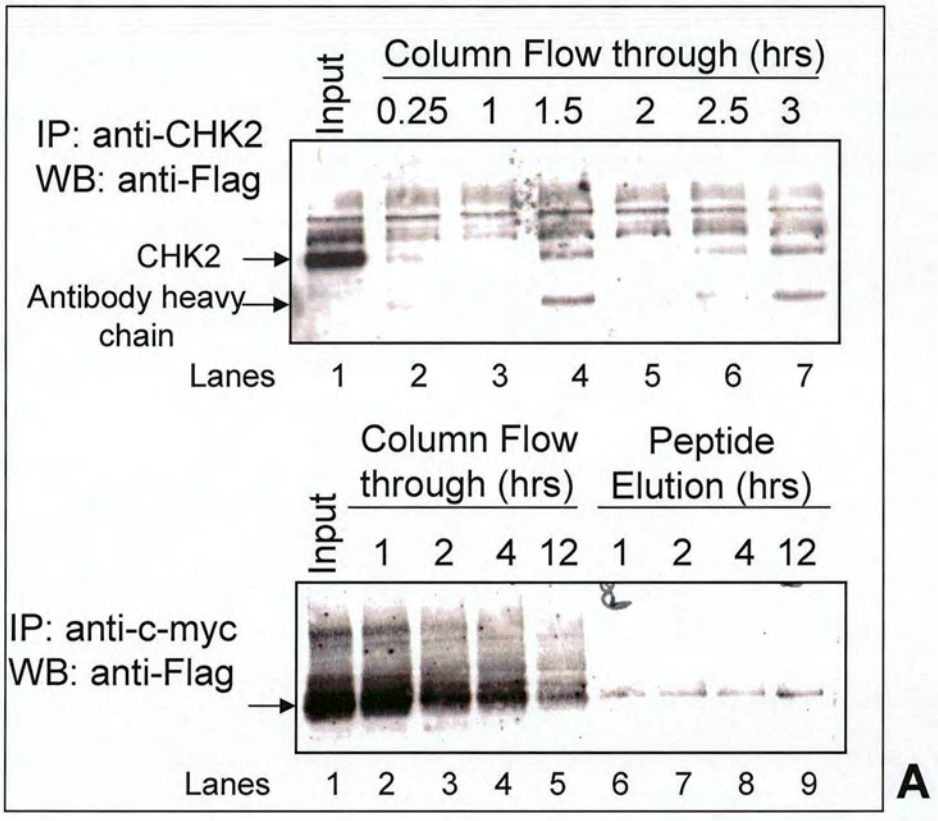
Column Flow through (hrs)
Input
0.25 1 1.5 2 2.5 3
IP: anti-CHK2
WB: anti-Flag
CHK2
Antibody heavy chain
Lanes 1 2 3 4 5 6 7
Column Flow through (hrs)
Peptide Elution (hrs)
Input
1 2 4 12 1 2 4 12
IP: anti-c-myc
WB: anti-Flag
Lanes 1 2 3 4 5 6 7 8 9
A

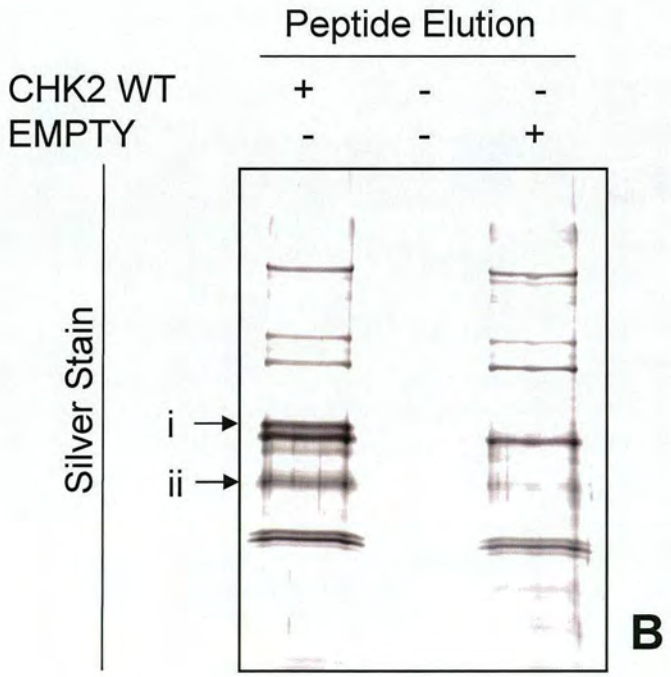
Peptide Elution
CHK2 WT + - -
EMPTY - - +
Silver Stain
i
ii
B

Figure 5.7 (cont.)

C

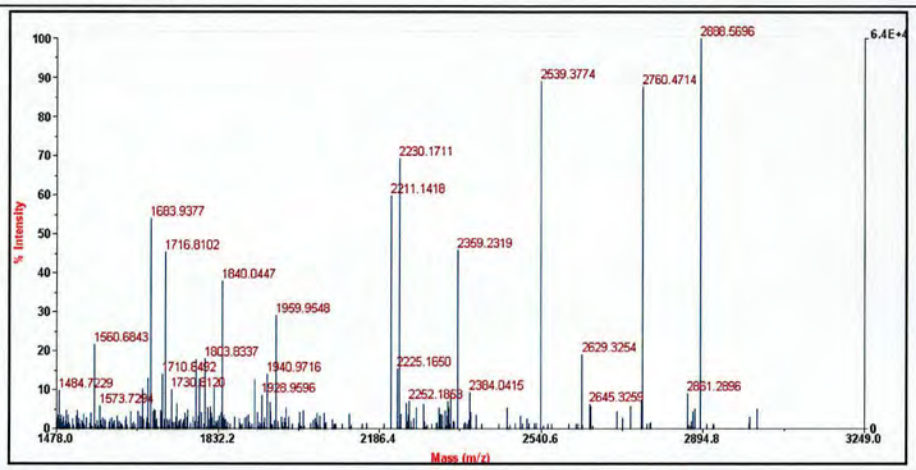

ProFound - Search Result Summary

Version 4.10.5
The Rockefeller University Edition

Protein Candidates for search B7C16631-0540-78881B41 [34820 sequences searched]

Rank	Probability	Est'd Z	Protein Information and Sequence Analyse Tools (T)	%	pI	kDa	
+1	1.0e+000	2.37	T gi|6005830|ref|NP_009125.1| protein kinase CHK2 isoform a; checkpoint-like protein CHK2; serine/threonine-protein kinase CHK2; CHK2 (checkpoint, S.pombe) homolog [Homo sapiens]	41	5.6	61.64	
2	2.2e-041	-	T gi|27469381|gb|AAH42110.1| FLJ34512 protein [Homo sapiens]	33	8.9	48.76	
3	5.6e-044	-	T gi|21753394|dbj|BAC03472.1| unnamed protein product [Homo sapiens]	19	6.9	57.81	
+4	4.2e-044	-	T gi|6851600|gb|AAC24716.1| p21 activated kinase 1B [Homo sapiens]	19	5.3	62.10	

Matched peptides shown in **Bold Red**

```
   1 MSRESDVEAQ QSHGSSACSQ PHGSVTQSQG SSSQSQGISS SSTSTMPNSS
  51 QSSHSSSGTL SSLETVSTQE LYSIPEDQEP EDQEPEEPTP APWARLWALQ
 101 DGFANLETES GHVTQSDLEL LLSSDPPASA SQSAGIRGVR HHPRPVCSLK
 151 CVNDNYWFGR DKSCEYCFDE PLLKRTDKYR TYSKKHFRIF REVGPKNSYI
 201 AYIEDHSGNG TFVNTELVGK GKRRPLNNNS EIALSLSRNK VFVFFDLTVD
 251 DQSVYPKALR DEYIMSKTLG SGACGEVKLA FERKTCKKVA IKIISKRKFA
 301 IGSAREADPA LNVETEIEIL KKLNHPCIIK IKNFFDAEDY YIVLEIMEGG
 351 ELFDKVVGNK RLKEATCKLY FYQMLLAVQY LHENGIIHRD LKPENVLLSS
 401 QEEDCLIKIT DFGHSKILGE TSLMRTLCGT PTYLAPEVLV SVGTAGYNRA
 451 VDCWSLGVIL FICLSGYPPF SEHRTQVSLK DQITSGKYNF IPEVWAEVSE
 501 KALDLVKKLL VVDPKARFTT EEALRHPWLQ DEDMKRKFQD LLSEENESTA
 551 LPQVLAQPST SRKRPREGEA EGAETTKRPA VCAAVL
```

D

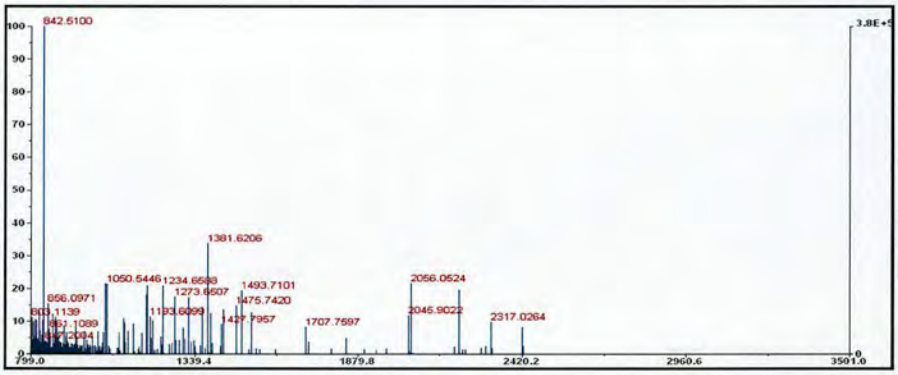

ProFound - Search Result Summary

Version 4.10.5
The Rockefeller University Edition

Protein Candidates for search B9311106-0429-74D0-C83E [34820 sequences searched]

Rank	Probability	Est'd Z	Protein Information and Sequence Analyse Tools (T)	%	pI	kDa	
+1	1.0e+000	2.17	T gi|4502993|ref|NP_002699.1| protein phosphatase 1B isoform 1; protein phosphatase 2C beta isoform; protein phosphatase 2C-like protein [Homo sapiens]	35	5.0	53.20	
+2	3.8e-010	-	T gi|547749|sp|P13645|K1CI_HUMAN Keratin, type I cytoskeletal 10 (Cytokeratin 10) (K10) (CK 10)	17	5.1	59.73	
+3	3.2e-012	-	T gi|134343|sp|P04264|K2C1_HUMAN Keratin, type II cytoskeletal 1 (Cytokeratin 1) (K1) (CK 1) (67 kDa cytokeratin) (Hair alpha protein)	23	8.3	66.17	
4	2.7e-013	-	T gi|220018|dbj|BAA00312.1| prolactin PRL precursor [Homo sapiens]	32	6.5	25.18	

Match to: **gi|12666523** Score: **48** Expect: **1.9** **protein phosphatase 1B1 43 kDa isoform [Homo sapiens]**

```
1 MGAFLDKPKT EKHNAHGAGN GLRYGLSSMQ GWRVEMEDAH TAVVGIPHGL 51
EDWSFFAVYD GHAGSRVANY CSTHLLEHIT TNEDFRAAGK SGSALELSVE 101
NVKNGIRTGF LKIDEYMRNF SDLRNGMDRS GSTAVGVMIS PKHIYFINCG 151
DSRAVLYRNG QVCFSTQDHK PCNPREKERI QNAGGSVMIQ RVNGSLAVSR 201
ALGDYDYKCV DGKGPTEQLV SPEPEVYEIL RAEEDEFIIL ACDGIWDVMS 251
NEELCEYVKS RLEVSDDLEN VCNWVVDTCL HKGSRDNMSI VLVCFSNAPK 301
VSDEAVKKDS ELDKHLESRV EEIMEKSGEE GMPDLAHVMR ILSAENIPNL 351
PPGGGLAGKR NVIEAVYSRL NPHRESDGGA GDLEDPW
```

Figure 5.7 Two-step purification of dual-tagged wild-type CHK2 and binding partners

(**A**) Expression vector (p3XFLAG-*myc*-CMV™-26) encoding wild-type CHK2 or empty vector control (8μg) were transfected in A549 cells. 24 hours post transfection cell lysates were incubated with anti-flag sepharose beads and the flow through from the column taken at 0.25, 1, 1.5, 2, 2.5 and 3 hours to determine the degree of binding of CHK2 to the column.
Top panel: Anti-flag immunoblot of degree of binding of bait wild-type CHK2 protein with time shows that a 15 minute incubation results in maximal binding to the flag-sepharose-resin (Top panel, *Lane 2 vs. 1*).
Bottom panel: Anti-flag immunoblot of 3xFlag-peptide elution from (**A**) shows that an overnight incubation results in maximal binding to the c-myc-sepharose-resin (Bottom panel, *Lane 5 vs. 1*). Overnight incubation with c-myc peptide results in maximal elution of bait CHK2 protein (Bottom panel, *Lane 9 vs.6)*.
(**B**) Expression vector (p3XFLAG-*myc*-CMV™-26) encoding wild-type CHK2 or empty vector control (8μg) were transfected in A549 cells. 24 hours post transfection the cell lysates were incubated with anti-flag sepharose beads for 30 minutes followed by 3xFlag peptide competitive elution. The 3x-flag peptide eluates were incubated overnight with anti-c-myc resin and competitively eluted overnight with c-myc peptide. The protein eluates were resolved on a 12% SDS-PAGE gel and silver-stained. Gel slices were excised from wild-type CHK2 and empty control eluates (i and ii arrows)
(**C**) MALDI-TOF-MS spectrum of gel slice (i), resulted in positive identification of CHK2 bait protein using MASCOT and Profound Search engines
(**D**) MALDI-TOF-MS spectrum of gel slice (ii), resulted in positive identification of protein phosphatase 1B1 (also known as PP2C beta) using MASCOT and Profound Search engines.

5.5 Discussion

Although most cases of classic Li-Fraumeni syndrome (LFS) and a subset of variant-LFS harbour germ-line mutations in p53, a small number of cases have mutations in CHK2 [220]. The similar phenotype conferred by germ-line mutations in p53 and CHK2, and the fact that tumours arising in CHK2-mutant family members may not carry somatic TP53 mutations, are consistent with CHK2 encoding a kinase responsible for the phosphorylation of p53 on Ser^{20} and its stabilization after DNA damage.

The mutants analysed in this study fall under two catagories. Firstly, structural and include mutations in the fork-head associated domain (FHA) which are $CHK2^{R145W}$ and $CHK2^{I157T}$ and secondly, frameshift mutations leading to the truncation within the catalytic kinase domain which are $CHK2_{delC1100}$ and $CHK2_{insA1368}$.

This study has highlighted that the inherent instability of $CHK2^{R145W}$, $CHK2_{insA1368}$ and $CHK2_{delC1100}$ when compared to wild-type and $CHK2^{I157T}$ was at the protein level and was partially blocked by addition of proteasome inhibitor MG132 in the case of $CHK2^{R145W}$ and $CHK2_{delc1100}$ but not $CHK2_{insA1368}$. In corroboration with this observation, transfected $CHK2^{R145W}$ had a shorter half-life (approx. 2 hrs) when compared to the more stable wild-type CHK2 or $CHK2^{I157T}$ (> 10 hrs). This study also demonstrated that $CHK2^{R145W}$ is hyperubiquitinated when compared to wild-type CHK2 and the other mutants, as defined by one-strep precipitation and immunoblotting with anti-ubiquitin, thereby confirming that CHK2 is degraded in a ubiquitin-proteasome dependent manner and that $CHK2^{R145W}$ may be susceptible to increased levels of proteasome degradation when compared to wild-type CHK2. As indicated in Figure 5.8, $CHK2^{R145W}$ and $CHK2^{I157T}$ are located on one face of the FHA β sandwich domain,

remote from the site of peptide binding. Ile^{157} is located at the C-terminal end of the β5-β6 loop, some 25 Å distant from the pThr site, and is largely solvent exposed. Arg^{145} is located on β5 and forms the core of a network of hydrogen bonding, nonpolar, and van der Waals interactions involving Asn^{112}, Trp^{114}, and Glu^{161} from adjacent β strands 3 and 6 together with Phe^{147} located on β5 [212].

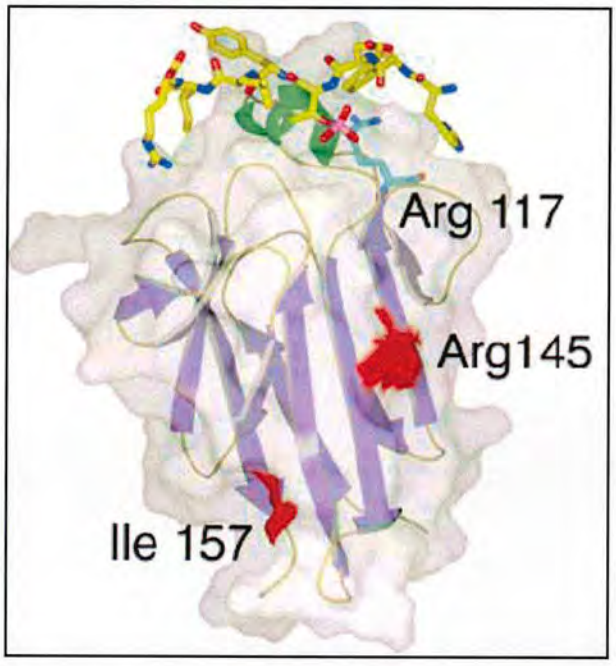

Figure 5.8 Structure of CHK2 and Fork Head Associated Domain[xii]

In view of this structural information and the above findings it is plausible to conclude that the deleterious effects of the $CHK2^{R145W}$ mutation which result in a higher level of ubiquitination and shorter half-life when compared to wild-type CHK2 and $CHK2^{I157T}$ are a result of a disruption of the FHA domain folding.

[xii] Figure 5.8: Bartek, J. and J. Lukas, *Chk1 and Chk2 kinases in checkpoint control and cancer.* Cancer Cell, 2003. **3**(5): p. 421-9. and Li, J., et al., *Structural and functional versatility of the FHA domain in DNA-damage signaling by the tumor suppressor kinase Chk2.* Mol Cell, 2002. **9**(5): p. 1045-54.

Zhang and co-workers have demonstrated that downregulation of CHK2 kinase expression in response to cisplatin was at the protein level and the degradation of CHK2 can be partially blocked by adding proteasome inhibitor MG132. The same authors conclude that proteasome inhibitors would be more potent when combined with cytotoxic agents such as cisplatin and MG132 for the killing of the H69 small cell lung cancer cells and A2780 ovarian cancer cells (wild-type CHK2)[221]. Such a dual pronged approach is likely, in theory, to have a significant approach in treatment of tumours bearing a wild-type CHK2 background but not necessarily for $CHK2^{R145W}$-bearing tumours since $CHK2^{R145W}$ cannot form a complex with p53 and both are defective in IR-induced p53 phosphorylation [222]. It is therefore important to genetically screen patients for CHK2 background before proceeding with such a therapeutic approach.

This study has also highlighted an interaction between CHK2 and protein phosphatase 1B isoform 1 (PPM1B; previously named protein phosphatase 2C beta isoform PP2Cbeta). Dozier *et al.* have shown that CHK2 interacts with the B' regulatory subunit of protein phosphatase 2A (PP2A) and this interaction allows the association of the checkpoint kinase (whatever its state of phosphorylation) with the fully assembled PP2A holoenzyme. Moreover, the same authors show that CHK2 can phosphorylate B' and, in so doing, increase PP2A activity. However, a negative feedback loop enables PP2A to dephosphorylate and inactivate CHK2 [223]. In another study, Cheng and co-workers demonstrate that PP2C-like enzymes specifically dephosphorylate Cdc28p (the major budding yeast CDK) at residue Thr^{169} and this dephosphorylation was inhibited by cyclin binding. The same authors showed that PP2C-like enzymes were the predominant human phosphatases acting on Thr^{160} of Cdk2

(a downstream target of CHK2) in a HeLa cell extract, indicating that the substrate specificity of PP2Cs against Cdks is evolutionary conserved [224].

Although the identification of substrates of PP2C *in vivo* has been hindered by the absence of specific inhibitors, PP2C exhibits a 20-fold preference for phosphothreonine-containing substrates compared with phosphoserine substrates *in vitro* [225] and substrates of PP2C *in vivo* have been proposed to be phosphorylated on threonine residues [226]. The FHA domain of CHK2 appears to bind phosphothreonine-containing peptides in vitro [212]. Taken together, the results from these studies and the novel PP2C:CHK2 interaction presented in this study might highlight a trimeric complex composed of CHK2, Cdk2 and PP2c. Under basal conditions, PP2C may serve to keep the CHK2 and Cdk2 kinases inactive and to CHK2 autophosphorylation impaired. In response to DNA damage, the buffering action of PP2C may be readily overcome allowing activation of CHK2 and Cdk2.

Another possible function of the CHK2:PP2C interaction involves the downstream target of CHK2, namely p53. Ofek and co-workers have shown that PP2Cα overexpression specifically activates p53 and stimulates its transcriptional activity [218]. The authors argue that PP2C might remove inhibitory phosphorylation sites in response to ionizing radiation thereby contributing to the DNA damage-induced stabilization of p53 [218]. Therefore, the CHK2:PP2C interaction discovered in this study may act in concert to activate p53.

6.0 Preliminary data on novel interactions of p53 with rps3, a DNA repair enzyme and ANT a mitochondrial pore protein

6.1 Introduction

In addition to many external agents that produce repairable DNA lesions, normal processes such as oxidative phosphorylation, lipid peroxidation, single carbon metabolism, and DNA replication errors directly produce DNA damage and damaging agents. These changes in DNA base chemistry include such modifications as methylation, oxidation, deamination, or the complete loss of bases. The cell's major line of defense is provided by the base excision repair (BER) system [227]. There are two main enzymes used, DNA glycosylases and AP (apurinic and apyrimidinic) endonucleases. The DNA glycosylase is used to break the β-N glycosidic bond to create an AP site. The AP endonuclease recognizes this site and nicks the damaged DNA on the 5' side (upstream) of the AP site creating a free 3'-OH. DNA polymerase, Pol I, extends the DNA from the free 3'-OH using its exonuclease activity to replace the nucleotide of the damaged base, as well as a few downstream, followed by sealing of the new DNA strand by DNA ligase.

Besides its ability to induce cell-cycle arrest and apoptosis via sequence-specific transcriptional activity, p53 has also been shown to physically interact with the BER multiprotein pathway [228]. Ref-1, also known as APE-1/Hap-1/APEX, is a DNA repair (A/P) endonuclease that plays a central role in the process of BER. Ref-1 functions by cleaving the DNA 5' to abasic sites, as well as to load DNA polymerase γ onto DNA [229]. The crystal structure of Ref-1 shows strong homology with two other DNA nucleases, DNase I from *Bos tauri* and exonuclease III from *Escherichia coli* [230] . In addition to its roles in BER, Ref-1 was shown previously to activate the AP-1

heterodimeric *fos-jun* transcription complex by changing the redox state of its DNA-binding-domain [231]. Gaiddon and co-workers have shown that Ref-1 interacts with p53 *in vitro* and *in vivo* and overexpression of the former leads to increased ability of p53 to stimulate endogenous p21 and cyclin G expression [232]. Moreover, Hanson and co-workers have shown that Ref-1 promotes tetramerization of p53 thereby enhancing p53 binding to target DNA [233].

On the other hand, mutant p53 has recently been shown to interact with key proteins involved in the DNA repair mechanism of double stranded breaks (DSBs). Song and co-workers showed that novel gain-of-function oncogenic mutant $p53^{R248W}$ and $p53^{R273H}$ interact with the nuclease Mre11 and suppress the binding of the Mre11-Rad50-NBS1 (MRN) complex to DSBs, leading to ATM activation [234].

p53 exerts its apoptotic and cell-cycle effects in a transcription-independent manner in addition to transcription-dependent means. Some transcriptional products of p53 include Bcl-2-associated X protein (BAX), NADPH oxidase activator 1 (NOXA), p53 acetate-induced protein 1 (p53AIP1) and p53-upregulated modulator of apoptosis (PUMA) which act directly on mitochondria and induce apoptosis [235-239]. In addition, in some cell types, a fraction of stabilized p53 rapidly translocates to mitochondria in response to a death stimulus. Mihara and co-workers have shown that exogenous p53 targets the mitochondria in p53 null cancer cells, and p53 was shown to be sufficient to launch apoptosis and suppress colony formation in a transcription-independent way. Moreover, endogenous mitochondrial p53 forms inhibitory complexes with anti-apoptotic Bcl-X and Bcl-2 proteins, resulting in cytochrome c release from mitochondria, thereby contributing to apoptosis by direct signalling at the mitochondria and amplifying transcription-dependent apoptosis also mediated by p53 [240].

The following preliminary data identify two potential p53-interactors that have a role in DNA repair and mitochondrial-dependent release of cytochrome C, namely ribosomal protein s3 and ADP/ATP translocase respectively.

6.2 Ribosomal protein s3 and ATP/ADP translocase identified as new binding partners to p53

DO-1 immunoprecipitates of $p53^{R175H}$-infected uninfected *Spodoptera frugiperda* were run on a 4-12% gradient gel (MOPS running buffer) and stained with colloidal blue stain. As shown in Figure 6.0 (**A**) low background was obtained in the empty vector (mock). All the visible bands in the gel were excised and subjected to analysis by LC-MS/MS., p53 was positively identified in all bands (data not shown) with the exception of the arrowed band Analysis of the arrowed band resulted in the identification of ATP/ADP translocase (ANT) (Figure 6.0 (**B**)) and ribosomal protein s3 (rps3) (Figure 6.0 (**C**)).

ANT is a component of the mitochondrial permeability transition pore (MPTP) which, in turn, is implicated in the release of pro-apoptotic factors such cytochrome C in response to intra or extra-cellular insults. ANT interacts with either Bax or Bcl-2, which influence ANT function in opposing manners. Bcl-2 maintains the translocase activity at high levels, whereas Bax inhibits the translocase function of ANT leading to release of cytochrome c after MPTP opening [241]. Since a fraction of p53 has been shown to localize with the mithochondria and specifically interact with Bcl-2 [240], further analysis should be carried out to investigate the interaction identified in this study, particularly, to elucidate whether it is specific to wild-type (promoting transcription-independent apoptosis via MPTP opening) or mutant p53 (gain-of-function by preventing apoptosis via MPTP blockage and possibly aided by ANT).

Alignment of human rps3 with human ref-1 by ClustalW protein alignment program revealed an identical GYSGV peptide motif in both proteins (Figure 6.0D). Interestingly the tyrosine residue in ref-1 (also conserved in DNase I (*Bos Taurus*)) has

been shown to be implicated in binding to the scissile phosphate group, adjacent to the extra-helical base [230]. Since Ref-1 has been shown to bind and transcriptionally activate p53 and rps3 has been associated with DNA repair activity, these observations coupled with the identification of the GYSGV motif in rps3 and Ref-1, prompted an investigation to see whether rps3 could activate p53 in a similar fashion as Ref-1. A p21-reporter dual luciferase assay was therefore employed. Briefly, H1299 cells were transfected with constant levels of p53 (50μg/well) (Figure 6.0 (**E**) *left panel*) or empty vector (50μg/well) (Figure 6.0 (**E**) *right panel*) and incremental amounts of rps3 DNA (0-2500 ng). The p21-reporter levels were normalized with internal standard Renilla-luciferase (*c.f.* Section 2.8.2). No significant effect on p53 transcriptional activity was observed following the addition of rps3. Furthermore no significant increase in p21 or BAX protein levels were observed following the titration of incremental amounts of rps3 (Figure 6.0 (**F**) *left panel Lanes 1-4 vs. 5-12*). Further studies should be performed to investigate whether an induction of base excistion repair (BER) by methyl methanesulfonate (MMS) activates p53 in an rps3 dependent way.

Interestingly, apart from its role in the ribosome rps3 has been identified as an *N*-glycosylase that liberates the modified or nonconventional base from DNA forming in its place an apurinic/apyrimidinic (AP) site [242]. Moreover, human rps3 interacts with BER enzymes *N*-glycosylase/AP lyase OGG1 promoting its activity and that of Ref-1. Since Ref-1 has been shown to interact with p53 (*c.f.* Section 6.0), the finding presented in this preliminary data might suggest a mega-DNA-repair-complex including rps3-OGG1-Ref-1-p53, which should be further elucidated.

Figure 6.0

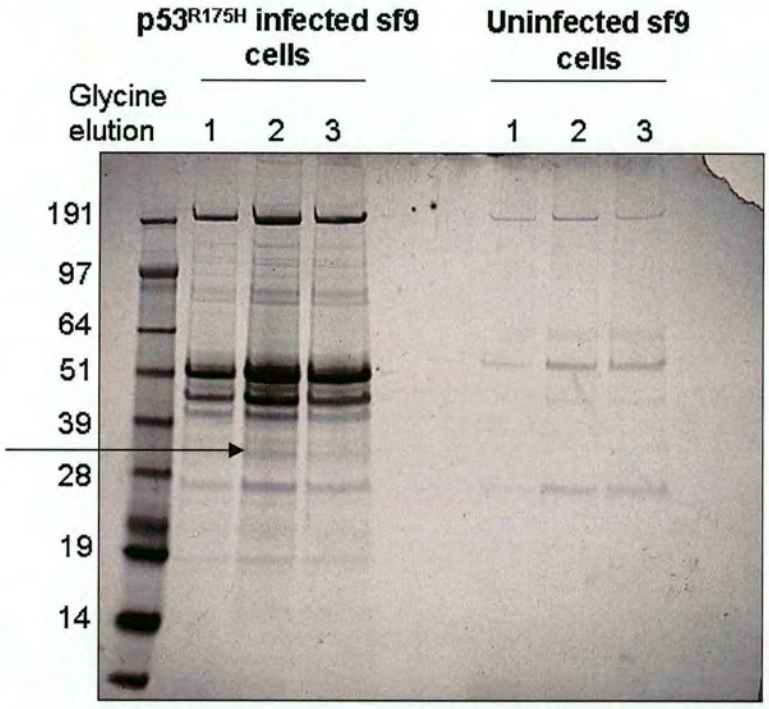

Match to: **gi|28261391** Score: **672 ADP/ATP translocase [Bombyx mori]**

1 MSNLADPVAF AK**DFLAGGIS AAVSKTAVAP IER**VK**LLLQV QHVSK**QIAAD
51 QRYK**GIVDAF VR**IPKEQGLL SFWR**GNFANV IRYFPTQALN FAFK**DKYKQV
101 FLGGVDKKTQ FWRYFAGNLA SGGAAGATSL CFVYPLDFAR TR**LAADVGKG**
151 **DGQR**EFSGLG NCISKIFK**SD GLIGLYR**GFG VSVQGIIIYR **ASYFGFYDTA**
201 **RGMLPDPK**NT PIVISWAIAQ TVTTVAGIIS YPFDTVRRRM MMQSGRAKSD
251 ILYKNTIHCW ATIAKTEGTS AFFK**GAFSNV LR**GTGGAFVL VLYDEIKKVL

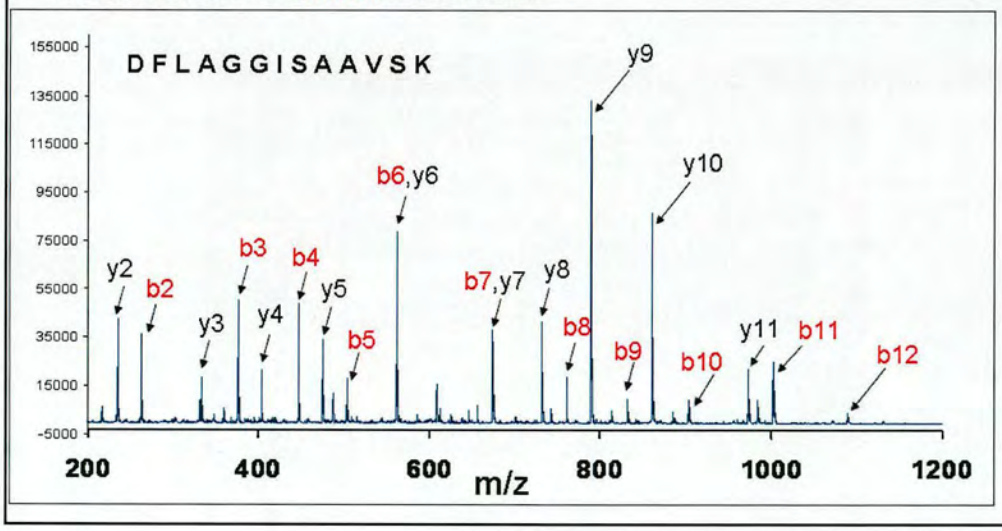

B

Figure 6.0 (cont.)

Match to: **gi|16566719** Score: **396 ribosomal protein S3 [Spodoptera frugiperda]**

1 MAVNNISKKR KFVGDGVFKA ELNEFLTREL AEDGYSGVEV RVTPTRSEII
51 IMATRTQSVL GEKGRRIREL TSVVQKRFNI PERSVELYAE KVATRGLCAI
101 AQAESLRYKL IGGLAVRRAC YGVLRFIMES GARGCEVVVS GKLRGQRAKS
151 MKFVDGLMIH SGDPCNDYVN TATRHVLLRQ GVLGIKVKIM LPWDQQGKNG
201 PKKPQPDHIL VTEPKDEPVP LEPTSDVRSL APAPLPQPVA AVA

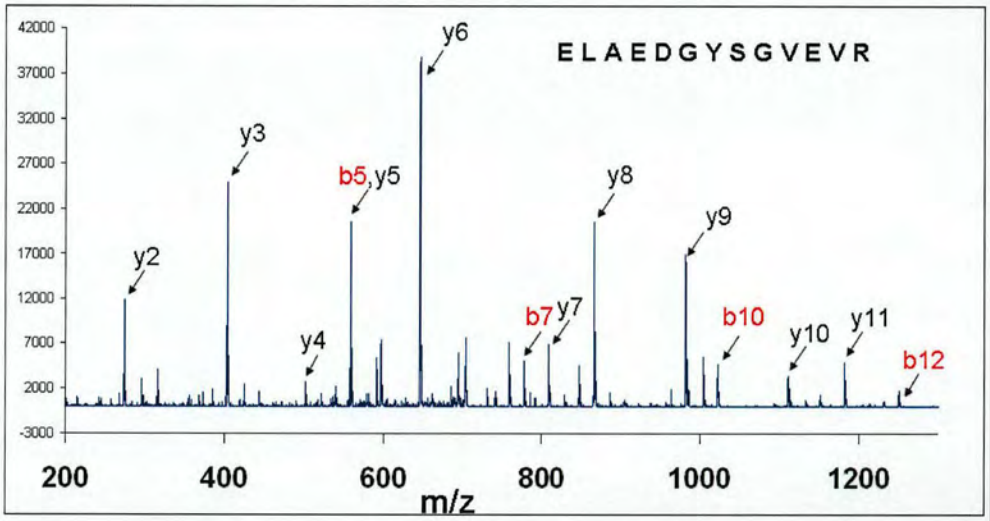

C

D

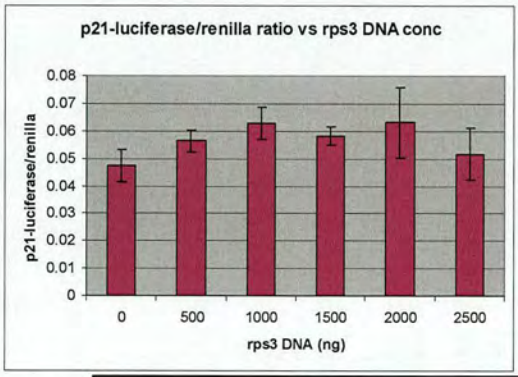

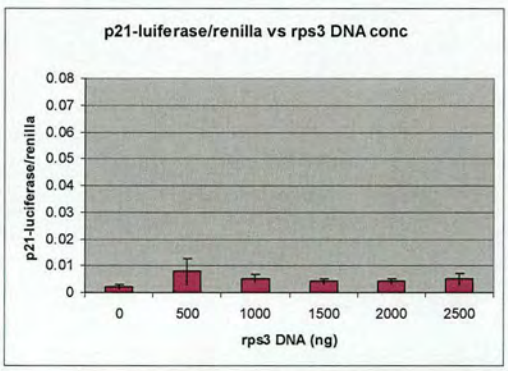

DO-1
α-p53

E

Figure 6.0 (cont.)

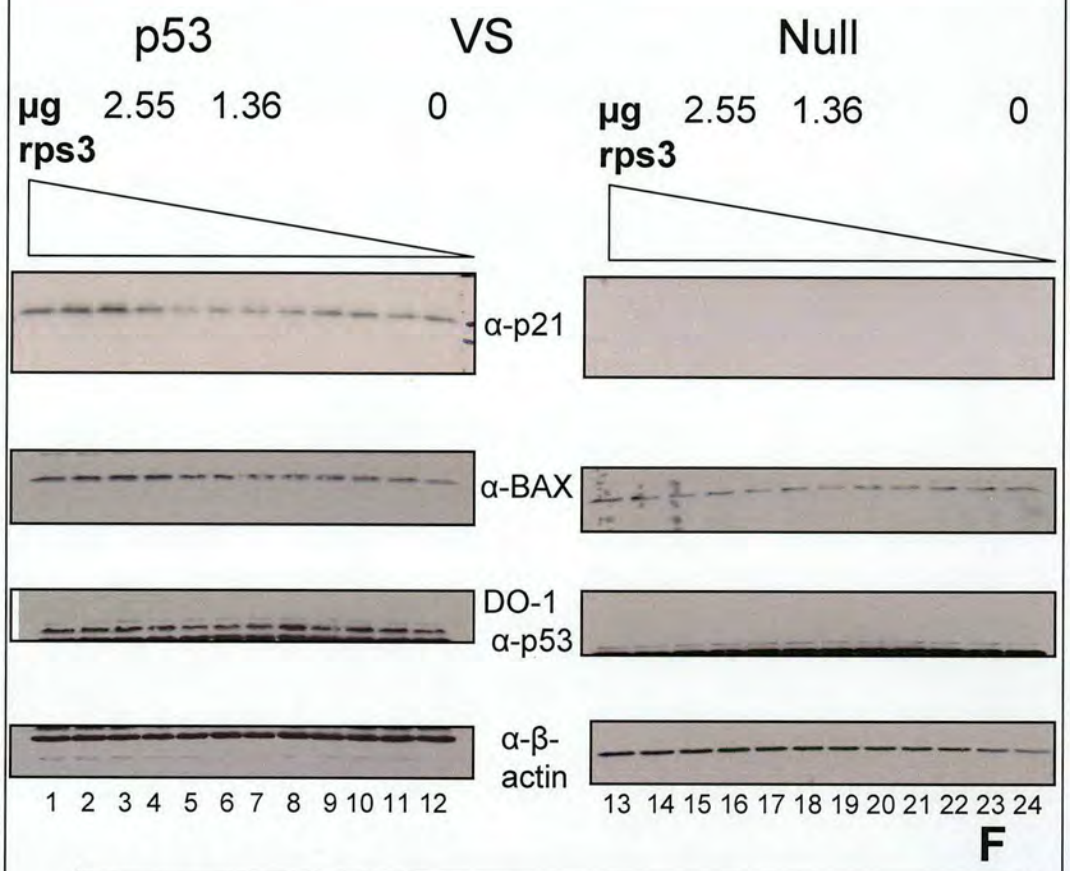

Figure 6.0 Identification of rps3 and ANT binding to p53^{R175H}

(**A**) Colloidal blue stain of eluates from DO-1 immunoprecipitated p53R175H infected Sf9 cells. Sf9 cells were infected with p53R175H baculovirus. Cells were harvested and lysed in Triton X-100 lysis buffer followed by DO-1 precipitation and 3 sequential glycine (0.1 M, pH 2.5) elutions. All bands were excised for analysis by LC-MS/MS. All bands were p53 positive except for the one indicated with an arrow.
(**B**) and (**C**) CID MS/MS spectra of single peptides from ANT and rps3 respectively showing *b* and *y* series of fragmentation.
(**D**) Clustal W alignment of rps3 with REF1 showing identity of GYSGV peptide in the two proteins.
(**E**) Dual luciferase p21-reporter assay. H1299 cells (24 well plates) were transfected with p53 (50 µg) (left panel) or equivalent amount of empty vector (right panel), incremental amounts of rps3 (500-2500 µg) , p21-consensus-luciferase and rinella-luciferase. Levels of p21 luciferase were normalised with levels obtained from internal standard renilla-luciferase.
(**F**) H1299 cells were transfected with p53 (50 µg) (left panel) or equivalent amount of empty vector (right panel), incremental amounts of rps3 (0.021-2.5 µg). 24 hrs post transfection the cells were lysed and immunoblotted for p21, BAX, p53 and β-actin.

7.0 Conclusions and future perspectives

In this thesis, primary focus was directed towards degradation of wild-type and mutant p53. Succinctly, and as illustrated in Figure 7.0, the following points were identified:

(**1**) Destabilizing, structural, missesense mutations in the DNA binding domain of p53 led to unfolding when compared to wild-type as defined by conformational antibodies.

(**2**) S10 β-sheet mutant $p53^{F270A}$ was hyperubiquitinated *in vivo* and in an *in vitro* translation assay which is MDM2 dependent.

(**3**) Mutant p53 interacted with a myriad of ribosomal proteins.

(**4**) Eef1a bound specifically to mutant p53.

(**5**) The molecular chaperone interactomes; "chaperomes" of mutant and wild-type p53 differed in that wild-type p53 bound preferentially to MDM2, Hsp40 and CHIP while mutant p53 bound Hsp70, CHIP and Hsp40 (with higher affinity than wild-type).

(**6**) A novel isoform of Hsp90 lacking the N-terminus (Hsp90ΔN) and TCP-1 beta (a chaperonin) were identified to specifically bind mutant p53.

(**7**) Wild-type p53 can be induced to bind to the Hsp90ΔN containing complex following the addition of Nutlin-3, 17-AAG.

As a side project, wild-type and naturally occurring mutations of the CHK2 gene were investigated. The following three points were been identified:

(**1**) $CHK2^{R145W}$ had a shorter half-life when compared to wild-type CHK2 and $CHK2^{I157T}$.

(**2**) $CHK2^{R145W}$ was hyperubiquitinated in cells when compared to wild-type CHK2.

(**3**) Protein phosphatase 1B1 (also known as PP2c beta) was identified as a binding partner of CHK2.

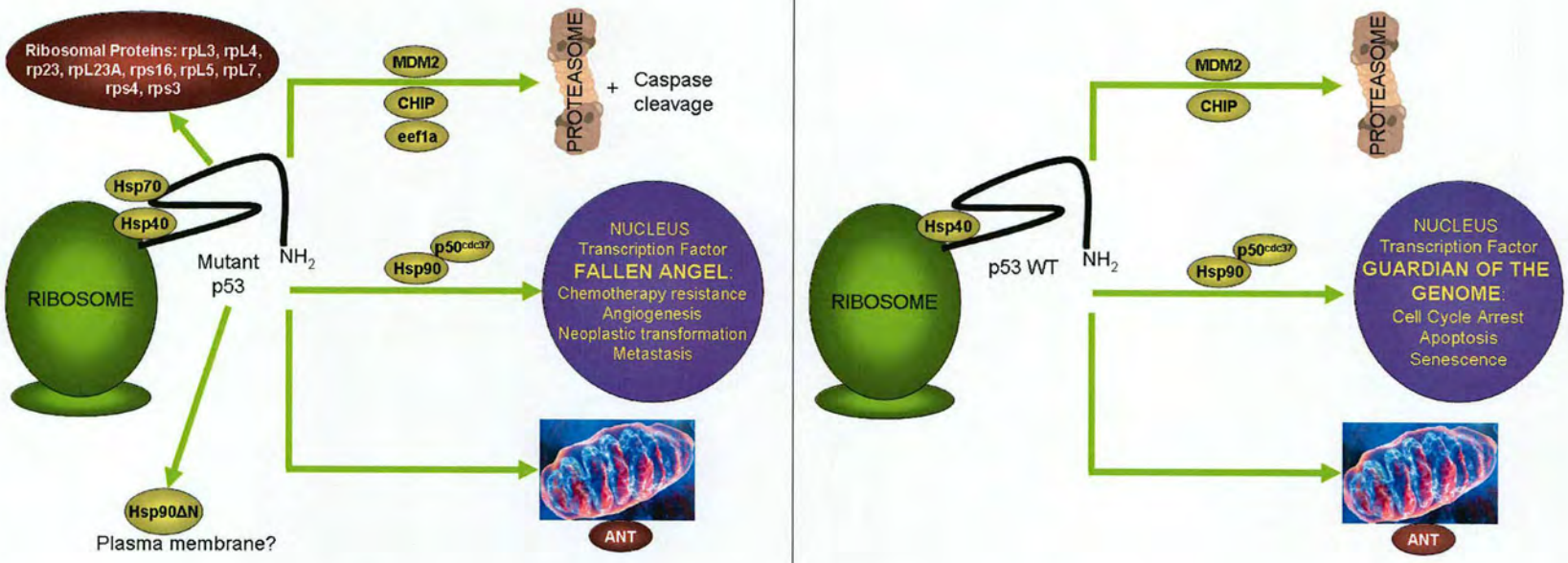

Figure 7.0 Summary of p53 interacting proteins. Proteins highlighted in yellow are molecular chaperones while proteins highlighted in purple have no chaperone activity known to date

7.1 The mutant p53:MDM2:eef1a interaction

A specific interaction between eef1a and mutant p53 was identified in this study. Furthermore, in a recent proteomic study MDM2 was found to bind eef1a without altering its translation function [140]. Elevated levels of eef1a have been found in primary human breast tissues [165] while high levels of MDM2 were found in a significant number of soft tissue sarcomas, osteosarcomas, gliomas and aggressive breast cancers [243-248]. It would therefore be interesting to perform a screen on these tumour types, particularly breast cancer, to investigate any correlation between gene amplification of eef1a and MDM2 and whether, a clinopathological significance exists for tumour progression (neoplasia) which is dependent on the p53:MDM2:eef1a interaction.

Biochemically, the interaction should be further characterised by knockdown of eef1a by siRNA. Current research efforts in Cathy Abbot's laboratory are directed towards the stable knockdown of eef1a in breast cancer cell lines. Once available, these cells (should they be viable) will be a useful tool for elucidating the role of eef1a:MDM2 in p53 degradation.

Moreover since eef1a has been shown to interact with the Rpt1 lid protein of the proteasome [131], it would be interesting to investigate the possible role of eef1a as a molecular chaperone that interacts with ubiquitinated p53 and directs the latter to the proteasome machinery for degradation. This study could be accomplished using specific mutant forms of eef1a, namely $eEF1A^{E286K}$ that shows poor interaction with the proteasome and $eEF1A^{D156N}$ which is hyperresistant to translation inhibitors but is more effective at eliminating damaged proteins [131].

7.2 Mutant and wild-type p53 interaction with Hsp90ΔN and $p50^{cdc37}$

In this study a specific interaction between Hsp90ΔN and mutant p53 was identified. Additionally, specific inhibitors designed for MDM2 and Hsp90, namely, Nutlin and 17-AAG appeared to enable WT p53 to form a complex with Hsp90ΔN. Current efforts in the laboratory are directed at disrupting the Hsp90ΔN:p53 complex by adding drugs that specifically inhibit the C-terminal ATPase activity of Hsp90 such as novobiocin. Briefly the experiment consists of transfecting H1299 cells with one-strep mutant and wildtype p53, following which the cells would be lysed and incubated with Novobiocin or excess ATP. The lysates would then be precipitated on strep-tactin columns and eluates immunoblotted for Hsp90ΔN, MDM2, Hsp70, Hsp90 and $p50^{cdc37}$. An siRNA approach to knockdown Hsp90ΔN could also be adopted and the effect of this silencing on ubiquitination of mutant/wild-type p53 ought to be investigated. A time-point experiment where cells are treated with 10 μM 17-AAG for incremental durations, i.e. 3, 10, 15, 30, 60 mins and 2, 5, 10 hours followed by analysis of Hsp90ΔN:p53 interaction would also be very informative. Treatment of cells for short periods of time would be enough to break hsp90 dependent complexes (including p53 chaperomes) without degrading the various hsp90-dependent clients substantially (Grammatikakis personal communication).

An interaction between p53 and the Hsp90 co-factor, $p50^{cdc37}$ was also identified in this study. Grammatikakis' laboratory kindly supplied us with a GST-fusion construct of $p50^{cdc37}$ in which the GST moiety has been modified by mutagenesis so that it does not bind p53, chaperones or other proteins specifically (Grammatikakis personal communication). This will hopefully prove to be a useful tool in further assessing the $p50^{cdc37}$: Hsp90ΔN:p53 complex and its effect on p53 ubiquitination/degradation.

Borek Votjesek's laboratory is currently preparing Hsp90ΔN specific antibodies for immunohistochemistry. These will be used to screen a wide array of primary human tumour samples (with p53 wild-type or mutant status) to assess the cellular sub-localization of Hsp90ΔN. Furthermore, Hsp90ΔN protein levels will also be screened in the same primary tumor samples.

7.3 p53 interaction with rps3

Ribosomal protein s3 (rps3) is a Janus-type protein with roles in polypeptide synthesis and DNA repair via the Base Excision repair pathway (BER). A specific interaction between rps3 and p53 was identified in this study. Recently work carried out by Deutsch's laboratory demonstrated that rps3 translocates from the cytoplasm to the nucleus following genotoxic stress. The translocation of rps3 is dependent on ERK1/2-mediated phosphorylation of a threonine residue (T42) of rps3. Moreover, rps3 was shown to co-localize with 7,8-dihydro-8-oxoguanine residues in DNA lesions associated with BER [249]. The rps3:p53 interaction should therefore be further investigated by observing the effect of specific rps3 knockdown by siRNA on BER and p53 activity in cells treated with BER inducing agents such as hydrogen peroxide and methyl methane sulphonate.

The Ref-1, DNA repair protein, has been shown to interact with p53 *in vitro* and *in vivo* and overexpression of the former leads to increased ability of p53 to stimulate endogenous p21 and cyclin G expression [232]. Ref-1 has also been shown to activate the AP-1 heterodimeric *fos-jun* transcription complex by changing the redox state of its DNA-binding-domain [231]. Current efforts in our laboratory are directed at elucidating

whether Ref-1 has a similar effect on key cysteines within the DNA-binding domain that bind zinc and are important residues for p53 conformation. If this were the case and since Ref-1 binds rps3 [242] it would be interesting to investigate whether rps3 has any effect on altering the ability of Ref-1 to modify the redox state of target DNA-binding domains.

Initial efforts to identify binding partners to rps3 by trypsin digestion of onestrep eluates obtained from cells transfected with onestrep rps3 have proved elusive due to low recovery yields. Current efforts are directed to scale up the amount of recovered proteins.

In the post-genomic era, advances in tools and technologies have provided an excellent opportunity to better understand the complex nature of carcinogenesis. Interactomics is an emergent, exciting field of systems biology which is a shift from the so called reductionist paradigm and to quote Denis Noble it

> "*is about putting together rather than taking apart, integration rather than reduction. It requires that we develop ways of thinking about integration that are rigorous as our reductionist programmes, but different. It means changing our philosophy, in the full sense of the term*".

In my modest opinion, the complexity of biological systems is better tackled by investigating multiple components simultaneously and collating data from different sources by intensive data mining.

8.0 References

Books:

[i] Mayer, R.J., Ciechanover A., Rechsteiner [Ed] *Protein Degradation - The Ubiquitin-Proteasome System.* Wiley-VCH, Weinheim, 2006 ISBN-10: 3-527-31130-0 **Vol 2:** p. 158.

[ii] Mayer, R.J., Ciechanover A., Rechsteiner [Ed] *Protein Degradation - The Ubiquitin-Proteasome System.* Wiley-VCH, Weinheim, 2006 ISBN-10: 3-527-31130-0 **Vol 2:** p. 3.

[iii] Mayer, R.J., Ciechanover A., Rechsteiner [Ed] *Protein Degradation - The Ubiquitin-Proteasome System.* Wiley-VCH, Weinheim, 2006 ISBN-10: 3-527-31130-0 **Vol 2:** p. 7.

[iv] Dass, C., *Principles and Practice of Biological Mass Spectrometry* Wiley Interscience Series on Mass Spectrometry, John Wiley & Sons, New York, 2001 ISBN: 0471330531: p. 27

[v] Dass, C., *Principles and Practice of Biological Mass Spectrometry* Wiley Interscience Series on Mass Spectrometry, John Wiley & Sons, New York, 2001 ISBN: 0471330531: p. 27-28

[vi] Dass, C., *Principles and Practice of Biological Mass Spectrometry* Wiley Interscience Series on Mass Spectrometry, John Wiley & Sons, New York, 2001 ISBN: 0471330531: p. 37

[vii] Dass, C., *Principles and Practice of Biological Mass Spectrometry* Wiley Interscience Series on Mass Spectrometry, John Wiley & Sons, New York, 2001 ISBN: 0471330531: p. 40

[viii] Dass, C., *Principles and Practice of Biological Mass Spectrometry* Wiley Interscience Series on Mass Spectrometry, John Wiley & Sons, New York, 2001 ISBN: 0471330531: p. 73

[ix] Hardie, D.G.[Ed] *Protein Phosphorylation: A practical approach* IRL Press, New York, 1993, ISBN 0-19-963305-3: p97

Papers:

1. Motoyama, N.; Naka, K., DNA damage tumor suppressor genes and genomic instability. *Curr Opin Genet Dev* **2004,** 14, (1), 11-6.

2. Iliakis, G.; Wang, Y.; Guan, J.; Wang, H., DNA damage checkpoint control in cells exposed to ionizing radiation. *Oncogene* **2003,** 22, (37), 5834-47.

3. Bakkenist, C. J.; Kastan, M. B., DNA damage activates ATM through intermolecular autophosphorylation and dimer dissociation. *Nature* **2003,** 421, (6922), 499-506.

4. Craig, A. L.; Hupp, T. R., The regulation of CHK2 in human cancer. *Oncogene* **2004,** 23, (52), 8411-8.

5. Bartek, J.; Lukas, J., Chk1 and Chk2 kinases in checkpoint control and cancer. *Cancer Cell* **2003,** 3, (5), 421-9.

6. Schwarz, J. K.; Lovly, C. M.; Piwnica-Worms, H., Regulation of the Chk2 protein kinase by oligomerization-mediated cis- and trans-phosphorylation. *Mol Cancer Res* **2003,** 1, (8), 598-609.
7. Matsuoka, S.; Huang, M.; Elledge, S. J., Linkage of ATM to cell cycle regulation by the Chk2 protein kinase. *Science* **1998,** 282, (5395), 1893-7.
8. Falck, J.; Mailand, N.; Syljuasen, R. G.; Bartek, J.; Lukas, J., The ATM-Chk2-Cdc25A checkpoint pathway guards against radioresistant DNA synthesis. *Nature* **2001,** 410, (6830), 842-7.
9. Zhang, J.; Willers, H.; Feng, Z.; Ghosh, J. C.; Kim, S.; Weaver, D. T.; Chung, J. H.; Powell, S. N.; Xia, F., Chk2 phosphorylation of BRCA1 regulates DNA double-strand break repair. *Mol Cell Biol* **2004,** 24, (2), 708-18.
10. Stevens, C.; Smith, L.; La Thangue, N. B., Chk2 activates E2F-1 in response to DNA damage. *Nat Cell Biol* **2003,** 5, (5), 401-9.
11. Hirao, A.; Kong, Y. Y.; Matsuoka, S.; Wakeham, A.; Ruland, J.; Yoshida, H.; Liu, D.; Elledge, S. J.; Mak, T. W., DNA damage-induced activation of p53 by the checkpoint kinase Chk2. *Science* **2000,** 287, (5459), 1824-7.
12. Craig, A.; Scott, M.; Burch, L.; Smith, G.; Ball, K.; Hupp, T., Allosteric effects mediate CHK2 phosphorylation of the p53 transactivation domain. *EMBO Rep* **2003,** 4, (8), 787-92.
13. Craig, A. L.; Chrystal, J. A.; Fraser, J. A.; Sphyris, N.; Lin, Y.; Harrison, B. J.; Scott, M. T.; Dornreiter, I.; Hupp, T. R., The MDM2 ubiquitination signal in the DNA-binding domain of p53 forms a docking site for calcium calmodulin kinase superfamily members. *Mol Cell Biol* **2007,** 27, (9), 3542-55.
14. Parker, L. L.; Piwnica-Worms, H., Inactivation of the p34cdc2-cyclin B complex by the human WEE1 tyrosine kinase. *Science* **1992,** 257, (5078), 1955-7.
15. Booher, R. N.; Holman, P. S.; Fattaey, A., Human Myt1 is a cell cycle-regulated kinase that inhibits Cdc2 but not Cdk2 activity. *J Biol Chem* **1997,** 272, (35), 22300-6.
16. Liu, F.; Stanton, J. J.; Wu, Z.; Piwnica-Worms, H., The human Myt1 kinase preferentially phosphorylates Cdc2 on threonine 14 and localizes to the endoplasmic reticulum and Golgi complex. *Mol Cell Biol* **1997,** 17, (2), 571-83.
17. Galmarini, C. M.; Kamath, K.; Vanier-Viornery, A.; Hervieu, V.; Peiller, E.; Falette, N.; Puisieux, A.; Ann Jordan, M.; Dumontet, C., Drug resistance associated with loss of p53 involves extensive alterations in microtubule composition and dynamics. *Br J Cancer* **2003,** 88, (11), 1793-9.
18. Galmarini, C. M.; Falette, N.; Tabone, E.; Levrat, C.; Britten, R.; Voorzanger-Rousselot, N.; Roesch-Gateau, O.; Vanier-Viornery, A.; Puisieux, A.; Dumontet, C., Inactivation of wild-type p53 by a dominant negative mutant renders MCF-7 cells resistant to tubulin-binding agent cytotoxicity. *Br J Cancer* **2001,** 85, (6), 902-8.
19. Vogelstein, B.; Lane, D.; Levine, A. J., Surfing the p53 network. *Nature* **2000,** 408, (6810), 307-10.
20. Bouchet, B. P.; de Fromentel, C. C.; Puisieux, A.; Galmarini, C. M., p53 as a target for anti-cancer drug development. *Crit Rev Oncol Hematol* **2006,** 58, (3), 190-207.
21. Toledo, F.; Wahl, G. M., Regulating the p53 pathway: in vitro hypotheses, in vivo veritas. *Nat Rev Cancer* **2006,** 6, (12), 909-23.
22. Lu, H.; Levine, A. J., Human TAFII31 protein is a transcriptional coactivator of the p53 protein. *Proc Natl Acad Sci U S A* **1995,** 92, (11), 5154-8.

23. Gu, W.; Roeder, R. G., Activation of p53 sequence-specific DNA binding by acetylation of the p53 C-terminal domain. *Cell* **1997,** 90, (4), 595-606.
24. Iyer, N. G.; Chin, S. F.; Ozdag, H.; Daigo, Y.; Hu, D. E.; Cariati, M.; Brindle, K.; Aparicio, S.; Caldas, C., p300 regulates p53-dependent apoptosis after DNA damage in colorectal cancer cells by modulation of PUMA/p21 levels. *Proc Natl Acad Sci U S A* **2004,** 101, (19), 7386-91.
25. Leveillard, T.; Andera, L.; Bissonnette, N.; Schaeffer, L.; Bracco, L.; Egly, J. M.; Wasylyk, B., Functional interactions between p53 and the TFIIH complex are affected by tumour-associated mutations. *Embo J* **1996,** 15, (7), 1615-24.
26. Xiao, H.; Pearson, A.; Coulombe, B.; Truant, R.; Zhang, S.; Regier, J. L.; Triezenberg, S. J.; Reinberg, D.; Flores, O.; Ingles, C. J.; et al., Binding of basal transcription factor TFIIH to the acidic activation domains of VP16 and p53. *Mol Cell Biol* **1994,** 14, (10), 7013-24.
27. Walker, K. K.; Levine, A. J., Identification of a novel p53 functional domain that is necessary for efficient growth suppression. *Proc Natl Acad Sci U S A* **1996,** 93, (26), 15335-40.
28. Mantovani, F.; Tocco, F.; Girardini, J.; Smith, P.; Gasco, M.; Lu, X.; Crook, T.; Del Sal, G., The prolyl isomerase Pin1 orchestrates p53 acetylation and dissociation from the apoptosis inhibitor iASPP. *Nat Struct Mol Biol* **2007,** 14, (10), 912-20.
29. Craig, A. L.; Burch, L.; Vojtesek, B.; Mikutowska, J.; Thompson, A.; Hupp, T. R., Novel phosphorylation sites of human tumour suppressor protein p53 at Ser20 and Thr18 that disrupt the binding of mdm2 (mouse double minute 2) protein are modified in human cancers. *Biochem J* **1999,** 342 (Pt 1), 133-41.
30. Schon, O.; Friedler, A.; Bycroft, M.; Freund, S. M.; Fersht, A. R., Molecular mechanism of the interaction between MDM2 and p53. *J Mol Biol* **2002,** 323, (3), 491-501.
31. Kraiss, S.; Quaiser, A.; Oren, M.; Montenarh, M., Oligomerization of oncoprotein p53. *J Virol* **1988,** 62, (12), 4737-44.
32. Cho, Y.; Gorina, S.; Jeffrey, P. D.; Pavletich, N. P., Crystal structure of a p53 tumor suppressor-DNA complex: understanding tumorigenic mutations. *Science* **1994,** 265, (5170), 346-55.
33. Joerger, A. C.; Fersht, A. R., Structure-function-rescue: the diverse nature of common p53 cancer mutants. *Oncogene* **2007,** 26, (15), 2226-42.
34. Jeffrey, P. D.; Gorina, S.; Pavletich, N. P., Crystal structure of the tetramerization domain of the p53 tumor suppressor at 1.7 angstroms. *Science* **1995,** 267, (5203), 1498-502.
35. Hupp, T. R.; Lane, D. P., Allosteric activation of latent p53 tetramers. *Curr Biol* **1994,** 4, (10), 865-75.
36. Hupp, T. R.; Lane, D. P., Two distinct signaling pathways activate the latent DNA binding function of p53 in a casein kinase II-independent manner. *J Biol Chem* **1995,** 270, (30), 18165-74.
37. Waterman, M. J.; Stavridi, E. S.; Waterman, J. L.; Halazonetis, T. D., ATM-dependent activation of p53 involves dephosphorylation and association with 14-3-3 proteins. *Nat Genet* **1998,** 19, (2), 175-8.
38. Wang, Y.; Reed, M.; Wang, P.; Stenger, J. E.; Mayr, G.; Anderson, M. E.; Schwedes, J. F.; Tegtmeyer, P., p53 domains: identification and characterization of two autonomous DNA-binding regions. *Genes Dev* **1993,** 7, (12B), 2575-86.

39. Lee, S.; Elenbaas, B.; Levine, A.; Griffith, J., p53 and its 14 kDa C-terminal domain recognize primary DNA damage in the form of insertion/deletion mismatches. *Cell* **1995,** 81, (7), 1013-20.
40. Lomax, M. E.; Barnes, D. M.; Hupp, T. R.; Picksley, S. M.; Camplejohn, R. S., Characterization of p53 oligomerization domain mutations isolated from Li-Fraumeni and Li-Fraumeni like family members. *Oncogene* **1998,** 17, (5), 643-9.
41. Bakalkin, G.; Selivanova, G.; Yakovleva, T.; Kiseleva, E.; Kashuba, E.; Magnusson, K. P.; Szekely, L.; Klein, G.; Terenius, L.; Wiman, K. G., p53 binds single-stranded DNA ends through the C-terminal domain and internal DNA segments via the middle domain. *Nucleic Acids Res* **1995,** 23, (3), 362-9.
42. Dang, C. V.; Lee, W. M., Nuclear and nucleolar targeting sequences of c-erb-A, c-myb, N-myc, p53, HSP70, and HIV tat proteins. *J Biol Chem* **1989,** 264, (30), 18019-23.
43. Zhang, Y.; Xiong, Y., A p53 amino-terminal nuclear export signal inhibited by DNA damage-induced phosphorylation. *Science* **2001,** 292, (5523), 1910-5.
44. Soussi, T., p53 alterations in human cancer: more questions than answers. *Oncogene* **2007,** 26, (15), 2145-56.
45. Deb, D.; Chakraborti, A. S.; Lanyi, A.; Troyer, D. A.; Deb, S., Disruption of functions of wild-type p53 by hetero-oligomerization. *Int J Oncol* **1999,** 15, (3), 413-22.
46. Strano, S.; Dell'Orso, S.; Di Agostino, S.; Fontemaggi, G.; Sacchi, A.; Blandino, G., Mutant p53: an oncogenic transcription factor. *Oncogene* **2007,** 26, (15), 2212-9.
47. Cadwell, C.; Zambetti, G. P., The effects of wild-type p53 tumor suppressor activity and mutant p53 gain-of-function on cell growth. *Gene* **2001,** 277, (1-2), 15-30.
48. Di Agostino, S.; Strano, S.; Emiliozzi, V.; Zerbini, V.; Mottolese, M.; Sacchi, A.; Blandino, G.; Piaggio, G., Gain of function of mutant p53: the mutant p53/NF-Y protein complex reveals an aberrant transcriptional mechanism of cell cycle regulation. *Cancer Cell* **2006,** 10, (3), 191-202.
49. Scheffner, M.; Werness, B. A.; Huibregtse, J. M.; Levine, A. J.; Howley, P. M., The E6 oncoprotein encoded by human papillomavirus types 16 and 18 promotes the degradation of p53. *Cell* **1990,** 63, (6), 1129-36.
50. Ciechanover, A.; Heller, H.; Elias, S.; Haas, A. L.; Hershko, A., ATP-dependent conjugation of reticulocyte proteins with the polypeptide required for protein degradation. *Proc Natl Acad Sci U S A* **1980,** 77, (3), 1365-8.
51. Hershko, A.; Ciechanover, A.; Heller, H.; Haas, A. L.; Rose, I. A., Proposed role of ATP in protein breakdown: conjugation of protein with multiple chains of the polypeptide of ATP-dependent proteolysis. *Proc Natl Acad Sci U S A* **1980,** 77, (4), 1783-6.
52. Hershko, A.; Heller, H.; Elias, S.; Ciechanover, A., Components of ubiquitin-protein ligase system. Resolution, affinity purification, and role in protein breakdown. *J Biol Chem* **1983,** 258, (13), 8206-14.
53. Haas, A. L.; Warms, J. V.; Hershko, A.; Rose, I. A., Ubiquitin-activating enzyme. Mechanism and role in protein-ubiquitin conjugation. *J Biol Chem* **1982,** 257, (5), 2543-8.
54. Lorick, K. L.; Jensen, J. P.; Fang, S.; Ong, A. M.; Hatakeyama, S.; Weissman, A. M., RING fingers mediate ubiquitin-conjugating enzyme (E2)-dependent ubiquitination. *Proc Natl Acad Sci U S A* **1999,** 96, (20), 11364-9.
55. Seol, J. H.; Feldman, R. M.; Zachariae, W.; Shevchenko, A.; Correll, C. C.; Lyapina, S.; Chi, Y.; Galova, M.; Claypool, J.; Sandmeyer, S.; Nasmyth, K.; Deshaies,

R. J.; Shevchenko, A.; Deshaies, R. J., Cdc53/cullin and the essential Hrt1 RING-H2 subunit of SCF define a ubiquitin ligase module that activates the E2 enzyme Cdc34. *Genes Dev* **1999,** 13, (12), 1614-26.
56. Orlicky, S.; Tang, X.; Willems, A.; Tyers, M.; Sicheri, F., Structural basis for phosphodependent substrate selection and orientation by the SCFCdc4 ubiquitin ligase. *Cell* **2003,** 112, (2), 243-56.
57. Zheng, N.; Wang, P.; Jeffrey, P. D.; Pavletich, N. P., Structure of a c-Cbl-UbcH7 complex: RING domain function in ubiquitin-protein ligases. *Cell* **2000,** 102, (4), 533-9.
58. Baumeister, W.; Walz, J.; Zuhl, F.; Seemuller, E., The proteasome: paradigm of a self-compartmentalizing protease. *Cell* **1998,** 92, (3), 367-80.
59. Lowe, J.; Stock, D.; Jap, B.; Zwickl, P.; Baumeister, W.; Huber, R., Crystal structure of the 20S proteasome from the archaeon T. acidophilum at 3.4 A resolution. *Science* **1995,** 268, (5210), 533-9.
60. Bogyo, M.; McMaster, J. S.; Gaczynska, M.; Tortorella, D.; Goldberg, A. L.; Ploegh, H., Covalent modification of the active site threonine of proteasomal beta subunits and the Escherichia coli homolog HslV by a new class of inhibitors. *Proc Natl Acad Sci U S A* **1997,** 94, (13), 6629-34.
61. Jones, S. N.; Roe, A. E.; Donehower, L. A.; Bradley, A., Rescue of embryonic lethality in Mdm2-deficient mice by absence of p53. *Nature* **1995,** 378, (6553), 206-8.
62. Honda, R.; Tanaka, H.; Yasuda, H., Oncoprotein MDM2 is a ubiquitin ligase E3 for tumor suppressor p53. *FEBS Lett* **1997,** 420, (1), 25-7.
63. Marechal, V.; Elenbaas, B.; Piette, J.; Nicolas, J. C.; Levine, A. J., The ribosomal L5 protein is associated with mdm-2 and mdm-2-p53 complexes. *Mol Cell Biol* **1994,** 14, (11), 7414-20.
64. Kubbutat, M. H.; Ludwig, R. L.; Ashcroft, M.; Vousden, K. H., Regulation of Mdm2-directed degradation by the C terminus of p53. *Mol Cell Biol* **1998,** 18, (10), 5690-8.
65. Rodriguez, M. S.; Desterro, J. M.; Lain, S.; Lane, D. P.; Hay, R. T., Multiple C-terminal lysine residues target p53 for ubiquitin-proteasome-mediated degradation. *Mol Cell Biol* **2000,** 20, (22), 8458-67.
66. Maki, C. G., Oligomerization is required for p53 to be efficiently ubiquitinated by MDM2. *J Biol Chem* **1999,** 274, (23), 16531-5.
67. Shimizu, H.; Burch, L. R.; Smith, A. J.; Dornan, D.; Wallace, M.; Ball, K. L.; Hupp, T. R., The conformationally flexible S9-S10 linker region in the core domain of p53 contains a novel MDM2 binding site whose mutation increases ubiquitination of p53 in vivo. *J Biol Chem* **2002,** 277, (32), 28446-58.
68. Wallace, M.; Worrall, E.; Pettersson, S.; Hupp, T. R.; Ball, K. L., Dual-site regulation of MDM2 E3-ubiquitin ligase activity. *Mol Cell* **2006,** 23, (2), 251-63.
69. Honda, R.; Yasuda, H., Association of p19(ARF) with Mdm2 inhibits ubiquitin ligase activity of Mdm2 for tumor suppressor p53. *Embo J* **1999,** 18, (1), 22-7.
70. Weber, J. D.; Taylor, L. J.; Roussel, M. F.; Sherr, C. J.; Bar-Sagi, D., Nucleolar Arf sequesters Mdm2 and activates p53. *Nat Cell Biol* **1999,** 1, (1), 20-6.
71. Tao, W.; Levine, A. J., P19(ARF) stabilizes p53 by blocking nucleo-cytoplasmic shuttling of Mdm2. *Proc Natl Acad Sci U S A* **1999,** 96, (12), 6937-41.
72. Dai, M. S.; Lu, H., Inhibition of MDM2-mediated p53 ubiquitination and degradation by ribosomal protein L5. *J Biol Chem* **2004,** 279, (43), 44475-82.

73. Hodges, M.; Tissot, C.; Freemont, P. S., Protein regulation: tag wrestling with relatives of ubiquitin. *Curr Biol* **1998,** 8, (21), R749-52.
74. Fogal, V.; Gostissa, M.; Sandy, P.; Zacchi, P.; Sternsdorf, T.; Jensen, K.; Pandolfi, P. P.; Will, H.; Schneider, C.; Del Sal, G., Regulation of p53 activity in nuclear bodies by a specific PML isoform. *Embo J* **2000,** 19, (22), 6185-95.
75. Osaka, F.; Kawasaki, H.; Aida, N.; Saeki, M.; Chiba, T.; Kawashima, S.; Tanaka, K.; Kato, S., A new NEDD8-ligating system for cullin-4A. *Genes Dev* **1998,** 12, (15), 2263-8.
76. Gong, L.; Yeh, E. T., Identification of the activating and conjugating enzymes of the NEDD8 conjugation pathway. *J Biol Chem* **1999,** 274, (17), 12036-42.
77. Xirodimas, D. P.; Saville, M. K.; Bourdon, J. C.; Hay, R. T.; Lane, D. P., Mdm2-mediated NEDD8 conjugation of p53 inhibits its transcriptional activity. *Cell* **2004,** 118, (1), 83-97.
78. Schubert, U.; Anton, L. C.; Gibbs, J.; Norbury, C. C.; Yewdell, J. W.; Bennink, J. R., Rapid degradation of a large fraction of newly synthesized proteins by proteasomes. *Nature* **2000,** 404, (6779), 770-4.
79. Hohfeld, J.; Cyr, D. M.; Patterson, C., From the cradle to the grave: molecular chaperones that may choose between folding and degradation. *EMBO Rep* **2001,** 2, (10), 885-90.
80. Wickner, S.; Maurizi, M. R.; Gottesman, S., Posttranslational quality control: folding, refolding, and degrading proteins. *Science* **1999,** 286, (5446), 1888-93.
81. Ellis, R. J., Molecular chaperones: assisting assembly in addition to folding. *Trends Biochem Sci* **2006,** 31, (7), 395-401.
82. Mayer, M. P.; Bukau, B., Hsp70 chaperones: cellular functions and molecular mechanism. *Cell Mol Life Sci* **2005,** 62, (6), 670-84.
83. Young, J. C.; Agashe, V. R.; Siegers, K.; Hartl, F. U., Pathways of chaperone-mediated protein folding in the cytosol. *Nat Rev Mol Cell Biol* **2004,** 5, (10), 781-91.
84. Hartl, F. U.; Hayer-Hartl, M., Molecular chaperones in the cytosol: from nascent chain to folded protein. *Science* **2002,** 295, (5561), 1852-8.
85. Frydman, J.; Hohfeld, J., Chaperones get in touch: the Hip-Hop connection. *Trends Biochem Sci* **1997,** 22, (3), 87-92.
86. Mosser, D. D.; Morimoto, R. I., Molecular chaperones and the stress of oncogenesis. *Oncogene* **2004,** 23, (16), 2907-18.
87. Caplan, A. J.; Mandal, A. K.; Theodoraki, M. A., Molecular chaperones and protein kinase quality control. *Trends Cell Biol* **2007,** 17, (2), 87-92.
88. Esser, C.; Alberti, S.; Hohfeld, J., Cooperation of molecular chaperones with the ubiquitin/proteasome system. *Biochim Biophys Acta* **2004,** 1695, (1-3), 171-88.
89. Wiederkehr, T.; Bukau, B.; Buchberger, A., Protein turnover: a CHIP programmed for proteolysis. *Curr Biol* **2002,** 12, (1), R26-8.
90. Arndt, V.; Rogon, C.; Hohfeld, J., To be, or not to be - molecular chaperones in protein degradation. *Cell Mol Life Sci* **2007,** 64, (19-20), 2525-41.
91. Mayer, M. P.; Brehmer, D.; Gassler, C. S.; Bukau, B., Hsp70 chaperone machines. *Adv Protein Chem* **2001,** 59, 1-44.
92. Bukau, B.; Horwich, A. L., The Hsp70 and Hsp60 chaperone machines. *Cell* **1998,** 92, (3), 351-66.
93. Rudiger, S.; Germeroth, L.; Schneider-Mergener, J.; Bukau, B., Substrate specificity of the DnaK chaperone determined by screening cellulose-bound peptide libraries. *Embo J* **1997,** 16, (7), 1501-7.

94. Zhu, X.; Zhao, X.; Burkholder, W. F.; Gragerov, A.; Ogata, C. M.; Gottesman, M. E.; Hendrickson, W. A., Structural analysis of substrate binding by the molecular chaperone DnaK. *Science* **1996,** 272, (5268), 1606-14.
95. Ballinger, C. A.; Connell, P.; Wu, Y.; Hu, Z.; Thompson, L. J.; Yin, L. Y.; Patterson, C., Identification of CHIP, a novel tetratricopeptide repeat-containing protein that interacts with heat shock proteins and negatively regulates chaperone functions. *Mol Cell Biol* **1999,** 19, (6), 4535-45.
96. Hohfeld, J.; Minami, Y.; Hartl, F. U., Hip, a novel cochaperone involved in the eukaryotic Hsc70/Hsp40 reaction cycle. *Cell* **1995,** 83, (4), 589-98.
97. Gassler, C. S.; Wiederkehr, T.; Brehmer, D.; Bukau, B.; Mayer, M. P., Bag-1M accelerates nucleotide release for human Hsc70 and Hsp70 and can act concentration-dependent as positive and negative cofactor. *J Biol Chem* **2001,** 276, (35), 32538-44.
98. Hohfeld, J.; Jentsch, S., GrpE-like regulation of the hsc70 chaperone by the anti-apoptotic protein BAG-1. *Embo J* **1997,** 16, (20), 6209-16.
99. Buchner, J., Hsp90 & Co. - a holding for folding. *Trends Biochem Sci* **1999,** 24, (4), 136-41.
100. Caplan, A. J., Hsp90's secrets unfold: new insights from structural and functional studies. *Trends Cell Biol* **1999,** 9, (7), 262-8.
101. Scheufler, C.; Brinker, A.; Bourenkov, G.; Pegoraro, S.; Moroder, L.; Bartunik, H.; Hartl, F. U.; Moarefi, I., Structure of TPR domain-peptide complexes: critical elements in the assembly of the Hsp70-Hsp90 multichaperone machine. *Cell* **2000,** 101, (2), 199-210.
102. Connell, P.; Ballinger, C. A.; Jiang, J.; Wu, Y.; Thompson, L. J.; Hohfeld, J.; Patterson, C., The co-chaperone CHIP regulates protein triage decisions mediated by heat-shock proteins. *Nat Cell Biol* **2001,** 3, (1), 93-6.
103. Xu, Z.; Horwich, A. L.; Sigler, P. B., The crystal structure of the asymmetric GroEL-GroES-(ADP)7 chaperonin complex. *Nature* **1997,** 388, (6644), 741-50.
104. Saibil, H. R.; Ranson, N. A., The chaperonin folding machine. *Trends Biochem Sci* **2002,** 27, (12), 627-32.
105. Meyer, A. S.; Gillespie, J. R.; Walther, D.; Millet, I. S.; Doniach, S.; Frydman, J., Closing the folding chamber of the eukaryotic chaperonin requires the transition state of ATP hydrolysis. *Cell* **2003,** 113, (3), 369-81.
106. Thulasiraman, V.; Yang, C. F.; Frydman, J., In vivo newly translated polypeptides are sequestered in a protected folding environment. *Embo J* **1999,** 18, (1), 85-95.
107. Meacham, G. C.; Patterson, C.; Zhang, W.; Younger, J. M.; Cyr, D. M., The Hsc70 co-chaperone CHIP targets immature CFTR for proteasomal degradation. *Nat Cell Biol* **2001,** 3, (1), 100-5.
108. Esser, C.; Scheffner, M.; Hohfeld, J., The chaperone-associated ubiquitin ligase CHIP is able to target p53 for proteasomal degradation. *J Biol Chem* **2005,** 280, (29), 27443-8.
109. Lukashchuk, N.; Vousden, K. H., Ubiquitination and Degradation of Mutant P53. *Mol Cell Biol* **2007**.
110. Karas, M.; Hillenkamp, F., Laser desorption ionization of proteins with molecular masses exceeding 10,000 daltons. *Anal Chem* **1988,** 60, (20), 2299-301.
111. Dreisewerd, K., The desorption process in MALDI. *Chem Rev* **2003,** 103, (2), 395-426.

112. Nemes, P.; Marginean, I.; Vertes, A., Spraying mode effect on droplet formation and ion chemistry in electrosprays. *Anal Chem* **2007,** 79, (8), 3105-16.
113. Juraschek, R.; Dulcks, T.; Karas, M., Nanoelectrospray--more than just a minimized-flow electrospray ionization source. *J Am Soc Mass Spectrom* **1999,** 10, (4), 300-8.
114. Cotter, R. J.; Woods, A. S.; Cornish, T. J., Biological applications of time-of-flight mass spectrometry. *Biochem Soc Trans* **1994,** 22, (2), 539-42.
115. Brown, R. S.; Lennon, J. J., Mass resolution improvement by incorporation of pulsed ion extraction in a matrix-assisted laser desorption/ionization linear time-of-flight mass spectrometer. *Anal Chem* **1995,** 67, (13), 1998-2003.
116. Kaufmann, R.; Spengler, B.; Lutzenkirchen, F., Mass spectrometric sequencing of linear peptides by product-ion analysis in a reflectron time-of-flight mass spectrometer using matrix-assisted laser desorption ionization. *Rapid Commun Mass Spectrom* **1993,** 7, (10), 902-10.
117. McLuckey, S. A.; Van Berkel, G. J.; Goeringer, D. E.; Glish, G. L., Ion trap mass spectrometry. Using high-pressure ionization. *Anal Chem* **1994,** 66, (14), 737A-743A.
118. Boyd, R. K.; Bott, P. A.; Beer, B. R.; Harvan, D. J.; Hass, J. R., Computer-based mass measurement of fragment ion spectra from tandem magnetic sector mass spectrometers with an electrically floated collision cell. *Anal Chem* **1987,** 59, (1), 189-93.
119. Kaiser, R. E., Jr.; Williams, J. D.; Lammert, S. A.; Cooks, R. G.; Zakett, D., Thermospray liquid chromatography-mass spectrometry with a quadrupole ion trap mass spectrometer. *J Chromatogr* **1991,** 562, (1-2), 3-11.
120. McLuckey, S. A.; Goeringer, D. E.; Glish, G. L., Collisional activation with random noise in ion trap mass spectrometry. *Anal Chem* **1992,** 64, (13), 1455-60.
121. Patterson, S. D., Matrix-assisted laser-desorption/ionization mass spectrometric approaches for the identification of gel-separated proteins in the 5-50 pmol range. *Electrophoresis* **1995,** 16, (7), 1104-14.
122. Yates, J. R., 3rd; Eng, J. K.; McCormack, A. L.; Schieltz, D., Method to correlate tandem mass spectra of modified peptides to amino acid sequences in the protein database. *Anal Chem* **1995,** 67, (8), 1426-36.
123. Roepstorff, P.; Fohlman, J., Proposal for a common nomenclature for sequence ions in mass spectra of peptides. *Biomed Mass Spectrom* **1984,** 11, (11), 601.
124. Leng, R. P.; Lin, Y.; Ma, W.; Wu, H.; Lemmers, B.; Chung, S.; Parant, J. M.; Lozano, G.; Hakem, R.; Benchimol, S., Pirh2, a p53-induced ubiquitin-protein ligase, promotes p53 degradation. *Cell* **2003,** 112, (6), 779-91.
125. Dornan, D.; Wertz, I.; Shimizu, H.; Arnott, D.; Frantz, G. D.; Dowd, P.; O'Rourke, K.; Koeppen, H.; Dixit, V. M., The ubiquitin ligase COP1 is a critical negative regulator of p53. *Nature* **2004,** 429, (6987), 86-92.
126. Rajendra, R.; Malegaonkar, D.; Pungaliya, P.; Marshall, H.; Rasheed, Z.; Brownell, J.; Liu, L. F.; Lutzker, S.; Saleem, A.; Rubin, E. H., Topors functions as an E3 ubiquitin ligase with specific E2 enzymes and ubiquitinates p53. *J Biol Chem* **2004,** 279, (35), 36440-4.
127. Chen, D.; Kon, N.; Li, M.; Zhang, W.; Qin, J.; Gu, W., ARF-BP1/Mule is a critical mediator of the ARF tumor suppressor. *Cell* **2005,** 121, (7), 1071-83.
128. Yamasaki, S.; Yagishita, N.; Sasaki, T.; Nakazawa, M.; Kato, Y.; Yamadera, T.; Bae, E.; Toriyama, S.; Ikeda, R.; Zhang, L.; Fujitani, K.; Yoo, E.; Tsuchimochi, K.;

Ohta, T.; Araya, N.; Fujita, H.; Aratani, S.; Eguchi, K.; Komiya, S.; Maruyama, I.; Higashi, N.; Sato, M.; Senoo, H.; Ochi, T.; Yokoyama, S.; Amano, T.; Kim, J.; Gay, S.; Fukamizu, A.; Nishioka, K.; Tanaka, K.; Nakajima, T., Cytoplasmic destruction of p53 by the endoplasmic reticulum-resident ubiquitin ligase 'Synoviolin'. *Embo J* **2007,** 26, (1), 113-22.
129. Yang, W.; Rozan, L. M.; McDonald, E. R., 3rd; Navaraj, A.; Liu, J. J.; Matthew, E. M.; Wang, W.; Dicker, D. T.; El-Deiry, W. S., CARPs are ubiquitin ligases that promote MDM2-independent p53 and phospho-p53ser20 degradation. *J Biol Chem* **2007,** 282, (5), 3273-81.
130. Kudo, T.; Katayama, T.; Imaizumi, K.; Yasuda, Y.; Yatera, M.; Okochi, M.; Tohyama, M.; Takeda, M., The unfolded protein response is involved in the pathology of Alzheimer's disease. *Ann N Y Acad Sci* **2002,** 977, 349-55.
131. Chuang, S. M.; Chen, L.; Lambertson, D.; Anand, M.; Kinzy, T. G.; Madura, K., Proteasome-mediated degradation of cotranslationally damaged proteins involves translation elongation factor 1A. *Mol Cell Biol* **2005,** 25, (1), 403-13.
132. Cook, A.; Milner, J., Evidence for allosteric variants of wild-type p53, a tumour suppressor protein. *Br J Cancer* **1990,** 61, (4), 548-52.
133. Mendoza, H. M.; Shen, L. N.; Botting, C.; Lewis, A.; Chen, J.; Ink, B.; Hay, R. T., NEDP1, a highly conserved cysteine protease that deNEDDylates Cullins. *J Biol Chem* **2003,** 278, (28), 25637-43.
134. Kussie, P. H.; Gorina, S.; Marechal, V.; Elenbaas, B.; Moreau, J.; Levine, A. J.; Pavletich, N. P., Structure of the MDM2 oncoprotein bound to the p53 tumor suppressor transactivation domain. *Science* **1996,** 274, (5289), 948-53.
135. Yun, E. Y.; Goo, T. W.; Kim, S. W.; Choi, K. H.; Hwang, J. S.; Kang, S. W.; Kwon, O. Y., Changes in cellular secretory processing during baculovirus infection. *Biotechnol Lett* **2005,** 27, (14), 1041-5.
136. Dai, M. S.; Zeng, S. X.; Jin, Y.; Sun, X. X.; David, L.; Lu, H., Ribosomal protein L23 activates p53 by inhibiting MDM2 function in response to ribosomal perturbation but not to translation inhibition. *Mol Cell Biol* **2004,** 24, (17), 7654-68.
137. Mauro, V. P.; Edelman, G. M., The ribosome filter hypothesis. *Proc Natl Acad Sci U S A* **2002,** 99, (19), 12031-6.
138. Hotokezaka, Y.; Tobben, U.; Hotokezaka, H.; Van Leyen, K.; Beatrix, B.; Smith, D. H.; Nakamura, T.; Wiedmann, M., Interaction of the eukaryotic elongation factor 1A with newly synthesized polypeptides. *J Biol Chem* **2002,** 277, (21), 18545-51.
139. Dumont, P.; Leu, J. I.; Della Pietra, A. C., 3rd; George, D. L.; Murphy, M., The codon 72 polymorphic variants of p53 have markedly different apoptotic potential. *Nat Genet* **2003,** 33, (3), 357-65.
140. Frum, R.; Busby, S. A.; Ramamoorthy, M.; Deb, S.; Shabanowitz, J.; Hunt, D. F.; Deb, S. P., HDM2-binding partners: interaction with translation elongation factor EF1alpha. *J Proteome Res* **2007,** 6, (4), 1410-7.
141. Schmidt, M.; Kloetzel, P. M., Biogenesis of eukaryotic 20S proteasomes: the complex maturation pathway of a complex enzyme. *Faseb J* **1997,** 11, (14), 1235-43.
142. Burch, L.; Shimizu, H.; Smith, A.; Patterson, C.; Hupp, T. R., Expansion of protein interaction maps by phage peptide display using MDM2 as a prototypical conformationally flexible target protein. *J Mol Biol* **2004,** 337, (1), 129-45.
143. Yu, G. W.; Rudiger, S.; Veprintsev, D.; Freund, S.; Fernandez-Fernandez, M. R.; Fersht, A. R., The central region of HDM2 provides a second binding site for p53. *Proc Natl Acad Sci U S A* **2006,** 103, (5), 1227-32.

144. Joerger, A. C.; Ang, H. C.; Fersht, A. R., Structural basis for understanding oncogenic p53 mutations and designing rescue drugs. *Proc Natl Acad Sci U S A* **2006,** 103, (41), 15056-61.
145. Marston, N. J.; Jenkins, J. R.; Vousden, K. H., Oligomerisation of full length p53 contributes to the interaction with mdm2 but not HPV E6. *Oncogene* **1995,** 10, (9), 1709-15.
146. O'Neill, M.; Campbell, S. J.; Save, V.; Thompson, A. M.; Hall, P. A., An immunochemical analysis of mdm2 expression in human breast cancer and the identification of a growth-regulated cross-reacting species p170. *J Pathol* **1998,** 186, (3), 254-61.
147. Wawrzynow, B.; Zylicz, A.; Wallace, M.; Hupp, T.; Zylicz, M., MDM2 Chaperones the p53 Tumor Suppressor. *J Biol Chem* **2007,** 282, (45), 32603-12.
148. Chan, W. M.; Mak, M. C.; Fung, T. K.; Lau, A.; Siu, W. Y.; Poon, R. Y., Ubiquitination of p53 at multiple sites in the DNA-binding domain. *Mol Cancer Res* **2006,** 4, (1), 15-25.
149. Krummel, K. A.; Lee, C. J.; Toledo, F.; Wahl, G. M., The C-terminal lysines fine-tune P53 stress responses in a mouse model but are not required for stability control or transactivation. *Proc Natl Acad Sci U S A* **2005,** 102, (29), 10188-93.
150. Metspalu, A.; Toots, I.; Saarma, M.; Villems, R., The ternary complex consisting of rat liver ribosomal 5 S RNA, 5.8 S RNA and protein L5. *FEBS Lett* **1980,** 119, (1), 81-4.
151. Fontoura, B. M.; Atienza, C. A.; Sorokina, E. A.; Morimoto, T.; Carroll, R. B., Cytoplasmic p53 polypeptide is associated with ribosomes. *Mol Cell Biol* **1997,** 17, (6), 3146-54.
152. Lee, J. C.; Henry, B.; Yeh, Y. C., Binding of proteins from the large ribosomal subunits to 5.8 S rRNA of Saccharomyces cerevisiae. *J Biol Chem* **1983,** 258, (2), 854-8.
153. Sherr, C. J.; Weber, J. D., The ARF/p53 pathway. *Curr Opin Genet Dev* **2000,** 10, (1), 94-9.
154. Rubbi, C. P.; Milner, J., Non-activated p53 co-localizes with sites of transcription within both the nucleoplasm and the nucleolus. *Oncogene* **2000,** 19, (1), 85-96.
155. Klibanov, S. A.; O'Hagan, H. M.; Ljungman, M., Accumulation of soluble and nucleolar-associated p53 proteins following cellular stress. *J Cell Sci* **2001,** 114, (Pt 10), 1867-73.
156. Dunbar, D. A.; Dragon, F.; Lee, S. J.; Baserga, S. J., A nucleolar protein related to ribosomal protein L7 is required for an early step in large ribosomal subunit biogenesis. *Proc Natl Acad Sci U S A* **2000,** 97, (24), 13027-32.
157. Kramer, G.; Rauch, T.; Rist, W.; Vorderwulbecke, S.; Patzelt, H.; Schulze-Specking, A.; Ban, N.; Deuerling, E.; Bukau, B., L23 protein functions as a chaperone docking site on the ribosome. *Nature* **2002,** 419, (6903), 171-4.
158. Bukau, B.; Deuerling, E.; Pfund, C.; Craig, E. A., Getting newly synthesized proteins into shape. *Cell* **2000,** 101, (2), 119-22.
159. Patzelt, H.; Rudiger, S.; Brehmer, D.; Kramer, G.; Vorderwulbecke, S.; Schaffitzel, E.; Waitz, A.; Hesterkamp, T.; Dong, L.; Schneider-Mergener, J.; Bukau, B.; Deuerling, E., Binding specificity of Escherichia coli trigger factor. *Proc Natl Acad Sci U S A* **2001,** 98, (25), 14244-9.

160. Deuerling, E.; Patzelt, H.; Vorderwulbecke, S.; Rauch, T.; Kramer, G.; Schaffitzel, E.; Mogk, A.; Schulze-Specking, A.; Langen, H.; Bukau, B., Trigger Factor and DnaK possess overlapping substrate pools and binding specificities. *Mol Microbiol* **2003,** 47, (5), 1317-28.
161. Caldas, T. D.; El Yaagoubi, A.; Richarme, G., Chaperone properties of bacterial elongation factor EF-Tu. *J Biol Chem* **1998,** 273, (19), 11478-82.
162. Suzuki, H.; Ueda, T.; Taguchi, H.; Takeuchi, N., Chaperone properties of mammalian mitochondrial translation elongation factor Tu. *J Biol Chem* **2007,** 282, (6), 4076-84.
163. Amsterdam, A.; Sadler, K. C.; Lai, K.; Farrington, S.; Bronson, R. T.; Lees, J. A.; Hopkins, N., Many ribosomal protein genes are cancer genes in zebrafish. *PLoS Biol* **2004,** 2, (5), E139.
164. Rajasekhar, V. K.; Viale, A.; Socci, N. D.; Wiedmann, M.; Hu, X.; Holland, E. C., Oncogenic Ras and Akt signaling contribute to glioblastoma formation by differential recruitment of existing mRNAs to polysomes. *Mol Cell* **2003,** 12, (4), 889-901.
165. Chen, L.; Madura, K., Increased proteasome activity, ubiquitin-conjugating enzymes, and eEF1A translation factor detected in breast cancer tissue. *Cancer Res* **2005,** 65, (13), 5599-606.
166. Lukashchuk, N.; Vousden, K. H., Ubiquitination and degradation of mutant p53. *Mol Cell Biol* **2007,** 27, (23), 8284-95.
167. Jolly, C.; Morimoto, R. I., Role of the heat shock response and molecular chaperones in oncogenesis and cell death. *J Natl Cancer Inst* **2000,** 92, (19), 1564-72.
168. Blagosklonny, M. V.; Toretsky, J.; Bohen, S.; Neckers, L., Mutant conformation of p53 translated in vitro or in vivo requires functional HSP90. *Proc Natl Acad Sci U S A* **1996,** 93, (16), 8379-83.
169. Sugito, K.; Yamane, M.; Hattori, H.; Hayashi, Y.; Tohnai, I.; Ueda, M.; Tsuchida, N.; Ohtsuka, K., Interaction between hsp70 and hsp40, eukaryotic homologues of DnaK and DnaJ, in human cells expressing mutant-type p53. *FEBS Lett* **1995,** 358, (2), 161-4.
170. Whitesell, L.; Sutphin, P. D.; Pulcini, E. J.; Martinez, J. D.; Cook, P. H., The physical association of multiple molecular chaperone proteins with mutant p53 is altered by geldanamycin, an hsp90-binding agent. *Mol Cell Biol* **1998,** 18, (3), 1517-24.
171. King, F. W.; Wawrzynow, A.; Hohfeld, J.; Zylicz, M., Co-chaperones Bag-1, Hop and Hsp40 regulate Hsc70 and Hsp90 interactions with wild-type or mutant p53. *Embo J* **2001,** 20, (22), 6297-305.
172. Arkin, M. R.; Wells, J. A., Small-molecule inhibitors of protein-protein interactions: progressing towards the dream. *Nat Rev Drug Discov* **2004,** 3, (4), 301-17.
173. Vassilev, L. T.; Vu, B. T.; Graves, B.; Carvajal, D.; Podlaski, F.; Filipovic, Z.; Kong, N.; Kammlott, U.; Lukacs, C.; Klein, C.; Fotouhi, N.; Liu, E. A., In vivo activation of the p53 pathway by small-molecule antagonists of MDM2. *Science* **2004,** 303, (5659), 844-8.
174. Pochampally, R.; Fodera, B.; Chen, L.; Lu, W.; Chen, J., Activation of an MDM2-specific caspase by p53 in the absence of apoptosis. *J Biol Chem* **1999,** 274, (21), 15271-7.
175. Workman, P.; Burrows, F.; Neckers, L.; Rosen, N., Drugging the Cancer Chaperone HSP90: Combinatorial Therapeutic Exploitation of Oncogene Addiction and Tumor Stress. *Ann N Y Acad Sci* **2007,** 1113, 202-16.

176. Tripathi, V.; Ali, A.; Bhat, R.; Pati, U., CHIP chaperones wild type p53 tumor suppressor protein. *J Biol Chem* **2007,** 282, (39), 28441-54.
177. Lee, H.; Mok, K. H.; Muhandiram, R.; Park, K. H.; Suk, J. E.; Kim, D. H.; Chang, J.; Sung, Y. C.; Choi, K. Y.; Han, K. H., Local structural elements in the mostly unstructured transcriptional activation domain of human p53. *J Biol Chem* **2000,** 275, (38), 29426-32.
178. Davidoff, A. M.; Iglehart, J. D.; Marks, J. R., Immune response to p53 is dependent upon p53/HSP70 complexes in breast cancers. *Proc Natl Acad Sci U S A* **1992,** 89, (8), 3439-42.
179. Blagosklonny, M. V.; Toretsky, J.; Neckers, L., Geldanamycin selectively destabilizes and conformationally alters mutated p53. *Oncogene* **1995,** 11, (5), 933-9.
180. Csermely, P.; Schnaider, T.; Soti, C.; Prohaszka, Z.; Nardai, G., The 90-kDa molecular chaperone family: structure, function, and clinical applications. A comprehensive review. *Pharmacol Ther* **1998,** 79, (2), 129-68.
181. Grammatikakis, N.; Vultur, A.; Ramana, C. V.; Siganou, A.; Schweinfest, C. W.; Watson, D. K.; Raptis, L., The role of Hsp90N, a new member of the Hsp90 family, in signal transduction and neoplastic transformation. *J Biol Chem* **2002,** 277, (10), 8312-20.
182. Sreedhar, A. S.; Kalmar, E.; Csermely, P.; Shen, Y. F., Hsp90 isoforms: functions, expression and clinical importance. *FEBS Lett* **2004,** 562, (1-3), 11-5.
183. Perdew, G. H.; Wiegand, H.; Vanden Heuvel, J. P.; Mitchell, C.; Singh, S. S., A 50 kilodalton protein associated with raf and pp60(v-src) protein kinases is a mammalian homolog of the cell cycle control protein cdc37. *Biochemistry* **1997,** 36, (12), 3600-7.
184. Hunter, T.; Poon, R. Y., Cdc37: a protein kinase chaperone? *Trends Cell Biol* **1997,** 7, (4), 157-61.
185. Pratt, W. B., The role of heat shock proteins in regulating the function, folding, and trafficking of the glucocorticoid receptor. *J Biol Chem* **1993,** 268, (29), 21455-8.
186. Kimura, Y.; Rutherford, S. L.; Miyata, Y.; Yahara, I.; Freeman, B. C.; Yue, L.; Morimoto, R. I.; Lindquist, S., Cdc37 is a molecular chaperone with specific functions in signal transduction. *Genes Dev* **1997,** 11, (14), 1775-85.
187. Grammatikakis, N.; Lin, J. H.; Grammatikakis, A.; Tsichlis, P. N.; Cochran, B. H., p50(cdc37) acting in concert with Hsp90 is required for Raf-1 function. *Mol Cell Biol* **1999,** 19, (3), 1661-72.
188. Gattoni, R.; Mahe, D.; Mahl, P.; Fischer, N.; Mattei, M. G.; Stevenin, J.; Fuchs, J. P., The human hnRNP-M proteins: structure and relation with early heat shock-induced splicing arrest and chromosome mapping. *Nucleic Acids Res* **1996,** 24, (13), 2535-42.
189. Jiang, J.; Ballinger, C. A.; Wu, Y.; Dai, Q.; Cyr, D. M.; Hohfeld, J.; Patterson, C., CHIP is a U-box-dependent E3 ubiquitin ligase: identification of Hsc70 as a target for ubiquitylation. *J Biol Chem* **2001,** 276, (46), 42938-44.
190. Smith, D. F.; Whitesell, L.; Katsanis, E., Molecular chaperones: biology and prospects for pharmacological intervention. *Pharmacol Rev* **1998,** 50, (4), 493-514.
191. Young, J. C.; Schneider, C.; Hartl, F. U., In vitro evidence that hsp90 contains two independent chaperone sites. *FEBS Lett* **1997,** 418, (1-2), 139-43.
192. Scheibel, T.; Weikl, T.; Rimerman, R.; Smith, D.; Lindquist, S.; Buchner, J., Contribution of N- and C-terminal domains to the function of Hsp90 in Saccharomyces cerevisiae. *Mol Microbiol* **1999,** 34, (4), 701-13.

193. Soti, C.; Racz, A.; Csermely, P., A Nucleotide-dependent molecular switch controls ATP binding at the C-terminal domain of Hsp90. N-terminal nucleotide binding unmasks a C-terminal binding pocket. *J Biol Chem* **2002,** 277, (9), 7066-75.
194. Soti, C.; Vermes, A.; Haystead, T. A.; Csermely, P., Comparative analysis of the ATP-binding sites of Hsp90 by nucleotide affinity cleavage: a distinct nucleotide specificity of the C-terminal ATP-binding site. *Eur J Biochem* **2003,** 270, (11), 2421-8.
195. Martin, J.; Langer, T.; Boteva, R.; Schramel, A.; Horwich, A. L.; Hartl, F. U., Chaperonin-mediated protein folding at the surface of groEL through a 'molten globule'-like intermediate. *Nature* **1991,** 352, (6330), 36-42.
196. Creighton, T. E., Molecular chaperones. Unfolding protein folding. *Nature* **1991,** 352, (6330), 17-8.
197. Agard, D. A., To fold or not to fold. *Science* **1993,** 260, (5116), 1903-4.
198. Ellis, R. J., Protein folding. Chaperonin duet. *Nature* **1993,** 366, (6452), 213-4.
199. Frydman, J.; Nimmesgern, E.; Erdjument-Bromage, H.; Wall, J. S.; Tempst, P.; Hartl, F. U., Function in protein folding of TRiC, a cytosolic ring complex containing TCP-1 and structurally related subunits. *Embo J* **1992,** 11, (13), 4767-78.
200. Todd, M. J.; Viitanen, P. V.; Lorimer, G. H., Dynamics of the chaperonin ATPase cycle: implications for facilitated protein folding. *Science* **1994,** 265, (5172), 659-66.
201. Weissman, J. S.; Kashi, Y.; Fenton, W. A.; Horwich, A. L., GroEL-mediated protein folding proceeds by multiple rounds of binding and release of nonnative forms. *Cell* **1994,** 78, (4), 693-702.
202. Kubota, H.; Hynes, G.; Willison, K., The chaperonin containing t-complex polypeptide 1 (TCP-1). Multisubunit machinery assisting in protein folding and assembly in the eukaryotic cytosol. *Eur J Biochem* **1995,** 230, (1), 3-16.
203. Dobrzynski, J. K.; Sternlicht, M. L.; Farr, G. W.; Sternlicht, H., Newly-synthesized beta-tubulin demonstrates domain-specific interactions with the cytosolic chaperonin. *Biochemistry* **1996,** 35, (49), 15870-82.
204. Llorca, O.; Martin-Benito, J.; Grantham, J.; Ritco-Vonsovici, M.; Willison, K. R.; Carrascosa, J. L.; Valpuesta, J. M., The 'sequential allosteric ring' mechanism in the eukaryotic chaperonin-assisted folding of actin and tubulin. *Embo J* **2001,** 20, (15), 4065-75.
205. Krecic, A. M.; Swanson, M. S., hnRNP complexes: composition, structure, and function. *Curr Opin Cell Biol* **1999,** 11, (3), 363-71.
206. Bomsztyk, K.; Denisenko, O.; Ostrowski, J., hnRNP K: one protein multiple processes. *Bioessays* **2004,** 26, (6), 629-38.
207. Howell, M.; Borchers, C.; Milgram, S. L., Heterogeneous nuclear ribonuclear protein U associates with YAP and regulates its co-activation of Bax transcription. *J Biol Chem* **2004,** 279, (25), 26300-6.
208. Kukalev, A.; Nord, Y.; Palmberg, C.; Bergman, T.; Percipalle, P., Actin and hnRNP U cooperate for productive transcription by RNA polymerase II. *Nat Struct Mol Biol* **2005,** 12, (3), 238-44.
209. Wei, C. C.; Guo, D. F.; Zhang, S. L.; Ingelfinger, J. R.; Chan, J. S., Heterogenous nuclear ribonucleoprotein F modulates angiotensinogen gene expression in rat kidney proximal tubular cells. *J Am Soc Nephrol* **2005,** 16, (3), 616-28.
210. Chen, Y.; Schnetz, M. P.; Irarrazabal, C. E.; Shen, R. F.; Williams, C. K.; Burg, M. B.; Ferraris, J. D., Proteomic identification of proteins associated with the

osmoregulatory transcription factor TonEBP/OREBP: functional effects of Hsp90 and PARP-1. *Am J Physiol Renal Physiol* **2007,** 292, (3), F981-92.
211. Moumen, A.; Masterson, P.; O'Connor, M. J.; Jackson, S. P., hnRNP K: an HDM2 target and transcriptional coactivator of p53 in response to DNA damage. *Cell* **2005,** 123, (6), 1065-78.
212. Li, J.; Williams, B. L.; Haire, L. F.; Goldberg, M.; Wilker, E.; Durocher, D.; Yaffe, M. B.; Jackson, S. P.; Smerdon, S. J., Structural and functional versatility of the FHA domain in DNA-damage signaling by the tumor suppressor kinase Chk2. *Mol Cell* **2002,** 9, (5), 1045-54.
213. Wu, X.; Webster, S. R.; Chen, J., Characterization of tumor-associated Chk2 mutations. *J Biol Chem* **2001,** 276, (4), 2971-4.
214. Staalesen, V.; Falck, J.; Geisler, S.; Bartkova, J.; Borresen-Dale, A. L.; Lukas, J.; Lillehaug, J. R.; Bartek, J.; Lonning, P. E., Alternative splicing and mutation status of CHEK2 in stage III breast cancer. *Oncogene* **2004,** 23, (52), 8535-44.
215. Prajapati, S.; Verma, U.; Yamamoto, Y.; Kwak, Y. T.; Gaynor, R. B., Protein phosphatase 2Cbeta association with the IkappaB kinase complex is involved in regulating NF-kappaB activity. *J Biol Chem* **2004,** 279, (3), 1739-46.
216. Hanada, M.; Ninomiya-Tsuji, J.; Komaki, K.; Ohnishi, M.; Katsura, K.; Kanamaru, R.; Matsumoto, K.; Tamura, S., Regulation of the TAK1 signaling pathway by protein phosphatase 2C. *J Biol Chem* **2001,** 276, (8), 5753-9.
217. Cheng, A.; Kaldis, P.; Solomon, M. J., Dephosphorylation of human cyclin-dependent kinases by protein phosphatase type 2C alpha and beta 2 isoforms. *J Biol Chem* **2000,** 275, (44), 34744-9.
218. Ofek, P.; Ben-Meir, D.; Kariv-Inbal, Z.; Oren, M.; Lavi, S., Cell cycle regulation and p53 activation by protein phosphatase 2C alpha. *J Biol Chem* **2003,** 278, (16), 14299-305.
219. Hirao, A.; Cheung, A.; Duncan, G.; Girard, P. M.; Elia, A. J.; Wakeham, A.; Okada, H.; Sarkissian, T.; Wong, J. A.; Sakai, T.; De Stanchina, E.; Bristow, R. G.; Suda, T.; Lowe, S. W.; Jeggo, P. A.; Elledge, S. J.; Mak, T. W., Chk2 is a tumor suppressor that regulates apoptosis in both an ataxia telangiectasia mutated (ATM)-dependent and an ATM-independent manner. *Mol Cell Biol* **2002,** 22, (18), 6521-32.
220. Bell, D. W.; Varley, J. M.; Szydlo, T. E.; Kang, D. H.; Wahrer, D. C.; Shannon, K. E.; Lubratovich, M.; Verselis, S. J.; Isselbacher, K. J.; Fraumeni, J. F.; Birch, J. M.; Li, F. P.; Garber, J. E.; Haber, D. A., Heterozygous germ line hCHK2 mutations in Li-Fraumeni syndrome. *Science* **1999,** 286, (5449), 2528-31.
221. Zhang, P.; Gao, W.; Li, H.; Reed, E.; Chen, F., Inducible degradation of checkpoint kinase 2 links to cisplatin-induced resistance in ovarian cancer cells. *Biochem Biophys Res Commun* **2005,** 328, (2), 567-72.
222. Falck, J.; Lukas, C.; Protopopova, M.; Lukas, J.; Selivanova, G.; Bartek, J., Functional impact of concomitant versus alternative defects in the Chk2-p53 tumour suppressor pathway. *Oncogene* **2001,** 20, (39), 5503-10.
223. Dozier, C.; Bonyadi, M.; Baricault, L.; Tonasso, L.; Darbon, J. M., Regulation of Chk2 phosphorylation by interaction with protein phosphatase 2A via its B' regulatory subunit. *Biol Cell* **2004,** 96, (7), 509-17.
224. Cheng, A.; Ross, K. E.; Kaldis, P.; Solomon, M. J., Dephosphorylation of cyclin-dependent kinases by type 2C protein phosphatases. *Genes Dev* **1999,** 13, (22), 2946-57.

225. Donella Deana, A.; Mac Gowan, C. H.; Cohen, P.; Marchiori, F.; Meyer, H. E.; Pinna, L. A., An investigation of the substrate specificity of protein phosphatase 2C using synthetic peptide substrates; comparison with protein phosphatase 2A. *Biochim Biophys Acta* **1990,** 1051, (2), 199-202.
226. Das, A. K.; Helps, N. R.; Cohen, P. T.; Barford, D., Crystal structure of the protein serine/threonine phosphatase 2C at 2.0 A resolution. *Embo J* **1996,** 15, (24), 6798-809.
227. Singer, B.; Hang, B., What structural features determine repair enzyme specificity and mechanism in chemically modified DNA? *Chem Res Toxicol* **1997,** 10, (7), 713-32.
228. Jayaraman, L.; Murthy, K. G.; Zhu, C.; Curran, T.; Xanthoudakis, S.; Prives, C., Identification of redox/repair protein Ref-1 as a potent activator of p53. *Genes Dev* **1997,** 11, (5), 558-70.
229. Bennett, R. A.; Wilson, D. M., 3rd; Wong, D.; Demple, B., Interaction of human apurinic endonuclease and DNA polymerase beta in the base excision repair pathway. *Proc Natl Acad Sci U S A* **1997,** 94, (14), 7166-9.
230. Gorman, M. A.; Morera, S.; Rothwell, D. G.; de La Fortelle, E.; Mol, C. D.; Tainer, J. A.; Hickson, I. D.; Freemont, P. S., The crystal structure of the human DNA repair endonuclease HAP1 suggests the recognition of extra-helical deoxyribose at DNA abasic sites. *Embo J* **1997,** 16, (21), 6548-58.
231. Xanthoudakis, S.; Curran, T., Identification and characterization of Ref-1, a nuclear protein that facilitates AP-1 DNA-binding activity. *Embo J* **1992,** 11, (2), 653-65.
232. Gaiddon, C.; Moorthy, N. C.; Prives, C., Ref-1 regulates the transactivation and pro-apoptotic functions of p53 in vivo. *Embo J* **1999,** 18, (20), 5609-21.
233. Hanson, S.; Kim, E.; Deppert, W., Redox factor 1 (Ref-1) enhances specific DNA binding of p53 by promoting p53 tetramerization. *Oncogene* **2005,** 24, (9), 1641-7.
234. Song, H.; Hollstein, M.; Xu, Y., p53 gain-of-function cancer mutants induce genetic instability by inactivating ATM. *Nat Cell Biol* **2007,** 9, (5), 573-80.
235. Miyashita, T.; Reed, J. C., Tumor suppressor p53 is a direct transcriptional activator of the human bax gene. *Cell* **1995,** 80, (2), 293-9.
236. Oda, E.; Ohki, R.; Murasawa, H.; Nemoto, J.; Shibue, T.; Yamashita, T.; Tokino, T.; Taniguchi, T.; Tanaka, N., Noxa, a BH3-only member of the Bcl-2 family and candidate mediator of p53-induced apoptosis. *Science* **2000,** 288, (5468), 1053-8.
237. Oda, K.; Arakawa, H.; Tanaka, T.; Matsuda, K.; Tanikawa, C.; Mori, T.; Nishimori, H.; Tamai, K.; Tokino, T.; Nakamura, Y.; Taya, Y., p53AIP1, a potential mediator of p53-dependent apoptosis, and its regulation by Ser-46-phosphorylated p53. *Cell* **2000,** 102, (6), 849-62.
238. Nakano, K.; Vousden, K. H., PUMA, a novel proapoptotic gene, is induced by p53. *Mol Cell* **2001,** 7, (3), 683-94.
239. Yu, J.; Zhang, L.; Hwang, P. M.; Kinzler, K. W.; Vogelstein, B., PUMA induces the rapid apoptosis of colorectal cancer cells. *Mol Cell* **2001,** 7, (3), 673-82.
240. Mihara, M.; Erster, S.; Zaika, A.; Petrenko, O.; Chittenden, T.; Pancoska, P.; Moll, U. M., p53 has a direct apoptogenic role at the mitochondria. *Mol Cell* **2003,** 11, (3), 577-90.
241. Belzacq, A. S.; Vieira, H. L.; Verrier, F.; Vandecasteele, G.; Cohen, I.; Prevost, M. C.; Larquet, E.; Pariselli, F.; Petit, P. X.; Kahn, A.; Rizzuto, R.; Brenner, C.;

Kroemer, G., Bcl-2 and Bax modulate adenine nucleotide translocase activity. *Cancer Res* **2003,** 63, (2), 541-6.
242. Hegde, V.; Wang, M.; Deutsch, W. A., Human ribosomal protein S3 interacts with DNA base excision repair proteins hAPE/Ref-1 and hOGG1. *Biochemistry* **2004,** 43, (44), 14211-7.
243. Cordon-Cardo, C.; Latres, E.; Drobnjak, M.; Oliva, M. R.; Pollack, D.; Woodruff, J. M.; Marechal, V.; Chen, J.; Brennan, M. F.; Levine, A. J., Molecular abnormalities of mdm2 and p53 genes in adult soft tissue sarcomas. *Cancer Res* **1994,** 54, (3), 794-9.
244. Ladanyi, M.; Cha, C.; Lewis, R.; Jhanwar, S. C.; Huvos, A. G.; Healey, J. H., MDM2 gene amplification in metastatic osteosarcoma. *Cancer Res* **1993,** 53, (1), 16-8.
245. Leach, F. S.; Tokino, T.; Meltzer, P.; Burrell, M.; Oliner, J. D.; Smith, S.; Hill, D. E.; Sidransky, D.; Kinzler, K. W.; Vogelstein, B., p53 Mutation and MDM2 amplification in human soft tissue sarcomas. *Cancer Res* **1993,** 53, (10 Suppl), 2231-4.
246. Oliner, J. D.; Kinzler, K. W.; Meltzer, P. S.; George, D. L.; Vogelstein, B., Amplification of a gene encoding a p53-associated protein in human sarcomas. *Nature* **1992,** 358, (6381), 80-3.
247. Reifenberger, G.; Liu, L.; Ichimura, K.; Schmidt, E. E.; Collins, V. P., Amplification and overexpression of the MDM2 gene in a subset of human malignant gliomas without p53 mutations. *Cancer Res* **1993,** 53, (12), 2736-9.
248. Courjal, F.; Cuny, M.; Rodriguez, C.; Louason, G.; Speiser, P.; Katsaros, D.; Tanner, M. M.; Zeillinger, R.; Theillet, C., DNA amplifications at 20q13 and MDM2 define distinct subsets of evolved breast and ovarian tumours. *Br J Cancer* **1996,** 74, (12), 1984-9.
249. Yadavilli, S.; Hegde, V.; Deutsch, W. A., Translocation of human ribosomal protein S3 to sites of DNA damage is dependant on ERK-mediated phosphorylation following genotoxic stress. *DNA Repair (Amst)* **2007,** 6, (10), 1453-62.